SYNTHESIS AND CHARACTERIZATION OF TWO STAGE CROSSLINKABLE RESINS

A THESIS SUBMITTED

TO THE

UNIVERSITY OF PUNE

FOR THE DEGREE OF

DOCTOR OF PHILOSOPHY

IN CHEMISTRY

BY

SANGAVE DADASAHEB VITTHAL

POLYMER SCIENCE AND ENGINEERING DIVISION

NATIONAL CHEMICAL LABORATORY

PUNE-411008, INDIA

MARCH 2012

CERTIFICATE

This is to certify that the work incorporated in the thesis entitled **"Synthesis and Characterization of Two Stage Crosslinkable Resins"** submitted by **Mr. Sangave Dadasaheb Vitthal** was carried out under my supervision. Such material as has been obtained from other sources has been duly acknowledged in the thesis.

Date: **Dr. M. G. Kulkarni**

National Chemical Laboratory, **(Research Guide)**

Pune 411008.

DECLARATION

I hereby declare that the work presented in the thesis entitled **"Synthesis and Characterization of Two Stage Crosslinkable Resins"** submitted for Ph. D. degree to the University of Pune has been carried out under the supervision of **Dr. M. G. Kulkarni** at the Division of Polymer Science and Engineering, National Chemical Laboratory, Pune, India. The work is original and has not been submitted in part or full by me for any degree or diploma to this or any other University.

Date: **Sangave Dadasaheb Vitthal**

National Chemical Laboratory, **(Research Student)**

Pune-411008.

Acknowledgment

This dissertation represents the successful completion of long awaited dream and that would not have been possible without the efforts, advice, encouragement and support from many people:

Emotions can not be adequately expressed in words, therefore my acknowledgment are many times more than that I am expressing here. Knowledge can only be acquired with the help of an able, experienced "Guruvarya". I am really fortunate to have Dr. M. G. Kulkarni, Head, PSE, NCL, as my research guide, who, in his unique way gave valuable guidance, constant encouragement, constructive criticism and suggestions throughout the tenure of this investigation.

I am extremely fortunate for having an opportunity to express my heartiest gratitude to Prof. V. Ramgopal Rao, IITB, Powai, Mumbai, for his support, both scientifique and financial and stimulating discussions and ideas. Thanks are also due to his kind and caring nature.

I would like to thank Dr. Badiger, Mr. M. J. Thakar and Dr. Rathna for the support given to me during this work.

I'm also thankful to Dr. Nitin Kale, Dr. Nageshwari, Dr. Jayashree, Dr. Sheetal and Dr. Mrinmoy from IITB, Powai, Mumbai, for supporting my Lithography Characterizations.

I would like to thank the Council of Scientific and Industrial Research, New Delhi for the award of fellowship in the form of JRF and SRF and Director, NCL for providing facilities, which enabled me to carry out my research in such a prestigious research laboratory.

I am grateful to all my friends Santanu, Vijaya, Shweta, Vijay, Amit, Suresha, Ujwal, Dr. Hemant, Dr. Ramesh, Dr. Gahininath, Dr. Gore, Dr. Jiten, Dr. Amit, Dr. Arun,

Dr. Swarnendu, Dr. Kiran, Dr. Narayan, Dr. Jayant, Dr. Raman, Dr. Rupali, Dr. Smitha, Dr. Anupa, Dr. Sunita, Dr. Prerana, Dr. Shubhangi, Dr. Jyotsna, Aarti, Manjusha, Trupti, Satish, Sameera, Swapnil, Sandeep, Vinod, Muntazim, Arpita, Neelam, Vishal, Tushar, Narhari, Anumon, Pawan, for timely help, co-operation and making my stay at NCL pleasant.

My deepest gratitude goes to my labmate Nivika's family close to me for their unflagging love and support throughout, this dissertation is simply impossible without them. I am indebted to her "Papa" Rajendra, as a typical father for his motivation, care and love towards me. I remember their constant support when I encountered difficulties and I remember, most of all, her delicious dishes "Mumma" prepared. In the most difficult moments, I tried to look at things through the eyes of this family including Swapnil who always had enough of positive spirit for a dozen people.

I am also thankful to Mr. Dhavale, Mr. Kokane, Mr. Bharati and Mr. Mahajan for their assistance.

Completion of this thesis would not have been possible without the unconditional support and faith bestowed by my wife Manju.

Bhau, Arunabai, Chababai, Anna, Aaba, and Bapu, for your unconditional support, freedom for career will remain my inspiration throughout my life, your patience, sacrifice, and faith in education gave me the strength to pursue for PhD…

Dadasaheb Sangave
March 2012

Dedicated to my family

TABLE OF CONTENTS

Chapter 1

Literature survey

1.1.	Introduction	2
1.2.	Microlithography	3
1.3.	Types of microlithography	4
1.3.1.	Photolithography	4
1.3.1.1.	Exposure techniques	5
1.3.1.1.1.	Contact printing	5
1.3.1.1.2.	Proximity printing	5
1.3.1.1.3.	Projection printing	6
1.3.1.2.	Processing steps in lithography	6
1.3.1.2.1.	Vapour prime	6
1.3.1.2.2.	Spin coat	7
1.3.1.2.3.	Soft bake	7
1.3.1.2.4.	Exposure to radiation	7
1.3.1.2.5.	Post exposure bake	7
1.3.1.2.6.	Resist development	8
1.3.1.2.7.	Hard bake	8
1.3.1.2.8.	Develop / Inspect	9
1.3.1.3.	Optical lithography resists	9

1.3.1.3.1.	Polymers with pendant epoxide groups	9
1.3.1.3.2.	Polymers with pendant chalcone groups	10
1.3.1.3.3.	Polymers with pendant abietate groups	11
1.3.1.3.4.	Polymers with pendant vinyl groups	12
1.3.2.	Electron beam lithography	14
1.3.2.1.	Electron gun	15
1.3.2.2.	Electron optical column	16
1.3.2.3.	Substrate	17
1.3.2.4.	Techniques	17
1.3.2.4.1.	Electron beam direct write lithography	17
1.3.2.4.2.	Electron solid interactions	18
1.3.2.4.3.	Multiple electron beam direct-write lithography	20
1.3.2.5.	Electron beam writing approaches	21
1.3.2.5.1.	Vector writing approach	21
1.3.2.5.2.	Raster writing approach	22
1.3.2.6.	Electron beam resist	22
1.3.2.6.1.	Polymeric resists	23
1.3.2.6.2.	Molecular resist	24
1.3.2.6.2.1.	Molecular glass resists	24
1.3.2.6.2.2.	Calixarene derivatives	27
1.3.2.6.2.3.	Dendrimeric resists	28
1.3.2.6.2.4.	Triphenylene derivative	29
1.3.3.	Chemically amplified resist	30
1.3.4.	Resist characterization	33

1.3.4.1. Line edge roughness (LER) 33

1.3.4.2. Sensitivity and contrast 35

1.3.5. Next generation lithography 36

1.4. References 37

Chapter 2

Objective and scope of the work

2.1. Preamble 43

2.2. Objectives 43

2.3. Scope of the present research investigation 44

Chapter 3

Polymer containing latent vinyl groups for lithographic applications

3.1. Introduction 46

3.2. Experimental section 48

3.2.1 Materials 48

3.2.2. Synthesis 48

3.2.2.1. Monomer synthesis 48

3.2.2.1.1. Cumyl methacrylate monomer (CM) 48

3.2.2.1.2. 1-Naphthol methacrylate (NM) 50

3.2.2.2. Synthesis of inclusion complex (IC) of the crosslinker 51

3.2.2.2.1. βCD-TMPTMA IC (CD-T) 51
3.2.2.2.2. βCD-EGDMA IC (CD-E) 51
3.2.2.3. Copolymer synthesis 51
3.2.2.3.1. Poly (CM-co-CD-E), 20/80 51
3.2.2.3.2. Poly (CM-co-CD-T), 20/80 52
3.2.2.4. Characterization 53
3.2.2.5. Lithographic evaluation of negative-tone photoresist 54
3.3. Results and Discussion 54
3.3.1. Choice of the method 54
3.3.2. Inclusion complex: Characterization by ^{1}H-NMR 55
3.3.2.1. ^{1}H-NMR-CD-T IC 55
3.3.2.2. ^{1}H-NMR CD-E IC 56
3.3.3. Polymer characterization 56
3.3.3.1. Solubility 56
3.3.3.2. Molecular weights 57
3.3.3.3. Determination of unsaturation in copolymers 58
3.3.3.3.1. Qualitative determination by FTIR spectroscopy 58
3.3.3.3.2. Quantitative evaluation by ^{1}H-NMR spectroscopy 60
3.3.3.4. Thermal properties 63
3.3.3.4.1. Thermogravimetric analysis 63
3.3.3.4.2. Glass transition temperature (T_g) 65
3.3.3.5. Transmittance studies 68
3.3.3.6. Lithographic evaluation 69

3.3.3.6.1.	Sensitivity curve	69
3.3.3.6.2.	Lithography	70
3.4.	Conclusion	75
3.5.	References	76

Chapter 4

Synthesis, characterization and evaluation of linear polymers containing pendant epoxy groups as negative photoresist for optical lithography

4.1.	Introduction	79
4.2.	Experimental	80
4.2.1.	Materials	80
4.2.2.	Synthesis	80
4.2.2.1.	Monomer synthesis	80
4.2.2.1.1.	Bisphenol-A methacrylate (BPMA)	80
4.2.2.1.2.	1, 5-dihydroxynaphthalene methacrylate (1, 5-DHNMA)	81
4.2.2.2.	Homopolymer synthesis	81
4.2.2.2.1.	Poly (BPMA)	81
4.2.2.2.2.	Poly (1, 5-DHNMA)	81
4.2.2.3.	Copolymer synthesis	81
4.2.2.3.1.	Poly (BPMA-co-CM) (70:30)	81
4.2.2.3.2.	Poly (BPMA-co-CM) (50:50)	82
4.2.2.3.3.	Poly (BPMA-co-CM) (30:70)	82

4.2.2.3.4.	Poly (1, 5-DHNMA-co-NM) (70:30)	82
4.2.2.3.5.	Poly (1, 5-DHNMA-co-NM) (50:50)	82
4.2.2.3.6.	Poly (1, 5-DHNMA-co-NM) (30:70)	82
4.2.2.4.	Epoxide conjugation	82
4.2.2.4.1.	Poly (BPMA) epoxide	82
4.2.2.4.2.	Poly (1, 5DHNMA) epoxide	83
4.2.3.	Characterization	83
4.2.4.	Lithographic evaluation	83
4.3.	Results and Discussion	84
4.3.1.	Choice of the system	84
4.3.2.	Synthesis of epoxy conjugated polymers	84
4.3.3.	Polymer characterization	86
4.3.3.1.	Solubility	86
4.3.3.2.	Molecular weights	87
4.3.3.3.	^{1}H NMR spectroscopy	87
4.3.3.3.1.	^{1}H NMR of BPMA and 1, 5-DHNMA	87
4.3.3.3.2.	^{1}H NMR of Poly (BPMA) and Poly (1,5-DHNMA) before and after epoxide conjugation	89
4.3.3.4.	Thermal properties	91
4.3.3.4.1.	Thermogravimetric analysis (TGA)	91
4.3.3.4.2.	Glass transition temperature (T_g)	92
4.3.4.	Lithography	93
4.4.	Conclusion	98
4.5.	References	99

Chapter 5

Chemically amplified negative photoresists based on first generation dendrimers for electron-beam lithography

5.1.	Introduction	101
5.2.	Experimental section	103
5.2.1.	Materials	103
5.2.2.	Synthesis	104
5.2.2.1.	Preparation of G_1-Tris	104
5.2.2.2.	Preparation of G_1-Bis	104
5.2.2.3.	Preparation of G_1-Dhn	104
5.2.2.4.	Preparation of G_1-Tris-epoxide	104
5.2.2.5.	Preparation of G_1-Bis-epoxide	105
5.2.2.6.	Preparation of G_1-Dhn-epoxide	105
5.2.3.	Characterization	106
5.2.4.	Lithographic evaluation	106
5.3.	Results and Discussion	106
5.3.1.	Design of first generation dendrimers	106
5.3.2.	Synthesis of FGDs	108
5.3.3.	FGDs characterization	110
5.3.3.1.	Solubility	110
5.3.3.2.	IR spectroscopy	110

5.3.3.3.	^{1}H-NMR spectroscopy	111
5.3.3.4.	Molecular weights	113
5.3.3.5.	Thermal properties	113
5.3.3.5.1.	Thermal degradation	113
5.3.3.5.2.	The glass transition temperature	114
5.3.3.6.	X-ray diffraction (XRD)	117
5.3.3.7.	Lithographic evaluation	118
5.3.3.7.1.	Sensitivity curve for the FGDs	118
5.3.3.7.2.	Post exposure bake optimization	121
5.3.3.7.3.	Electron beam lithography	121
5.3.3.7.4.	Scanning electron microscopy	122
5.3.3.7.5.	Line edge roughness (LER)	123
5.4.	Conclusions	125
5.5.	References	126

Chapter 6

Chemically amplified positive resists based on first generation dendrimers for electron-beam lithography

6.1.	Introduction	130
6.2.	Experimental	131
6.2.1.	Materials	131
6.2.2.	Synthesis	131

6.2.2.1.	G_1-Tris-t-BOC100	131
6.2.2.2.	G_1-Tris-t-BOC80	131
6.2.2.3.	G_1-Tris-t-BOC60	132
6.2.2.4.	G_1-Tris-t-BOC50	132
6.2.2.5.	G_1-Bis-t-BOC100	132
6.2.2.6.	G_1-Bis-t-BOC80	132
6.2.2.7.	G_1-Bis-t-BOC60	132
6.2.2.8.	G_1-Bis-t-BOC50	133
6.2.2.9.	G_1-Dhn-t-BOC100	133
6.2.2.10.	G_1-Dhn-t-BOC80	133
6.2.2.11.	G_1-Dhn-t-BOC60	133
6.2.2.12.	G_1-Dhn-t-BOC50	133
6.2.3.	Characterization	134
6.2.4.	Lithographic evaluation of positive tone FGDs	134
6.3.	Results and Discussion	134
6.3.1.	Choice of dendrimers	134
6.3.2.	Synthesis of FGDs	136
6.3.3.	FGDs characterization	137
6.3.3.1.	Solubility	137
6.3.3.2.	FTIR spectroscopy	138
6.3.3.3.	^{1}H-NMR spectroscopy	139
6.3.3.4.	Molecular weights	140
6.3.3.5.	Thermal properties	141
6.3.3.5.1.	Thermal degradation	141

6.3.3.5.2. The glass transition temperature 144

6.3.3.6. X-ray diffraction (XRD) 147

6.3.3.7. Adhesion measurements 148

6.3.4. Lithographic evaluation 149

6.3.4.1. Sensitivity curves for the FGD resists 149

6.3.4.2. Post exposure bakes (PEB) and development time optimization 151

6.3.4.3. Electron beam lithography 152

6.3.4.4. Scanning electron microscopy (SEM) 153

6.3.4.4.1. Positive-tone resists 153

6.3.4.4.2. Line edge roughness (LER) 154

6.4. Conclusions 155

6.5. References 157

Chapter 7

Chemically amplified negative resists based on first generation dendrimers for optical lithography

7.1. Introduction 160

7.2. Experimental section 161

7.2.1. Characterization 161

7.2.2. Lithographic evaluation 161

7.3. Results and Discussion 162

7.3.1. Lithography 162

7.3.2. Patterns for gate area device 165

7.3.3. Reactive ion etching (RIE) 166

7.4. Conclusions 171

7.5. References 172

Chapter 8

Conclusions and recommendations for further work

8.1 Major conclusions arrived at from this investigation 174

8.2 Recommendations for future work 175

List of Figures XVII

List of Tables XXV

Abbreviations XXVII

List of Figures

Chapter 1

Figure 1.1:	Moore's Law	3
Figure 1.2:	UV wavelength used in photolithography	4
Figure 1.3:	Schematic of photolithography	4
Figure 1.4:	Schematic of optical exposure techniques	6
Figure 1.5:	Processing steps in lithography	8
Figure 1.6:	Methacrylate polymer containing pendant epoxide	9
Figure 1.7:	Structure of SU-8 polymer	10
Figure 1.8:	Polymer containing pendant chalcone groups	11
Figure 1.9:	Synthesis of methacrylate polymer containing abietate group	12
Figure 1.10:	Polyferrocenylsilanes methacrylate containing pendant vinyl groups	13
Figure 1.11:	Synthesis of poly (HEMA-co-t-MMA) and post functionalization	13
Figure 1.12:	Schematic of an electron beam exposure system	14
Figure 1.13:	Schematic of the electron gun	15
Figure 1.14:	Schematic of the electron optical column	16
Figure 1.15:	Schematic of beam control elements in electron beam direct writing lithography	18
Figure 1.16:	Schematic representation of electron solid interactions (Monte Carlo simulation)	19
Figure 1.17:	Schematic representation of electron scattering with beam acceleration	19

Figure 1.18:	Schematic representation of multiple electron beam direct write system	20
Figure 1.19:	Vector writing approach	21
Figure 1.20:	Raster writing approach	22
Figure 1.21:	Resist classification	23
Figure 1.22:	Chemical structure of calixa[n]rene with functional groups R1 and R2	27
Figure 1.23:	Schematic of a triphenylene derivative with functional groups R1 and R2	30
Figure 1.24:	Acid-catalysed deprotection of the t-BOC resist	31
Figure 1.25:	Crosslinking of an epoxy resin via acid-catalysed ring opening	32
Figure 1.26:	Chemical amplification imaging mechanism	33
Figure 1.27:	Schematic of the LER for the polymers and molecular	34
Figure 1.28:	Sensitivity curves for positive and negative resist	36

Chapter 3

Figure 3.1:	Synthesis of monomers CM and NM	49
Figure 3.2:	CD-T and CD-E IC synthesis	50
Figure 3.3:	Synthesis of EGDMA copolymers	52
Figure 3.4:	Synthesis of TMPTMA copolymers	53
Figure 3.5:	1H-NMR D-T IC	55
Figure 3.6:	1H-NMR EGDMA-β-CD IC	56
Figure 3.7:	FTIR spectra of polymers P1-P4	59
Figure 3.8:	FTIR spectra of polymers P5-P8	59

Figure 3.9: FTIR spectra of polymers P9-P12 60

Figure 3.10: FTIR spectra of polymers P13-P16 60

Figure 3.11: 1H NMR spectra of polymers P1-P4 61

Figure 3.12: 1H NMR spectra of polymers P5-P8 61

Figure 3.13: ^{1}H NMR spectra of polymers P9-P12 62

Figure 3.14: ^{1}H NMR spectra of polymers P13-P16 62

Figure 3.15: TGA thermograms of P1-P4 63

Figure 3.16: TGA thermograms of P5-P8 64

Figure 3.17: TGA thermograms of P9-P12 64

Figure 3.18: TGA thermograms of P13-P16 65

Figure 3.19: DSC thermograms of polymers P1-P4 66

Figure 3.20: DSC thermograms of polymers P5-P8 66

Figure 3.21: DSC Thermograms of polymers P12 and P16 68

Figure 3.22: Transmittance of copolymers 69

Figure 3.23: Characteristic UV-exposure curves 70

Figure 3.24: SEM images of Polymer P1. 72

Figure 3.25: SEM images of Polymer P9. 72

Figure 3.26: SEM images of Polymer P5. 73

Figure 3.27: SEM images of Polymer P13. 73

Figure 3.28: Images of resist P1 (A) and P9 (B) 74

Figure 3.29: Images of resist P5 (A) and P13 (B) 74

Chapter 4

Figure 4.1:	Synthesis of bisphenol-A based polymers containing pendant epoxy groups: A) DMF, 65°C; D) KOH, polyethylene glycol-400, epichlorohydrin.	85
Figure 4.2:	Synthesis of 1,5-dihydroxynaphthalene based polymers containing pendant epoxy groups: A) Methacryloyl chloride, TEA, THF; B) AIBN, DMF, 65°C; C) AIBN, 1-HNMA, DMF, 65°C; D) KOH, polyethylene glycol-400, epichlorohydrin.	86
Figure 4.3:	1H NMR spectra of BPMA	88
Figure 4.4:	1H NMR spectra of 1,5-DHNMA	88
Figure 4.5:	1H NMR spectra of Poly (BPMA)	89
Figure 4.6:	1H NMR spectra Poly (BPMA) epoxide	89
Figure 4.7:	1H NMR spectra of Poly (1,5-DHNMA)	90
Figure 4.8:	1H NMR spectra of Poly (1,5-DHNMA) epoxide	90
Figure 4.9:	Thermograms of P1-P4	91
Figure 4.10:	Thermograms of P5-P8	91
Figure 4.11:	DSC thermograms of polymers P1-P4 before (a) and after (b) photocrosslinking P5-P8 before (c) and after (d) photocrosslinking.	92
Figure 4.12:	SEM images of P1	94
Figure 4.13:	SEM images of P2	94
Figure 4.14:	SEM images of the resist P5	95
Figure 4.15:	SEM images of the resist P6	95
Figure 4.16:	SEM images of the SU-8	96
Figure 4.17:	Optical images of gate area patterns with SU-8 (A), P2 (B) and P6 (C)	97

Chapter 5

Figure 5.1a:	Synthesis of G_1-Tris-epoxide; a) K_2CO_3, DMF, 60°C; b) KOH, Epichlorohydrin, PEG-400, 60°C	109
Figure 5.1b:	Structures of G_1-Bis, G_1-Dhn, G_1-Bis-epoxide and G_1-Dhn-epoxide	109
Figure 5.2a:	FTIR spectrum of G_1-Tris and G_1-Tris-epoxide	110
Figure 5.2b:	FTIR spectrum of G_1-Bis and G_1-Bis-epoxide	111
Figure 5.2c:	FTIR spectrum of G_1-Dhn and G_1-Dhn-epoxide	111
Figure 5.3a:	NMR spectrum of G_1-Tris	112
Figure 5.3b:	^{1}H-NMR spectrum of G_1-Tris-epoxide	112
Figure 5.4a:	Thermograms of unmodified FGDs	114
Figure 5.4b:	Thermograms of epoxide conjugated FGDs	114
Figure 5.5a:	DSC thermograms of FGDs, scan rate 10 °C/min	116
Figure 5.5b:	DSC thermograms of FGDs-epoxide, scan rate 10 °C/min.	116
Figure 5.5c:	T_gs of FGDs before and after epoxide conjugation	116
Figure 5.6:	XRD of dendrimers	117
Figure 5.7:	Relative resist thickness vs. exposure dose for the FGDs: A) 5 wt % PAG, B) 10 wt% Of PAG	119
Figure 5.8:	SEM images of G_1-Tris-epoxide used for sensitivity and contrast calculation: A) 5 wt %; B) 10 wt. % PAG	119
Figure 5.9:	SEM images of A) G_1-Tris-epoxide and B) G_1-Bis-epoxide EBL pattern. Line thickness 500, 200, 100 and 50 nm bottom upward	122
Figure 5.10:	A) SEM image of 50 nm lines at 1:2 nm pitch for G_1-tris-epoxide; B) 50 nm lines at 1:10 nm pitch for G_1-Dhn-epoxide	123

Figure 5.11: 30 nm lines at pitch 1:10 (A), 1:2 (B), 1:1(C) G_1-tris-epoxide 123

Figure 5.12: 30 nm lines at pitch 1:10 (A), 1:2 (B) and 1:1 (C) G_1-Bis-epoxide 123

Figure 5.13: Images of patterns of G_1-Tris-epoxide used for LER calculation 124

Chapter 6

Figure 6.1: Synthesis of t-BOC conjugated FGDs, (a) K_2CO_3, DMF, 60^oC; (b) NMP, DMAP, and di-t-butyldicarbonate at room temperature. 136

Figure 6.2: Structures of G1-Bis-t-BOC100 and G_1-Dhn-t-BOC100 137

Figure 6.3a: FTIR of G_1-Tris-t-BOC 138

Figure 6.3b: FTIR of G_1-Bis-t-BOC 138

Figure 6.3c: FTIR of G_1-Dhn-t-BOC 139

Figure 6.4a: 1H NMR spectrum of G_1-Tris 140

Figure 6.4b: 1H NMR spectrum of G_1-Tris-BOC100 140

Figure 6.5a: TGA thermograms of G_1-Tris-t-BOC 142

Figure 6.5b: TGA thermograms of G_1-Bis-t-BOC 142

Figure 6.5c: TGA thermograms of G_1-Dhn-t-BOC 143

Figure 6.6a: Tg of G_1-Tris and t-BOC derivatives 145

Figure 6.6b: Tg of G_1-Bis and t-BOC derivatives 145

Figure 6.6c: Tg of G_1-Dhn and t-BOC derivatives 146

Figure 6.7: XRD of t-BOC conjugated FGDs 147

Figure 6.8: Effect of t-BOC protection on adhesion of FGDs 149

Figure 6.9:	SEM image of G_1-Tris-t-BOC80 used for sensitivity and contrast	150
Figure 6.10:	Exposure characteristics curves for FGDs containing 80 % t-BOC	150
Figure 6.11:	Development of G_1-tris-t-BOC in TMAH at varying time A) 40 sec; B) 50 sec and C) 70 sec.	152
Figure 6.12:	SEM images of 100 nm lines at pitch 1:2 (A), 1:1(B), 1:0.7 (C); 50 nm lines at pitch 1:2 (D), 1:1 (E) and 30 nm lines at pitch 1:3 (F), 1:2 (G) and 1:1 (H) for G_1-Tris-BOC 80.	153
Figure 6.13:	SEM images of 100 nm lines at pitch 1:2 (A); 50 nm lines at pitch 1:2 (B), 1:1 (C) and 30 nm lines at pitch 1:3 (D), 1:2 (E) and 1:1 (F) for G_1-Bis-BOC 80.	154
Figure 6.14:	SEM images of G_1-Dhn-BOC 80 at pitch 1:2; (A) 100, (B) 50 nm lines.	154

Chapter 7

Figure 7.1:	Line pattern of the G_1-Tris-epoxide resist	163
Figure 7.2:	Line pattern of the G_1-Bis-epoxide resist	164
Figure 7.3:	Line pattern of the G_1-Dhn-epoxide resist	164
Figure 7.4:	Line pattern of the SU-8 resist	165
Figure 7.5:	Images of the resist SU-8 (A), G_1-Tris-epoxide (B), G_1-Bis-epoxide (C) and G_1-Dhn-epoxide (D)	166
Figure 7.6:	SEM images of the resist A) SU-8, B) G_1-Tris-epoxide, C) G_1-Bis-epoxide and D) G_1-Dhn-epoxide	167
Figure 7.7:	Thickness of the squares patterns on silicon oxide before (A) and after (B) RIE	168
Figure 7.8:	AFM images of SU-8 before and after RIE	169

Figure 7.9: AFM images of G_1-Tris-epoxide before and after RIE 170

Figure 7.10: AFM images of G_1-Bis-epoxide before and after RIE 170

Figure 7.11: AFM images of G_1-Dhn-epoxide before and after RIE 171

List of Tables

Chapter 1

Table 1.1: Structure of molecular glasses 25

Table 1.2: Structure of Dendrimers 29

Chapter 3

Table 3.1: Copolymers of EGDMA 57

Table 3.2: Copolymers of TMPTMA 58

Table 3.3: Thermal properties of copolymers 67

Table 3.4: % Transmittance and film thickness 69

Chapter 4

Table 4.1: Molecular weights of Poly (BPMA-co-CPMA) epoxide 87

Table 4.2: Molecular weights of Poly (1, 5-DHNMA-co-1-HNMA) epoxide 87

Table 4.3: Characterization of polymers. 93

Chapter 5

Table 5.1: Characterization of FGDs 117

Table 5.2: Comparison of the FGDs with SU-8 and calixarene based resists 120

Table 5.3: LER values comparison 125

Chapter 6

Table 6.1: Molecular weights of FGDs 141

Table 6.2: t-BOC content from 1H-NMR and TGA analysis 143

Table 6.3: Tg of FGDs 146

Table 6.4: Work of adhesion for t-BOC films on silicon substrate 148

Table 6.5: LER values for FGD resists 155

Chapter 7

Table 7.1 RIE conditions 168

Table 7.2 Reactive ion etching (RIE) of the FGDs and SU-8 169

Abbreviations

Acetone-d_6	Deuterated acetone
AFM	Atomic force microscope
AIBN	Azo-bis-isobutyronitrile
Bisphenol- A	1, 3, 5-tris (bromomethyl) benzene
BPMA	Bisphenol-A methacrylate
CAR	Chemically Amplified Resists
CAR	Chemically amplified resists
$CDCl_3$	Deuterated Chloroform
CM	Cumyl methacrylate
DCM	Dichloromethane
1,5- Dhn	1,5-Dihydroxy naphthalene
DMAP	4-Dimethylaminopyridine
DMF	N, N-Dimethylformamide
DMSO	Dimethylsulphoxide
DMSO-d_6	Deuterated dimethyl sulphoxide
DRAM	Dynamic random access memories
DSC	Differential scanning calorimetery
DUV	Deep Ultraviolet
EA	Ethyl acetate
EBL	Electron Beam Lithography
EGDMA	Ethylene glycol dimethacrylate
EUV	Extreme ultraviolet

FGDs	First Generation Dendrimers
FTIR	Fourier Transform Infra-red
G_1-Bis	FGDs based on Bisphenol-A
G_1-Dhn	FGDs based on 1, 5-Dhn
G_1-Tris	FGDs based on Trisphenol
GMA	Glycidyl methacrylate
GPC	Gel Permeation Chromatography
HEMA	Hydroxy ethyl methacrylate
HMDS	Hexamethyldisilazane
IC	Integerated Circuit
IC	Inclusion Complex
K_2CO_3	Potassium carbonate
KOH	Potassium hydroxide solution
^{1}H NMR	Proton nuclear magnetic resonance
LER	Line edge roughness
MEMS	Micro Electro Mechanical Systems
MGs	Molecular Glasses
Min	minutes
MMA	Methyl methacrylate
$\mu C/cm^2$	Micro coulomb per centimeter square
Mn	Number average
Mw	Weight average
n-BA	n-butyl acrylate
Nm	nanometer

NM	1-naphthol methacrylate
NMP	N-methyl-2-pyrrolidone
PAG	Photo acid generator
PEB	Post Exposure Bake
PEG-400	Polyethylene glycol
PGMEA	propylene glycol methyl ether acetate
PMMA	Poly (methyl methacrylate)
ppm	parts per million
RIE	Reactive Ion Etching
SEM	Scanning electron microscopy
t-BMA	Butyl methacrylate
t-BOC	Di-t-butyloxy dicarbonate
T_g	Glass transition temperature
TGA	Thermo gravimetric analyses
THF	Tetrahydrofuran
Tm	Melting Temperature
TMAH	Tetramethyl ammonium hydroxide
TMMGU	Tetrakis-(methoxylmethyl)- glycoluril
TMPTMA	Trimethylol propane trimethacrylate
Trisphenol	1, 1, 1-tris-p-4-hydroxyphenyl ethane
UV	Ultra- violet
W_{ad}	Work of Adhesion
Wt%	Weight percent
XRD	X-Ray Diffraction

Chapter 1

Literature survey

1.1. Introduction

Over the past 30 years, the semiconductor industry has made significant progress in the technology for mass production of devices with enhanced performance. The first semiconductor transistor designed by Bardeen, Brattain, and Shockley in 1947 was a milestone in the field of electronics (Morton and Gabriel, 2004). Because of its high efficiency and small size, the transistor promised to replace the bulky vacuum tubes. Manufacture of commercially available transistors started in the early 1950s. A variety of transistors such as the point contact transistor and the junction transistor were initially supplied to the defence and mass consumer market. In 1959, the integrated circuit (IC) were introduced (Kilby, 1964; Noyce, 1961). The IC allows an entire electronic circuit containing transistors, passive components, and interconnecting wiring to be integrated onto a single semiconductor chip. ICs were commercialised in the 1960s. Replacement of vacuum tubes in semiconductor transistor helped to enhance number of transistors and electronics components in smaller chips, resulting in faster and more powerful devices at reduced production costs (Moore, 1965). Moore's prediction that the number of transistors in integrated circuits would double about every two years came to be known as Moore's Law (Figure 1.1). This increase also led to a range of electronic and microelectronics application. New technologies demand more complex circuits in smaller devices. Number of transistors can be increased by reducing the size, which are then integrated together in the same chip. Advancement in lithographic technology has played a major role in this regard. Lithography is a well established technique for the fabrication of silicon based microelectronic devices (Reichmanis et al., 1991). Since last 40 years, the development of new lithographic techniques and photoresist materials has been an active research area, as it is realized that without these developments lithography will no longer be able to meet the performance demands of the future. During the past decade, availability of new resists and lithographic technologies has helped to reduce the size of semiconductor devices and has resulted in increased number of sub-devices leading to an increase in the processor speed (Thompsons et al., 1983; Reichmanis et al., 2001., Reichmains and Thompson 1989; Dai et al., 2006).

The device performance is expected to be further enhanced by the successful development of newer resists such as dendrimers and molecular glasses, and

processing techniques such as UV lithography, Deep ultra-violet (DUV), EUV and e-beam lithography. E-beam (Felix et al., 2008) and EUV (De Silva et al., 2008, De Silva et al., 2008, De Silva and Ober 2008, Wang et al., 2007) technologies resolve features below 100 nm.

This chapter reviews the literature on materials and lithographic techniques pertinent to the scope of the investigation. The coverage is illustrative rather than encyclopaediac.

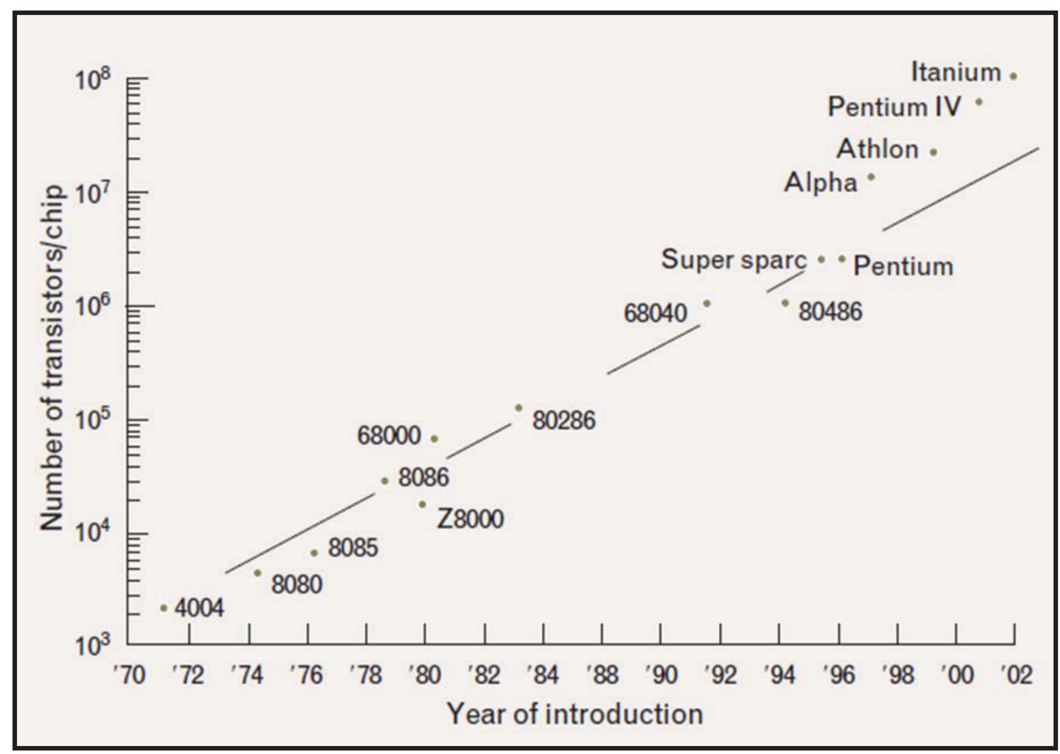

Figure 1.1: Moore's Law

(Rothschild et al., 2003)

1.2. Microlithography

Microlithography is the process of printing a pattern on a silicon substrate. In semiconductor manufacture, lithography is used to produce a patterned mask on a semiconductor. It plays a critical role in IC fabrication as it determines the feature size and density of devices on the chip. The most commonly used techniques for microlithography are photolithography and electron beam lithography.

1.3. Types of microlithography

1.3.1. Photolithography

Photolithography uses light sources of specific wavelength (Figure 1.2) to expose the resist through a patterned mask.

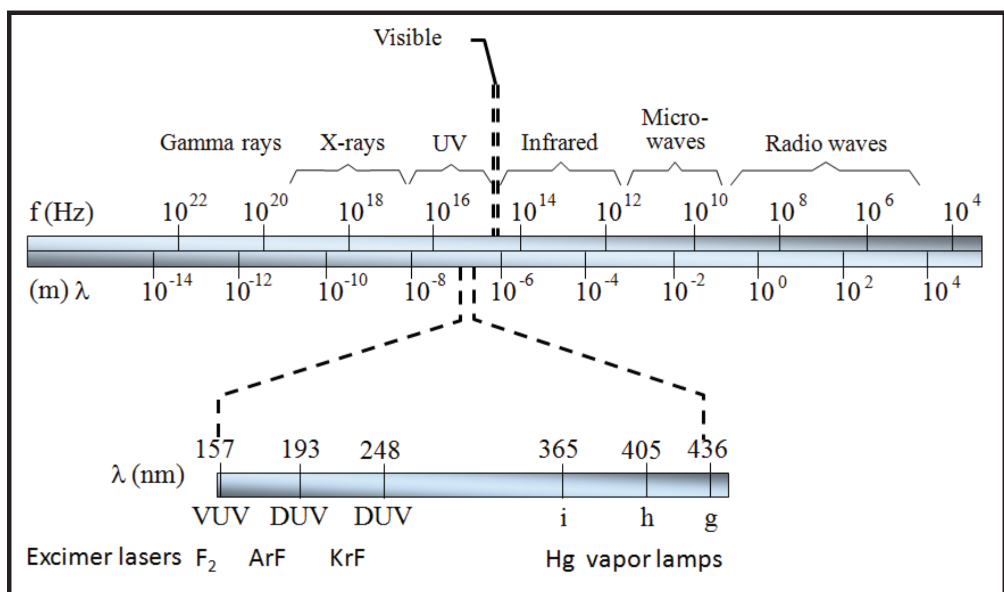

Figure 1.2: UV wavelength used in photolithography

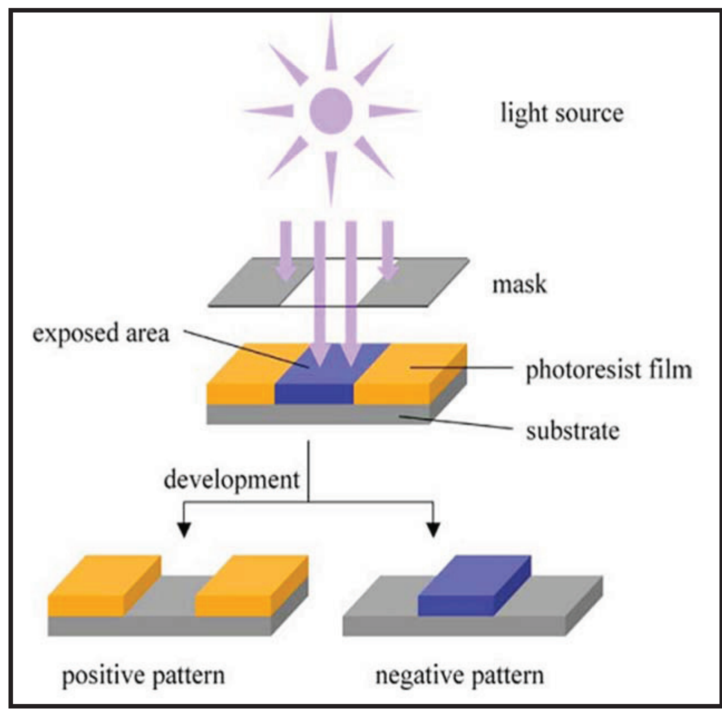

Figure 1.3: Schematic of photolithography

The basic steps involved in the photolithographic process are schematically illustrated in Figure 1.3. A substrate is coated with a thin film of photosensitive material called a photoresist, which is exposed to light through mask. The solubility of the photoresist in the developer solvent is altered by exposure to radiation, typically light in the ultraviolet (UV) region. Exposed area of the resist film can be removed leaving a positive tone resist pattern on the substrate. On the other hand unexposed area of the resist film is removed leaving a negative tone resist pattern on the substrate after development. The resist pattern acts as a temporary mask in the etching process and can be removed in the last step.

1.3.1.1. Exposure techniques

1.3.1.1.1. Contact printing

In this exposure technique the mask is pressed against the coated resist wafer at a certain pressure (Figure 1.4). This pressure is in the range of 0.05-0.3 atmospheres. In this technique, typically 365 nm wavelength is used, which is capable of attaining resolutions up to 0.5µ. However, the presence of contact between the mask and the resist somewhat diminishes the uniformity of resolution attainable across the wafer. To ease this problem, masks used in contact printing must be thin and flexible to allow better contact over the whole wafer. Contact printing can result in defects such as pinholes and scratches in masks and the wafers. Notwithstanding these drawbacks, this technique yields better resolution than the proximity printing and hence is widely used.

1.3.1.1.2. Proximity printing

Proximity printing is another optical lithography technique. In this method, there is no contact between the mask and the wafer (Figure 1.4). The masks used in this technique have longer life than those used in contact printing. During proximity printing, the mask is usually only 20-50 µ away from the wafer. Since the diffraction of light results from a small gap between the mask and the resist coated wafer, the resolution achieved by proximity printing is not as good as that attained during contact printing.

1.3.1.1.3. Projection printing

Projection printing involves no contact between the mask and the wafer (Figure 1.4). This technique employs a large gap between the mask and the wafer. The technique is employed in most modern optical lithography equipment. Projection printers use a well designed objective lens between the mask and the wafer which collects diffracted light from the mask and projects it onto the wafer. The capability of a lens to collect diffracted light and project this onto the wafer is measured by its numerical aperture. The numerical aperture values of lenses used in projection printers typically range from 0.16 to 0.40. The resolution achieved by projection printers depends on the wavelength of the incident light and the numerical aperture of the lens. Use of a lens with a higher numerical aperture will result in better resolution of the patterned structures.

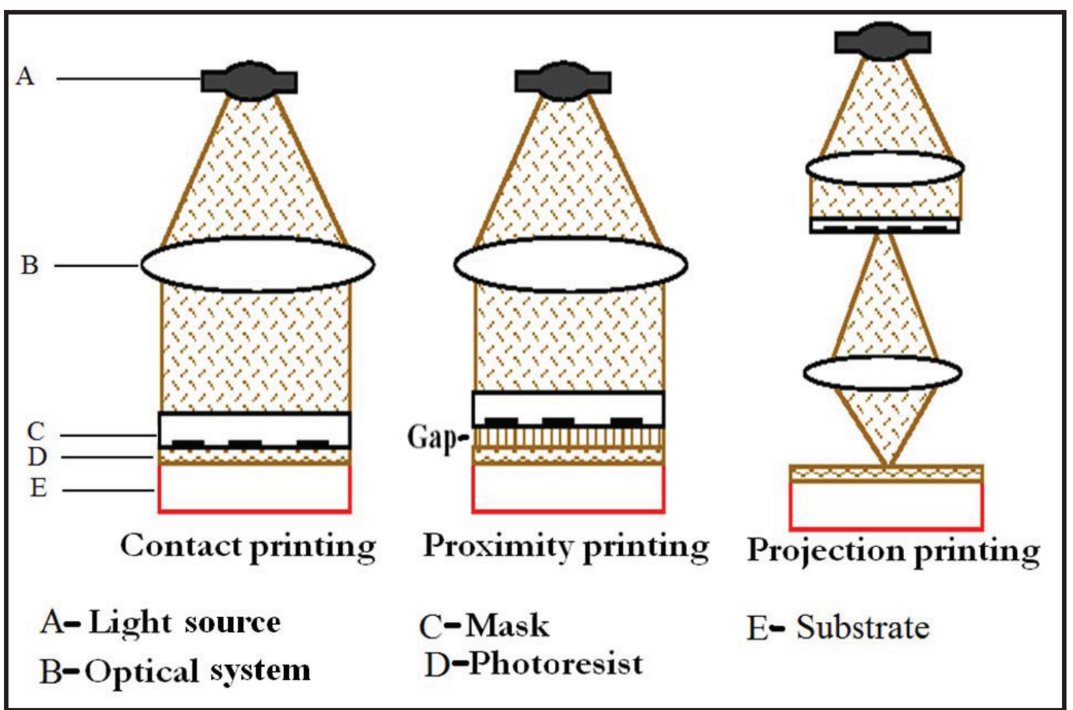

Figure 1.4: Schematic of optical exposure techniques

1.3.1.2. Processing steps in lithography

1.3.1.2.1. Vapour prime

Adhesion of photoresist to the substrate is critical, and governs the replication of the resist patterns. In order to minimise the moisture effects on the resist adhesion, vapour prime surface treatment using hexamethyldisilazane (HMDS) is given. The hydrated

surface of the wafer reacts with HMDS. The reaction releases ammonia resulting in low surface tension (Figure 1.5a).

1.3.1.2.2. Spin coat

Several methods are available by which resist can be coated on the substrate. In this process controlled amount of the resist is dispensed on the substrate. The substrate is spun at lower speed for a specific time and then at higher speed for preset time to produce a resist film of uniform thickness on the substrate (Figure 1.5b).

1.3.1.2.3. Soft bake

After coating, solvent content in the film is reduced but traces of solvent still remain. In order to remove residual solvent from the resist, soft bake step employed. Soft bake increases resist density which helps improve the resolution, adhesion, film uniformity and line-width control (Figure 1.5c).

1.3.1.2.4. Exposure to radiation

After soft baking, resist coated wafer is exposed to radiation that produces the pattern image on the resist. The patterns are formed on the wafer using a mask, which defines which areas of the resist surface will be exposed to radiation. Irradiated regions of positive photoresists will become more soluble in the developer, so positive resists form a positive image of the mask on the wafer. Negative resists form a negative image of the mask on the wafer because the exposed regions become insoluble in the developer (Figure 1.5d).

1.3.1.2.5. Post exposure bake

The post exposure bake (PEB) step is performed after radiation exposure. Acid generated in the radiation exposure step reacts with the resist component. PEB accelerates the deprotection reaction for the positive resist and crosslinking reaction in the case of negative resist. It helps to transfer a geometric pattern from a photo-mask to a photoresist in the form of negative or positive tone (1.5e).

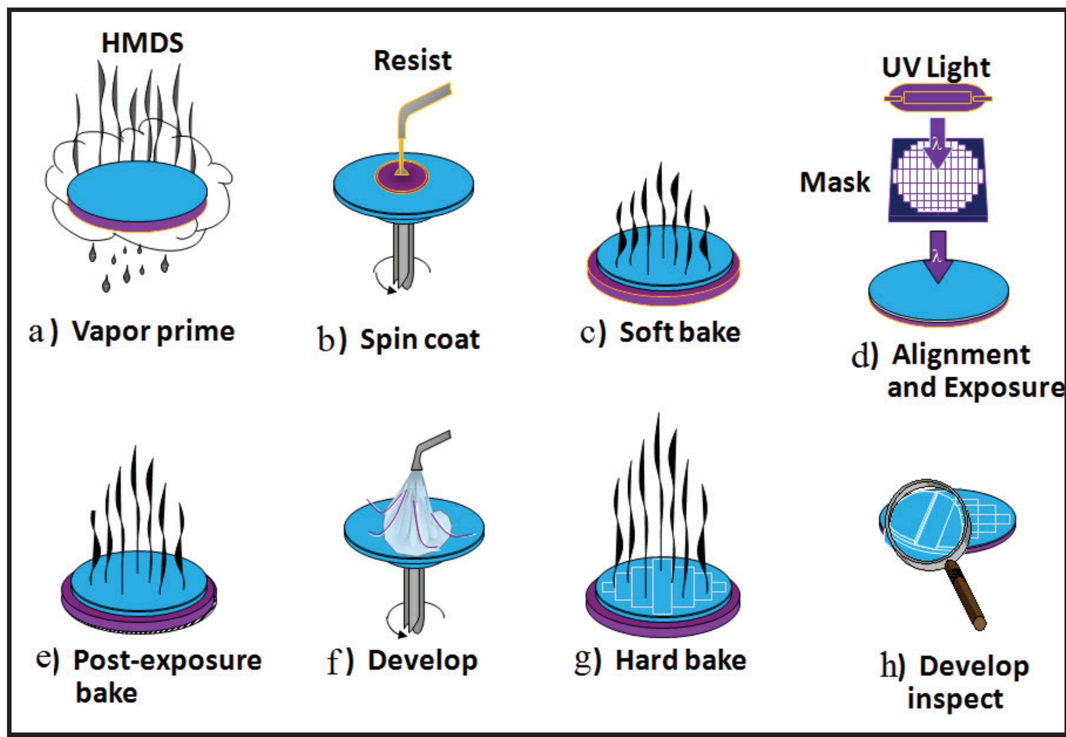

Figure 1.5: Processing steps in lithography

1.3.1.2.6. Resist development

After completion of deprotection or crosslinking reaction during PEB, next most important step is development. Depending on the positive tone or negative tone of the photoresist, development process either dissolves the resist that has been exposed or the photoresist that has been not exposed. Visible patterns appear on the wafer as windows or as islands. The developer needs to remove the photoresist where removal is desired where as photoresist has low solubility where dissolution is not desired which helps to avoid distortion in the resulting photoresist patterns (Figure 1.5f).

1.3.1.2.7. Hard bake

After development, hard bake is performed in order to remove all traces of solvents used during the development. Hard bake temperatures are limited by pattern distortion or decomposition of photoresist. Generally hard bake temperatures are 120 to 140°C as compared to soft bake temperatures which are typically in the range of 90-100 ^{o}C (Figure 1.5g).

1.3.1.2.8. Develop / Inspect

This process uses SEM, typically an automated operation to inspect the patterns. It helps to verify the quality of the pattern, identify defects, and characterize the performance of the photolithography process (Figure 1.4h).

1.3.1.3. Optical lithography resists

A wide range of materials have been explored and developed over the last four decades. Here we summarize more recent efforts pertinent to our investigation.

1.3.1.3.1. Polymers with pendant epoxide groups

Polymers containing pendant epoxy groups can be readily synthesized (Figure 1.6), since monomers, like glycidyl acrylate, glycidyl methacrylate and others monomers are available commercially. Also polymers containing hydroxyl group can be reacted with epichlorohydrin to yield polymers containing pendant cyclic ether groups.

These monomers can be polymerized or copolymerized readily by a free-radical mechanism to yield polymeric materials with pendant epoxy groups. Negative photoresists based on epoxy resins are used extensively in electronics industry (Chae and Park., 2004) as they offer a unique combination of properties like high strength, thermal stability, moisture resistance, chemical and corrosion resistance, adhesion and requisite mechanical as well as electrical properties (Rwei et al., 2005**;** Wang and Lee., 2000).

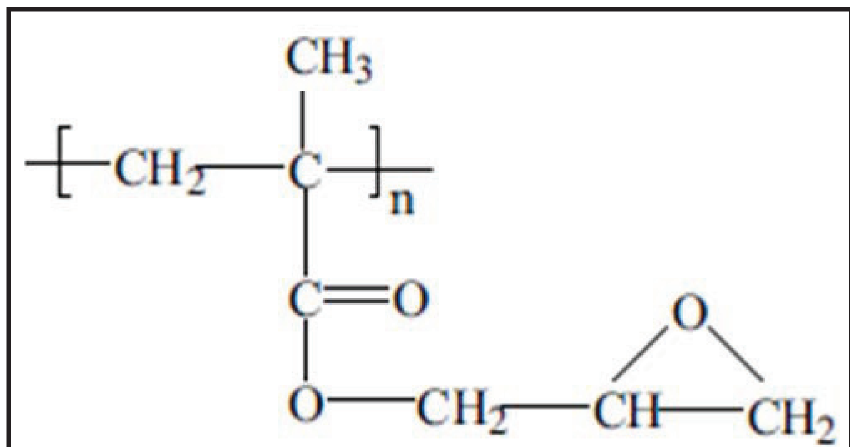

Figure 1.6: Methacrylate polymer containing pendant epoxide

The most commonly used conventional epoxy resins are those obtained via the reaction of epichlorohydrin with bisphenol-A. To improve the thermal and mechanical properties of epoxy resins, the modification of backbone and an increase in the number of the epoxy groups are explored**.** Conventional method for the preparation of Novolac resin is condensation polymerization between aldehyde and phenol in presence of acid catalysts. Novolac epoxy resins, being multifunctional, can provide denser cross linked network**.** The properties of cured epoxy polymers largely depend on the nature of the chemical structure of starting resins. The SU-8 (Figure 1.7) photoresist is a negative tone epoxy based resist initially developed by IBM (Day, 1994), which provides good lithographic performance and low etching rate (Bilenberg et al., 2006) and is extensively used for applications in lithography, for moulding and packaging in semiconductor industry.

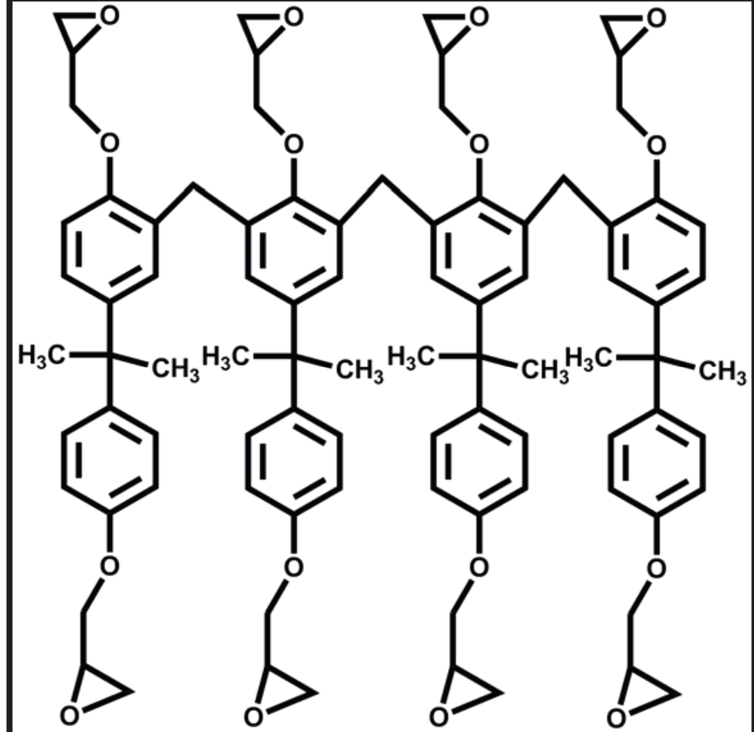

Figure 1.7: Structure of SU-8 polymer

1.3.1.3.2. Polymers with pendant chalcone groups

Pendant chalcone groups on polymers behave like pendant cinnamate groups. Thus, photocrosslinkable polymer can be formed, for instance, from Poly (vinyl alcohol) by

the reaction with 4'-substituted-4-carboxychalcone in dimethyl formamide solution, using 2,4,6-trinitrochlorobenzene as the condensing agent (Watanabe et al., 1986).
The photosensitivity of this polymer is in the range 1 to 5 mJ/cm^2. The R group shown in Figure 1.8 is *p*-Br, *m*-NO_2, or $(CH_3)_2N$. The crosslinking occurs via formation of bi-radicals derived from the double bonds of the cinnamoyl groups. Rehab, (1998) reported negative photoresist, containing pendant chalcone moiety.
Allyl-chalcone monomer was used for homopolymerization and co-polymerization. However, lithographic evaluation of the polymer was not reported. These polymers are very attractive as a source of negative photoresist, because of good solubility, the ability to form films, high photosensitivity, resistance towards solvents after crosslinking, thermal stability and resistance towards plasmas and etching agents, which are critical for commercial negative photoresist materials.

Figure 1.8: Polymer containing pendant chalcone groups

1.3.1.3.3. Polymers with pendant abietate groups

Kwak et al, (2007) synthesized polymer containing abietic acid functionality. Abietic acid was first reacted under pressure with ethylene oxide.
The condensation reaction of modified abietic acid with methacrylic acid led to the monomer methacryloyloxyethyl abietate, as a gummy liquid at 68% yield. Polymer containing pendant abietate group (Figure 1.9), easily underwent photodimerization of the conjugated carbon-carbon double bonds to crosslinking reaction by UV irradiation and was transparent in visible region. The resist resolved 30 μ features using light intensity 5 J/cm^2.

Figure 1.9: Synthesis of methacrylate polymer containing abietate group (Kwak et al., 2007)

1.3.1.3.4. Polymers with pendant vinyl groups

Cyr et al, (2004) reported polyferrocenyl silanes Methacrylate. Polyferocenyl silanes were synthesized using Pt-catalyst. The halide functionality on the polymer backbone was further modified by hydroxyethyl methacrylate to yield polyferrocenylsilanes bearing pendant photopolymerizable methacrylate groups (Figure 1.10). In the structure depicted in Figure 1.10, R could be a methyl or ethyl group and R" could be methyl or phenyl group. The polymers photocrosslink through the methacrylate group.

Another methodology involves the synthesis of linear, soluble copolymers containing pendant hydroxyl functionality and its subsequent modification (Figure 1.11). Koo et al, (2002 and 2003) synthesized Poly (methyl methacrylate / 2-hydroxy ethyl methacrylate) based copolymers, having pendant hydroxyl groups which were further conjugated with methacrylic anhydride. The resulting polymer containing pendant vinyl groups were used in wave-guide applications (Koo et al., 2002). Similarly copolymerization of silyl protected HEMA i.e. HEMA-TMS with various co-monomers such as glycidyl methacrylate (GMA), methyl methacrylate (MMA), t-

butyl methacrylate (t-BMA), n-butyl acrylate (n-BA), t-butyl methacrylate (t-BMA), acrylic acid (AA) was carried out over a range of co-monomer feed ratios.

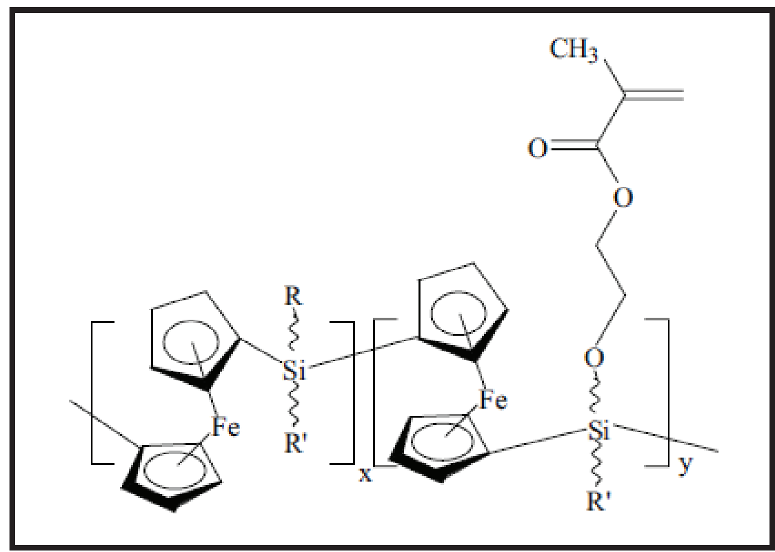

Figure 1.10: Polyferrocenylsilanes methacrylate containing pendant vinyl groups

(Cyr et al., 2004)

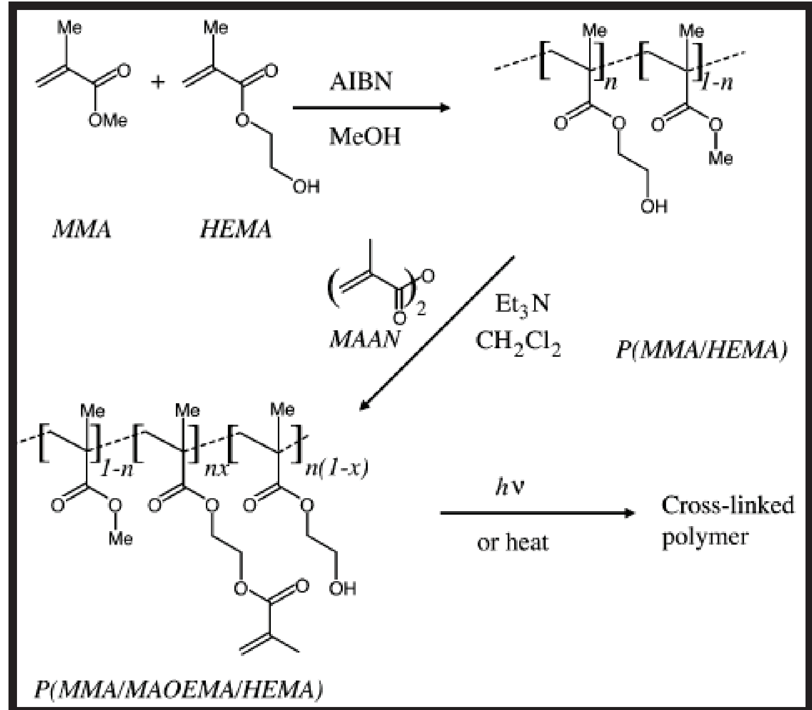

Figure 1.11: Synthesis of poly (HEMA-*co*-t-MMA) and post functionalization

(Koo et al., 2002)

The pendant hydroxyl groups of these co-polymers were then functionalized using methacryloyl / acryloyl chloride or methacrylic anhydride to obtain polymers containing pendant double bonds. These polymers were shown to be useful as positive photoresists (Liu et al., 2001).

1.3.2. Electron beam lithography

The need for increasing processing speed of devices calls for decreasing feature sizes. Because of diffraction limitations, conventional optical lithography is increasingly inadequate to meet the requirements for lower feature sizes. This has spurred materials and process development research in industrial laboratories and universities. Electron beam lithography (EBL) involves irradiation of the radiation sensitive resist to electrons by means of focused electron beam. The structural changes taking place on exposure to irradiation, characterize the materials as negative or positive tone resist.

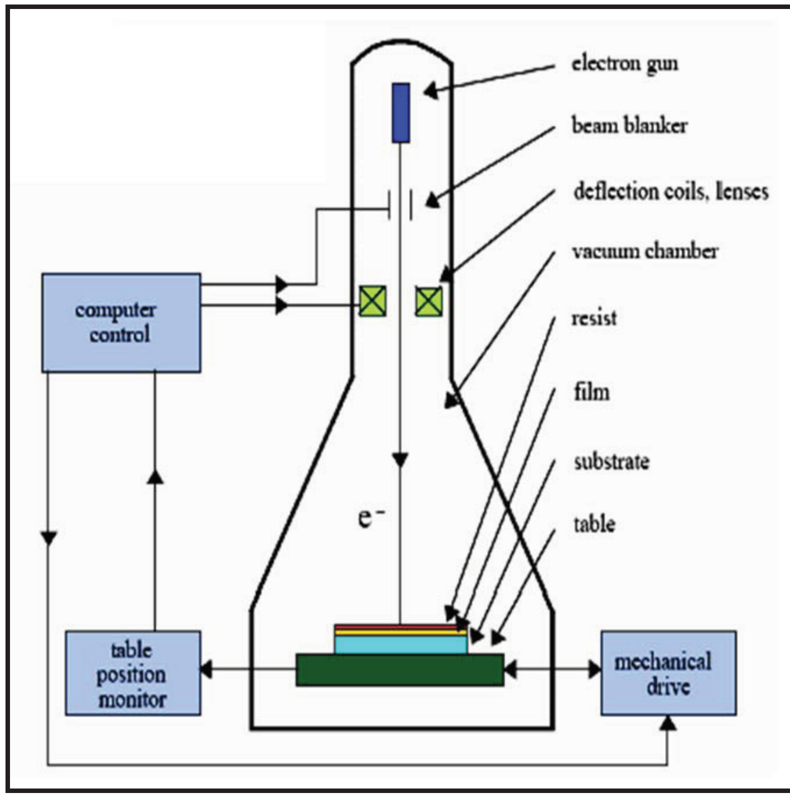

Figure 1.12: Schematic of an electron beam exposure system

(Thomson et al., 1983)

The three major sources of electrons are thermionic emitters, photo emitters, and field emitters. EBL is used for writing complex patterns directly on resist coated on silicon wafers. Lithographic procedures involved in EBL are almost similar to that in photolithography. The most commonly used electron beam photo resist is polymethylmethacrylate (PMMA). PMMA breaks down into monomer upon exposure to electrons, which is later developed using tetramethyl ammonium hydroxide (TMAH).

The EBL process is shown in (Figure 1.12), but the equipment required is quite complex. Instead of getting in to the complex instrumentation of EBL it would be more appropriate to understand some of the important components in EBL such as electron gun, electron optical column and substrate.

1.3.2.1. Electron gun

Figure 1.13 shows the schematic of the electron gun. The electron gun is able to discharge a beam of electrons from a filament tip in a particular direction.

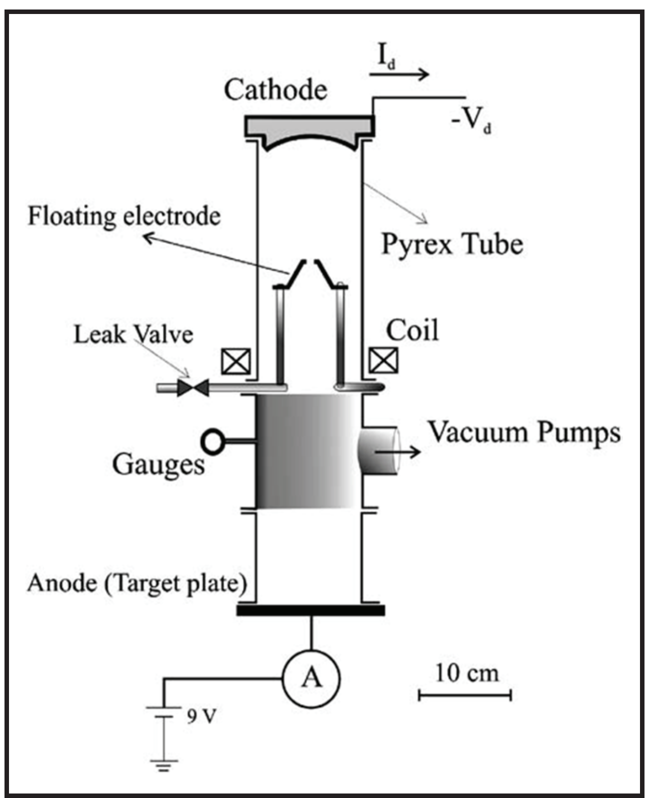

Figure 1.13: Schematic of the electron gun
(Amir et al., 2004)

Two common e-beam emitters are lanthanum hexaboride crystal and a zirconium oxide coated tungsten needle. The emitter is first heated to produce and excite electrons on the surface. Then, when a high voltage is applied, the excited electrons accelerate towards the anode. By varying the voltage, the path and the focus of the beam can be manipulated.

1.3.2.2. Electron optical column

The electrons emitted are focused into a beam using electromagnetic lenses, which define the diameter of the spot size of the beam.

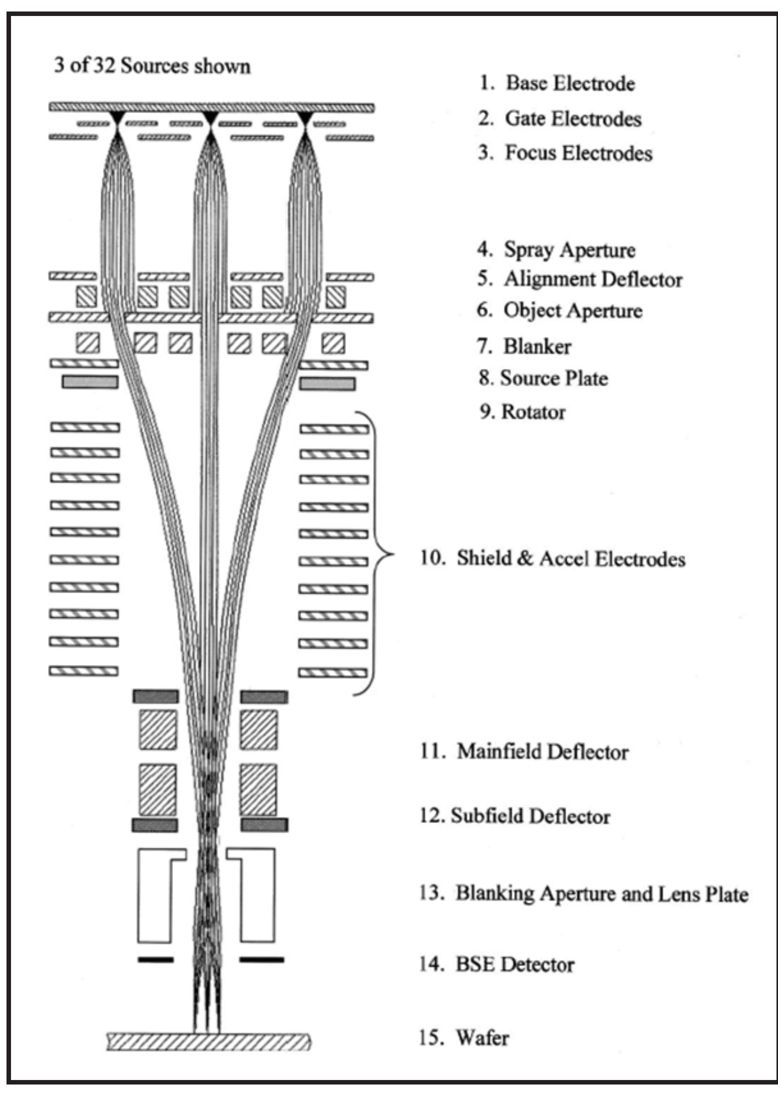

Figure 1.14: Schematic of the electron optical column
(Yin et al., 2000)

Electron optical column is a crucial part of the EBL because it isolates the beam from any outside interference as shown in Figure 1.14. It is a system of lenses that, by a combination of electromagnetism and optics, focus the electrons into a concentrated beam in the required direction. Two parallel plates inside the column can be electrostatically charged to a precise degree. The resulting electric field is able to bend the beam in the desired direction.

1.3.2.3. Substrate

After the beam is directed by the optical column, it is ready to be focused on the resist coated surface. High energy electron bombardment will cause chemical changes in resist materials. When the beam hits the resist, either an additive or subtractive reaction takes place. An additive writing method uses the electrons to induce a deposition of a resist on the surface. Subtractive writing methods use the e-beam to remove the sections of the resist. This method is common in creating masks for optical lithography.

1.3.2.4. Techniques

1.3.2.4.1. Electron beam direct write lithography

Since the 1960s EBL has been used in the integrated circuit (IC) industry. In an EBL instrument, the electron beam is accelerated and focused onto a resist sample under vacuum environment. Patterning requires a deflection and a blanking system which uses electrostatic or electromagnetic lenses to control the beam position, as shown schematically in Figure 1.15. EBL instrument can be used to draw an arbitrary pattern without using a mask, hence it is called as a maskless lithography. EBL is the most promising lithographic technique among lithographic technologies in terms of resolution capability.

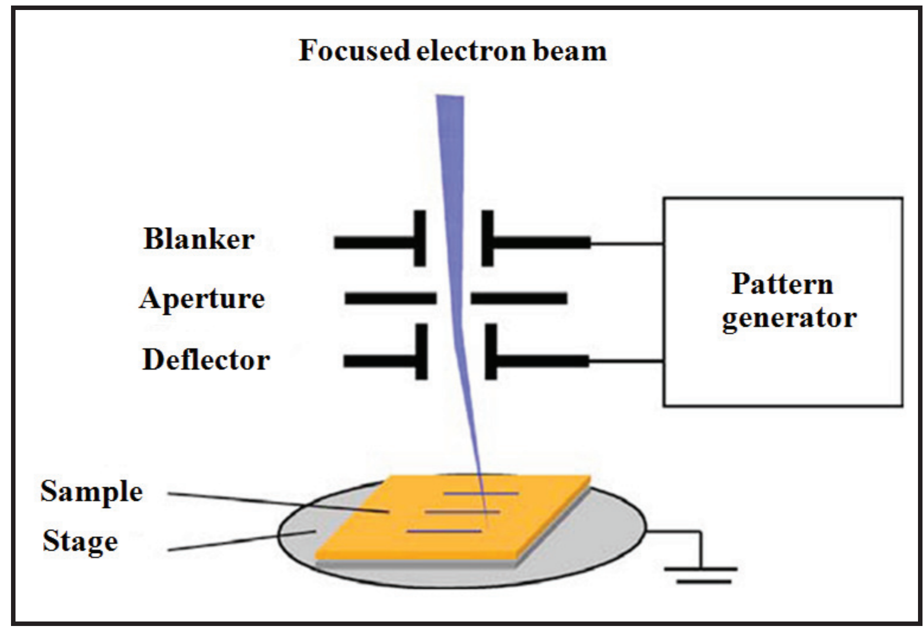

Figure 1.15: Schematic of beam control elements in electron beam direct writing lithography.
(Pfeiffer 2009)

1.3.2.4.2. Electron solid interactions

Although the electron beam in EBL instrument can be tightly focussed to yield an extremely small beam diameter of a few nanometres it is unusual to achieve nanometer size feature in the resist film. As the electrons penetrate the resist, a fraction of electrons undergo small angle scattering within the resist. The parameters that influence the accuracy of the pattern definition and transfer process become more and more critical as the feature sizes are lowered. As primary electrons hit the resist, they exhibit both forward and backward scattering, as shown in Figure 1.16. Forward scattering causes incident electrons to change their path by a small angle, broadening the beam diameter as electrons penetrate toward the bottom of the resist film. This forward scattering can result in a significantly broader beam profile at the bottom of the resist than at the top which limits the final resolution (Figure 1.17).

Backward scattering is a large angle scattering which usually occurs when primary electrons collide with a heavy ion core. Some backscattered electrons pass through the resist at a range as far as micrometer away from the incident beam. These backscattered electrons are responsible for the proximity effect in which scattered electrons expose unexposed areas of a resist film. The extent of exposure due to backscattered electrons depends on the energy of the primary electrons (Figure 1.17).

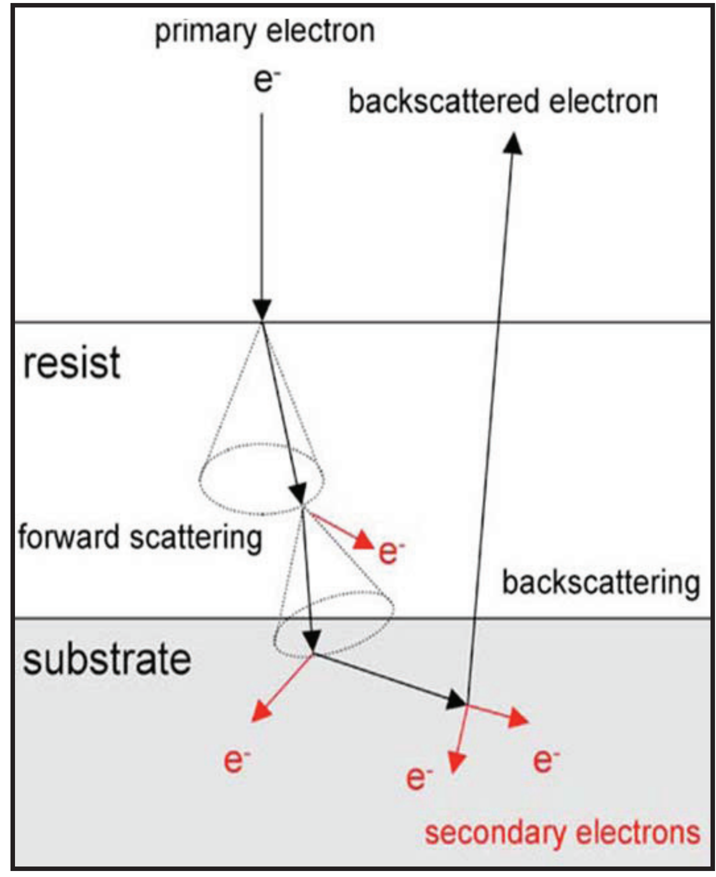

Figure 1.16: Schematic representation of electron solid interactions (Shimizu and Ze-Jun., 1992)

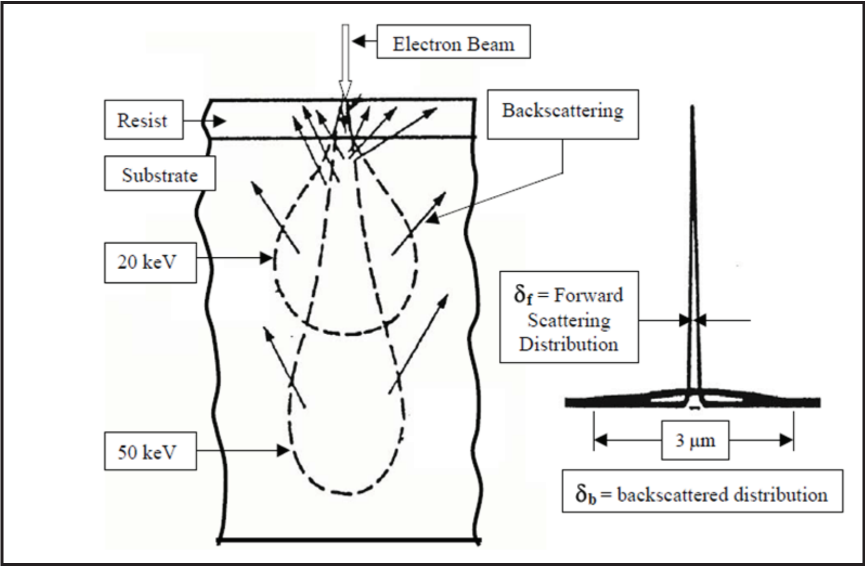

Figure 1.17: Schematic of electron scattering with beam acceleration (Henderson, 2007)

A primary electron with higher energy allows the backscattered electron to travel a longer distance. The energy dissipation continues and generates a number of secondary electrons along the pathway of the primary electrons until the primary electrons lose all energy. They are considered to cause additional beam diameter widening as they can travel a short distance of the order of nanometers, in the resist before reacting with a resist molecule.

1.3.2.4.3. Multiple electron beam direct-write lithography

The major disadvantage of EBL is its extremely slow writing speed, achieving less than one wafer per hour in contrast to 50-100 wafers per hour which can be patterned by optical lithography. An example of next generation EBL is maskless lithography based on multibeam technology, including multiple aperture pixel by pixel enhancement of resolution (MAPPER) and projection maskless lithography. The MAPPER concept is based on parallel direct writing electron beams, each of which is programmed to operate independently with the assistance of high speed optical data transfer (Wieland, et al, 2009). A schematic of the MAPPER system is illustrated in Figure 1.18.

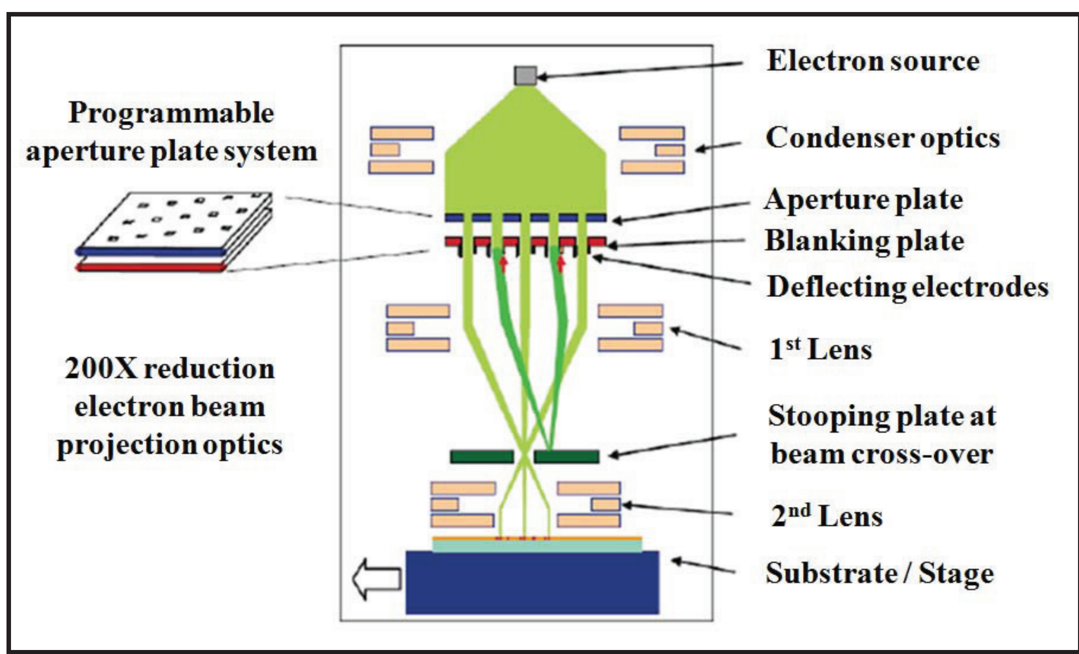

Figure 1.18: Schematic representation of multiple electron beam direct write system (Pfeiffer 2009)

In the MAPPER system, electrons are generated from a high brightness electron source and they are collimated to cover the aperture plate using a collimator lens. A single collimated beam is split up into 13,000 electron beams at the aperture array. The beams are finally focused by the projection lens array onto the wafer on the moving stage. In this setup, the data system takes control of beam writing through switching of 13,000 light beams, one for each beam blanker, so that each electron beam has its own blanking system, allowing thousands of electron beams to work independently. Electron beam lithography provides excellent resolution due to the small wavelength and a small probe size, whereas the resolution in optical lithography is limited by the wavelength of the light used for exposure. In addition, EBL is a flexible patterning technique that can work with a variety of materials. There are several advantages of using EBL over optical lithography, as it offers resolution up to 20 nm, and can print complex computer generated patterns directly on the wafer. The technique can work with variety of materials and with almost infinite number of patterns. The technique however suffer from disadvantages like high capital and maintenance cost, forward scattering and back scattering and slower writing speed.

1.3.2.5. Electron beam writing approaches

There are two types of writing methods employed in electron beam lithography.

1.3.2.5.1. Vector writing approach

Vector Scan utilizes the method of jumping from one patterned area to the next rather than scanning serially over the entire wafer area (Figure 1.19).

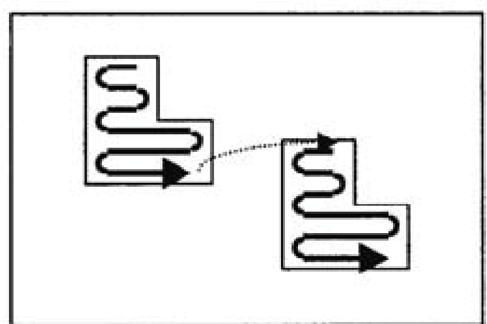

Figure 1.19: Vector writing approach
(Fontana et al., 2002)

Since there is no need to visit every point in the pattern, the vector scan approach is faster than raster scan for sparse patterns. Adjustments to dose can be accomplished easily. A disadvantage is that longer beam settling time is required which results in increased difficulty in maintaining placement accuracy.

1.3.2.5.2. Raster writing approach

Herriott et al., in 1975 employed a method whereby the beam is swept across the entire field, pixel element by pixel element, with the beam being turned off and on (blanked and unblanked) as needed to expose the desired pattern (Figure 1.20). This strategy is based on a relatively simple architecture that is easy to calibrate. The disadvantage is that because the beam is scanned across the entire writing field, sparse patterns take just as long to write as dense patterns. An additional drawback is that dose adjustment within the pattern, to correct for proximity effect, is inherently difficult.

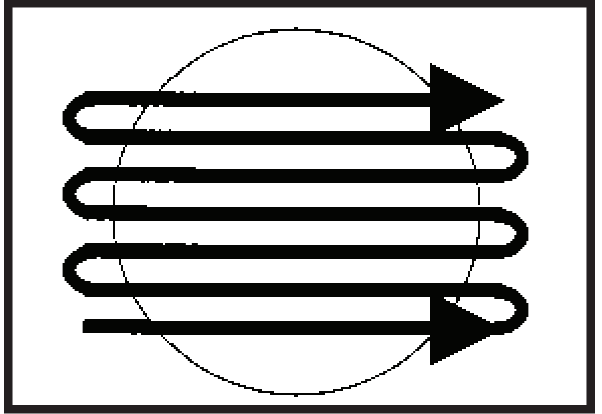

Figure 1.20: Raster writing approach
(Fontana et al., 2002)

1.3.2.6. Electron beam resists

The resists are the radiation sensitive compounds. The main components in the resist are resin (polymeric, dendrimeric and molecular glass materials), a photoacid generator (PAG) and a film casting solvent. They form a thin film on the substrate by spin coating technique. The resin changes structure when exposed to specific radiation source. The solvent allows spin coating and formation of thin homogeneous film on the substrate whereas PAG controls the chemical reaction in the resist. Resists are

mainly classified as positive or negative, according to the response to radiation (Figure 1.21). In the case of positive resist mask image is same as that of wafer image, the exposed resist softens and is washed out with developer. In the case of negative resist mask image is opposite to that of wafer image. The exposed resist becomes crosslinked and is insoluble in developer.

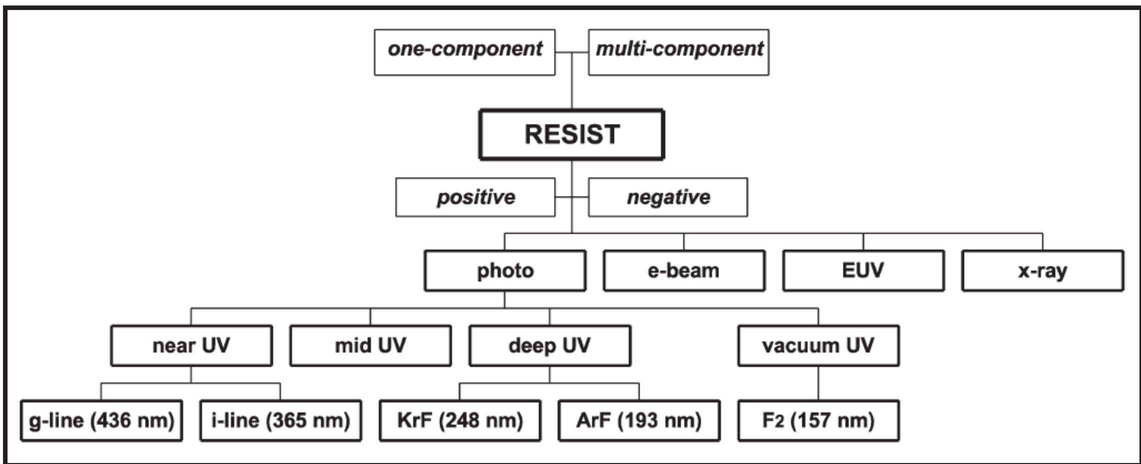

Figure 1.21: Resist classification

(Ito, 2005)

1.3.2.6.1. Polymeric resists

The conventional resists for electron beam lithography are polymers. They are high T_g materials and are able to form a smooth film on substrates by spin coating. Poly (methyl methacrylate) (PMMA) was one of the first polymer developed for e-beam lithography. PMMA is typically used as a positive tone resist although it can act as negative tone resist (Duan et al., 2010) at twice the magnitude used for positive tone resist. Upon e-beam irradiation the polymer can undergo either bond breaking or crosslinking. The bond breaking dominates in the positive tone of PMMA leading to a lowering in the molecular weight of the polymer hence increases solubility in particular developer. Crosslinking forming a high molecular weight polymer which is insoluble, dominates the negative tone mode of PMMA. PMMA has a capability for high resolution and is considered high resolution resist. Lines with resolution below 5 nm were demonstrated in positive tone using PMMA (Yasin et al., 2001), whereas 12 nm isolated lines were also achieved in negative tone PMMA (Hoole et al., 1997). Its

limitations are poor sensitivity ≈350 μC/cm^2 at 50 kV beam acceleration and poor etch resistance to plasma etching.

1.3.2.6.2. Molecular resists

Electronic circuit density in semiconductor devices has been increasing, and the minimum feature size required for device fabrication is decreasing continuously. While 1Gbit dynamic random access memories (DRAM) with a resolution of 130 nm were produced in 2001 and the goal was to fabricate 4 Gbit DRAM chips with a resolution of 65 nm. Both new lithographic processes and new resist materials for nanolithography of the future are being extensively explored. Polymers have been used as photo and e-beam resist materials owing to their ability to form uniform amorphous films (Reichmanis et al., 2001). However, a serious problem encountered with polymer resists for the fabrication of nanometer scale patterns is the variation of line patterns resulting from their large molecular size and broad molecular weight distribution, which leads to edge and surface roughness. Reducing the molecular size is an effective approach towards higher resolution in future nanolithography. Use of low molecular weight resists such as dendrimers and calixarene and molecular glasses offer advantages such as high purity, well defined structures as well as low molecular weights and lack of chain entanglement. Molecular resists are amorphous molecular materials with resist properties which offer advantages over polymer resist materials because of their smaller molecular size and the absence of molecular weight distribution. Amorphous molecular resists, which form uniform, amorphous films by spin coating from solution, are expected to be increasingly used in future nanolithography, enabling the fabrication of nanometer-scale line patterns with low LER relative to those fabricated with polymer resists (Yoshizwa, et al., 1996; De Silva et al., 2008).

1.3.2.6.2.1. Molecular glass resists

Small organic molecules generally tend to crystallize, as they are usually crystalline below their melting temperatures. However, recent studies have showed that small organic molecules can also form stable amorphous glasses above room temperature if their molecular structures are properly designed (Shirota, 2000). These low molecular weight molecules that readily form stable amorphous glasses above room temperature

are called amorphous molecular materials. Molecular glasses were synthesized based on benzene or phenol as central core (Kadota et al., 2004) in order to increase the rigidity of the system and hence T_g (Yang et al., 2006; Dai et al., 2006). Phenolic segment not only provides high T_g but also etch resistance and base solubility. Most of the phenol based molecular glasses reported in the literature suffer from low T_g and probability of crystallization due to the small size, compact shapes and pi-pi stacking in the system (De Silva and Ober, 2008). Similarly, most of the symmetric 100% t-BOC protected MGs exhibited tendency to crystallize (De Silva et al., 2008) and hence necessitude different isomeric forms and various degree of protection to inhibit crystallization. In such cases problems may arise during development in basic media, due to the free hydroxyl functionality which may react with base in the developer and hence LER may increase.

Table 1.1: Structure of molecular glasses

Sr No	**Structure**	**Name**	**Reference**
1	HO, HO, O, O, OH, OH	6,6’,7,7’-teterahydroxy -4,4,4’4’-tetramethyl-2,2’-spirobichroman	Yang et al., 2006
2	HO, HO, OH, OH	4-[4-[1,1-Bis(4-hydroxyphenyl)ethyl]]-R,R-dimethylbenzylphenol	Dai, et al., 2006

3		5,5’,6,6’-Tetrahydroxy-3,3,3’,3’-tetramethyl-1,1’-spirobisindane	Dai, et al., 2006
4		Modified calix[4]resorcinarene	Felix et al., 2008
5		1,3,5-tris-(p-(p-hydroxyphenyl)-phenyl)benzene	Hattori et al., 2009
6		5,5-bis-(tert-butoxycar bonyloxy) phenyl-5-[4,4-bis(tert-butoxycarbo nyloxy)-1,1:3 ,1-terphenyl-50-yl]-1,1:3,1:3,1:3,1-quinquephenyl	Kadota et al., 2004

A summary of design principles for tailoring molecular glasses (MGs) for lithographic applications which overcome the limitations of polymeric resists in sub 50 nm features has been recently provided by De Silva et al., (2008). The advantage of MGs lies in the fact that the free volume is distributed into much smaller units compared to that in polymers, which governs diffusion in these matrices which in turn influences resolution and LER. They can be tailored to offer higher thermal stability, film forming ability and amorphous character. In order to increase T_g, translational, rotational and vibrational motions of the molecules are restricted by incorporating rigid and bulky side groups such as tert-butyl, naphthalene, biphenyl, triphenyl and fluorine moieties (De Silva et al., 2008; Shirota 2005; Kinoshita et al., 2002) and by increasing the crosslink density (Wang and Lee 2000). Recent studies further illustrate that thin films of molecular glass resists demonstrate consistently lower LER values due to the smaller segment of free volume in molecular glass system that can inhibit the acid diffusion.

1.3.2.6.2.2. Calixarene derivatives

Calixarene based molecular resist systems used in both positive and negative tone resists have been reported by many researchers (Felix et al., 2008; Sailer et al., 2004; Fugita et al., 1996; Ohnishi et al., 1997). Base calixarene is a cyclic oligomer containing repeating units of phenolic hydroxyl groups linked with methylene bridges as shown in Figure 1.22.

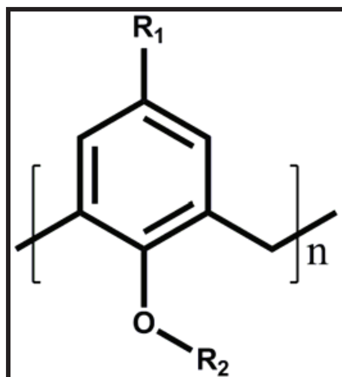

Figure 1.22: Chemical structure of calixa[n]rene with functional groups R_1 and R_2

Various calix[n]arene derivatives have been studied as the negative tone resists for e-beam lithography (Fujita et al., 1995; Fujita et al., 1996; Sailer et al., 2002., Sailer et

al., 2004; Ishida et al., 2003). The low molecular size material has the potential for high resolution lithography. Sub 10 nm feature resolution was achieved by using methyl-acetoxycalix[6]arene (Sailer et al., 2002; Ohnishi et al., 1997; Yasin et al., 2001).

However, its sensitivity varied between 6-10 mC/cm^2. Sailor et al., (2004) reported chemical amplification of a calix[4]arene epoxide modified derivative through cationic polymerisation. Using calix[4]arene derivative resist, 20 nm patterns were resolved at sensitivity of 15 μC/cm^2 at 30 kV beam acceleration.

1.3.2.6.2.3. Dendrimeric resists

Use of dendrimers has attracted applications in lithography owing to their excellent properties like highly compact, globular shaped, amorphous nature and monodisperse spherical structures, which reduce chain entanglement, yielding low LER (Tully et al., 2000). The advantages of using dendrimers as a photoresist have been acknowledged in the literature (Tully et al., 2000; Mori, et al., 2006; Haba et al., 1999; Ito et al., 2008).

In order to ensure the formation of stable amorphous films it is essential that the low molecular weight resist structures are non planar and inhibit crystallization. In this context spherical, branched or star shaped molecules have specific advantages. Structural attributes which result in low free volume and restricted molecular rotation lead to an enhanced T_g. High T_g is critical as such materials form stable thin films and can be subjected to PEB, structure development and plasma etching. The presence of bulkier molecule at the periphery results in lower free volume and increase in T_g. Chemically amplified resists (CAR) are generally preferred as these can be processed at low dose in EBL. Mori et al., (2006) reported FGDs containing peripheral furan groups having T_g 55°C which were crosslinked using (4,4-methylenbis[2,6-bis(hydroxymethyl phenol). The resist was processed at 50 kV using a dose of 20μC/cm^2.

Features upto 200 nm lines with a pitch 1:2 could be successfully processed. Tully et al., (2000) explored the role of dendrimer based CARs for fabricating features up to 50 nm. The t-BOC conjugated dendrimers had a T_g 73-77 ^{o}C. Since the resist was not cured, the solubility difference between exposed and unexposed resist resolved 50 nm negative patterns (Tully et al., 2000). Mike and Andy, (2000) synthesized dendritic

polymer resists which resolved 75 nm lines using 30 kV beam acceleration at 1000–2000 mC/cm^2 sensitivity.

Table 1.2: Structure of Dendrimers

Sr No	Structure	Name	Reference
1		α, α, α-tris (4-hydroxy phenyl)-1-ethyl-4-isopropyl benzene based FGD	Mori et al., 2006
2		1, 1, 1-tris-p-4-hydroxyphenyl ethane based dendrimer	Tully et al., 2000

1.3.2.6.2.4. Triphenylene derivative

A triphenylene molecule consisting of four benzene rings bound together as shown in Figure 1.23 was used as negative tone (Robinson et al., 1999; Robinson et al., 2000; Tada, et al., 2000) as well as positive tone e-beam resist. Triphenylene derivative having negative resist properties showed sensitivity in the range 1.5-6.5 mC/cm^2 at 20 kV beam acceleration. A high resolution of 14 nm was achieved in the same derivative using 30 kV beam and development in monochlorobenzene. The etch resistance of the triphenylene derivatives was about twice that of a common novolac

resist. Chemical amplification of the triphenylene derivatives has been demonstrated (Robinson, et al., 2006; Robinson, et al., 2008; Zaid, et al., 2007).

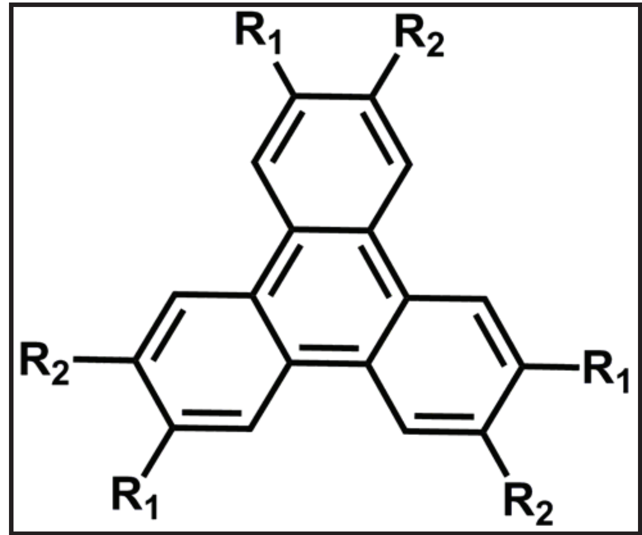

Figure 1.23: Schematic of a triphenylene derivative with functional groups R_1 and R_2

1.3.3. Chemically amplified resists

The concept of chemical amplification of resists was proposed by Ito and Willson (1983) to tackle the issue of the poor photosensitivity of resists for DUV lithography (Ito and Willson 1983; Ito et al., 1985; Ito, 2005). In a chemically amplified resist (CAR) system, a single photo event produces a catalyst by photoreaction of a photoactive compound upon irradiation, which then induces a cascade of chemical reactions. Therefore a single irradiation event can lead to multiple resist exposure events, increasing the photosensitivity. This is an advantage over using irradiating energy to change solubility in conventional resists. The CARs are being increasingly explored for new resist materials. Chemical amplification chemistry has been studied for positive tone and negative tone images (Ito, 2005). The CAR system consists of a polymer protected with an acid labile functional group and a photo acid generator (PAG) used to initiate acid catalysis reaction. In first step photoreaction of PAG and radiation generates a strong acid. In the second step, the acid catalyses a reaction in which an acid labile group is deprotected from the main polymer chain and the acid is regenerated to repeat deprotection reactions. The deprotection of the acid sensitive group changes the polarity of the polymer, and hence the solubility of the exposed

polymers is altered. To promote the deprotection reaction, post exposure bake (PEB) at an elevated temperature is required.

The first CAR used in the manufacture of DRAM using Deep UV lithography (wavelength-248 nm) was IBM's resist containing poly (4-*tert*-butoxycarbonyloxystyrene) mixed with 4.75 wt% of triphenylsulfonium hexafluoro-antimonate as PAG (Ito, 1997). The poly (4-*tert*-butoxycarbonyloxystyrene) is a poly (4-hydroxystyrene) with the phenolic units protected using tert-butoxycabonyl (t-BOC) functional group. After protection with (t-BOC) the polymer became insoluble in polar solvents. The CA mechanism of the t-BOC resist is shown in Figure 1.24.

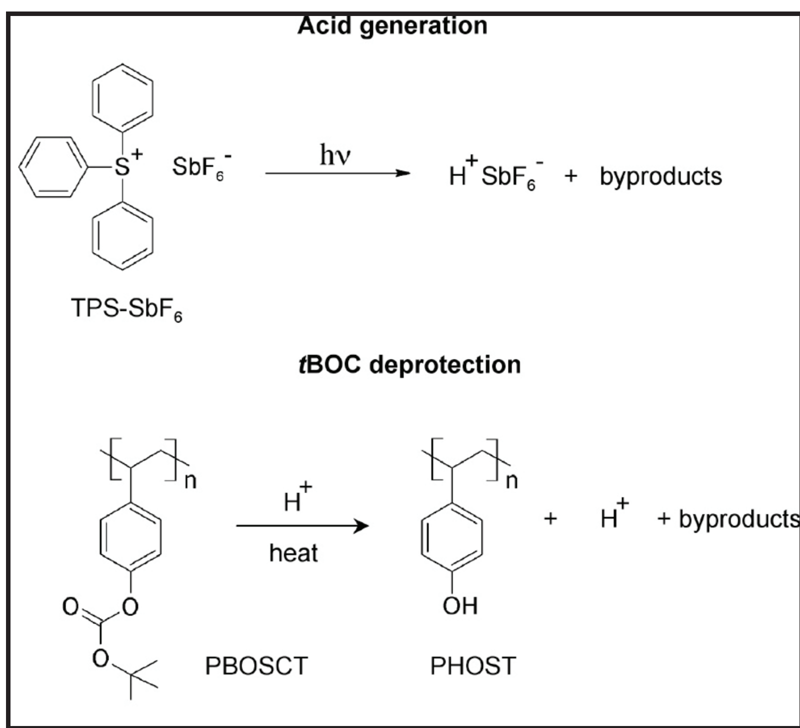

Figure 1.24: Acid-catalysed deprotection of the t-BOC resist (Ito, 2005)

Upon exposure to Deep UV radiation, the PAG generates a strong acid, which cleaves the acid labile t-BOC group in the PEB step at 100 ^{o}C. The t-BOC group releases isobutene and carbon dioxide as by-products, and produces another acid. The resist acts as positive tone or a negative tone resist, depending on the development process. A positive tone image is achieved when developed in aqueous base developer in which an exposed area is readily dissolved in the developer solvent and washed away. A widely used aqueous base is tetramethylammonium hydroxide (TMAH) at 0.26 N

concentration. In contrast, a negative tone image is generated when developed in an organic solvent such as anisole in which unexposed area is removed, leaving a negative pattern.

Polymer crosslinking is the chemical amplification mechanism for negative tone resist. Crosslinking by acid-catalysed ring-opening of an epoxide functional group was proposed for use in a negative tone CAR (Ito and Willson, 1983). The resist containing blend of a resin having pendant epoxide group and onium salt was used as a PAG (Dektar and Hacker, 1990; Crivello, 1999).

Figure 1.25 Crosslinking of an epoxy resin via acid-catalysed ring opening (Ito, 2005)

The generated acid in photoreaction reacts with epoxide ring producing a highly reactive site which reacts with another epoxide ring. As a result, the three-dimensional crosslinked network forms in the exposed area and becomes insoluble in an organic developer. The crosslinking mechanism of the epoxy resin is illustrated in Figure 1.25.

Another example of a commercially available resist based on epoxy crosslinking is SU-8. It is used for transferring pattern onto a silicon substrate by etching in a range of applications (Pepin et al., 2004; Bilenberg et al., 2006). Main limitation in negative

tone resist for high resolution patterning is swelling of crosslinked feature, which results during development process, as the organic solvent penetrates into the crosslinked network and distorts the pattern. Chemical amplification resists are further classified based on their imaging mechanism (Ito, 2005) (Figure 1.26).

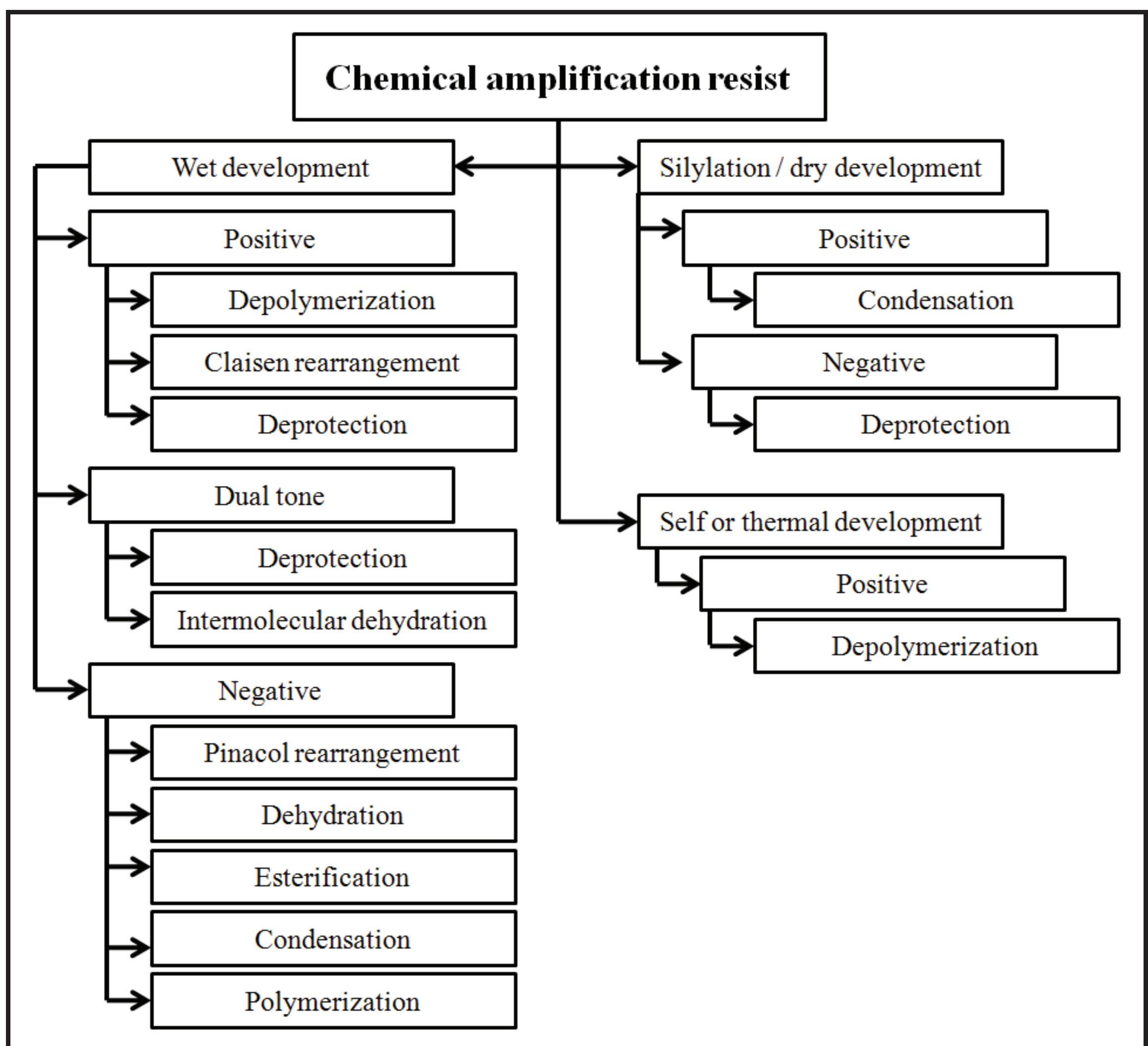

Figure 1.26: Chemical amplification imaging mechanism (Ito, 2005)

1.3.4. Resist characterization

1.3.4.1. Line edge roughness (LER)

LER is random fluctuation at the edge of a resist feature that changes the feature size adversely. There are numerous potential contributors to LER in the lithographic process. As feature dimensions shrink, LER has become an increasing by critical

factor in lithographic processing. Although all the causes of poor LER are not clearly understood, many factors are believed to affect LER. LER has been attributed to a number of material factors such as the molecular weight of resist component (Figure 1.27) (De Silva et al, 2008; Yamaguchi et al., 2004; Leunissen, et al., 2005; Patsis et al., 2004; Patsis, et al., 2005) molecular weight distribution (Yoshimura et al., 1993), molecular structure (Fedynyshyn et al., 2006, Fedynyshyn et al., 2008), resist aggregation (De Silva 2008) and distribution of resist components (Hirayama et al., 2005; Kozawa et al., 2009). It has been suggested that reduction of LER can be achieved by using resists with low molecular weight and with low polydispersity (De silva et al., 2008).

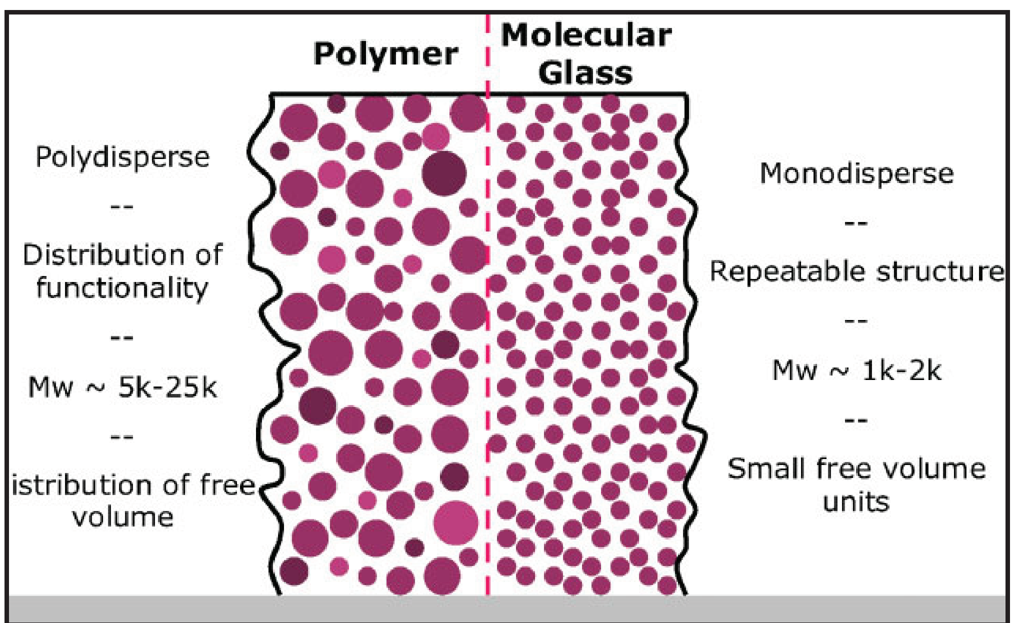

Figure 1.27: Schematic of the LER for the polymers and molecular materials (De Silva et al., 2008)

Moreover a contribution from the lithography processes to LER is also reported. The presence of mask defects (Reynolds et al., 1999), a poor aerial image contrast (Shin et al., 2001; Shin et al., 2002), shot noise effects (Leunissen et al., 2005; Rau et al., 1998; Kruit et al., 2004) and unoptimized development processes (Yasin et al., 2004; Yasin et al., 2004; Flanagin, et al., 1999) can lead to an increase in LER. Studies of chemical reactions and transport effects in resist films, especially in the case of chemically amplified resist reveal that the acid diffusion increases LER (Leunissen et al., 2005; Patsis et al., 2004; Yoshizawa et al., 2002). Line edge roughness (LER)

control is one of the most difficult challenge to be overcome in sub-100 nm lithography.

1.3.4.2. Sensitivity and contrast

Sensitivity and contrast are basic properties of a resist material, depending on wavelength or energy of the radiation source as well as process conditions such as baking and development. The sensitivity of a resist is the minimum dose of radiation required to complete chemical conversion for the resist, Dose in photolithography is the energy exposed onto a resist per unit area, usually expressed in mJ/cm^2, whereas in electron beam lithography it is the amount of electric charge or the number of electrons per unit area, expressed as $\mu C/cm^2$. The resolution and contrast of a resist material are important. To achieve high resolution a photoresist must possess relatively high contrast and sensitivity to exposed radiation. The resolution specifies the smallest feature size which can be patterned under a given set of conditions. Contrast (γ) of a resist is directly related to the resolution, resist profiles, and linewidth control. Both sensitivity and contrast of the resist can be determined from a response curve obtained by plotting the thickness remaining after the development process versus the irradiation dose (Figure 1.28). An ideal resist should have both high contrast and high sensitivity. The contrast (γ) is calculated from the formula $\gamma^{-1} = \log D_1 - \log D_0$ (Bilenberg et al., 2006). For the negative resist, D_0 is the highest dose at which the resist is not crosslinked and is washed out completely on development, D_1 is the minimum dose where the resist thickness is the same as that of coated film after development. In the case of positive resist D_0 is the maximum dose where the resist thickness before development and after development is identical and $D_1$is the minimum dose at which the exposed resist in completely deprotected and washed out after development. For thick resist layers and large structures, these curves are easy to generate. In general, the resist thickness remaining after the development process is measured with SEM or surface profilometer. When thin resist layers (< 10 nm) are used, reliable measurements are difficult, even using an atomic force microscope (AFM) operating in tapping mode.

In this case, the contrast is measured and is defined as the slope of the linear portion of the graph of the linewidth measured after the development plotted versus the

logarithm of the dose. Resist with higher contrast results in better resolution than that which exhibits low contrast.

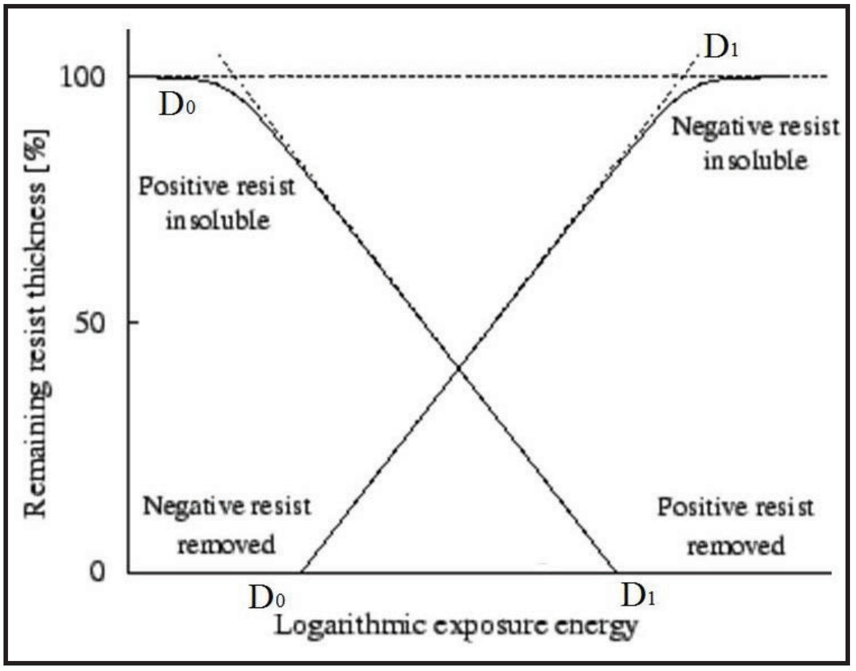

Figure 1.28: Sensitivity curves for positive and negative resist

1.3.5. Next generation lithography

Although features achieved by photolithography are already smaller than the radiation wavelength (Hughes et al., 2008), the need for fabricating complex structures and lower critical feature size continues. Alternative technologies currently being developed for next generation lithography includes, 193 nm immersion with multiple patterning lithography, extreme ultraviolet (EUV) lithography, imprint lithography, and maskless lithography. The greatest challenge is to increase resolution capability of lithography.

In summary, the review of literature reveals the need to develop new resists for photolithography and e-beam lithography. We have explored two approaches viz copolymerization of cyclodextrin inclusion complexes of methacrylate monomers and epoxide functionalized methacrylate monomers as negative resists for photolithography. Subsequently we have explored functionalized first generation dendrimers as negative as well as positive resists for electron beam lithography and photolithography. The results show that these materials exhibited lithographic performance comparable to SU-8 and hold promise for the future.

1.4. References

1. Amir H, S., Mahmood, G., Henrich, H., Frederic, O., Reinhard, H., Mohammad R, H., Nima, B., J. Plasma Fusion Res. Series, 2004, **6**, 735-737.
2. Bilenberg, B., Jacobsen, S., Schmidt, M. S., Skjolding, L.H.D., Shi, P., Boggild, P., Tegenfeldt, J.O., Kristensen, A., Microelectronic Engineering 2006, **83,** 1609–1612.
3. Chae, K. H., Park, J. H. Macromolecular Research 2004, **12**, 4, 352-358.
4. Crivello, J. V., J. Polym.Sci. Part A: Polym. Chem. 1999, **37**, 4241-4254.
5. Cyr, P. W., Rider, D. A., Kulbaba, K., Manners, I**.** Macromolecules, 2004, **37**, 11, 3959-3961.
6. Dai, J., Chang, S. W., Hamad, A., Yang, D., Felix, N., Ober, C. K. Chem. Mater. 2006, **18**, 3404-3411.
7. Day, R. A., U.S. Pat. 5304457, 1994.
8. Dektar, J. L., Hacker, N. P., J. Am. Chem. Soc. 1990, **112**, 6004-6015.
9. De Silva, A., Felix, N. M., Ober, C. K. Adv. Mater. 2008, **9999**, 1–7.
10. De Silva, A., Lee J. K., Andre X., Felix N. M., Cao H. B., Deng H., Ober C. K., Chem. Mater., 2008, **20**, 1606–1613.
11. De Silva, A., Ober C. K., J. Mater. Chem., 2008, **18**, 1903–1910.
12. Duan, H., Winston, D., Yang, J. K. W., Cord, B. M., Manfrinato, V. R., Berggren, K. K., J. Vac. Sci. Technol. B 2010., **28,** 6, C6C58-C6C62.
13. Fedynyshyn, T. H., Pottebaum, I., Astolfi, D. K., Cabral, A., Roberts, J., Meagley, R., J. Vac. Sci. Technol. B 2006, **24,** 6, 3031-3039.
14. Fedynyshyn, T. H., Astolfi, D. K., Goodman, R. B., Cann, S., Roberts, J., J. Vac. Sci. Technol. B, 2008, **26,** 6, 2281-2289.
15. Felix, N. M., De Silva, A., Ober, C. K. Adv. Mater. 2008, **20**, 1303–1309.
16. Flanagin, L. W., Singh, V. K., Willson, C. G., J. Vac. Sci. Technol. B 1999, **17**, 4, 1371-1379.
17. Fontana, R. E., Katine, J., Rooks, M., Viswanathan, R., Lille, J., MacDonald, S., Kratschmer, E., Tsang, C., Nguyen, S., Robertson, N., Kasiraj, P. IEEE Transactions on Magnetics, 2002, **38**, 1, 95-100.
18. Fujita, J., Ochiai, Y., Nomura, E., Matsui, S., Appl. Phys. Lett. 1995, **68,** 9, 1297-1299.

19. Fujita, J., Ochiai, Y., Nomura, E., Matsui, S., J. Vac Sci. Technol. B 1996, **14**, 4272-4276.
20. Haba, O., Haga,K.,Ueda, M. Chem. Mater. 1999**, 11**, 427-432.
21. Hattori, S., Yamada, A., Saito, S., Asakawa, K., Koshiba, T., Nakasugi, T. J. Vac. Sci. Technol. B 2009, **27**, 5, 2138-2144.
22. Henderson, C. L., http://henderson.chbe.gatech.edu/
23. Herriott, D. R., Collier, R. J., Alles, D. S., Stafford, J. W. IEEE Trans. Electron Devices 1975, **22**, 385-388.
24. Hirayama, T., Shiono, D., Matsumaru, S., Ogata, T., Hada, H., Onodera, J., Arai, T., Sakamizu, T., Yamaguchi, A., Shiraishi, H., Fukuda H., Ueda, M., Jpn. J. Appl. Phys. 2005, **44,** 7B, 5484-5488.
25. Hoole, A. C. F., Welland, M. E., Broers, A. N., Semicond. Sci. Technol, 1997, **12** 1166-1170.
26. Hughes, G., Litt, L. C., Wuest, A., Palaiyanur, S., Proc. SPIE 2008, 70280-70281.
27. Ito, H., Willson, C. G., Polym. Eng. Sci. 1983, **23,** 18, 1012-1018.
28. Ito, H., Willson, C. G., Frechet, J. M. J., U. S. Patent, 4,491,628, 1985.
29. Ito, H., Adv. Polym. Sci. 2005, **172**, 37-245.
30. Ito, H., IBM J. Res. Dev. 1997, **44,** 1, 119-130.
31. Ito, Y., Higashihara, T., Ueda, M., Journal of Photopolymer Science and Technology 2008, **21,** 799-803.
32. Ishida, M., Fujita, J., Ogura1, T., Ochiai, Y., Ohshima, E., Momoda, J., Jpn. J. Appl. Phys. 2003, **42**, 3913-3916.
33. Kadota, T., Kageyama, H., Wakaya, F., Kenji, G., Shirota, Y., Chemistry Letters 2004, **33**, 6, 706-707.
34. Kilby, J. S., U.S. Patent 3,138,743, 1964.
35. Kinoshita, M., Kita, H., Shirota, Y. Adv. Fun. Mater. 2002, **12,** 11-12, 780-786.
36. Koo, J.S., Smith, P. G. R., Williams, R. B. Chem. Mater. 2002**, 14**, 5030-5036.
37. Koo, J.S., Smith, P. G. R., Williams, R. B. Riziotis, C., Grossel, M. C. Optical Materials, 2003, **23**, 583–592.

38. Kozawa, T., Oizumi, H., Itani, T., Tagawa, S., Jpn. J. Appl. Phys. 2009, **48**, 126004-12007.
39. Kruit, P., Steenbrink, S., Jager, R., Wieland, M., J. Vac. Sci. Technol. B 2004, **22**, 2948-2955.
40. Kwak, G., Choi, J. U., Seo, K. H., Park, L. S., Hyun, S. H., Kim, W. S. Chem. Mater. 2007**, 19**, 2898-2902.
41. Leunissen, L. H. A., Ercken, M., Patsis, G. P., Microelectron. Eng. 2005, **78-79**, 2-10.
42. Liu, J-H.; Lin, S-H.; Shih, J-C., J. Appl. Polym. Sci. 2001, **80***,* 328-333.
43. Mike, W., Andy, N., J. Vac. Sci. Technol. B 2000, **18**, 6, 3345-3448.
44. Moore, G. E., Electronics 1965, **38**, 8, 114-117.
45. Mori, H., Nomura, E., Hosoda, A., Miyake, Y., Taniguchi, H., Macromol. Rapid Commun. 2006, **27**, 1792–1796.
46. Morton, J., D. L., Gabriel, J., Electronics: the life story of a technology, Westport, CT: Greenwood Press, 2004, 29-34.
47. Noyce, R. N., U.S. Patent 2,981,877, 1961.
48. Onishi, Y., Fujita, J., Ochiai, Y., Matsui,S., Microelectron. Eng. 1997, **35**, 117-120.
49. Patsis, G. P., Constantoudis, V., Gogolides, E., Microelectron. Eng. 2004, **75**, 207-308.
50. Patsis, G. P., Gogolides, E., Van Werden, K., Jpn. J. Appl. Phys. 2005, **44,** 8, 6341-6348.
51. Pfeiffer, H. C., SPIE Proc. 2009, **7378,** 737802, 1-12.
52. Pepin, A., Studer, V., Decanini, D., Chen, Y., Microelectronic Engineering 2004, **73–74**, 233–237.
53. Rau, N., Stratton, F., Fields, C., Ogawa, T., Neureuther, A., Kubena, R., Willson G., J. Vac. Sci. Technol. B 1998, **16**, 3784-3788.
54. Reichmanis, E., Nalamasu, O., Houlihan, F. M., Macromol. Symp. 2001, **175**, 185-196.
55. Reichmains, E., Thompson, L. F., Chem.Rev.1989, **89**, 1273-1289.
56. Rehab, H. Eur. Polym. J. 1998, **34**, 12, 1845-1855.
57. Reynolds, G. W., Taylor, J. W., J. Vac. Sci. Technol. B 1999, **17**, 2, 334-344.

58. Robinson, A. P. G., Palmer, R. E., Tada, T., Kanayama, T., Allen, M. T., Preece, J. A., Harris, K.D. M., J. Phys. D: Appl. Phys. 1999, **32**, L75-L78.
59. Robinson, A. P. G., Palmer, R. E., Tada, T., Kanayama, T., Allen, M. T., Preece, J. A., Harris, K.D. M., J. Vac. Sci. Technol. B 2000, **18**, 6, 2730-2736.
60. Robinson, A. P. G., Zaid, H. M., Gibbons, F. P., Palmer R. E., Manickam, M., Preece, J. A., Brainard, R., Zampini, T., O'Connell, K., Microelectron. Eng. 2006, **83**, 4-9, 1115-1118.
61. Robinson, A.P.G., Zaid, H.M., Manickam, M., Preece, J.A., Palmer R.E., Microelectron. Eng. 2008, **85**, 7, 1540-1544.
62. Rothschild, M., Bloomstein, T. M., Fedynyshyn, T. H., Kunz, R. R., Liberman, V., Switkes, M., Efremow, Jr, N. N., Palmacci, S.T., Sedlacek, J. H. C., Hardy, D. E., Grenville, A. Lincoln Laboratory journal 2003, **14,** 2, 221-236.
63. Rwei, S. P, Cheng, C.Y., Liou, G. S., Cheng, K. C., Polym Eng Sci 2005; **45**, 478-486.
64. Sailer, H., Ruderisch, A., Kern, D. P., Schurigb, V. J. Vac. Sci. Technol. B 2002, **20**, 6, 58-61.
65. Sailer, H., Ruderisch, A., Henschel, W., Schurig, V., Kern, D.P., J. Vac. Sci. Technol. B 2004, **22**, 6, 3485-3488.
66. Shimizu, R., Ze-Jun, D., Rep. Prog. Phy**s.**1992, 487-531.
67. Shin, J., Han, G., Ma, Y., Moloni, K., Cerrina, F. J., Vac. Sci. Technol. B 2001, **19**, 6, 2890-2895.
68. Shin, J. Ma, Y. Cerrina F., J. Vac. Sci. Technol. B 2002, **20**, 6, 2927-2931.
69. Shirota, Y., J. Mater. Chem., 2000, **10**, 1-25.
70. Tada, T., Kanayama, T., Robinson, A. P. G., Palmer, R. E., Allen, M. T., Preece, J. A., Harris, K.D. M., Microelectron. Eng. 2000, **53**, 425-428.
71. Thompson, L. F., Wilson, C. G., Bowden, M. J., Acs, Symposium Series 1983, 219, 47-85.
72. Tully, D. C., Trimble, A. R., Frechet, J. M. J. Adv. Mater. 2000, **12**, 15, 1118-1122.
73. Wang, C. S., Lee, M. C., Polymer 2000, **41**, 3631-3638.
74. Wang, M., Gonsalves, K. E., Rabinovich, M, Yuehb., W., Roberts, J. M., J. Mater. Chem. 2007, **17**, 1699–1706.

75. Watanabe, S., Harashima, S., Tsukada, N., J. Polymer. Sci., Chem. Ed., 1986, **24**, 1227- 1234.
76. Wieland, M. J., De Boer G., Ten Berge, G. F., Jager, R., Van de Peut, T., Peijster, J. J. M., Slot, E., Steenbrink, S. W. H. K., Teepen, T. F., Van Veen, A. H. V., Kampherbeek, B. J., MAPPER: high throughput maskless lithography, SPIE Proc, 2009, 7271.
77. Yamaguchi, T., Yamazaki, K., Namatsu, H., J. Vac. Sci. Technol. B 2004, **22**, 6, 2604-2610.
78. Yang, D., Chang, S. W., Ober, C. K. J. Mater. Chem., 2006, **16**, 1693–1696.
79. Yasin, S., Hasko, D. G., Carecanac, F., J. Vac. Sci. Technol. B, 2001, **19**, 311-315.
80. Yasin, S., Hasko, D. G., Ahmed, H., Appl. Phys. Lett. 2001, **78**, 2760-2762.
81. Yasin, S., Khalid, M. N., Hasko, D. G., Ahmed, H., Microelectron. Eng. 2004, **73-74**, 259-264.
82. Yasin, S., Hasko, D. G., Khalid, M. N., Weaver, D. J., Ahmed, H., J. Vac. Sci. Technol. B 2004, **22**, 2, 574-578.
83. Yin, E., Brodie, A. D., Tsai, F. C., Guo, G. X., Parker, N. W. J. Vac. Sci. Technol. B, **18,** 6, 3126-3131.
84. Yoshimura, T., Shiraishi, H., Yamamoto, J., Okazaki, S., Appl. Phys. Lett. 1993, **63**, 764-766.
85. Yoshizawa, M., Moriya, S., J. Vac. Sci. Technol. B 2002, **20**, 1342-1347.
86. Yoshizawa, M., Kageyama, H., Shirota, Y., Wakaya, F., Gamo, K., Takai, M., Appl. Phys. Lett 1996, **69**, 2605-2610.
87. Zaid H. M., Robinson, A. P. G., Palmer, R. E., Manickam, M., Preece J. A., Adv. Funct. Mater. 2007, **17,** 14, 2522-2527.

Chapter 2

Objective and scope of the work

2.1. Preamble

The challenge in lithography is to reduce the feature size by developing new lithographic techniques and resist materials, such as linear and hyper branched polymers. Molecular glasses and dendrimers are being explored to overcome the problems encountered with polymeric resists during the fabrication of nanometer-scale patterns because of high molecular weight and molecular weight distribution leading to the irregularity of line patterns resulting from chain entanglement, aging, poor miscibility and aggregation.

This investigation has been focused on design and evaluation of copolymer resists containing new crosslinking chemistries and first generation dendrimers in photolithography and electron beam lithography.

The major objectives and scope of the proposed investigation are summarized below.

2.2. Objectives

1. To synthesize negative resists which can be crosslinked in two stages by copolymerizing inclusion complexes of multivinyl monomers and β-cyclodextrin with the methacrylate monomers.
2. Evaluate the effect of crosslink density on thermal properties (TGA and T_g) of the copolymers.
3. Control crosslink density in the copolymers and evaluate its effect on their performance in optical lithography.
4. Synthesize and characterize soluble linear polymers containing pendant epoxide functionality.
5. Synthesize and characterize soluble linear polymers containing different degrees of epoxide substitution.
6. Evaluate effect of cross linking density on thermal properties (TGA and T_g) of the polymers synthesized in 5.
7. Evaluate the polymers synthesized in 5 for optical lithography.
8. Synthesize and characterize new chemically amplified resists based on first generation dendrimers consisting bisphenol-A, 1, 5-dihydroxynaphthalene and trisphenol units for optical and electron beam lithography.
9. Characterize and evaluate properties of the linear polymers, copolymers and first generation dendrimers by instrumental techniques such as FTIR, NMR, GPC, XRD, TGA and DSC.

10. Evaluate first generation dendrimers resist synthesized in 8 as negative tone electron beam resists.
11. Modify first generation dendrimers synthesized in 8 and evaluate their performance as positive resists in electron beam lithography.
12. Evaluate first generation dendrimers as negative tone optical resists and explore their utility in device fabrication.

2.3. The scope of the present research investigation is outlined below more precisely

1. Synthesis of two stage soluble co-polymers consisting CuMA-co-EGDMA, 1-HNMA-co-EGDMA, CuMA-co-TMPTMA and 1-HNMA-co-TMPTMA containing pendant vinyl unsaturation for optical lithography.
2. Synthesis of linear soluble polymers CuMA-co-BPMA and 1-HNMA-co-1, 5-DHNMA, containing pendant epoxides for optical lithography.
3. Structural characterization of resists by instrumental techniques such as FTIR, NMR, GPC, DSC, XRD, AFM and ESEM.
4. Evaluation of effect of variation of crosslink density on performance in optical lithography.
5. Comparison of the lithographic performance of linear polymers containing pendant epoxide with SU-8 resist.
6. Synthesis and characterization of FGDs based on 1,3,5-trisbromomethylbenzene as core and bisphenol-A, trisphenol and 1,5-dihydroxynaphthalene as peripheral moiety.
7. Epoxide conjugation of FGDs synthesized in 6 and evaluation of the negative resist in electron beam lithography to establish the lowest feature size and highest feature density that can be achieved.
8. Conjugation of FGDs synthesized in 6 with t-BOC to yield positive tone resist and evaluate their performance in electron beam lithography to establish the lowest feature size and highest pattern density that can be achieved.
9. Evaluation of negative tone photoresist based on epoxide conjugated FGDs in optical lithography and comparison with SU-8 resist.

Chapter 3

Polymer containing latent vinyl groups for lithographic applications

3.1. Introduction

Advances in lithography have resulted in significant enhancement in the performance of semiconductor devices. In microelectronics industries, this has resulted in reduction in size of microstructures (Reichmanis and Thompson, 1989; Reichmanis et al., 1999; Cyr et al., 2004). One of the prerequisites of photoresists is the ability to exhibit differentiatial solubility in developer solvents upon exposure to UV light (Wu and Gonsalves, 2001). Polymers have been classified as positive and negative photoresists based on solubility towards developer following irradiation. The photocrosslinkable polymers have received significant attention in the field of microlithography (Chen and Yin, 2004; Fang et al., 2002); tissue engineering, (Fisher et al., 2003) and waveguides (Koo et al., 2002).

Negative photoresists are further classified based on photocrosslinking mechanism as polymers containing vinyl functionality, epoxide rings and halide groups (Reichmanis and Thompson, 1989). In literature, synthesis of negative photoresists has been achieved by different approaches.

First approach which is most commonly used, involves conjugation of photosensitive moieties to polymer backbones. Chen and Yin, (2004) developed negative photosensitive hyperbranched polymers, having free hydroxyl functionality, which was subsequently converted into vinyl functionality by reacting with methacryloyl chloride. Koo et al, (2002 and 2003) synthesized Poly (methyl methacrylate / 2-hydroxy ethyl methacrylate) based copolymers, having pendant hydroxyl groups which were further conjugated with methacrylic anhydride. Cyr et al, 2004 developed polyferrocenylsilane methacrylates. Polyferrocenylsilanes were synthesized using Pt-catalyst. The halide functionality on the polymer backbone was further modified by hydroxyethyl methacrylate leading to polyferrocenylsilanes bearing pendant photocrosslinkable methacrylate groups. Han et al., (2007) synthesized block copolymers of styrene / methyl methacrylate / hydroxyethyl methacrylate and styrene / methyl methacrylate / glycidyl methacrylate, wherein photo-crosslinkable acryloyl group was incorporated by esterification of hydroxyl groups in hydroxyethyl methacrylate.

The approach suffers from following limitations. The results of pendant group functionalization are not consistent, and the product, which varied in nature from a free flowing powder to a sticky solid, is difficult to isolate (Koo et al., 2002).

Methacrylic anhydride is less reactive than methacryloyl chloride but is suitable for the preparation of esters only under mild conditions (Koo et al., 2002). In both cases a stabilizer e.g. *p*-benzoquinone needs to be added during the reaction to inhibit cross-linking. Subsequent removal of stabilizers is difficult. Residual stabilizers lower the rate of polymerization and conversion of pendant groups is incomplete. Attempts to increase conversion result in homo polymerization of modifier as well as cross-linking of the functionalized polymers.

Second approach involves polymerization of monomers containing photosensitive moieties. Kwak et al, (2007) synthesized methacrylate based homopolymer and copolymers containing abietate groups. Monomer methacryloyloxyethyl abietate was synthesized from abietic acid incorporating an ethyl spacer and was further copolymerized with methylmethacrylate. Photodimerization of unsaturation in abietic acid resulted in crosslinking. However, the crosslinking was not complete as was demonstrated by separated from significant fractions extracted in solvent. Rehab (1998) reported negative photoresist, containing pendant chalcone moiety. Allyl-chalcone monomer was used for homopolymerization and co-polymerization. However, lithographic evaluation of the polymer was not reported. Lee and Hong (2002) developed an acrylic rosin (Levopimaric acid) based negative photoresist which showed sensitivity 12.6- 84.6 mJ/cm^2 and resolution 2.2-10 μm.

This approach suffers from multiple steps required for synthesis and purification. We report a new approach which involves synthesis of photosensitive copolymers containing latent crosslinking sites. In previous work from our group we reported inclusion complexes of β-cyclodextrin with EGDMA and TMPTMA. During free radical polymerization these crosslinkers behave as monovinyl monomers and yield solvent soluble polymers containing pendant unsaturations that could be crosslinked further in the second stage by thermal or photochemical stimulus. Solvent soluble Poly (EGDMA) and Poly (TMPTMA) reported previously are brittle in nature and have poor adhesion properties. These polymers exhibit low glass transition temperature even after crosslinking e.g. Poly (EGDMA) has T_g of 93.05 ^{o}C (Satav et al., 2006) while Poly (TMPTMA) has T_g 57.41 ^{o}C (Satav et al., 2007). Moreover aliphatic resins are generally not preferred for the device applications due to their low thermal stability (Reichmanis et al., 1991). High glass transition temperature (T_g) is an important requisite for photoresist to form stable films and withstand post exposure

bake. The photoresist performance viz. sensitivity, resolution, and PEB depend on its T_g. For finer resolution, it is necessary that the PEB temperature be lower than T_g. Polymers containing phenyl and naphthalene rings exhibit better thermal stability and moisture resistance (Xu et al., 2004; Ratnaprabha and Daliya, 2005; Duann et al., 2004). Copolymerization of these vinyl monomers with monomers containing multiple unsaturated sites like ethylene glycol dimethacrylate (EGDMA), trimethylol propane trimethacrylate (TMPTMA), results in crosslinked products. Alternatively inclusion complexes of EGDMA and TMPTMA can be copolymerized with rigid monomers like cumyl methacrylate (CM) and 1-naphthol methacrylate (NM), which would be expected to exhibit better thermal stability, film formation and adhesion of cast films. In this chapter, solvent soluble copolymers of CPMA and 1-HNMA with EGDMA and TMPTMA in varying ratios were synthesized. These exhibited high T_g and photocrosslinkability and were evaluated as negative resist in photolithography.

3.2. Experimental section

3.2.1. Materials

EGDMA, TMPTMA, 1-Naphthol, cumylphenol, methacrylic acid, 1-hydroxy cyclohexyl phenyl ketone were procured from Aldrich chemicals (USA). Benzyl chloride, azo-bis-isobutyronitrile (AIBN) were procured from spectrochem. β-Cyclodextrin was procured from Himedia. AIBN was recrystallized from Acetone and petether. N, N-dimethylformamide (DMF), dichloromethane (DCM), tetrahydrofuran (THF) and ethyl acetate (EA) were from Merck chemicals.

3.2.2. Synthesis

3.2.2.1. Monomer synthesis

3.2.2.1.1. Cumyl methacrylate monomer (CM)

Cumyl phenol 20 g (9.4×10^{-2} moles) was dissolved in dry dichloromethane (150 ml) in a clean, dry, two-neck 250 ml round-bottom flask under dry nitrogen atmosphere with magnetic stirring. Triethylamine 13 ml (9.4×10^{-2} moles) was added and stirred well for 10 minutes. The reaction flask was then placed in an ice bath. Methacryloyl chloride 10 ml (9.4×10^{-2} moles) in 20 ml DCM was added slowly so that the temperature of the reaction mixture was maintained between 0 ^{o}C to

5 ^{o}C. After addition was complete, the ice bath was removed and stirring was continued for 3-4 h. The reaction mixture was extracted with ethyl acetate. The solvent was evaporated and the CM monomer was recovered by column chromatography, using petroleum ether and ethyl acetate (95:05 v/v) as elutant. Yield 24.3 g (92 %).

^{1}H NMR ($CDCl_3$-*d*$_6$)**;** CM [ppm]: 1.68 (6H, -C $(CH_3)_2$ of Cumyl phenol), 2.05 (3H, -CH_3 adjacent to allyl group), 5.73 and 6.33 (2H, vinyl protons), 7.0-7.21 (9 H, aromatic protons).

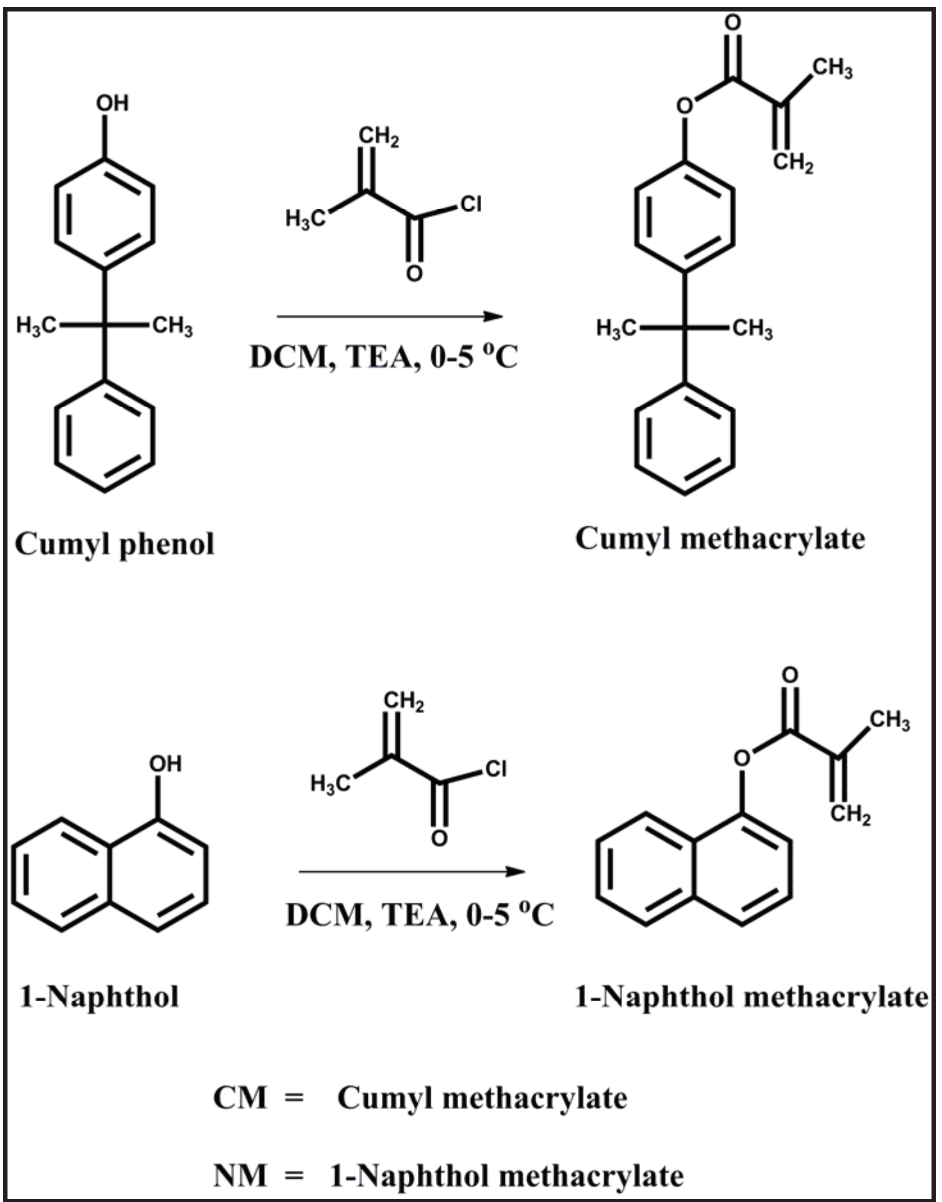

Figure 3.1: Synthesis of monomers CM and NM

Figure 3.2: CD-T and CD-E IC synthesis

3.2.2.1.2. 1-Naphthol methacrylate (NM)

1-Naphthol 20 g (0.138 moles) was dissolved in dry dichloromethane (150 ml) in a clean, dry, 250 ml round-bottom flask under dry nitrogen atmosphere with magnetic stirring. Triethylamine 19 ml (0.138 moles) was added and stirred well for 10

minutes. The reaction flask was then placed in an ice bath. Methacryloyl chloride 15 ml (0.138 moles) in 30 ml DCM was added slowly so that the temperature of the reaction mixture was maintained between 0 ^oC to 5 ^oC. After addition was complete, the ice bath was removed and stirring was continued for 3-4 h. The reaction mixture was extracted with ethyl acetate. The solvent was evaporated and the NM monomer was recovered by column chromatography, using petroleum ether and ethyl acetate (90:10 v/v) as elutant. Yield 26.2 g (89 %).

^1H NMR ($CDCl_3$-d_6)**;** NM [ppm]: 2.08 (3H, -CH_3 adjacent to allyl proton), 5.98 and 6.42 (2H, vinyl protons), 6.9-8.7 (7 H, aromatic protons).

3.2.2.2. Synthesis of inclusion complex (IC) of the crosslinker

3.2.2.2.1. β-CD-TMPTMA IC (CD-T)

30 g (2.6 X 10^{-2} moles) β-CD was dissolved in 1650 ml water. To this 4.47 g (1X 10^{-2} moles) TMPTMA was added and stirred for 24 h at room temperature. The complex slowly precipitated out. It was filtered and washed with distilled water to remove uncomplexed β-CD, followed by petroleum ether to remove TMPTMA. The complex was characterized by ^1H NMR.

3.2.2.2.2. β-CD-EGDMA IC (CD-E)

11.35 g (1 X 10^{-2} moles) β-CD was dissolved in 615 ml water. To this 1.99 g (1X 10^{-2} moles) EGDMA was added and stirred for 24 h at room temperature. The complex slowly precipitated out. It was filtered and washed with distilled water to remove uncomplexed β-CD, followed by petroleum ether to remove EGDMA. The complex was characterized by ^1H NMR.

3.2.2.3. Copolymer synthesis

3.2.2.3.1. Poly (CM-co-CD-E), 20/80

2 g (7.13 X 10^{-3} moles) of CM monomer and 38 g (2.8 X 10^{-2} moles) CD-E complex were dissolved in 400 ml DMF. 0.15 g (2 wt %) AIBN was added as an initiator, 0.2 g (3.5 X 10^{-3} moles) mercaptoethanol was used as a chain transfer reagent and reaction mixture was purged for 30 min with nitrogen. The reaction was carried out at 65 ^oC in water bath for 24 h. The reaction mixture was precipitated in excess water and

filtered. The precipitate thus obtained was dissolved in DMF and reprecipitated into methanol, filtered and dried under vacuum. The copolymer was characterized by ^{1}H NMR. Yield 5.7 g (75 %).

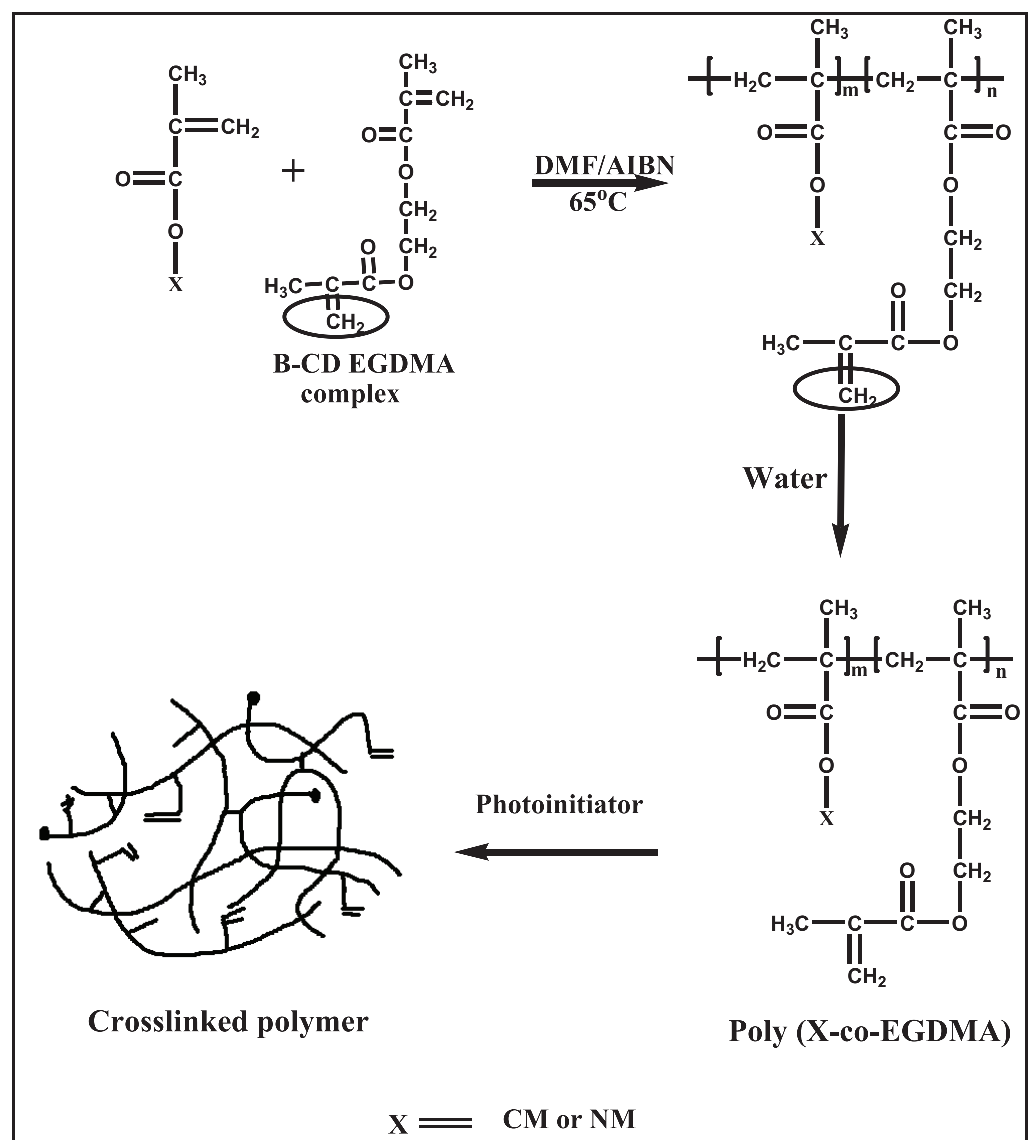

Figure 3.3: Synthesis of EGDMA copolymers

3.2.2.3.2. Poly (CM-co-CD-T), 20/80

2 g (7.13 X 10 $^{-3}$ moles) of CM monomer and 73 g (2.8 X 10 $^{-2}$ moles) CD-T complex were dissolved in 700 ml of DMF. 0.23 g (2 wt %) AIBN was added as an initiator, 0.2 g (3.5 X 10^{-3} moles) mercaptoethanol was used as a chain transfer reagent and reaction mixture was purged for 30 min with nitrogen. The reaction was carried out at 65 ^{o}C in water bath for 24 h. The reaction mixture was precipitated by pouring it into excess water and filtered. The precipitate thus obtained was dissolved in DMF and

reprecipitated in to methanol, filtered and dried under vacuum. The copolymer was characterized by ^{1}H NMR. Yield 7.9 g (69 %).

Copolymers of CM and NM with CD-E and CD-T (Figure 3.3 and 3.4) in varying monomer ratios were prepared as described above. The extent of incorporation of EGDMA and TMPTMA units in copolymers was calculated by ^{1}H-NMR, values are summarized in Table 3.1, 3.2.

Figure 3.4: Synthesis of TMPTMA copolymers

3.2.2.4. Characterization

The ^{1}H-NMR spectra were recorded in $CDCl_3$ at 25°C on Bruker-200 MHz spectrometer. IR spectra were recorded on a Perkin Elmer spectrometer (DRS mode) over the frequency range 4000-400 cm^{-1}. The weight average (M_w) and number average (M_n) molecular weights of polymers were measured by gel permeation

chromatography (GPC) using two 60 cm 100 Å polystyrene-DVB cross-linked gel columns from PSS GmbH using chloroform as eluent at a flow rate of 1 ml min^{-1}. Digital micrometer (Mitutoya-IP 65 range 0.25 mm-0.001mm) was used to measure the film thickness used to monitor transparency. Shimadzu spectrophotometer (UV-160 1PC) was used to measure the percent transmittance of polymers.

The differential scanning calorimetery (DSC) and thermo gravimetric analysis (TGA) were performed on TA Instrument DSC Q-10 and TGA-7 Perkin Elmer at a heating rate 10 ^{o}C/min. The resists were spin coated on silicon wafers at 3000 rpm. Karl Suss MJB-3 Mask Aligner, Germany, was used for resist patterning. Olympus optical microscope, Japan was used for imaging. Raith 150^{TWO}, Germany, was used to measure resist film thickness.

3.2.2.5. Lithographic evaluation of negative-tone photoresist

High T_g copolymers P1, P5, P9 and P13 were selected for lithography. The solutions containing 10 wt % polymers in γ-butyrolactone were used for lithographic evaluation. 1-hydroxy-cyclohexylphenyl ketone 10 wt % with respect to resist was added. The polymer resists were spin coated on silicon wafers at 3000 rpm for 30 sec. The thicknesses of the resist were 330 nm for P1, 309 nm for P5, 289 nm for P9 and 293 nm for P13. Coated samples were pre-baked on a hot-plate at 60 °C for 5 min. Samples were exposed to UV light using a soft-contact mask-aligner with an intensity of 2 mW/cm^2 at 365 nm wavelength for 60 sec. Post exposure bake (PEB) was carried out at 50 ^{o}C for 10 min. The patterns were developed using PGMEA, rinsed with isopropanol and dried with a nitrogen blower.

3.3. Results and Discussion

3.3.1. Choice of the method

Polymers containing vinyl unsaturation have been synthesized by reacting polymers containing functional groups such as hydroxyls with methacryloyl chloride or anhydride. Complete conversion of such reactions is difficult and efforts to force complete conversion result in crosslinking. We recently reported synthesis of vinyl monomers containing multiple unsaturations by forming inclusion complexes wherein methacrylate groups are encapsulated within cyclodextrin cavity (Satav et al., 2006;

Satav et al, 2007). Homopolymers of EGDMA and TMPTMA as well as their copolymers with methyl methacrylate (MMA) were prepared. However these are brittle and do not posses good film forming properties. As mentioned in the introduction, higher T_g is often a pre-requisite for photoresists. We therefore identified CM and NM as rigid monomers which would impart higher T_gs and also result in better film formation. In the following sections we describe synthesis of the inclusion complexes of two crosslinkers with β-cyclodextrin, copolymers of the complexes with CM and NM in various ratios, characterization of the copolymers for composition, thermal characteristics and evaluation of the polymers as negative resist by UV lithography (365 nm).

3.3.2. Inclusion complex: Characterization by ^{1}H-NMR

3.3.2.1. ^{1}H-NMR-CD-T IC

Figure 3.5 shows ^{1}H-NMR spectrum of CD-T IC. The stoichiometry of the complex (CD-T IC) was established by integrating the peak at 4.16 ppm, which corresponds to 6 protons of TMPTMA ($-OCH_2$), and the peaks at 4.49 and 4.82 ppm, which correspond to 7 protons of *β*-CD for ($-CH_2-OH$) and (C1-H) respectively. The integration confirmed 1:2 stoichiometry of CD-T complex.

β-CD-TMPTMA IC: 0.87 ppm (3H, CH_2-CH_3 of TMPTMA), 1.52 ppm (2H, CH_2-CH_3 of TMPTMA), 1.85 ppm (9H, CH_3 adjacent to vinyl group of TMPTMA), 4.11 ppm (6H, OCH_2 of TMPTMA), 5.67 ppm and 6.01 ppm (6H, vinyl protons of TMPTMA).

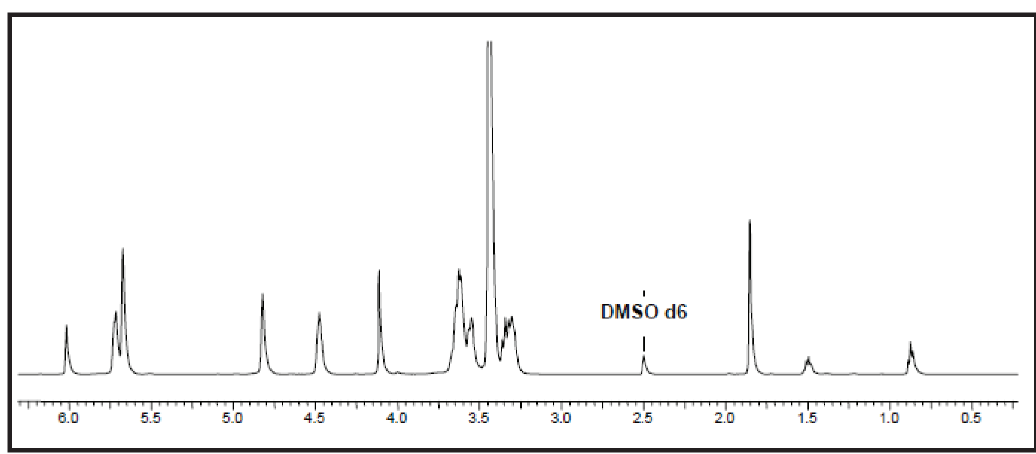

Figure 3.5: ^{1}H-NMR D-T IC

3.3.2.2. ^{1}H-NMR CD-E IC

Figure 6 shows ^{1}H-NMR spectrum of CD-E IC. The stoichiometry of the complex was established by integrating the peak at 4.34 ppm, which corresponds to four protons of EGDMA (-OCH_2-CH_2O-) and the peak at 4.48 ppm which corresponds to seven protons of β-CD (-CH_2OH) and the peak at 4.82 ppm which corresponds to seven protons of β-CD (C1-H). The integration confirmed 1:1 stoichiometry of CD-E complex (Figure 3.6).

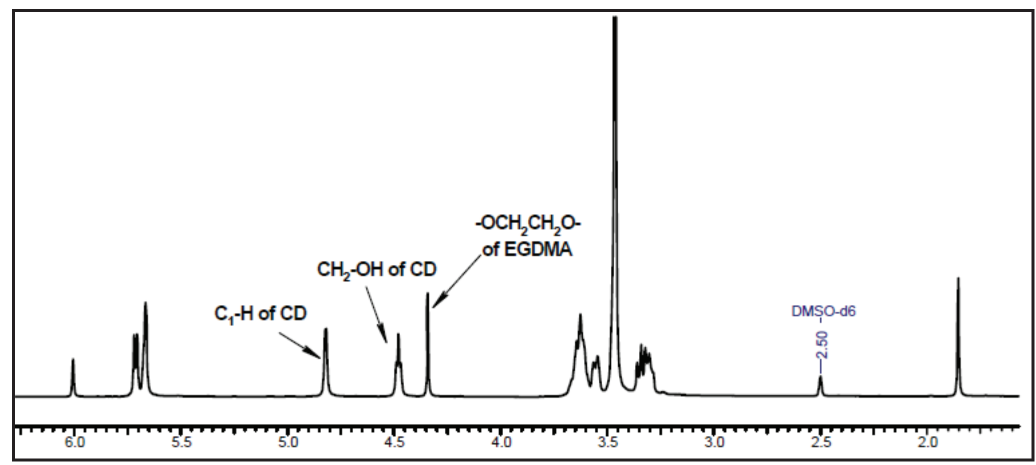

Figure 3.6: ^{1}H-NMR EGDMA-β-CD IC

β-CD-EGDMA IC: 1.85 ppm (6H, 2-CH3 groups of EGDMA), 4.34 ppm (4H, -OCH2CH2O- of EGDMA), 5.67 ppm and 6.01 ppm (4H, allyl protons of EGDMA), 5.72 ppm (C2–OH of β-CD), 5.71 ppm (C3–OH of β-CD), 4.48 ppm (C6-OH of β-CD), 4.82, ppm (C1-H of β-CD), 3.30 ppm (C2-H of β-CD), 3.34 ppm (C4-H of β-CD), 3.55 ppm (C5-H of β-CD), 3.61 ppm (C3-H of β-CD), 3.64 ppm (C6, Ha and Hb of β-CD).

3.3.3. Polymer characterization

3.3.3.1. Solubility

Solubility of the photoresist is one of the essential requirements as poor miscibility of the resist leads to structural defects during lithography. The solubility of the copolymers was tested in solvents which are commonly used for resist formulation. All the polymers were easily soluble in γ-butyrolactone, ethyl lactate, propylene

glycol methyl ether acetate (PGMEA), cyclohexanone and 2-methoxyethanol. The polymers were insoluble in methanol, ethanol and isopropanol.

3.3.3.2. Molecular weights

The weight average (M_w), number average (M_n) molecular weights and the polydispersity index (M_w/M_n) of the copolymers were determined using gel permeation chromatography.

Table 3.1: Copolymers of EGDMA

Sr. No	Copolymer	Feed Ratio (R : A)	X (%)	M_w	M_n	M_w/M_n
CM-co-EGDMA						
1	P1	20 : 80	61	1.73 X 10^4	7.50 X 10^3	2.30
2	P2	40 : 60	48	8.65 X 10^3	4.34 X 10^3	1.99
3	P3	50 : 50	36	1.30 X 10^4	7.07 X 10^3	1.84
4	P4	80 : 20	10	7.18 X 10^3	4.27 X 10^3	1.67
NM- co-EGDMA						
1	P5	20 : 80	70	8.56 X 10^3	4.09 X 10^3	2.09
2	P6	40 : 60	53	8.86 X 10^3	4.34 X 10^3	2.03
3	P7	50 : 50	40	6.99 X 10^3	3.58 X 10^3	1.95
4	P8	80 : 20	12	8.04 X 10^3	3.83 X 10^3	2.10

R= CM or NM, A= EGDMA or TMPTMA, X= actual crosslinker content in the polymer.

The copolymers up to 150000-180000 molecular weights could be synthesized. However these polymers yielded very high solution viscosities for spin coating. In order to lower molecular weights, 10 mole % mercaptoethanol was used as chain transfer agent. The values of molecular weights are summarized in table 3.1 and 3.2.

In all the cases crosslinker content in the polymer is less than that the feed. For any copolymerization system at a given feed composition incorporation of NM is lower than that of CM, because of the lower reactivity of the NM than that of the CM. Also at a given feed composition, the incorporation of TMPTMA is lower than that of GDMA. This is because TMPTMA forms 1:2 complex which is bulkier than the EGDMA complex which is 1:1.

Table 3.2: Copolymers of TMPTMA

Sr. No	Copolymer	Feed Ratio (R : A)	X (%)	M_w	M_n	M_w/M_n
CM-co-TMPTMA						
1	P9	20 : 80	44	1.13×10^4	3.95×10^3	2.86
2	P10	40 : 60	41	1.29×10^4	5.37×10^3	2.40
3	P11	50 : 50	28	1.32×10^4	4.06×10^3	3.25
4	P12	80 : 20	12	1.22×10^4	4.31×10^3	2.87
NM- co-TMPTMA						
1	P13	20 : 80	65	1.27×10^4	3.84×10^3	3.30
2	P14	40 : 60	49	1.38×10^4	4.35×10^3	3.17
3	P15	50 : 50	40	1.57×10^4	5.81×10^3	2.70
4	P16	80 : 20	13	1.34×10^4	3.91×10^3	3.42

R= CM or NM, A= EGDMA or TMPTMA, X= actual crosslinker content in the polymer.

3.3.3.3. Determination of unsaturation in copolymers

3.3.3.3.1. Qualitative determination by FTIR spectroscopy

The incorporation of crosslinker (EGDMA and TMPTMA) in copolymers was investigated by IR spectroscopy, 3 wt % copolymers in KBr were analyzed.

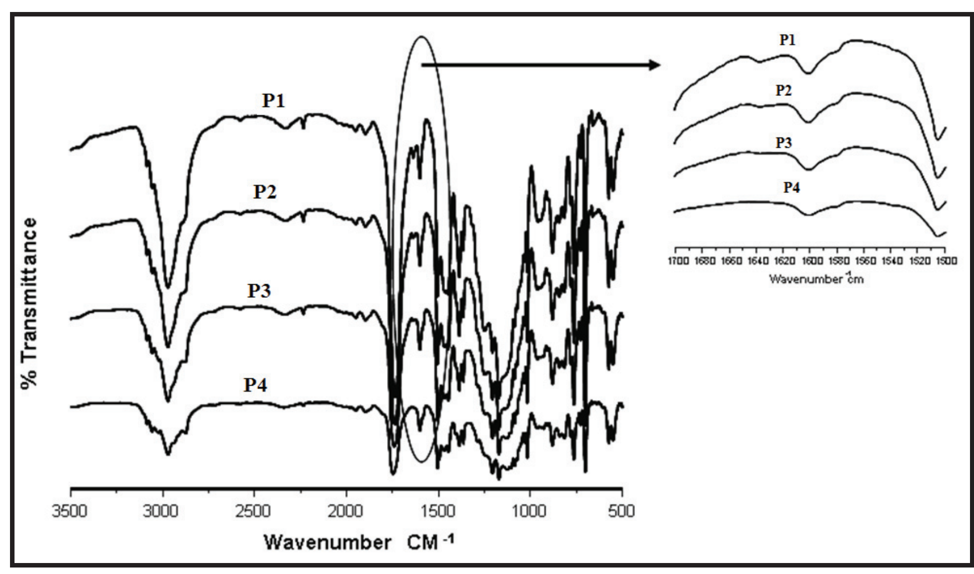

Figure 3.7: FTIR spectra of polymers P1-P4

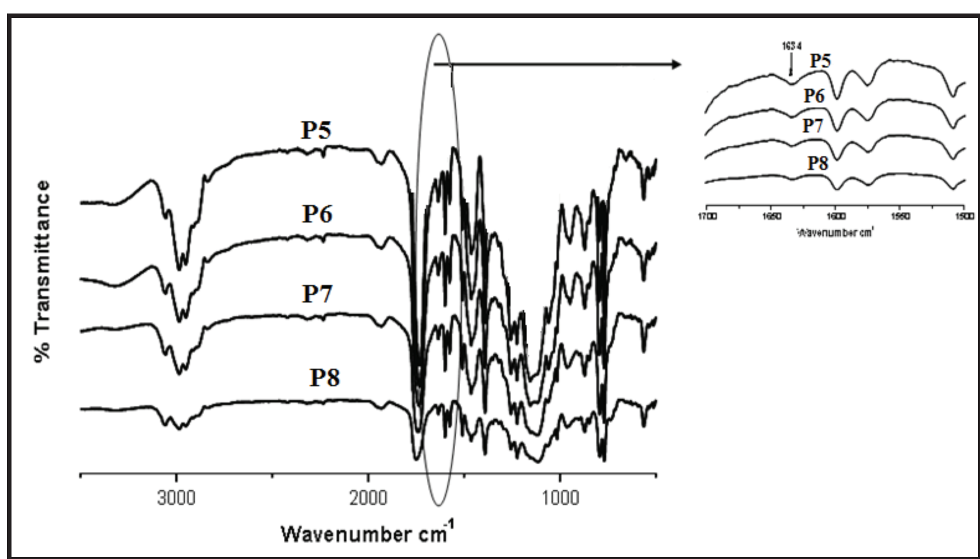

Figure 3.8: FTIR spectra of polymers P5-P8

The intensity of the peak at 1638 cm^{-1} which corresponds to EGDMA (Figures 3.7, 3.8) and at 1636 cm^{-1} which corresponds to TMPTMA (Figures 3.9, 3.10) increased gradually accompanied by decreasing intensity of peak at 3077 cm^{-1} (Figure 3.7, 3.9) and 3080 cm^{-1} (Figure 3.8, 3.10) corresponding to CM and NM respectively. Aromatic C–H stretching vibration, confirmed incorporation of CM and NM units in the polymer chain.

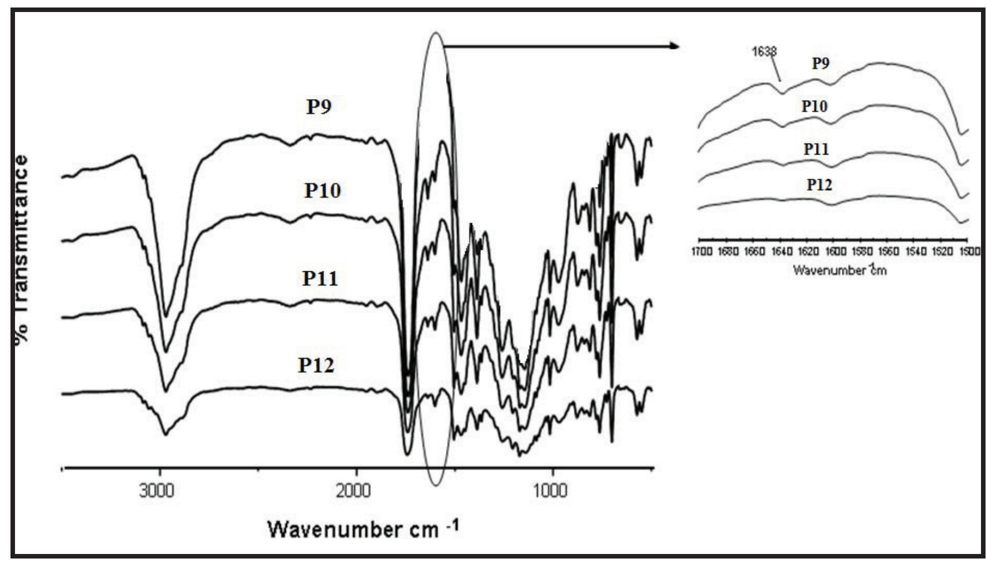

Figure 3.9: FTIR spectra of polymers P9-P12

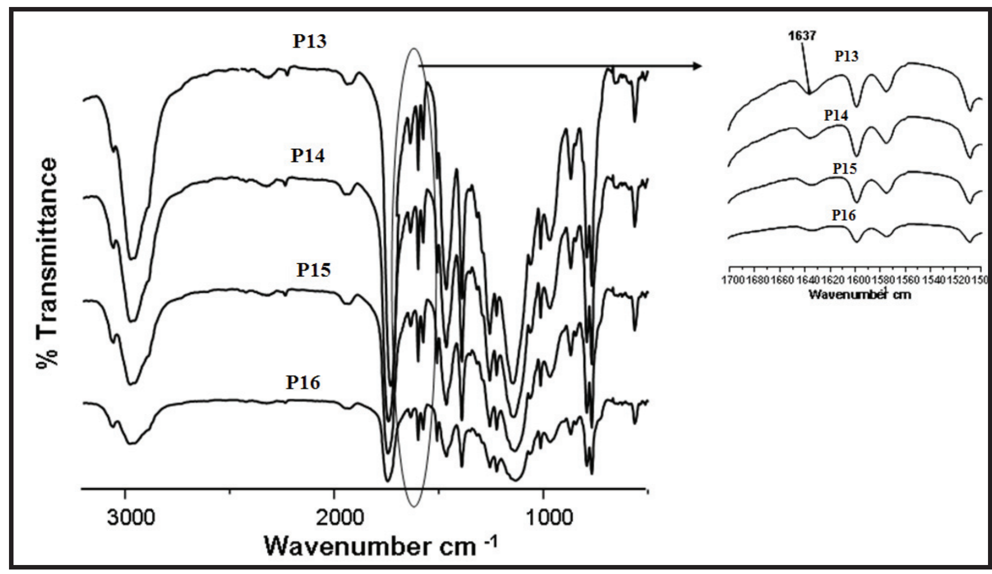

Figure 3.10: FTIR spectra of polymers P13-P16

3.3.3.3.2. Quantitative evaluation by ^{1}H-NMR spectroscopy

Incorporation of unsaturation was quantified from the ^{1}H-NMR spectra, comparing peak integrals of aromatic peaks of CM or NM with 4 protons of EGDMA unit and 6 protons of TMPTMA unit. Chemical shifts at 4.38 ppm (Figure 3.11) and 4.4 ppm (Figure 3.12) correspond to 4 protons of EGDMA (-OCH2CH2O-). Similarly peaks at 4.17 and 4.14 ppm (Figures 3.13, 3.14) correspond to 6 protons of TMPTMA units (-OCH2). Resonance signals at 6.13 ppm and 5.62 ppm (Figures 3.11, 3.12) correspond to the vinyl unsaturation in EGDMA.

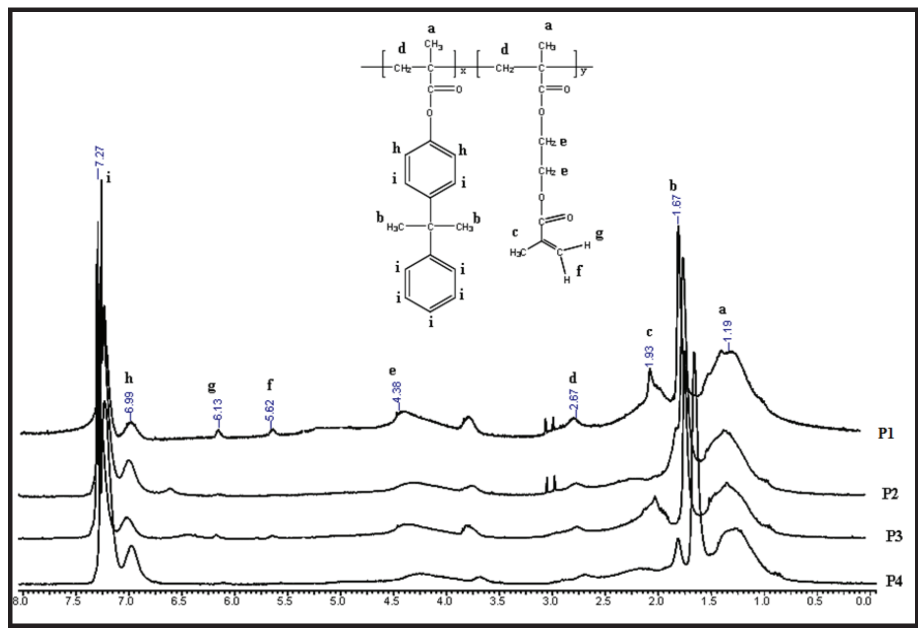

Figure 3.11: ^{1}H NMR spectra of polymers P1-P4

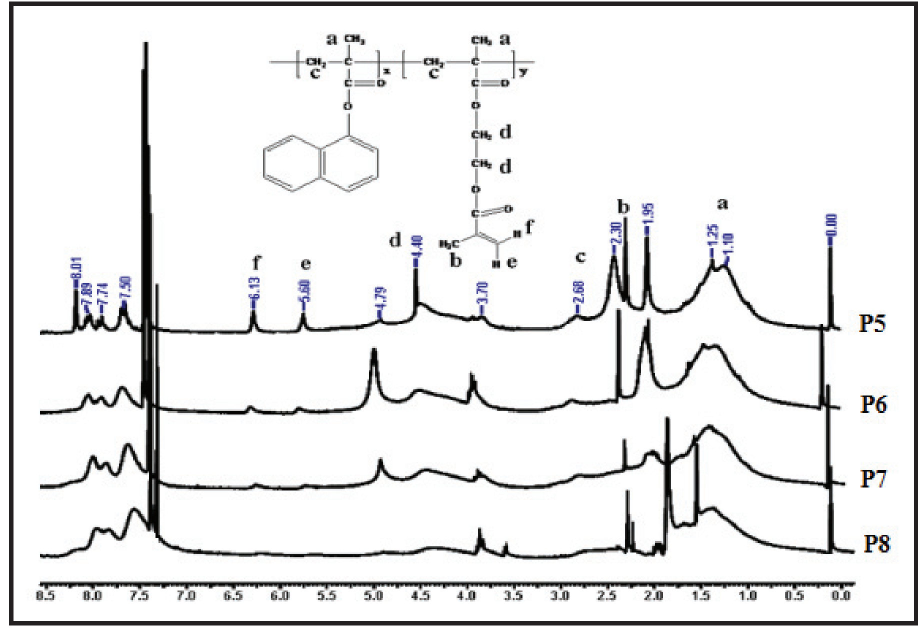

Figure 3.12: ^{1}H NMR spectra of polymers P5-P8

Peaks at 5.59 and 6.08 ppm (Figure 3.13, 3.14) correspond to vinyl protons of TMPTMA. Aromatic protons which correspond to CM appear in the range 6.99-7.21 ppm (Figures 3.11, 3.13) whereas, naphthalene ring protons appear in the range 7.3-8 ppm (Figure 3.12, 3.14). From the spectra it is clear that with increasing concentration of crosslinkers in the feed, intensity of vinyl protons in the polymer increases, while the peak intensity of the aromatic protons decreases. However in all the cases content

of the crosslinker in the polymer was lower than that in the feed. This is because the reactivity of the crosslinker is lowered as a result of inclusion complex formation. Similar results have been reported by Satav et al., (2006 and 2007).

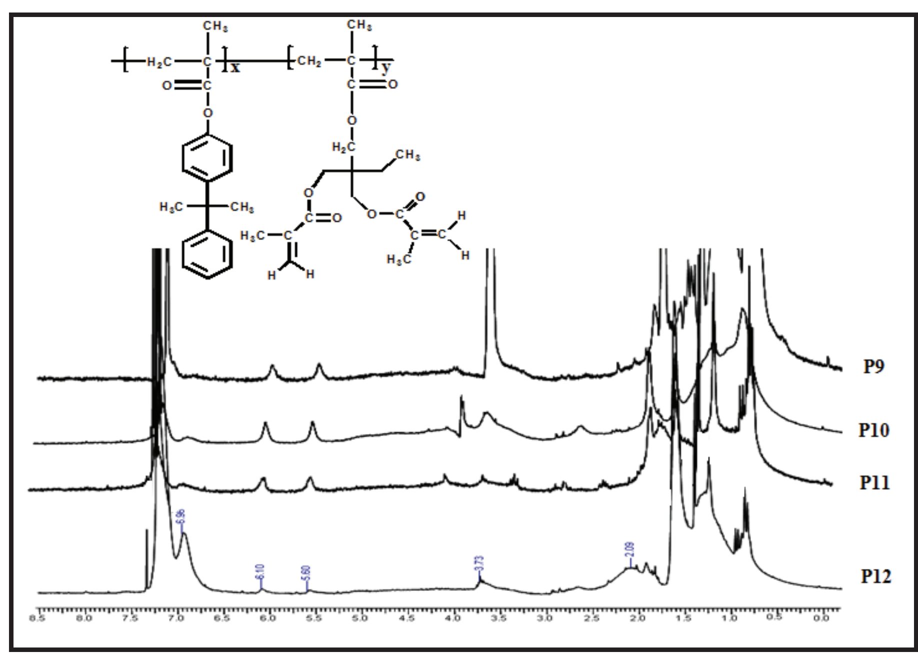

Figure 3.13: ^{1}H NMR spectra of polymers P9-P12

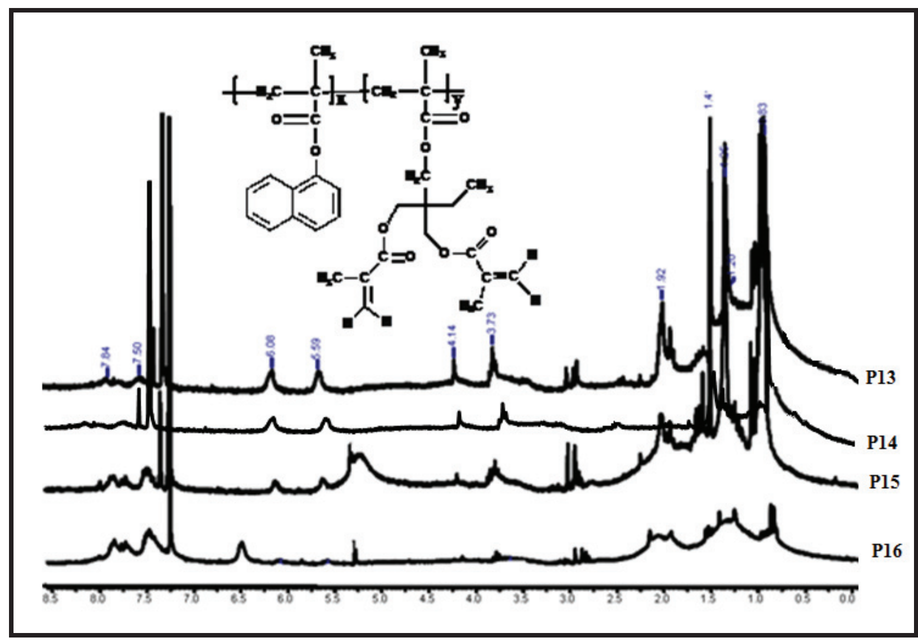

Figure 3.14: ^{1}H NMR spectra of polymers P13-P16

In all the cases incorporation of crosslinker content in the polymer is less than the feed. For any copolymerization system at a given feed composition incorporation of NM is lower than the CM, that is because of the reactivity of the NM is lower than CM. For any copolymerization system at a given feed composition the incorporation of TMPTMA is lower than that of EGDMA. This is because TPTMA forms 1:2 complex which is bulkier than the EGDA complex which is 1:1.

3.3.3.4. Thermal properties

3.3.3.4.1. Thermogravimetric analysis

Figures 3.15 to 3.18 show thermograms of the polymers P1, P5, P9 and P13 respectively. T_5 for Poly (CM-co-EGDMA) was greater than that for Poly (CM) only. This could be attributed crosslinking of EGDMA during heating, which increases thermal stability. T_5 therefore decreases as EGDMA content decreases. In the case of P4, thermal stability is lower than that of Poly (CM). This is because at 10 % incorporation of EGDMA, the enhancement in the thermal stability due to the copolymer crosslinking is not very effective.

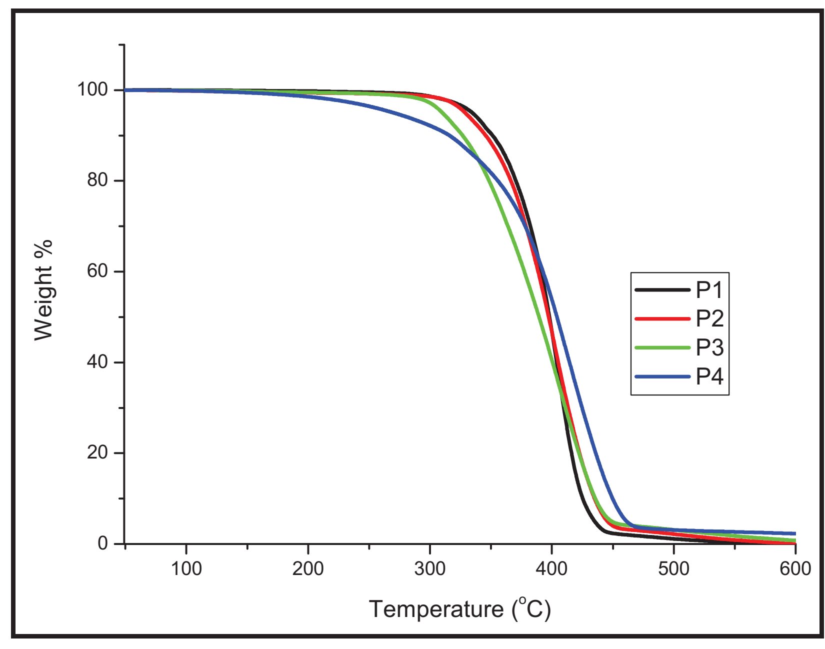

Figure 3.15: TGA thermograms of P1-P4

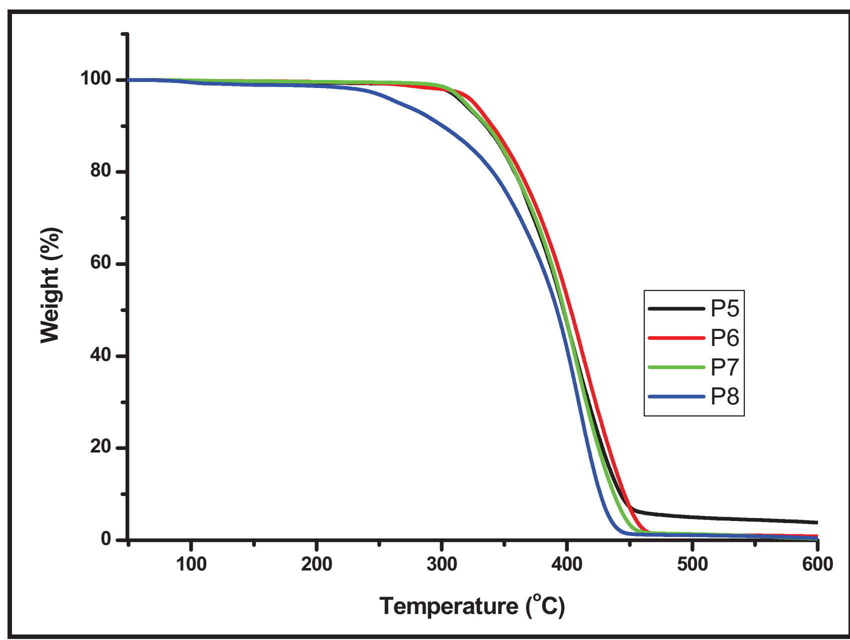

Figure 3.16: TGA thermograms of P5-P8

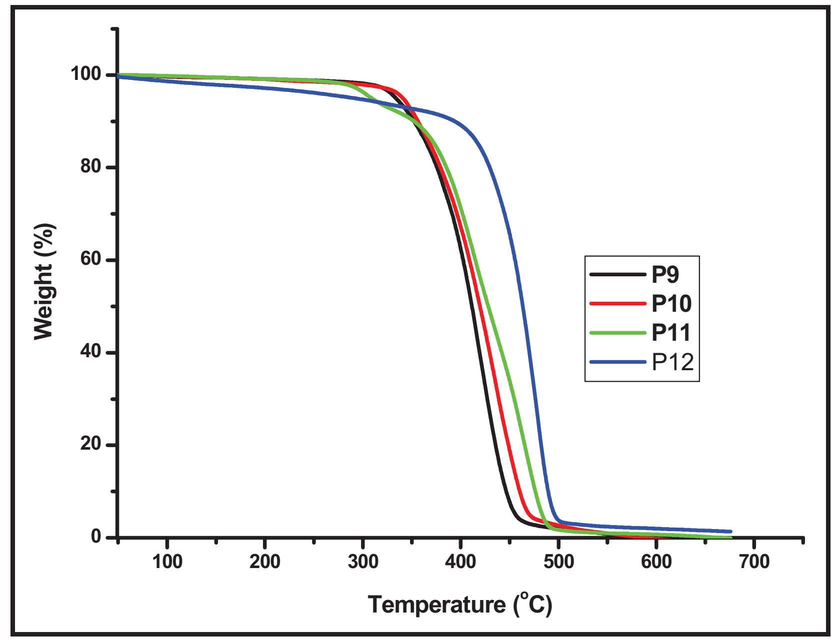

Figure 3.17: TGA thermograms of P9-P12

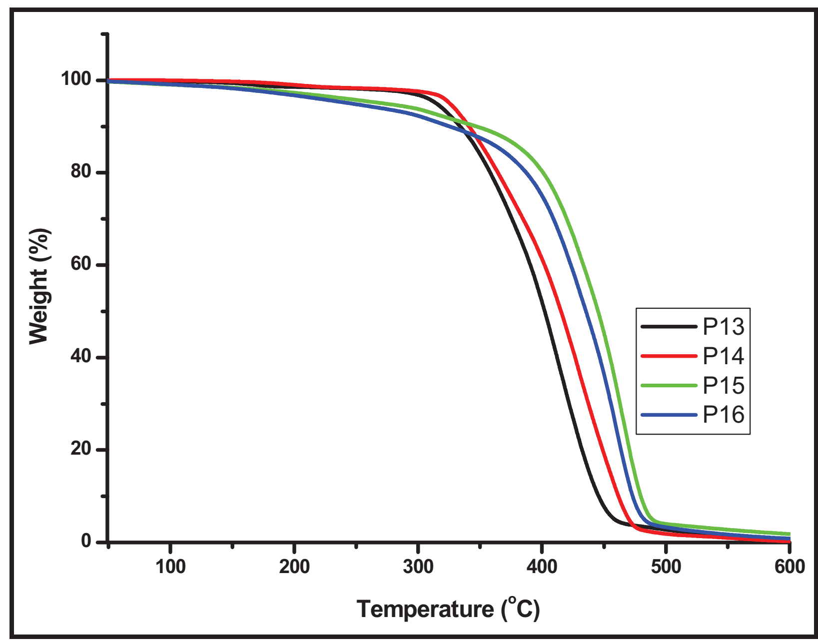

Figure 3.18: TGA thermograms of P13-P16

3.3.3.4.2. Glass transition temperature (T_g)

Thermograms for the copolymers P1, P5, P9 and P13 are shown in Figures 3.19-3.21. The values of the glass transition temperatures (T_g) of polymers are presented in Table 3.3. The T_g values for homopolymers of Poly (EGDMA) and Poly (TMPTMA) before crosslinking were 73.05 ^oC (Satav et al., 2006) and 41 ^oC (Satav et al., 2007) whereas for Poly (CM) and Poly (NM) the values are 97 ^oC and 103 ^oC respectively. From the above, it is seen that T_gs of aliphatic homopolymers (EGDMA and TMPTMA) are lower those that of aromatic homopolymers (CM and NM). This can be attributed to the fact that sterically rigid bulky moieties like CM and NM enhance T_g (Ratnaprabha and Daliya 2004; Pan et al., 2007). This also justifies our choice of monomers for the copolymer synthesis. The T_g of copolymers (125-198 ^oC) were found to be greater than those for corresponding homopolymers. This can be attributed to the crosslinking taking place during heating.

The copolymers synthesized in this work exhibited higher T_g than that for PMMA 105 ^oC (Kwak et al., 2007), and for Poly (MPAHEA-co-MMA) 122 ^oC (Lee and Hong, 2002). Homopolymers of methacryloyloxyethyl abietate (MAEA) showed T_g at 150 ^oC and copolymers of Poly (MMA-co-MAEA) exhibited T_gs in the range 134 to 146 ^oC depending on the composition (Kwak et al., 2007). Thus our results are comparable to those reported in the literature for methacrylate polymers containing

photocrosslinkable groups. Since the crosslinking densities in the case of TPTMA crosslinked polymers are higher than those of EGDMA crosslinked polymers. T_gs in these cases are too high to be detected.

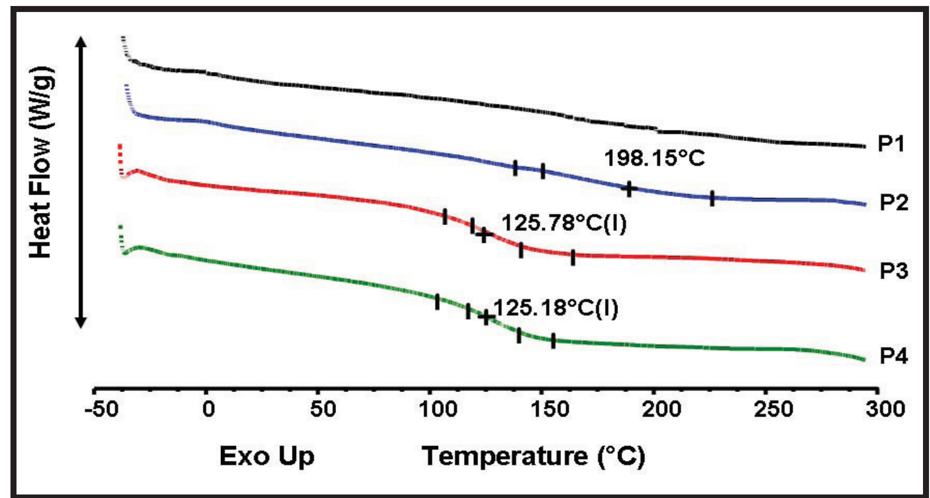

Figure 3.19: DSC thermograms of polymers P1-P4

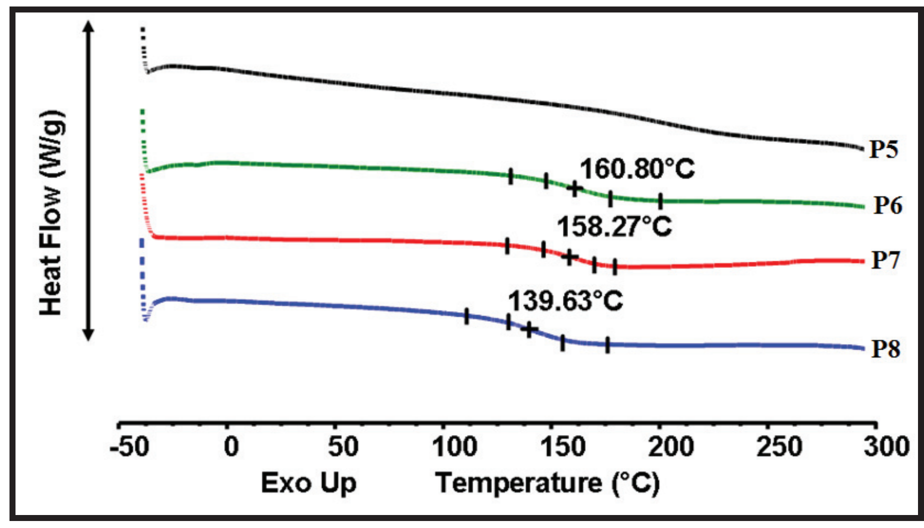

Figure 3.20: DSC thermograms of polymers P5-P8

As in Figure 3.19, the T_gs decreased with decreasing crosslinker content. The bulky geminal methyl groups in CM enhance the free volume of the system and lower T_g. Also corresponding decrease the crosslinker content also decreases crosslink density and their T_g. In contrast, in Figure 3.20 for NM containing copolymers, the NM itself being a bulky, fused ring structure provides rigidity. Hence poor mobility resulted in higher T_g. T_gs of the TMPTMA containing copolymers (Figure 3.21) follow the same argument as for the variation of crosslinker.

Table 3.3: Thermal properties of copolymers

Sr. No.	Polymer	T_g (°C)	$T_{5\%}$ wt loss (°C)
1	P1	*	334
2	P2	198	329
3	P3	126	310
4	P4	125	270
5	P5	*	317
6	P6	160.80	325
7	P7	158.27	318
8	P8	139.63	266
9	P9	*	333
10	P10	*	340
11	P11	*	308
12	P12	173.45	291
13	P13	*	314
24	P14	*	325
15	P15	*	271
16	P16	166	261
17	Poly-(CM)	93	293
18	Poly-(NM)	103	289
19	Poly-(EGDMA)	73	-
20	Poly-(TMPTMA)	49	-

*= T_g not observed

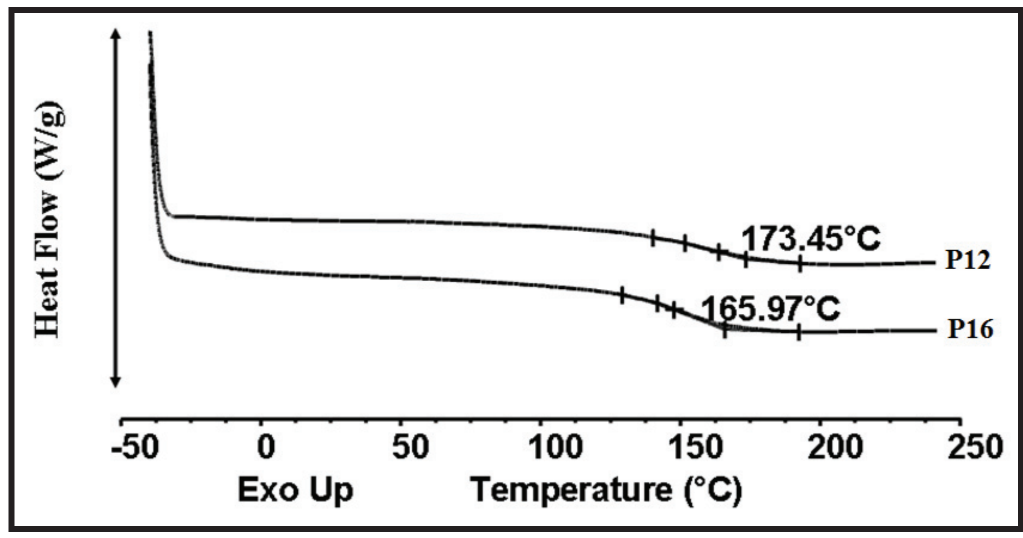

Figure 3.21: DSC Thermograms of polymers P12 and P16

In all the cases, T_g of TMPTMA based copolymers were higher than the corresponding copolymers based on EGDMA. This is to be expected since at the same crosslinker content, degree of crosslinking obtained in the TMPTMA copolymers is higher than that in the case of EGDMA based copolymers (Satav et al., 2006).

3.3.3.5. Transmittance studies

Photoresist must exhibit high transparency in visible region for application in display devices. Further during device fabrication processes resists are likely to exposed to higher temperatures and may undergo discoloration which results in loss of the transparency in the visible region. Figure 3.22 shows transmittance curves for P1, P5, P9 and P13 in the visible range 400-800 nm for polymer films prepared using formulation containing 20 wt % copolymer and 10 wt % PAG in γ-butyrolactone by drop casting. The films were exposed to 365 nm irradiation for 5 min and annealed for half an hour at 150 ^{o} C. The values of the thickness and transmittance are presented in Table 3.4.

The copolymer P1 exhibits excellent transmittance up to 94 % at a wavelength longer than 400 nm. These values are comparable to those for PMMA (92 %), inorganic glass (92 %) and poly-methacryloyloxyethyl abietate (90 %) (Kwak et al., 2007). Copolymers based on CM (P1 and P9) showed higher transmittance as compared to the NM based copolymers (P5 and P13) which are slightly colored and exhibit lower transmittance.

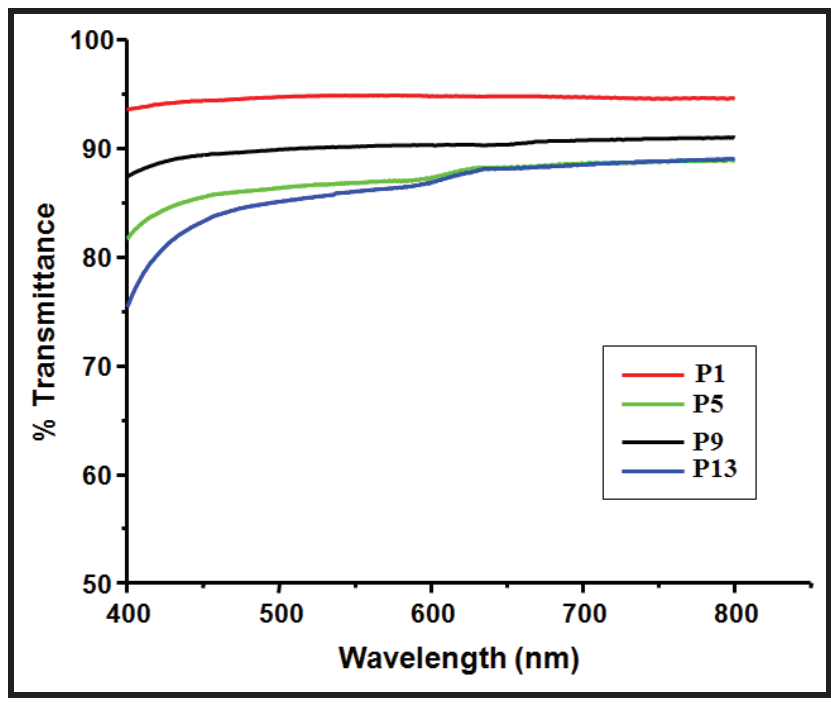

Figure 3.22: Transmittance of copolymers

Table 3.4: % Transmittance and film thickness

Sr. No.	Copolymers	Transmittance (%)	Thickness of film (mm)
1	P1	93.95	0.169
2	P5	87.49	0.149
3	P9	89.88	0.168
4	P13	86.98	0.174

3.3.3.6. Lithographic evaluation

3.3.3.6.1. Sensitivity curve

The sensitivity curves for the negative tone resists on exposure at 2 mW/cm^2 are shown in Figure 3.23. All the resists were formulated in γ-butyrolactone using 10 wt % copolymers and 10 wt. % 1-cyclohexyl phenyl ketone (Irgacure) on the basis of copolymer. The resists were spin coated on a silicon substrate and exposed to 365 nm

wavelength at intensity 2 mW/cm^2 upto 70 sec at 10 sec interval. The thicknesses of the patterned structures at various dose rates were measured using Raith 150^{Two} SEM.

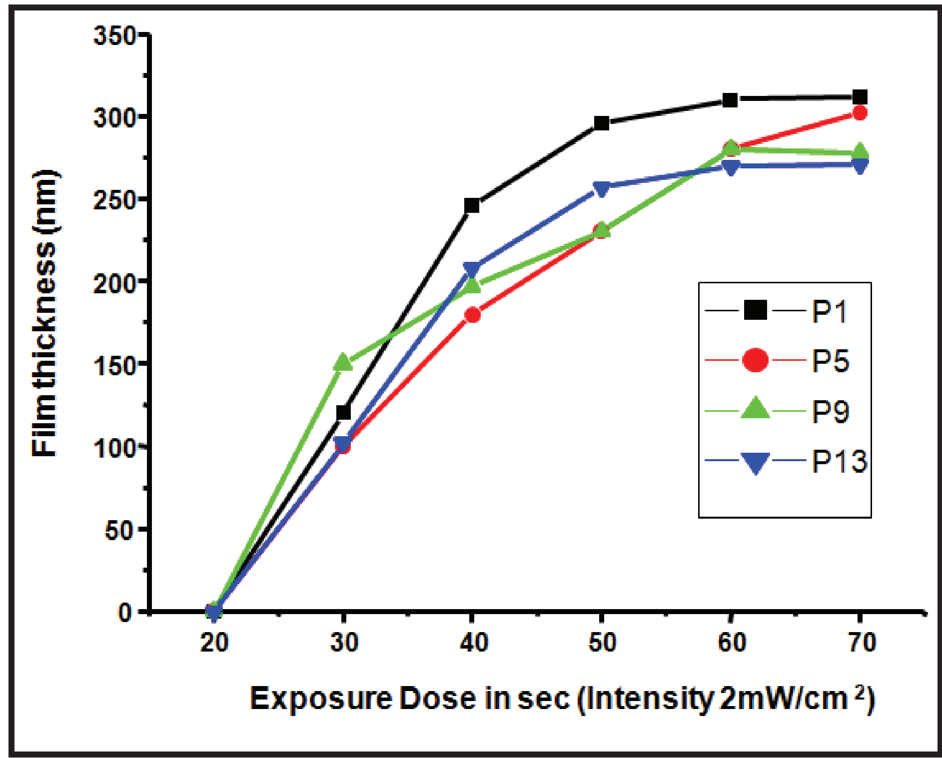

Figure 3.23: Characteristic UV-exposure curves

Sensitivity was defined as the dose at which thickness of the developed pattern was the same as that of the spin coated film. Copolymers containing CM (P1, P9) required 60 seconds exposure whereas copolymer containing NM (P5 and P13) required 60 and 70 sec exposure to reach the same thickness as the original film. P5 required 70 seconds exposure, since naphthalene containing resist are less reactive (Pan et al., 2007), whereas P13 required 60 sec exposure. Although, the P13 contains naphthalene which is less reactive, higher sensitivity may result from the incorporation of TMPTMA which enhances the crosslinking density.

3.3.3.6.2. Lithography

High T_g copolymers P1, P5, P9 and P13 were selected to investigate their performance as negative resist in optical lithography. For these experiments we used standard oxidized 2-inch silicon substrates to enhance adhesion of photoresist to the substrate. Resist containing 10 wt % copolymers and 10 wt % Irgacure based on

copolymers in γ-butyrolactone were spin coated at 3000 rpm. The coated samples were pre-baked on a hotplate at 60 °C for 5 min in order to avoid thermal crosslinking of the free vinyl groups. Resists P1, P9 and P13 were exposed to UV light using a soft-contact mask-aligner with an intensity of 2 mW/cm^2 at 365 nm wavelength for 60 sec, whereas P5 was exposed for 70 sec. Post exposure bake (PEB) was carried out at 50 ^oC for 10 min. The samples were then developed using propylene glycol methyl ether acetate for 60 sec, rinsed with IPA for 10 sec and dried with a nitrogen blower. We compared the performance of the polymers P1, P5, P9 and P13 for the lower feature sizes using mask containing line patterns at width ranging from 50 μ to 5 μ. Figures 3.24 to 3.27 show SEM images of the resist P1, P5, P9 and P13.

For all the polymer SEM images (Figures 3.24 to 3.27), the lithographic patterns were labelled as 50 μ lines at 50 μ spacing (a); 50 μ lines at 40 μ spacing (b); 50 μ lines at 30 μ spacing (c); 50 μ lines at 20 μ spacing (d); 50 μ lines at 10 μ spacing (e); 50 μ lines at 5 μ spacing (f); 40 μ lines at 40 μ spacing (g); 40 μ lines at 30 μ spacing (h); 40 μ lines at 20 μ spacing (i); 40 μ lines at 10 μ spacing (j); 40 μ lines at 5 μ spacing (k); 30 μ lines at 30 μ spacing (l); 30 μ lines at 20 μ spacing (m); 30 μ lines at 10 μ spacing (n); 30 μ lines at 5 μ spacing (o); 20 μ lines at 20 μ spacing (p); 20 μ lines at 20 μ spacing (q); 20 μ lines at 5 μ spacing (r); 10 μ lines at 10 μ spacing (s); 10 μ lines at 5 μ spacing (t).

From the SEM images it was seen that in all the cases lines upto 10 μ width could be resolved at spacing of 10 μ, while undeveloped lines were obtained in the case of lines at 5 μ width at 5 μ spacing. It may be noted that this does not necessarily reflect on the performance of the resins. During the fabrication of the mask, 5 μ line widths at 5 μ spacing were not resolved properly as a result of the limitation of the mask printing. Polymers based on CM show better lithographic performance as compared to NM based polymers. The pinholes obtained in the patterns in the case of NM polymers (Figures 3.28 and 3.29) are higher than in the case of the CM polymers.

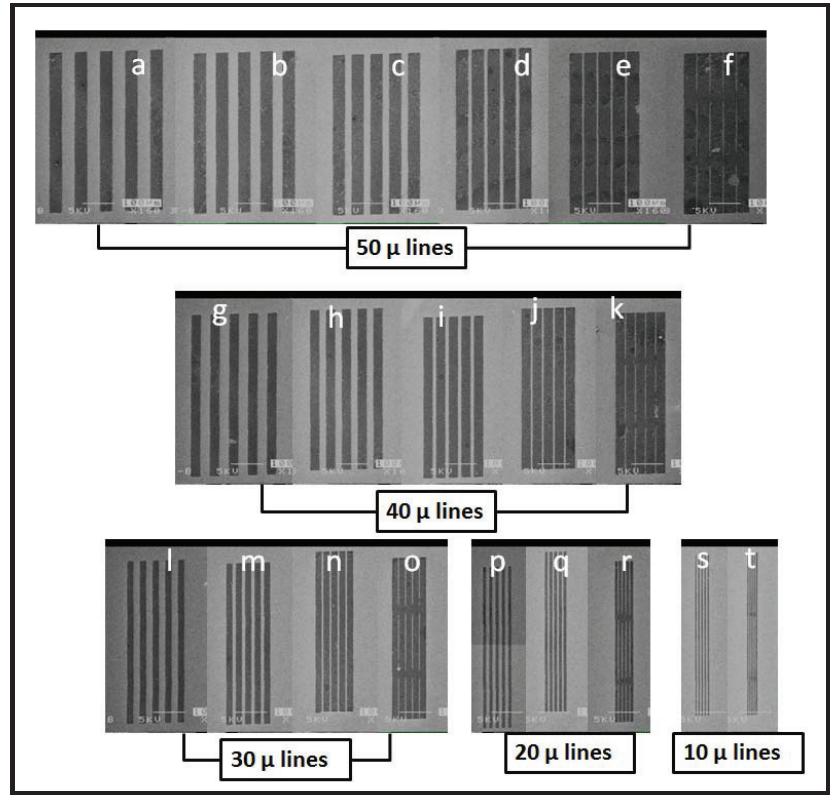

Figure 3.24: SEM images of Polymer P1.

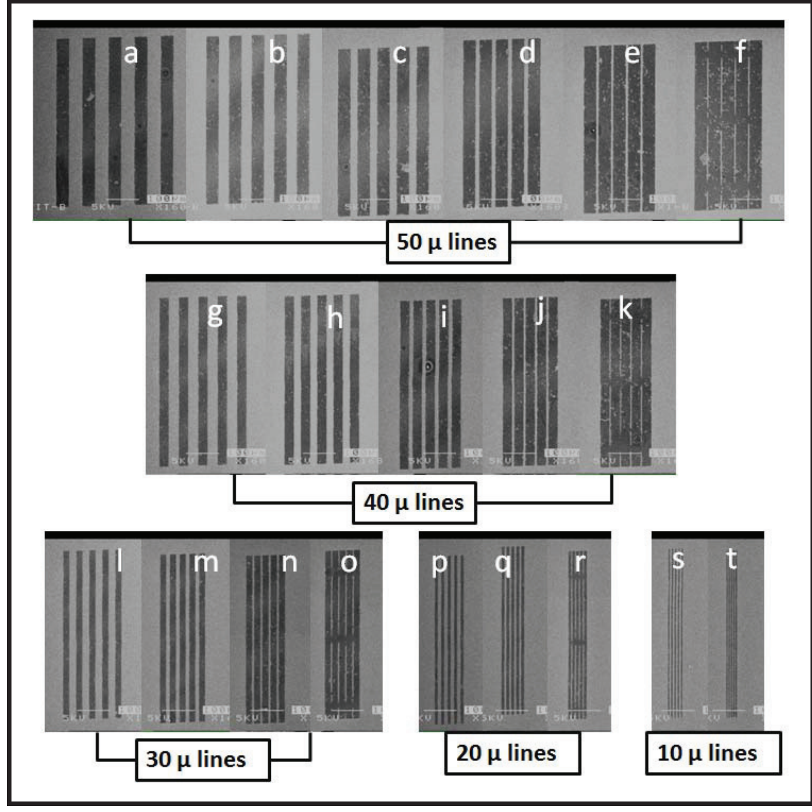

Figure 3.25: SEM images of Polymer P9.

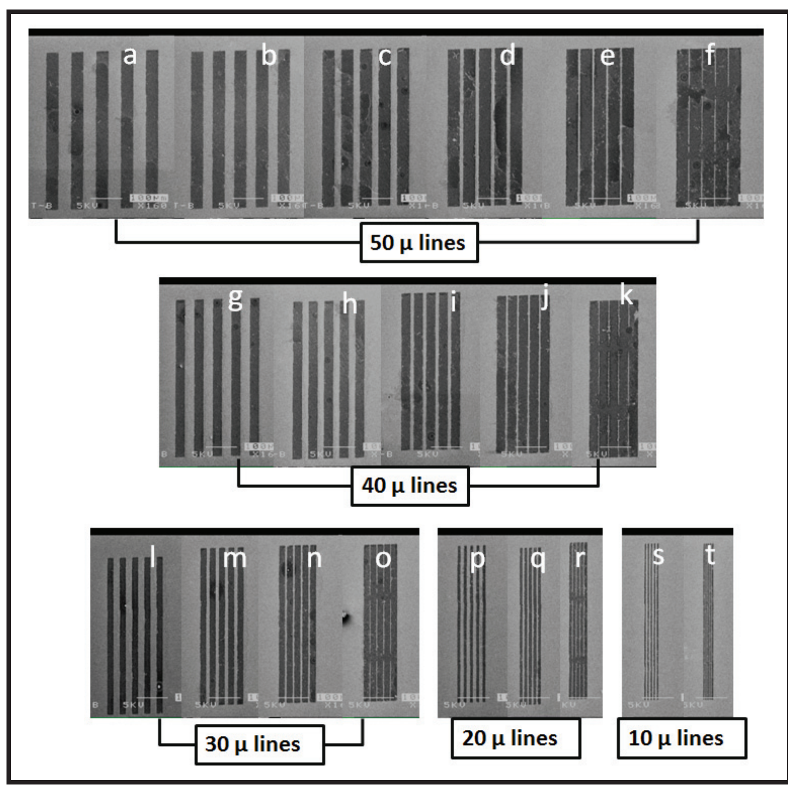

Figure 3.26: SEM images of Polymer P5.

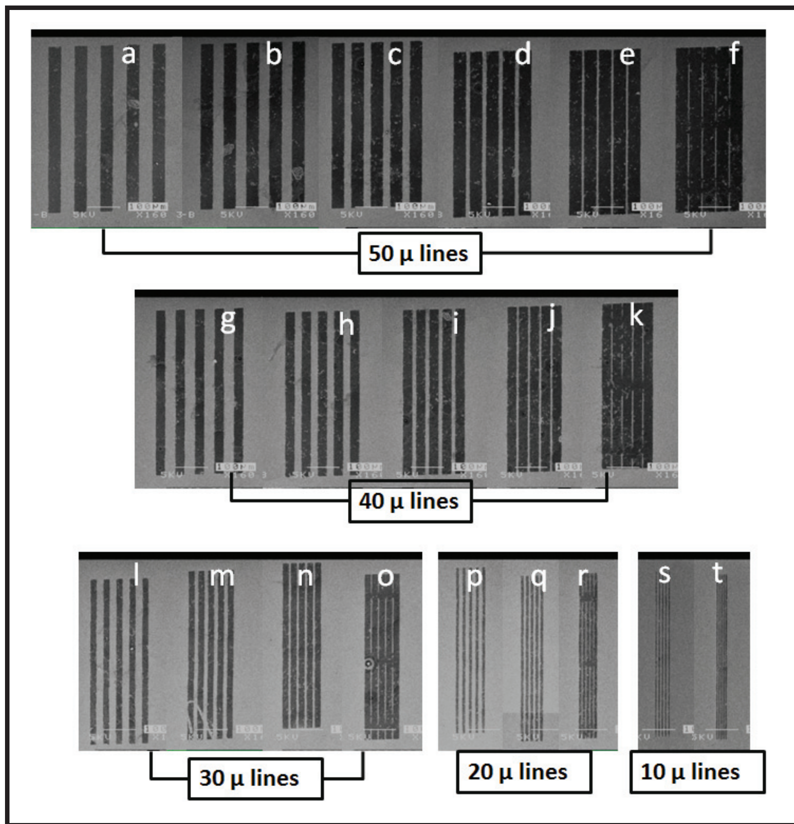

Figure 3.27: SEM images of Polymer P13.

Moreover, EGDMA based polymers show better lithographic performance compared to TMPTMA based polymers. We compared the performance of the polymers P1, P5, P9 and P13 for the complex mask designs containing three different shapes viz triangle (Δ), circle (○) and a square (□).

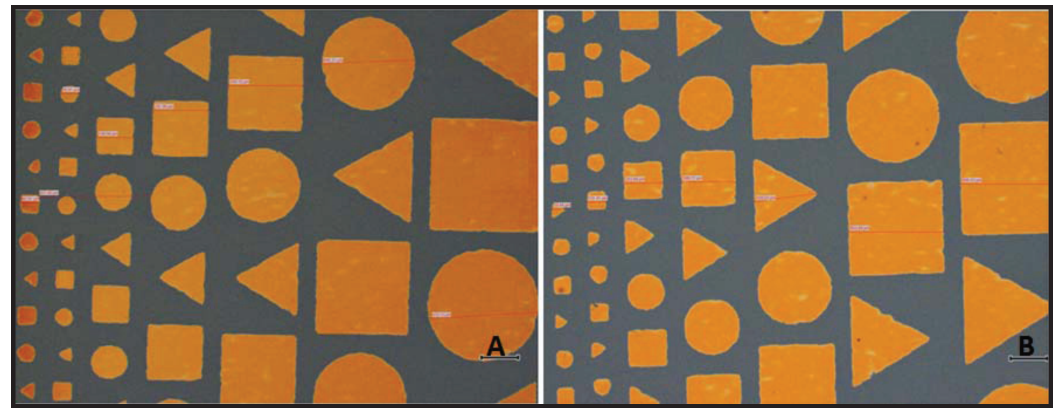

Figure 3.28: Images of resist P1 (A) and P9 (B)

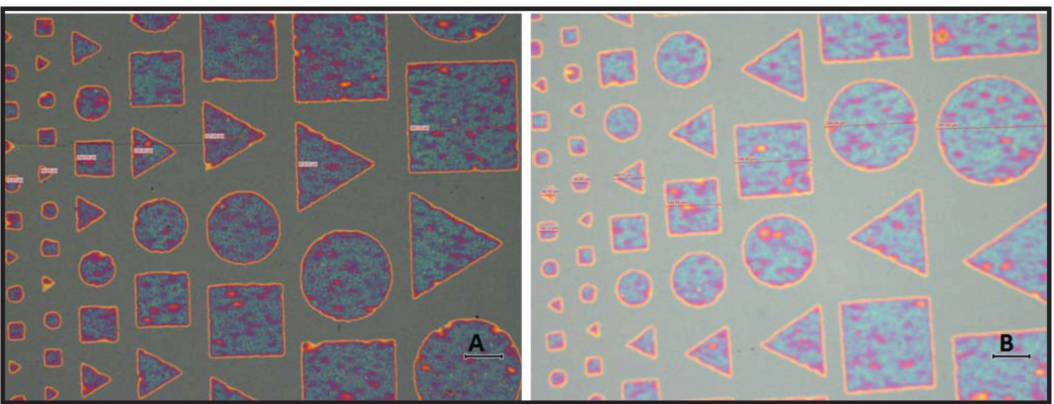

Figure 3.29: Images of resist P5 (A) and P13 (B)

Figures 3.28 A and B show colored optical images of the resist P1 and P9, whereas Figures 3.29 A and B show images of the resist P5 and P13 patterned through photolithography. It was found that P1 and P9 resists (Figures 3.28 A and B) show well resolved patterns up to 70 μ for all three shapes. Similarly, the structures obtained using P5 and P13 resolved similar features but showed roughness at the edges and pinholes (Figure 3.29 A and B). Thus lithographic performance of CM based copolymers is better than that of NM based copolymers.

3.4. Conclusion

Cumyl methacrylate and 1-naphthol methacrylate were copolymerized with cyclodextrin complexes of ethylene glycol dimethacrylate and trimethylol propane trimethacrylate to yield solvent soluble copolymers containing pendant vinyl unsaturations. The copolymers were characterized for thermal stability, glass transition temperature and transparency. $T_{5\%}$ at the copolymers was both function of the crosslinker content and the rigidity of the comonomers. The incorporation of aromatic methacrylate monomers enhanced both thermal stability and T_g of the copolymers. The lithographic evaluation showed that line patterns upto 10 μ width at the 10 μ spacing were resolved. It may be possible to resolve complex patterns at lower feature sizes. This needs to experimentally established.

3.5. References

1. Chen, H., Yin, J. Journal of Polymer Science: Part A: Polymer Chemistry 2004, **42**, 1735–1744.
2. Cyr, P. W., Rider, D. A., Kulbaba, K., Manners, I. Macromolecules, 2004, **37**, 11, 3959-3961.
3. De Silva, A., Ober, C. K. J. Mater. Chem., 2008, **18**, 1903–1910.
4. Duann, Y. F., Liu, T. M., Cheng, K. C., Su, W. F. Polymer Degradation and Stability 2004, **84**, 305-310.
5. Fang, S. W., Timpe, H. J., Gandini, A. Polymer 2002, **43**, 3505-3510.
6. Fisher, J. P., Holland, T. A., Dean, D., Mikos, A. G., Biomacromolecules 2003**, 4**, 1335-1342.
7. Han, E., In, I., Park, S. M., La, Y. H., Wang, Y., Nealey, P. F., Gopalan, P. Adv. Mater. 2007, **19**, 4448–4452.
8. Kaji, M., Nakahara, K., Ogami, K., Endo, T. Journal of Polymer Science: Part A: Polymer Chemistry, 1999, **37**, 3687–3693.
9. Koo, J.S., Smith, P. G. R., Williams, R. B. Chem. Mater. 2002**, 14**, 5030-5036.
10. Koo, J.S., Smith, P. G. R., Williams, R. B. Riziotis, C., Grossel, M. C. Optical Materials, 2003, **23**, 583–592.
11. Kwak, G., Choi, J. U., Seo, K. H., Park, L. S., Hyun, S. H., Kim, W. S. Chem. Mater. 2007**, 19**, 2898-2902.
12. Lee, S. J., Hong**,** S. I. European Polymer Journal, 2002, **38**, 387-392.
13. Pan, G., Du, Z., Zhang, C., Li, C., Yang, X., Li, H. Polymer 2007, **48,** 3686-3693.
14. Ratnaprabha, K., Daliya, P. K. Journal of Applied Polymer Science, 2005, **97**, 336–347.
15. Rehab, H. Eur. Polym. J. 1998, **34**, 12, 1845-1855.
16. Reichmanis, E., Thompson, L. F., Chem.Rev.1989, **89**, 1273-1289.
17. Reichmanis, E., Nalamasu, O., Houlihan, F. M. Acc. Chem. Res. 1999**, 32**, 659-667.
18. Reichmanis, E., Houlihan, F. M., Nalamasu, O., Neenan, T. X. Chem. Mater. 1991, **3**, 394-407.

19. Satav, S. S., Karmalkar, R. N., Kulkarni, M. G., Mulpuri, N., Sastry, G. N. J. Am. Chem. Soc. 2006, **128**, 7752-7753.
20. Satav, S. S., Karmalkar, R. N., Kulkarni, M. G., Mulpuri, N., Sastry, G. N. Macromolecules, 2007, **40**, 1824-1830.
21. Shirota, Y., Kageyama, H. Chem. Rev. 2007**, 107**, 953-1010.
22. Vijayanand, P. S., Kato, S., Satokawa, S., Kojima, T. Journal of Macromolecular Science, Part A: Pure and Applied Chemistry, 2007, **44**, 727–734.
23. Wu, H., Gonsalves, K. E. Adv. Mater. 2001, **13**, 3, 195-197.
24. Xu, K., Chen, M., Zhang, K., Hu, J. Polymer, 2004, **45**, 1133–1140.

Chapter 4

Synthesis, characterization and evaluation of linear polymers containing pendant epoxy groups as negative photoresist for optical lithography

4.1. Introduction

Polymers containing a photosensitive pendant epoxy moiety have been extensively used as photoresist materials (Reichmanis and Thompson, 1989). Efforts have been made to develop epoxy resins having good thermal stability, excellent chemical and corrosion resistance, mechanical and electrical properties, so that they find wide applications in electronics industry for printed circuits and as insulating materials (Pan et al., 2007). Increase in the number of epoxy groups and modification of the molecular backbone have been attempted to enhance the thermal and mechanical properties of epoxy resins (Wang and Lee., 1998). A number of epoxy resins based on aliphatic and aromatic monomers are commercially available. However, aliphatic epoxy resins are generally not preferred for applications in devices due to their low thermal stability (Reichmains et al., 1991).

SU-8 is a negative tone epoxy based photoresist most widely used in the fabrication of microstructures. Although SU-8 exhibits good lithographic performance, it also suffers from several disadvantages. Efforts are underway to develop materials which can overcome the limitations of SU-8 resist. Yang et al., (2007) came up with a new type of negative-tone photoresist based on blends of EPON resins 154 and 165 which differ in molecular weights. The two resins were mixed in gamma-butyrolactone in the ratio 40:60 and 50:50 respectively. The resists based on these blends could be used to fabricate microstructures with aspect-ratios >100 and ultra-thick resist layers of 1 mm suited for ultraviolet (UV) lithography.

In the previous chapter, we described resists containing latent crosslinking sites. β-Cyclodextrin complexes of EGDMA and TMPTMA were copolymerized with CM and NM comonomers to enhance the T_g of the copolymers. Thus methacrylate polymers, which are normally used as a positive resist, could be processed as a negative resist by incorporating latent crosslinking sites in the polymer structure. Negative tone patterns of 10 μm could be patterned by optical lithography.

In this chapter we report copolymers of CM and NM monomers and hydroxyl containing monomers, BPMA and 1, 5-DHNMA which are then converted into epoxy functionality so that the copolymers could be processed as negative resist using the same crosslinking chemistry as in SU-8. Depending upon the composition of the comonomers, polymers containing different levels of hydroxyl groups and hence the pendant epoxy groups were synthesized and evaluated as a negative resist for optical lithography. The advantages of this approach are ease of synthesis, isolation and

ability to manipulate crosslink density. The lithographic performance of the polymers based on bisphenol-A methacrylate was found to be comparable to that of SU-8 resins. These polymers would find applications in galvanoplating, sensors, photoresists, building micro fluidic structures and micro electro mechanical systems (MEMS).

4.2. Experimental

4.2.1. Materials

Bisphenol-A, 1-5-dihydroxy naphthalene, cumylphenol, 1-Naphthol, methacrylic acid, propylene glycol methyl ether acetate (PGMEA), triphenylsulfonium perfluoro-1-butanesulfonate (PAG) were obtained from Aldrich chemicals (USA). Benzyl chloride, sodium hydroxide (NaOH), Azo-bis-isobutyronitrile (AIBN), epichlorohydrin were procured from spectrochem. N, N-Dimethylformamide (DMF) obtained from Merck was distilled from CaH_2 under reduced pressure before use and all other reagents were used as received. Dichloromethane (DCM), tetrahydrofuran (THF), petether and ethyl acetate (EA) were from Merck chemicals.

4.2.2. Synthesis

4.2.2.1. Monomer synthesis

Synthesis of Cumyl methacrylate (CM) and 1-Naphthol methacrylate (NM) was discussed in chapter 3.

4.2.2.1.1. Bisphenol-A methacrylate (BPMA)

Bisphenol-A 10 g (4.3 X 10^{-2} moles) was dissolved in 70 ml THF, triethylamine 6.1 ml (4.3 X 10^{-2} moles) was added and stirred for 30 min. The reaction flask was then placed in an ice bath. Methacryloyl chloride 4.6 ml (4.3 X 10^{-2} moles) was added slowly such that the temperature of the reaction mixture was maintained between 0 ^{o}C to 5 ^{o}C. After addition was complete, the ice bath was removed and stirring was continued for 3-4 h. After completion of the reaction, the reaction mixture was extracted with ethyl acetate. The solvent was evaporated and the monomethacrylate monomer was recovered from the mixture of mono and dimethacrylate by column chromatography, using petroleum ether and ethyl acetate (95:05 v/v) as elutant. Yield was 9 g (70 %).

4.2.2.1.2. 1, 5-dihydroxynaphthalene methacrylate (1, 5-DHNMA)

1, 5-dihydroxynaphthalene methacrylate was prepared by the same method used for the preparation of BPMA using 1, 5-dihydroxynaphthalene 10 g (6.2 X 10^{-2} moles), 100 ml THF, triethylamine 8.8 ml (6.2 X 10^{-2} moles) as a base and methacryloyl chloride 6.5 ml (6.2 X 10^{-2} moles). Yield was 9.3 g (65%).

4.2.2.2. Homopolymer synthesis

4.2.2.2.1. Poly (BPMA)

5 g (1.68 X 10^{-2} moles) of bisphenol-A methacrylate was dissolved in 15 ml DMF. 0.1 g (2 wt %) AIBN initiator and 0.1 g (1.68 10^{-3} moles) (10 mole %) mercaptoethanol (chain transfer reagent) were added and stirred. Then nitrogen gas was purged for 30 minutes. The reaction was carried out for 12 hours at 65 ^{o}C in water bath. After complete reaction, the polymer was precipitated from methanol, filtered and dried under vacuum. Yield was 3.6 g (73%).

4.2.2.2.2. Poly (1, 5-DHNMA)

Poly (1, 5-Dhydroxynaphthalene methacrylate) was prepared using the same method described in section 2.2.2.1 from 5 g (3.1 X 10^{-2} moles) 1, 5-dihydroxynaphthalene methacrylate, 10 ml DMF, 0.1 g (2 wt %) AIBN initiator and 0.2 g (3.1 X 10^{-3}) mercaptoethanol. Yield was 3.3 g (67 %).

4.2.2.3. Copolymer synthesis

4.2.2.3.1. Poly (BPMA-co-CM) (70:30)

BPMA 5 g (1.68 X 10^{-2} moles) and CM 2 g (7.22 X 10^{-3} moles) were dissolved in 20 ml DMF. AIBN 0.14 g (2 wt %) was added as an initiator; 0.15 g (2.4 X 10^{-3} moles) (10 mole % on monomers) mercaptoethanol was used as a chain transfer reagent. The reaction was carried out at 65 ^{o}C in water bath for 24 hours. The polymer was precipitated from 70:30 v/v methanol: water. The polymer obtained was filtered and dried under vacuum. Yield 4.8 g (69 %).

Same synthetic procedure was used for all copolymer syntheses.

4.2.2.3.2. Poly (BPMA-co-CM) (50:50)

BPMA 3 g (1 X 10^{-2} moles), CM 2.9 g (1 X 10^{-2} moles), 20 ml DMF, AIBN 0.12 g (2 wt %), 0.12 g (2 X 10^{-3} moles) mercaptoethanol. Yield 3.9 g (67 %).

4.2.2.3.3. Poly (BPMA-co-CM) (30:70)

BPMA 2 g (6.70 X 10^{-3} moles), CM 4.4 g (1.57 X 10^{-2} moles), 20 ml DMF, AIBN 0.13 g (2 wt %), 0.14 g (2.2 X 10^{-3} moles) mercaptoethanol. Yield was 4 g (64 %).

4.2.2.3.4. Poly (1, 5-DHNMA-co-NM) (70:30)

1,5-DHNMA 5 g (2.2 X 10^{-2} moles), NM 2 g (9.4 X 10^{-3} moles), 20 ml DMF, AIBN 0.14 g (2 wt %), 0.2 g (3.1 X 10^{-3} moles) mercaptoethanol. Yield 4.6 g (66 %).

4.2.2.3.5. Poly (1, 5-DHNMA-co-NM) (50:50)

1,5-DHNMA 3 g (1.3 X 10^{-2} moles), NM 2.8 g (1.3 X 10^{-2} moles), 20 ml DMF, AIBN 0.12 g (2 wt %), 0.16 g (2.6 X 10^{-3} moles) mercaptoethanol. Yield 3.6 g (62 %).

4.2.2.3.6. Poly (1, 5-DHNMA-co-NM) (30:70)

1,5-DHNMA 2 g (8.7 X 10^{-3} moles), NM 4.3 g (2 X 10^{-2} moles), 20 ml DMF, AIBN 0.13 g (2 wt %), 0.17 g (2.8 X 10^{-3} moles) mercaptoethanol. Yield 3.6 g (62 %).

4.2.2.4. Epoxide conjugation

4.2.2.4.1. Poly (BPMA) epoxide

5 g (1.68 X 10^{-2} moles) Poly (BPMA), 0.1 g polyethylene glycol (PEG-400) as a phase transfer catalyst and 50 ml epichlorohydrin were added in to a 100 ml two necked flask equipped with stirrer. The reaction mixture was heated to 65 ^{o}C for one hour under nitrogen atmosphere. To this reaction mixture, dilute aqueous potassium hydroxide solution (KOH) 1.4 g (2.5 X 10^{-2} moles) in 10 ml water was added drop wise. After complete addition of alkali, the reaction was carried out for 2 h at 55 ^{o}C. The reaction mixture was then filtered and the organic phase was washed with water three times and dried over anhydrous sodium sulphate. Excess epichlorohydrin was subsequently distilled off to yield a semisolid mass which was precipitated from pet ether. The polymer was purified by dissolving it in to THF and reprecipitated from pet

ether to recover colourless polymer. All copolymers synthesized above were similarly conjugated to yield epoxide derivatives.

4.2.2.4.2. Poly (1, 5DHNMA) epoxide

Polymer was conjugated using procedure same as discussed in section 4.2.2.4.1 to yield epoxide derivatives.

4.2.3. Characterization

The ^{1}H-NMR spectra were recorded in $CDCl_3$ and DMSO-d_6 at 25°C on Bruker-200 MHz spectrometer. The Weight (M_w) and Number average (M_n) molecular weights of polymers were measured by gel permeation chromatography (GPC) using two polystyrene-DVB cross-linked gel columns 1 _ 60 cm 100 Å from PSS GmbH and chloroform as eluent at a flow rate of 1 mL min^{-1}. The differential scanning calorimetry (DSC) and thermo gravimetric analysis (TGA) were performed on TA Instrument DSC Q-10 and TGA-7 Perkin Elmer at a heating rate 10 ^{o}C/min. The resists were spin coated on silicon wafers at 3000 rpm. Optical litho tool, EVG 620 Automated Double Side Mask Aligner, Austria was used for resist patterning. Olympus optical microscope, Japan and Raith 150 ^{TWO}, Germany were used for imaging and thickness measurements.

4.2.4. Lithographic evaluation

The resists containing 14 wt % solutions in PGMEA were used to match the composition of SU-8 (2000.5). Commercially available triarylsulphonium hexafluoroantimonate (PAG) which is also used in SU-8 (2000.5), 10 wt % on the basis of polymers, was added. SU-8 (2000.5) was used as the standard resist for comparison. The polymer resists were spin coated on silicon wafers at 3000 rpm. SU-8 (2000.5) was first spin-coated onto the substrate to form a resist layer 460 nm thick. The thicknesses of the resists based on polymers P1-P8 are summarized in Table 4.3. Coated samples were pre-baked on a hotplate at 70 °C for 5 min and 90 ^{o}C for 1 min. Samples were exposed to UV light using a soft-contact mask-aligner of 60 mJ/cm^2 intensity at 365 nm wavelength for 5 sec. Post exposure bake (PEB) was carried out at 60 ^{o}C for 1 min and 95 ^{o}C for 1 min. The patterns were developed for 30 sec using PGMEA (SU-8 developer) at room temperature. The patterns were then rinsed with isopropanol and dried with a nitrogen blower.

4.3. Results and Discussion

4.3.1. Choice of the system

Polymethyl methacrylate (PMMA) is established as a positive working photoresist. To convert methacrylate based polymers into negative photoresist, MMA can be copolymerized with aliphatic comonomers such as HEMA, EGDMA and TMPTMA. Resists containing aliphatic methacrylate exhibit lower T_gs and are therefore not preferred (Reichmanis et al., 1991). To increase T_g and thermal stability, methacrylate based polymers, bulky and rigid moieties such as biphenyl, triphenyl and naphthalene need to be incorporated in the structure (Shirota, 2005). Kwak et al., (2007) synthesized negative resists by copolymerising methyl methacrylate and methacryloyloxyethyl abietate having T_g 149 ^oC. These negative resists resolved patterns upto 30 µm. Rehab (1998) developed methacrylate based negative photoresist containing pendant crosslinkable chalcone moiety. Negative resists based on epoxy acrylates of bisphenol-A diglycidyl ether and epoxy novolac showed good adhesion, hardness and chemical resistance (Chattopadhyay et al., 2005). The limitations of the novolac resins are their low T_g in the range of 70-120 ^oC (Reichmanis and Thompson, 1987). Therefore, it would be desirable to design and synthesize high T_g materials having crosslinking chemistry similar to that of novolac resins.

In this chapter we report design of negative photoresist based on bisphenol-A and 1, 5-dihydroxynaphthalene methacrylate. These monomers were copolymerized in varying ratios with CM and NM respectively to manipulate pendant hydroxyl group content. The polymers were further conjugated with epichlorohydrin to yield epoxide functionalities for crosslinking during processing. These architectures demonstrate the role of T_g and crosslink density on the resist performance in optical lithography.

4.3.2. Synthesis of epoxy conjugated polymers

The schematic procedures for the synthesis of epoxy modified polymers are outlined in Figures 4.1 and 4.2. Polymers were prepared by free-radical polymerization of BPMA with CM and 1, 5-DHNMA with NM in DMF varying molar feed ratios. The polymers were then reacted with excess epichlorohydrin to convert the pendant hydroxyl to epoxide groups. This approach was necessary since the efforts to vary

epoxide contents in homopolymers of Poly (BPMA) and Poly (1, 5-DHNMA) by varying the amount of epichlorohydrin resulted in crosslinked polymers.

Figure 4.1: Synthesis of bisphenol-A based polymers containing pendant epoxy groups: A) Methacryloyl chloride, TEA, THF; B) AIBN, DMF, 65°C; C) AIBN, CM, DMF, 65°C; D) KOH, polyethylene glycol-400, epichlorohydrin.

Figure 4.2: Synthesis of 1,5-dihydroxynaphthalene based polymers containing pendant epoxy groups: A) Methacryloyl chloride, TEA, THF; B) AIBN, DMF, 65°C; C) AIBN, NM, DMF, 65°C; D) KOH, polyethylene glycol-400, pichlorohydrin.

4.3.3. Polymer characterization

4.3.3.1. Solubility

Polymers containing pendant hydroxyl groups were soluble in most organic solvents including epichlorohydrin, acetone, ethyl acetate, γ-butyrolactone, THF, dimethylsulphoxide (DMSO), N, N-dimethylformamide (DMF). Epoxide conjugated polymers were readily soluble in most of the solvents commonly used for photoresist processing such as γ-butyrolactone, ethyl lactate, propylene glycol methyl ether acetate (PGMEA) and cyclopentanone, but were insoluble in methanol and ethanol.

4.3.3.2. Molecular weights

The weight average molecular weight (M_w), number average molecular weight (M_n) and the polydispersity index (M_w/M_n) of the polymers were determined using gel permeation chromatography in chloroform. Molecular weight for Poly (BPMA-co-CM) was 140000 and for Poly (1, 5-DHNM-co-NM) 80000. Such high molecular weights resulted in high solution viscosities which limited the film thickness which could be achieved during spin coating of films for resist applications. Molecular weights of the polymers were therefore regulated using 10 mole % mercaptoethanol as a chain transfer agent, values are summarized in Table 4.1 and 4.2. As a result, molecular weights could be lowered from 140000 to around 9000 in case of Poly (BPMA-co-CM) epoxide copolymers, and from 80000 to around 6000 for Poly (1, 5-DHNM-co-NM) epoxide.

Table 4.1: Molecular weights of Poly (BPMA-co-CM) epoxide

Polymer	BPMA:CM	M_w	M_n	M_w/M_n
P1	100 : 00	14000	8410	1.67
P2	70 : 30	14600	8120	1.84
P3	50 : 50	17300	9010	1.93
P4	30 : 70	18300	10500	1.75

Table 4.2: Molecular weights of Poly (1, 5-DHNMA-co-NM) epoxide

Polymer	1,5-DHNMA: NM	M_w	M_n	M_w/M_n
P5	100 : 00	11800	6330	1.87
P6	70 : 30	13400	7590	1.77
P7	50 : 50	17100	8340	2.05
P8	30 : 70	14000	6710	2.09

4.3.3.3. ^{1}H NMR spectroscopy

4.3.3.3.1. ^{1}H NMR of BPMA and 1, 5-DHNMA

Figure 4.3 shows ^{1}H-NMR spectrum of BPMA monomer in DMSO-d_6. Peak at 1.58 ppm corresponds to the geminal methyl protons of bisphenol-A.

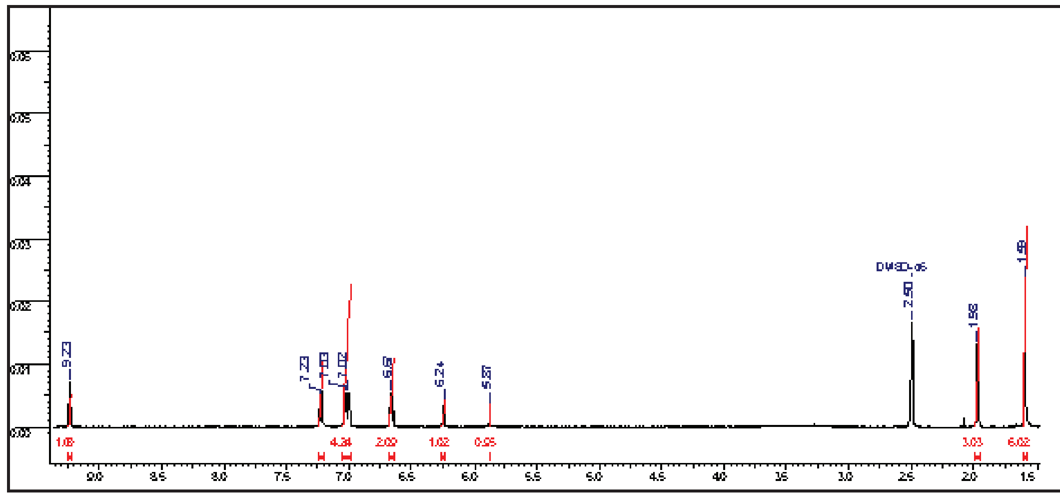

Figure 4.3: ^{1}H NMR spectra of BPMA

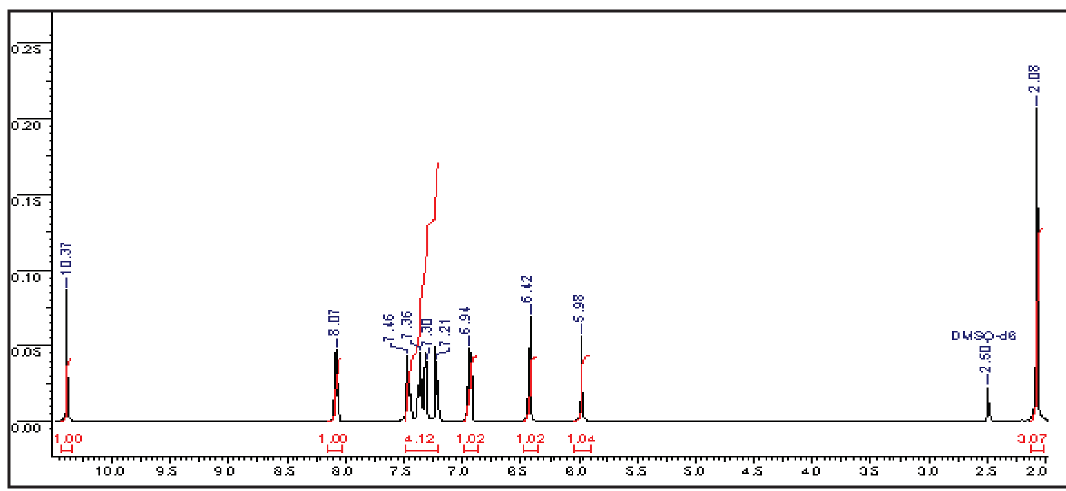

Figure 4.4: ^{1}H NMR spectra of 1, 5-DHNMA

Peaks in the range 6.6-7.23 ppm correspond to the aromatic protons. Peak at 1.96 ppm is attributed to the methyl protons adjacent to the vinyl unsaturation. The peaks at 5.82 ppm and 6.24 ppm correspond to vinyl unsaturation and peak at 9.23 ppm corresponds to the hydroxyl proton. Thus ^{1}H NMR confirmed that only one of the hydroxyl groups of the bisphenol moiety is converted to its methacrylate ester.

Figure 4.4 shows ^{1}H-NMR spectrum of 1, 5-DHNMA monomer in DMSO-d_6. Peak at 2.08 ppm corresponds to the methyl protons adjacent to the vinyl unsaturation. The peaks at 5.98 and 6.42 ppm correspond to the vinyl unsaturation and peak at 10.37 ppm corresponds to the hydroxyl proton. Peaks in the range 6.94-8.07 ppm correspond to the naphthalene ring protons.

4.3.3.3.2. ^{1}H NMR of Poly (BPMA) and Poly (1, 5-DHNMA) before and after epoxide conjugation

Figures 4.5 and 4.6 show ^{1}H-NMR spectra of Poly (BPMA) and Poly (BPMA) epoxide respectively.

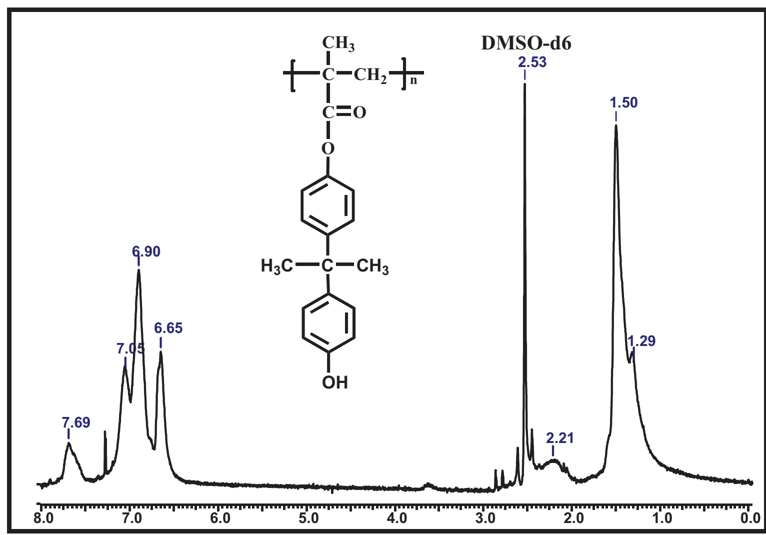

Figure 4.5: ^{1}H NMR spectra of Poly (BPMA)

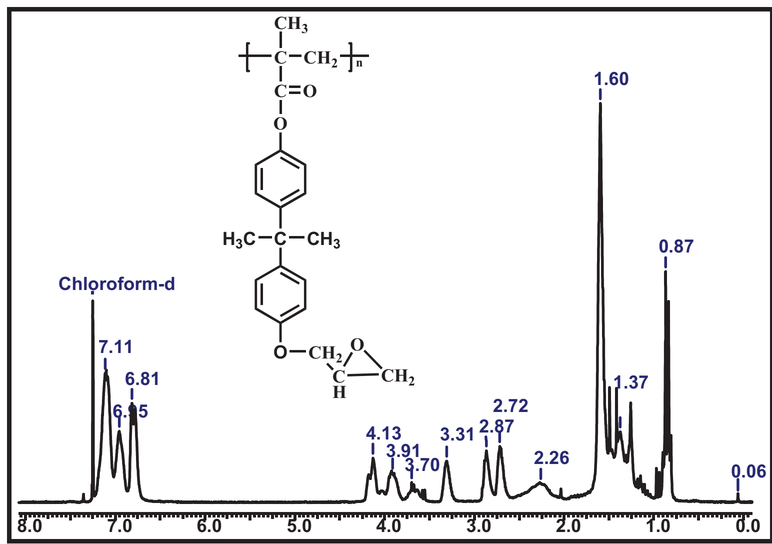

Figure 4.6: ^{1}H NMR spectra Poly (BPMA) epoxide

Chemical shifts at 1.29 ppm and 1.5 ppm correspond to three methyl protons of polymer backbone and six geminal methyl protons of bisphenol units. Similarly peaks at 2.21 ppm correspond to two methylene protons in the backbone of the chain (-CH_2) (Figure 4.5). In Figure 4.6 signals at 2.72 to 4.13 ppm crosspond to the protons of the pendant epoxy moiety. Aromatic protons corresponding to the bisphenol-A moiety

appear in the range 6.81-7.11ppm. There is no peak corresponding to the free hydroxyl group which confirms complete conversion to epoxide.

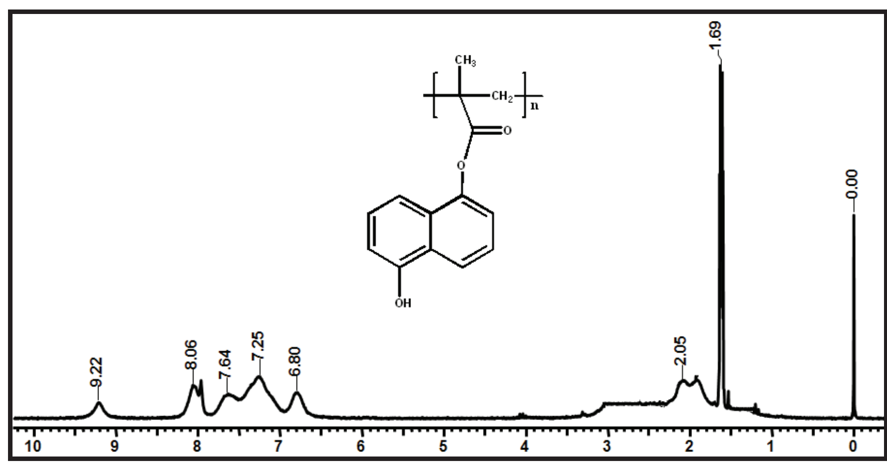

Figure 4.7: ^{1}H NMR spectra of Poly (1, 5-DHNMA)

Figure 4.7 shows the ^{1}H-NMR spectrum of Poly (1, 5-DHNMA) containing pendant free hydroxyl groups. Signals at 6.8-8.05 ppm correspond to the naphthalene ring protons. The backbone methylene (-CH_2) proton signals appear at 2.05 ppm. Signal at 9.22 ppm corresponds to the free hydroxyl groups. Figure 4.8 shows the ^{1}H-NMR spectrum of Poly (1, 5-DHNMA) epoxide. Peaks at 2.65-4.07 ppm correspond to the epoxide ring protons, which confirm the conversion of hydroxyl to epoxide group.

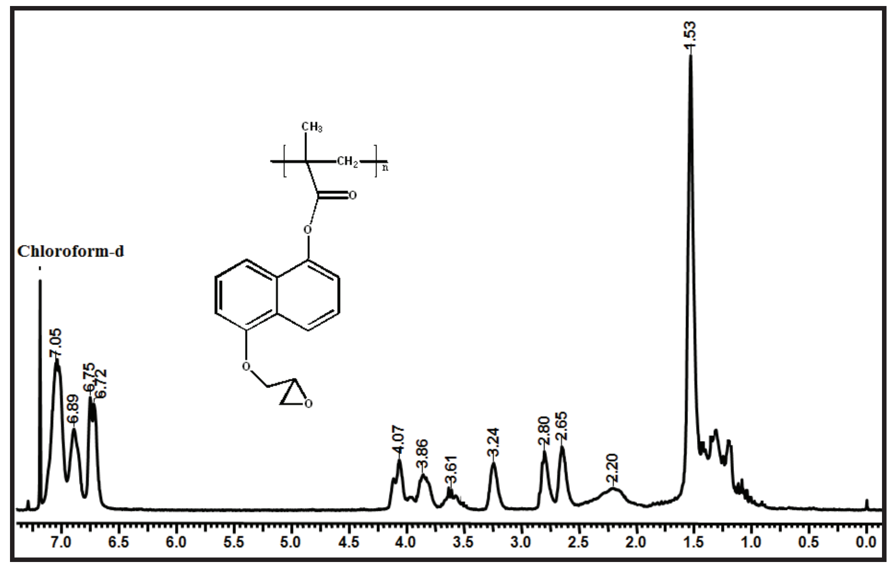

Figure 4.8: ^{1}H NMR spectra of Poly (1, 5-DHNMA) epoxide

4.3.3.4. Thermal properties

4.3.3.4.1. Thermogravimetric analysis (TGA)

The thermograms of epoxy conjugated polymers are shown in Figures 4.9 (P1-P4) and 4.10 (P5-P8) respectively. The temperature T_5 corresponding to 5 wt % loss was considered as the index of thermal stability. Values are summarized in Table 4.3. The TGA curves show that the polymers are thermally stable upto 300 ^{o}C owing to the rigid aromatic moieties and decompose in a single stage thereafter.

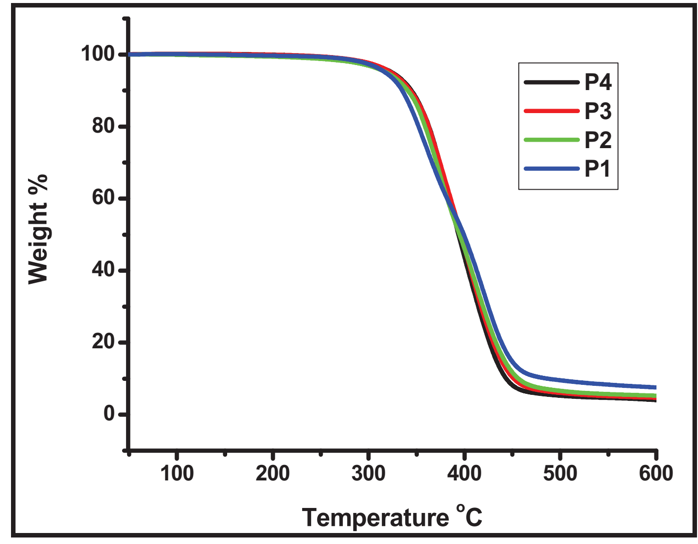

Figure 4.9: Thermograms of P1-P4

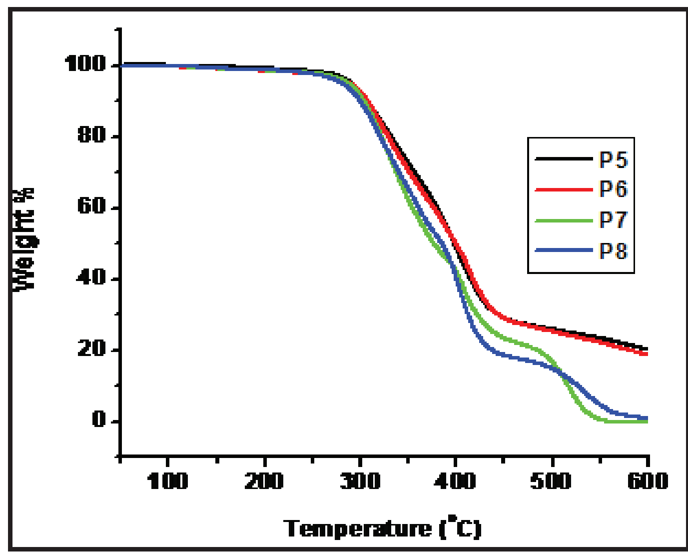

Figure 4.10: Thermograms of P5-P8

There is no significant difference in thermal stability of Poly (BPMA) and Poly (1,5-DHNMA). After epoxide conjgation, polymers based on bisphenol-A (P1-P4) undergo decomposition at relatively higher temperature than the polymers containing naphthalene moiety (P5-P8). The two methyl groups at the geminal position in the bisphenol moiety enhance molecular rigidity and hence thermal stability of the copolymers.

4.3.3.4.2. Glass transition temperature (T_g)

The thermal behaviour of the epoxy conjugated methacrylate copolymers was investigated by differential scanning calorimetry. DSC results summarized in Table 4.3 indicate that before crosslinking, polymers containing bisphenol-A (Figure 4.11 a) show lower T_gs compared to the polymers containing naphthalene (Figure 4.11 c). The geminal methyl groups in bisphenol-A and cumylphenol units increase free volume in the molecule, resulting in lower T_g (Uthirakumar et al., 2005). In contrast, fused ring structures of naphthalene are more rigid, which restrict chain rotation leading to higher T_g (Xu et al., 2004; Wang and Lee., 1998).

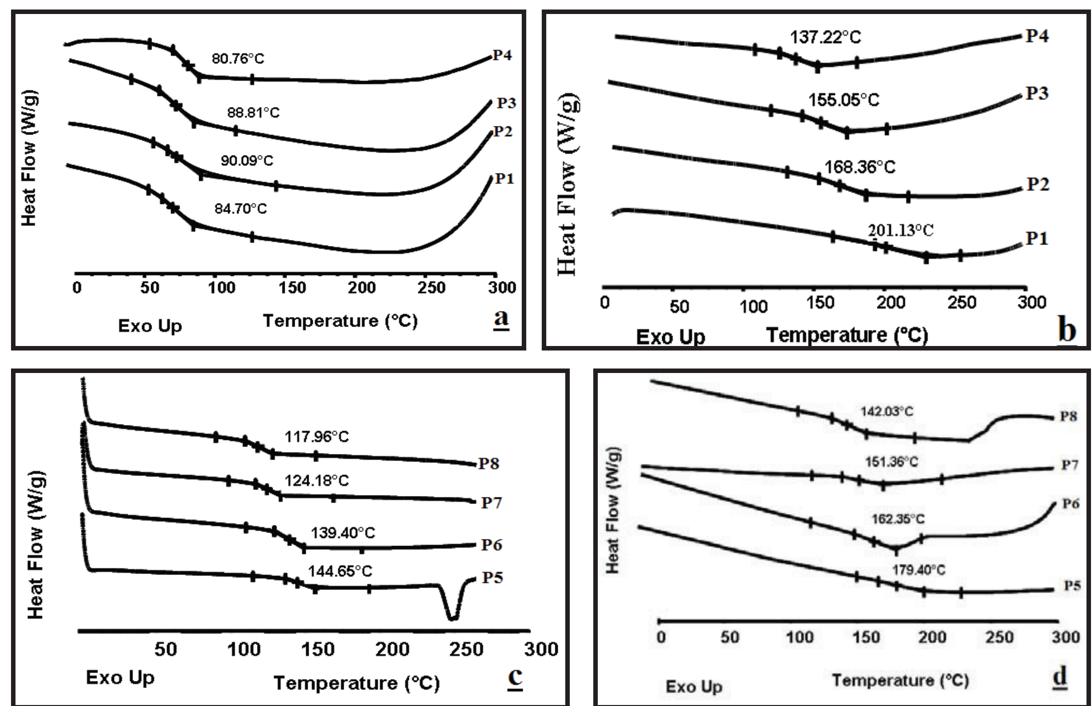

Figure 4.11: DSC thermograms of polymers P1-P4 before **(a)** and after **(b)** photocrosslinking P5-P8 before **(c)** and after **(d)** photocrosslinking.

The T_gs of the epoxide conjugated polymers containing bisphenol-A before crosslinking were found to be in the range 80-90 ^oC but did not exhibit a trend. The T_gs of the same polymers after crosslinking were found to decrease in the order P1> P2> P3>P4, which followed the same order as the degree of crosslinking (Wang and Lee., 2000). Polymers containing naphthalene moiety followed the same order. Upon crosslinking the geminal methyl groups in polymers P1-P4 (Figure 4.11 b) help in enhancing the T_g by increasing rigidity of the system and therefore these polymers show higher thermal stability as compared to P5-P8 (Figure 4.11 d).

Table 4.3: Characterization of Polymers

Polymer	Film thickness (nm)	(T_gs) (before crosslink) ^oC	(T_gs) (after crosslinking) ^oC	TGA at 5 wt % ^oC
P1	512	84.70	201.13	318
P2	507	90.09	168.36	319
P3	510	88.81	155.05	324
P4	518	80.76	137.22	325
P5	461	144.65	179.40	290
P6	470	139.40	162.36	289
P7	466	124.18	151.36	287
P8	457	117.96	142.03	280
p-BPMA	-	93	-	293
P-1,5-DHNMA	-	103	-	289
SU-8	460	50	200	-

4.3.4. Lithography

The goal of this investigation was to evaluate the effect of epoxy group density on the lithographic performance of the polymers. UV lithography was performed using the DSA tool, which is capable of fabricating 1μ features.

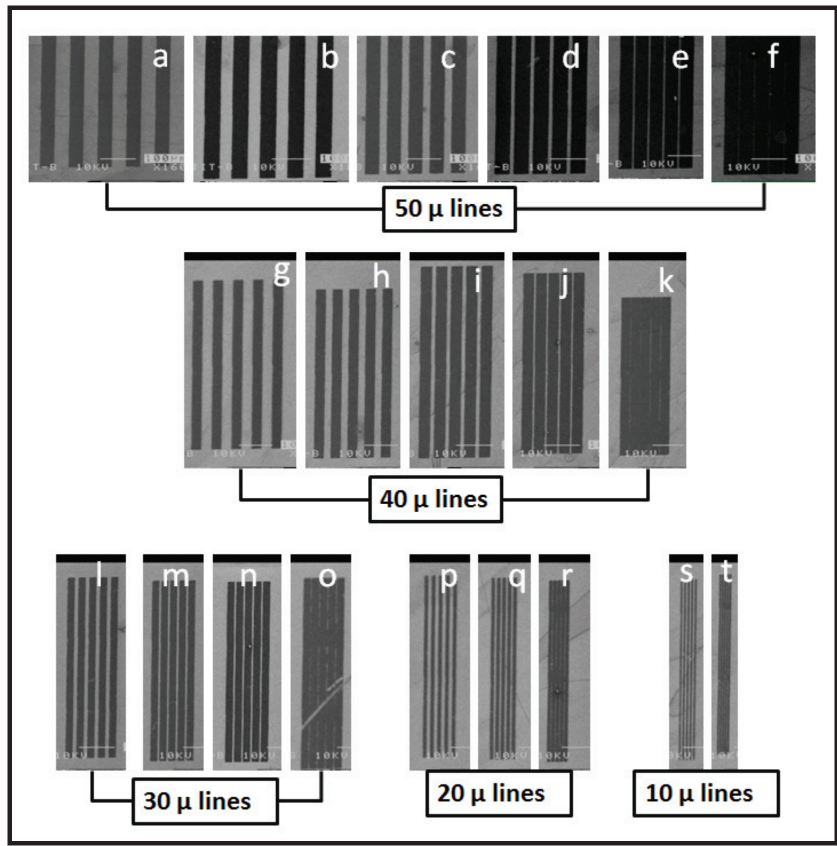

Figure 4.12: SEM images of P1

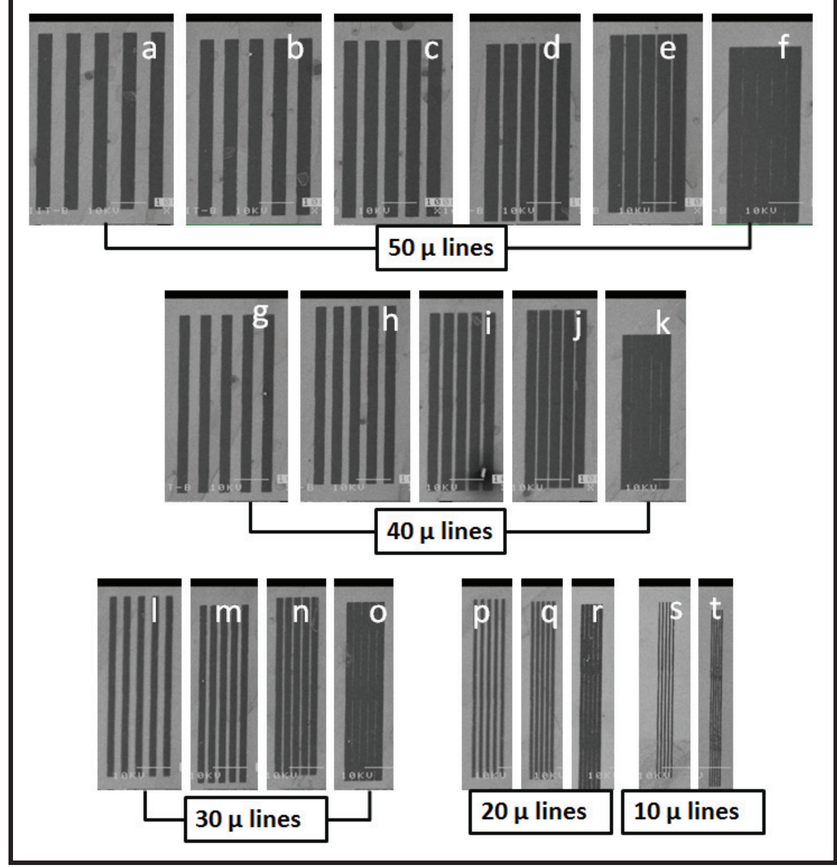

Figure 4.13: SEM images of P2

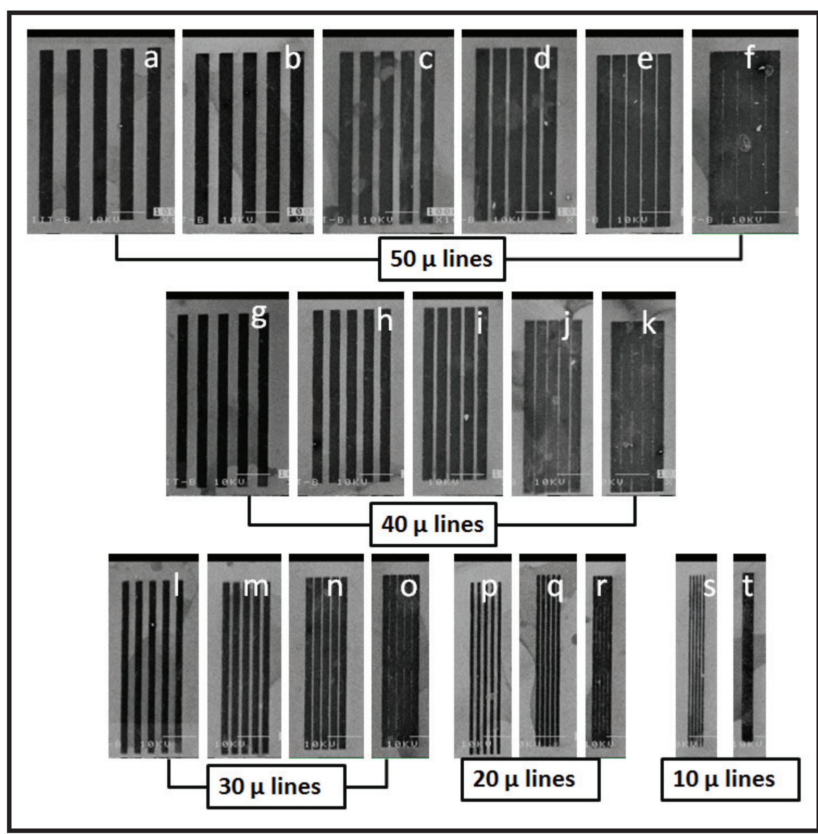

Figure 4.14: SEM images of the resist P5

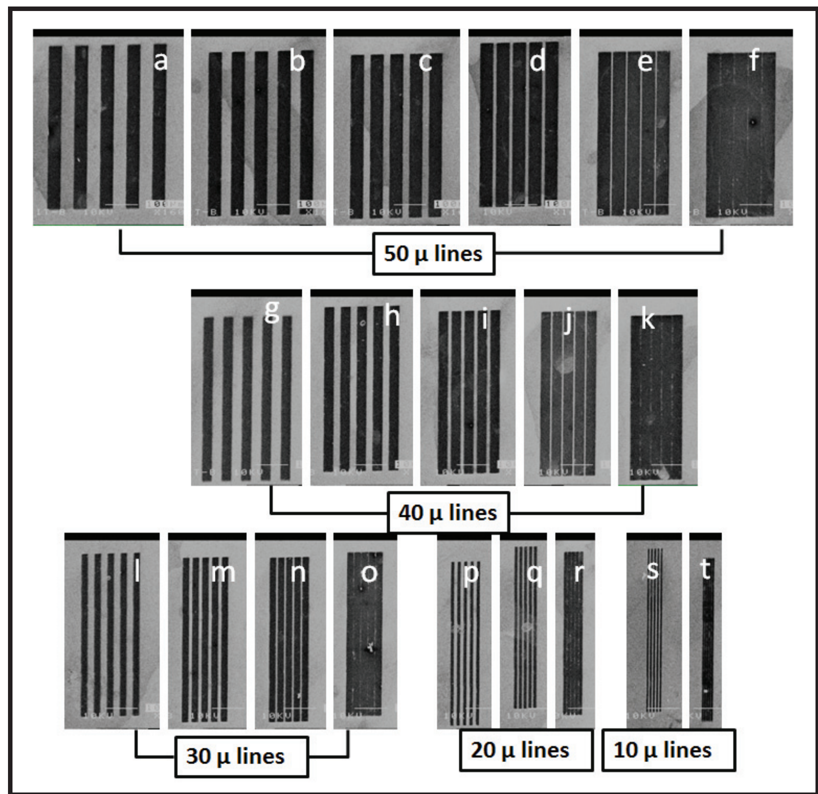

Figure 4.15: SEM images of the resist P6

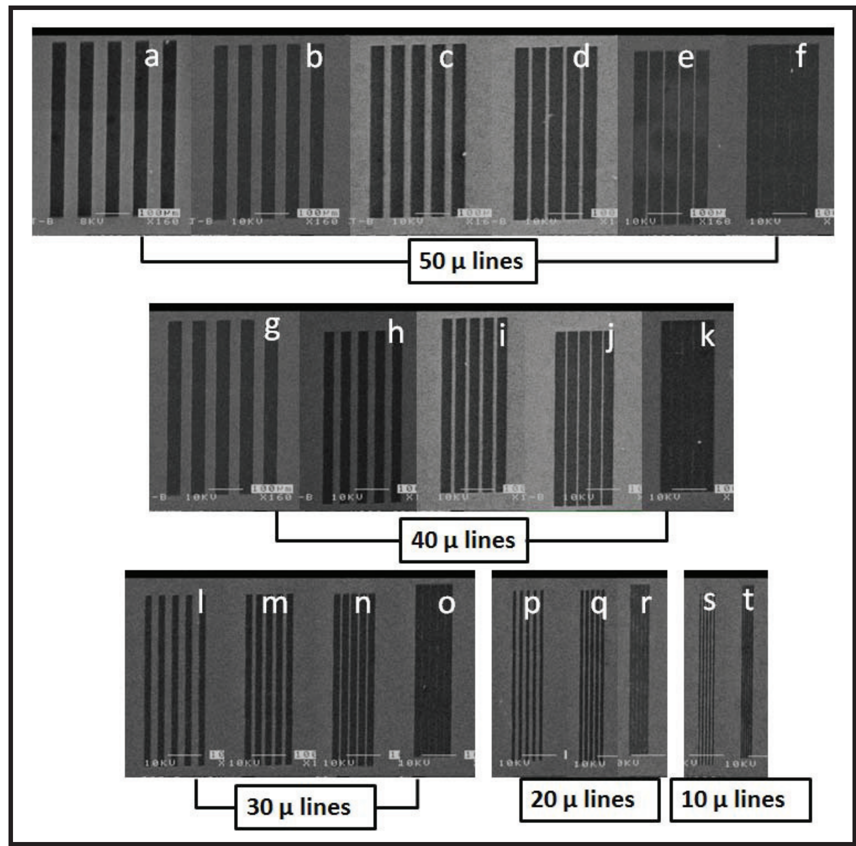

Figure 4.16: SEM images of the SU-8

Lithographic evaluation of polymers was carried using the same parameters for spin coating, pre-exposure bake, exposure time with fixed intensity, post exposure bake, and development that were optimized for the processing of SU-8 resist. For this comparative evaluation we selected two different masks, one containing 50-5 μ lines and second containing complex gate area device structures as discussed below. All the epoxide containing linear polymers based on bisphenol-A and 1, 5-dihydroxynaphthalene moieties were patterned using the lithographic conditions mentioned in experimental section. For all the polymer SEM images (Figures 4.12 to 4.16), the lithographic patterns were labelled as discussed in chapter 3. Figures 4.12 to 4.16 show the line patterns with widths ranging from 50 μ to 5 μ and spacing for polymers P1, P2, P5, P6 and SU-8 respectively. It was observed that in all the cases lines upto 10 μ width could be resolved at spacing of 10 μ, but not for the 5 μ width at 5 μ spacing.

It may be noted that this does not necessarily reflect on the performance of the resins. During the fabrication of the mask of 5 μ line width at 5 μ spacing, it was observed that the lines were not resolved due to the limitation of the equipment. We could thus

conclude that within the range investigated, the performance of the resins P1, P2, P5 and P6 was as good as SU-8 resists. This could be attributed to the high epoxide content of the resins which are reflected in higher T_gs of the crosslinked resins. In contrast, resins P3, P4, P7 and P8 polymers containing low epoxide contents and consequently low crosslink densities were washed out during development because of inadequate crosslinking.

In order to demonstrate the utility of resins synthesized by us in practical applications, we fabricated another mask containing gate area structure which would be used in CMOS fabrication to evaluate the lithographic performance of P2 and P6 resins vis a vis SU-8 resin. Lithography was performed using the conditions described in experimental section. The optical images were taken at 100X optical zoom using Olympus optical microscope, to identify the defects in the resists in the form of colour differentiation. Figure 4.17 shows coloured optical images of gate device area patterned using SU-8, P2 and P6 respectively. As compared to SU-8 (Figure 4.17 A) and P6 (Figure 4.17 C), P2 (Figure 4.17 B) could resolve defect free 5 μ line features in the gate device after development under identical conditions. It is visibly seen that the images obtained using SU-8 show roughness at the edges, a blurred shadow effect along the pattern edge as shown in Figure 4.17A. These defects are a result of poor film forming property and low adhesion of SU-8 resins (Yang et al., 2007; Sayah et al., 2007).

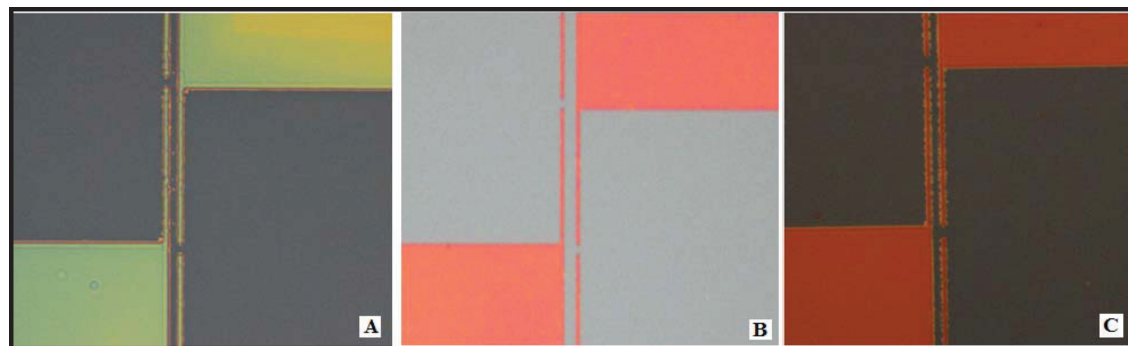

Figure 4.17: Optical images of gate area patterns with SU-8 (A), P2 (B) and P6 (C)

The polymer P2 (Figure 4.17B) showed defect free well resolved patterns after development under identical conditions as that of SU-8. In the case of polymer containing 1, 5- dihydroxynaphthalene (P6), greater line edge roughness was seen as compared to SU-8 and P2 resins (Figure 4.17C).

4.4. Conclusions

Photosensitive linear polymers containing methacrylate conjugates of bisphenol-A and 1, 5-dihydroxynaphthalene were synthesized. These polymers were further conjugated with epichlorohydrin to incorporate pendant epoxide groups as crosslinking sites. These polymers were characterized by TGA and DSC before and after photocrosslinking. The polymers were found to be thermally stable upto 300 ^{o}C. The DSC data show that the T_gs of bisphenol-A based polymers on crosslinking were greater than those of 1, 5-dihydroxynaphthalene based polymers. These polymers were evaluated for optical lithography. Polymers containing higher epoxide content resolved features upto 10 μ width at the 10 μ spacing. These polymers were further compared with the SU-8 resist by fabricating the gate area structure which is used in gate device. It was observed that P2 showed better lithographic performance than SU-8 resin. The resins containing lower degree of epoxide and hence low crosslink density could not be satisfactory processed.

4.5. References

1. Balakrishnan, M., Faccini, M., Diemeer, M. B. J., Verboom, W., Driessen, A., Reinhoudt, D.N., Leinse, A. Electronics Letters 2006, **42**, 1-2.
2. Feng, R., Farris, R.J. J. Micromech. Microeng. 2003, **13**, 80–88.
3. Jiguet, S., Bertsch, A., Judelewicz, M., Hofmann, H., Renaud, P. Microelectronic Engineering 2006, **83,** 1966–1970.
4. Kwak, G., Choi, J. U., Seo, K. H., Park, L. S., Hyun, S. H., Kim, W. S. Chem. Mater. 2007, **19**, 2898-2902.
5. Pan, G., Du, Z., Zhang, C., Li, C., Yang, X., Li, H. Polymer 2007, **48,** 3686-3693.
6. Reichmanis, E., Houlihan, F. M., Nalamasu, O., Neenan, T. X., Chem. Mater. 1991, **3**, 3, 394-407.
7. Reichmanis, E., Thompson, L. F., Chem.Rev.1989, **89**, 1273-1289.
8. Sayah, A., Parashar, V. K., Gijs, M. A. M. Journal of Microelectromechanical Systems, 2007, **16**, 3, 564-570.
9. Uthirakumar, P., Suh, E. K., Hong, C. H., Lee, Y. S., Polymer 2005, **46**, 4640–4646.
10. Wang, C. S., Lee, M. C., Polymer 2000, **41**, 3631–3638.
11. Wang, C. S., Lee, M. C., J Appl Polym Sci 1998, **70**, 10, 1907-1921.
12. Xu, K., Chen, M., Zhang,K., Hu, J., Polymer 2004, **45,** 1133–1140.
13. Yang, R., Soper, S. A., Wang, W., Sensors and Actuators A 2007, **135,** 625–636.

Chapter 5

Chemically amplified negative photoresists based on first generation dendrimers for electron-beam lithography

5.1. Introduction

Electron beam lithography (EBL) has been extensively investigated for enhancing the performance of photonic devices (Qualtieri et al., 2010); T-gates (Lee et al., 2005; Chen et al., 2004) and CMOS devices (Ming et al., 2004) because of the high-resolution it offers in the fabrication of nanostructures especially below 100 nm. The challenge in EBL is to fabricate features in sub 30 nm range. This calls for the development of new materials and processes.

The limitations of polymeric resists in the fabrication of nanometer scale patterns during EBL, arise from high molecular weight and broad molecular weight distribution, chain entanglement, aging, poor miscibility with chromophores, aggregation and swelling during pattern development (De Silva et al., 2008). As a part of newer lithography techniques developed to meet the demand for higher resolution and sensitivity and higher pattern densities at decreasing feature sizes. Duan et al., (2010) recently fabricated 10 nm half pitch features using PMMA as a negative resist at exposure as low as 2 kV. The contrast was 4 but the sensitivity was 5.8 mC/cm^2.

Amorphous low molecular weight resists are expected to form uniform films on spin coating and overcome the limitations of polymeric resists in terms of LER (Shirota, 2005). Use of low molecular weight resists such as dendrimers and molecular glasses offers advantages such as high purity, well defined structures, molecular weights and lack of chain entanglement. A summary of design principles for tailoring molecular glasses (MGs) for lithographic applications which overcome the limitations of polymeric resists in sub 50 nm features has been recently provided by De Silva et al., (2008). The advantage of MGs lies in the fact that the free volume is distributed into much smaller units compared to that in polymers, which governs diffusion in these matrices which in turn influences resolution and LER. They can be tailored to offer higher thermal stability, film forming ability and amorphous character. In order to increase T_g, translational, rotational and vibrational motions of the molecules are restricted by incorporating rigid and bulky side groups such as tert-butyl, naphthalene, biphenyl, triphenyl and fluorine moieties (De Silva et al., 2008; Shirota 2005; Kinoshita et al., 2002) and by increasing the crosslink density (Wang and Lee 2000).

In certain cases free hydroxyl groups or reactive furan rings (Mori et al., 2006), Powderlink 1174-(tetrakis(methoxylmethyl)-glycoluril (Dai et al., 2006) used as crosslinking moieties, result in loss of low molecular weight compounds which is

undesirable. Crosslinking of these systems during post exposure bake (PEB) results in the generation of small gas molecules such as water vapor and methanol, which may lead to pattern deformation especially at lower feature sizes. Carr et al., (2010) highlighted the importance of minimizing outgassing during resist processing, which primarily involves loss of solvent.

The most widely used photoresist systems are based on the crosslinking of epoxy resins. The crosslinking of negative photoresist containing epoxide groups is caused by the irradiation of a photoacid generator, which generates a reactive oxygen species that reacts with the epoxide moiety on a neighbouring polymer chain, resulting in the formation of a cross-link and corresponding propagating cation. This chain reaction leads to highly sensitive resists with high cross-linking efficiencies (Argitis et al., 1998).

SU-8 resist has been extensively used for EBL (Bilenberg et al., 2006; Aktary et al., 2003; Williamson and Shields, 2003, Wong and Pun, 2001). Nallani et al., (2003) patterned 500 nm features from 1.5 μ thick SU-8 films at 0.8 $\mu C/cm^2$ using 20 kV beam energy. Similarly 70 nm features at pitch 1:2.4 were fabricated from 200 nm thick films at 50 kV beam energy at sensitivity 3.6 $\mu C/cm^2$ (Pepin et al., 2004). However, generally it is difficult to reduce film thickness of SU-8 resists below 100 nm. Visible particles and pinholes are normally reported in SU-8 films at film thicknesses below 200 nm when prebaked. Minimum line width in SU-8 resist is governed by PAG diffusion during PEB and the pitch by the proximity effect. Bilenberg et al., (2006) processed SU-8 resin at 19.9 $\mu C/cm^2$ and 100 kV acceleration to resolve 24 nm features from 90 nm thick films at pitch 1:12.5 and contrast 0.8. The resin contains eight epoxide groups and has T_g 60 ^oC before crosslinking, which is enhanced to 240 ^oC when fully cross linked (Balakrishnan et al., 2006; Feng and Farris 2003). It is recognized that for negative photoresists, increase in T_g with crosslinking is desirable since increase in difference in T_g between the exposed and unexposed areas results in greater solubility difference, which can be expected to result in better resolution and contrast as well as low line edge roughness (LER). However, these resins suffer from brittleness, resulting from high cross link density, higher shrinkage and stress generated during crosslinking, which results in cracks and adhesion problems (Jiguet et al., 2006; Sayah et al., 2007; Feng and Farris 2003., Bystrova et al., 2007; Smith et al., 2010). Two types of epoxy based negative

photoresists have been investigated for EBL. The resist based on calix[4]arene bearing epoxide was reported by Sailer et al (2004). The resist was processed by EBL at 80 μC/cm^2 and 30 kV acceleration. 25 nm lines and 35 nm dots were resolved when pitch was set more than 1:6. The contrast was 2.1.

In summary, there is a need to design negative photoresist based on FGDs for EBL, which would enable fabrication of patterns upto 30 nm and a pitch 1:1, offering higher sensitivity and contrast.

We have synthesized FGDs starting with 1,3,5-trisbromo-methylbenzene as the core and dense, bulky, rigid 1, 1, 1-tris-p-4-hydroxyphenyl ethane, bisphenol-A and 1,5-dihydroxy naphthalene units at the periphery. The peripheral aromatic rigid molecules are connected to the central core through an ether linkage. These moieties were chosen as they are rigid, symmetric and thermally stable. FGD based on 1, 1, 1-tris-p-4-hydroxyphenyl ethane has six hydroxyls at the periphery, whereas FGDs based on bisphenol-A and 1,5-dihydroxynaphthalene have three hydroxyls, which helps to vary crosslink density. T_g could be manipulated by the choice of the peripheral aromatic group. The peripheral hydroxyls were reacted with epichlorohydrin to yield negative resists which were processed by EBL. The results show that these negative tone e-beam resists can be used to fabricate structures upto 30 nm width at a pitch 1:1 at 20 kV. The sensitivity, contrast and LER are comparable to those reported in the literature. It should be possible to resolve structures below these feature sizes at higher acceleration.

5.2. Experimental section

5.2.1. Materials

1, 5-Dihydroxy naphthalene (1,5-Dhn), Bisphenol-A, 1, 1, 1-tris-p-4-hydroxyphenyl ethane (Trisphenol), 1, 3, 5-tris (bromomethyl) benzene, propylene glycol methyl ether acetate (PGMEA), triphenylsulfonium perfluoro-1-butanesulfonate (PAG) were obtained from Aldrich chemicals (USA). Epichlorohydrin was procured from spectrochem, N, N-Dimethylformamide (DMF) obtained from Merck was distilled from CaH_2 under reduced pressure before use and all other reagents were used as received.

5.2.2. Synthesis

5.2.2.1. Preparation of G_1-Tris

Trisphenol 47 g (0.156 moles) was dissolved in 400 ml DMF, 97 g (0.702 moles) of anhydrous potassium carbonate was added and stirred for 30 min and maintained at 65°C, 2.8 g (7.8 X 10^{-3} moles) of 1, 3, 5-trisbromomethyl benzene in 20 ml DMF was added drop wise over 40 min. After the addition was complete, stirring was maintained for 12 h. DMF was recovered on rotary evaporator and reaction mixture was extracted with ethyl acetate. The solvent was evaporated and the G_1-Tris formed was purified by column chromatography, using petroleum ether and ethyl acetate (70:30 v/v) as elutant. G_1-Tris yield was 6.9 g (85%).

^{1}H NMR (DMSO-d_6): 9.28 δ (6H, -OH), 6.64-6.94 (36H, phenolic protons), 7.52 (3H, benzylic protons), 5.11 (6H, Ph-CH_2), 2.00 (9H, -CH_3).

5.2.2.2. Preparation of G_1-Bis

25.5 g (0.112 moles) bisphenol-A, 47g (0.336 moles) of K_2CO_3 in 150 ml DMF and 2 g (5.6 X 10^{-3} moles) of 1, 3, 5-trisbromomethyl benzene in 20 ml DMF were reacted as described above. G_1-Bis yield was 3.9 g (87%).

^{1}H NMR (DMSO-d_6): 8.19 δ (3H, -OH), 6.7-7.19 (24H, phenolic protons), 7.56 (3H, benzylic protons), 5.13 (6H, Ph-CH_2), 1.62 (18H, -CH_3).

5.2.2.3. Preparation of G_1-Dhn

18 g (0.112 moles) 1, 5-Dhn, 47g (0.336 moles) of K_2CO_3 in 150 ml DMF and 2 g (5.6 X 10^{-3} moles) of 1, 3, 5-trisbromomethyl benzene in 20 ml DMF were reacted as discussed in section 2.2.1. G_1-Dhn yield was 2.7 g (81%).

^{1}H NMR (DMSO-d_6)**:** 9.10 δ (3H, -OH), 6.94-7.85 (18H, naphthalene ring protons), 7.88 (3H, benzylic protons), 5.42 (6H, Ph-CH_2).

5.2.2.4. Preparation of G_1-Tris-epoxide

5 g (5 X 10^{-3} moles) G_1-Tris, 0.05 g polyethylene glycol-400 as a phase transfer catalyst and 50 ml epichlorohydrin were added to a 100 ml two necked flask equipped with a stirrer. The contents were heated to 70 ^{o}C for 1h. To this reaction mixture dilute aqueous potassium hydroxide solution (KOH) 1.70 g (3 X 10^{-2} moles) in 10 ml

water was added drop wise over 40 min. After addition of alkali was complete, the reaction was continued at 60 ^{o}C for further 2 h. The reaction mixture was filtered and the organic phase was washed with water three times and dried over anhydrous sodium sulphate. Excess epichlorohydrin was recovered over rotary evaporator under vacuum to yield a semisolid mass, which was then precipitated from pet ether. The product was purified by dissolving it in THF and reprecipitated from pet ether to recover a colourless product. The yield of G_1-Tris-epoxide was 6.4 g (97%).

^{1}H NMR ($CDCl_3$)**;** δ [ppm]: 6.77-7.01 (36H, phenolic protons), 7.45 (3H, benzylic protons), 5.04 (6H, Ph-CH2**)**, 2.09 (9H, -CH3), 2.72 to 2.92 ppm (12H, multiplet, protons of methylene in the oxirane ring), 3.33 ppm (6H, multiplet, protons of methine in the oxirane ring), 3.88 to 4.22 ppm (12H, multiplet, methylene protons connecting the phenoxy and the oxirane ring).

5.2.2.5. Preparation of G_1-Bis-epoxide

The compound was prepared by the same method used for G_1-Tris-epoxide using 2 g (2.5×10^{-3} moles) G_1-Bis, 0.02 g polyethylene glycol-400 as a phase transfer catalyst, 20 ml epichlorohydrin and potassium hydroxide 0.63 g (1.1×10^{-2} moles) in 4 ml water. G_1-Bis-epoxide yield was 2.4 g (98%).

^{1}H NMR ($CDCl_3$)**;** δ [ppm]: 6.79-7.15 (24H, phenolic protons), 7.44 (3H, benzylic protons), 5.04 (6H, Ph-CH2**)**, 1.63 (18H, -CH3), 2.72 to 2.92 ppm (6H, multiplet, protons of methylene in the oxirane ring), 3.43 ppm (3H, multiplet, protons of methine in the oxirane ring), 3.89 to 4.19 ppm (6H, multiplet, protons of methylene connecting the phenoxy and the oxirane ring).

5.2.2.6. Preparation of G_1-Dhn-epoxide

G_1-Dhn-epoxide was prepared using the same method described in section 2.2.5 from**,** 2 g (3.36×10^{-3} moles) G_1-Dhn, 0.02 g polyethylene glycol-400 as a phase transfer catalyst and 20 ml epichlorohydrin and potassium hydroxide 0.85 g (1.5×10^{-2} moles) in 5 ml water. G_1-Dhn-epoxide yield was 2.3 g (93%).

^{1}H NMR ($CDCl_3$)**;** δ [ppm]: 6.79-7.15 (24H, naphthalene ring protons), 7.44 (3H, benzylic protons), 5.29 (6H, Ph-CH2**)**, 2.83 to 2.99 ppm (6H, multiplet, protons of methylene in the oxirane ring), 3.47 ppm (3H, multiplet, protons of methine in the

oxirane ring), 3.86 to 4.41 ppm (6H, multiplet, protons of methylene connecting the naphthalene and the oxirane ring).

5.2.3. Characterization

The ^{1}H-NMR spectra recorded in $CDCl_3$ and DMSO-d_6 at 25°C on Bruker- 200 MHz spectrometer were used to estimate molecular weights of the FGDs. The IR spectra were recorded on a Perkin Elmer spectrometer (DRS mode). The differential scanning calorimetery (DSC) and thermo gravimetric analysis (TGA) were performed on TA Instrument DSC Q-10 and TGA-7 Perkin Elmer at a heating rate 10 ^{o}C/min. The resists were spin coated on silicon wafers at 6000 rpm. Raith 150^{TWO} was used a) to measure resist film thickness, b) for patterning, c) imaging the resists structures and d) LER measurements.

5.2.4. Lithographic evaluation

The FGDs were dissolved in propylene glycol methyl ether acetate (PGMEA) to obtain a 5 wt. % solution. Commercially available triphenylsulfonium perfluoro-1-butanesulfonate (PAG) 5 wt. % (Dai et al., 2006; De silva et al., 2008) and 10 wt. % (Ueda et al., 1998) on the basis of resist was used. The resulting solutions were filtered through a 200 nm filter and spin coated onto 2 inch oxidised silicon wafers (oxide thickness 200 nm) at 6000 rpm for 30 sec, leading to a film thickness of 66 nm for G_1-Tris-epoxide, 63 nm for G_1-Bis-epoxide and 62 nm for G_1-Dhn-epoxide as measured by Raith-150^{Two} SEM. This was subjected to prebaking at 70 ^{o}C for 5 min on hotplate and then exposed to e-beam using Raith-150^{Two}. Post exposure baking was done at 90 ^{o}C for 60 sec on a hotplate. The wafers were then developed using propylene glycol methyl ether acetate for 30 sec, rinsed with IPA for 10 sec and dried with a nitrogen blower.

5.3. Results and Discussion

5.3.1. Design of first generation dendrimers

In order to ensure the formation of stable amorphous films it is essential that the low molecular weight resist structures inhibit crystallization. In this context branched or star shaped molecules have specific advantages. Structural attributes which result in

low free volume and restrict molecular rotation, lead to enhanced T_g. High T_g is critical as such materials form stable thin films and can be subjected to PEB, structure development and plasma etching. Glass formation tendency is enhanced in branched systems containing rigid cores with short radiating arms conjugated with bulky peripheral moieties. Planar and nonplanar or tetrahedral cores have been explored to yield amorphous molecular glasses (De Silva 2008). The short length of arms and bulkier peripheral molecules, lead to low length-to-breadth ratio, increasing bulkiness and hence T_g. The presence of bulkier moieties in periphery results in lower free volume and increase in $T_{g.}$ Chemically amplified resists (CAR) are preferred as these can be processed at low dose in EBL.

Mori et al., (2006) reported FGDs containing peripheral furan groups having T_g 55°C which were crosslinked using (4,4- methylenbis[2,6-bis(hydroxymethyl phenol). The resist composition comprising 69 weight % resist / 20 weight % crosslinker and 10 weight % PAG was processed at 50 kV using a dose of 20μC/cm^2. 200 nm lines with a pitch 1:2 could be successfully processed. Surprisingly the resin having T_g 55 ^{o}C could be post exposure baked at 110 ^{o}C for 10 min. Tully et al., (2000) explored the role of dendrimer based CARs for fabricating features up to 50 nm. The t-BOC functionalized dendrimers had a T_g 73-77 ^{o}C. Since the resist was not cured, the solubility difference between exposed and unexposed resist resulted in 50 nm negative pattern. PEB had to be carried out at 60 ^{o}C and to achieve t-BOC deprotection, bake time upto 8 min had to be used. In our case the T_gs are lower than the PEB. The patterns still could be accurately reproduced because crosslinking accompanied the exposure, which resulted in an increase in T_g as the PEB proceeded.

While allyl modified calixarene were used as negative e-beam resist to fabricate patterns upto 10 nm, the dose at 50 kV varied between 6-10 mC/cm^2. This could be brought down from 5 mC/cm^2 to 2 mC/cm^2 by increasing the number of allyl units in the calixarene from 4 to 8 (Sailer et al., 2002). Sailer et al., (2004) reported that calyx(4)arene derivative bearing 4 epoxides at the lower rim can be processed in the presence of PAG based on mixed triaryl sulphonium salts using a dose of 15 μC/cm^2 at 25 kV.

FGDs in this work were designed to varry T_g, manipulate crosslink density and explore the possibility of fabricating patterns upto 30 nm. The structure used

contained 1, 3, 5-trisbromomethyl benzene as the core as it is reported that 1,3,5-branched structures lead to amorphous materials (De Silva et al., 2008). Dense, bulky, rigid Trisphenol; bisphenol-A and 1,5-Dhn units were conjugated at the periphery and subsequently converted to epoxide. Bisphenol-A has been used in SU-8 (Aktary et al., 2003), trisphenol as core in most of the dendrimers (Tully et al., 2000; Kamimura et al., 2005) and 1,5-Dhn units are expected to add to rigidity (Pan et al., 2007). The choice of the core and peripheral groups thus follow the criteria laid down in the literature. This approach is similar to epoxy modified calyx(4)arenes. Sensitivity and contrast values obtained have been compared with those reported by Sailer et al., (2004).

FGD based on trisphenol contained six hydroxyls at the periphery whereas, FGDs based on bisphenol-A and 1,5-Dhn contained three hydroxyl groups at the periphery. This architecture helps elucidate the role of crosslink density on the resist performance as will be discussed later. Use of bisphenol-A, 1,5-Dhn and trisphenol, as peripheral moieties enhanced T_g from 70 to 87 and to 139 ^oC. Another reason to design CARs based on FGDs is that LER is lower than in the non CARs as low acid diffusion smoothens roughness (Rio et al., 2009), which is critical in governing electrical characteristics of devices.

5.3.2. Synthesis of FGDs

We incorporated ether functionality on the benzene core as shown in Figures 5.1a and 5.1b**.** The first generation dendrimers were synthesized by reacting phenols and naphthols with 1, 3, 5-tris-bromomethylbenzene in the presence of potassium carbonate in DMF. The peripheral hydroxyls were conjugated with epichlorohydrin using KOH as a base and polyethylene glycol-400 as a phase transfer catalyst. An excess of epichlorohydrin was used to avoid crosslinking and addition reaction (Pielichowski and Czub., 1997).

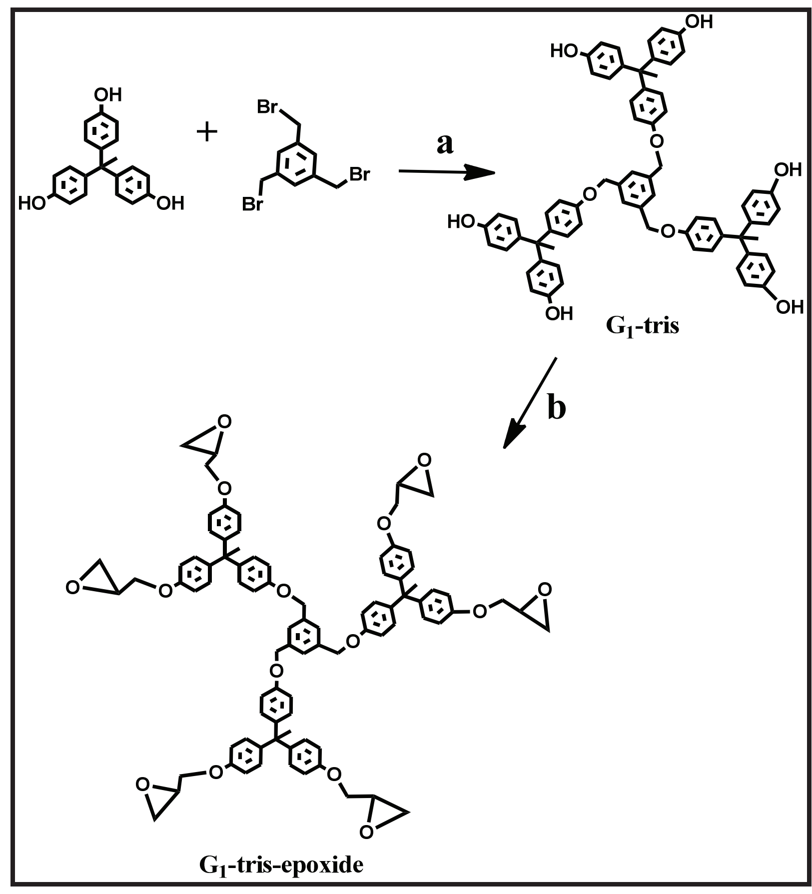

Figure 5.1a: Synthesis of G_1-Tris-epoxide; a) K_2CO_3, DMF, 60°C; b) KOH, Epichlorohydrin, PEG-400, 60°C

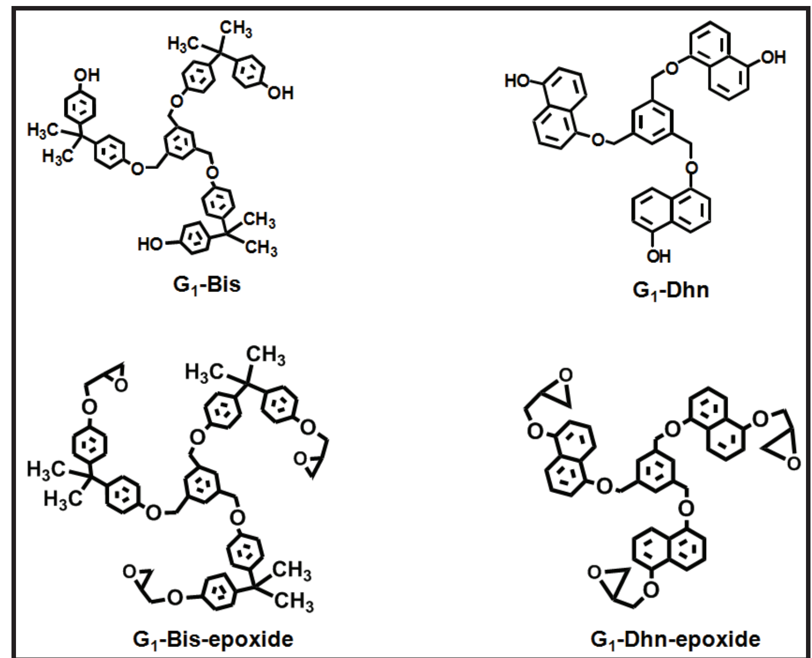

Figure 5.1b: Structures of G_1-Bis, G_1-Dhn, G_1-Bis-epoxide and G_1-Dhn-epoxide.

5.3.3. FGDs characterization

5.3.3.1. Solubility

FGDs based on Bisphenol-A, Trisphenol and 1, 5-Dhn bearing peripheral hydroxyl groups were readily soluble in most of the organic solvents like THF, acetone, DMF, ethyl acetate, γ-butyrolactone, epichlorohydrin, methanol, ethanol, ethyl lactate, propylene glycol methyl ether acetate (PGMEA), cyclohexanone and 2-methoxyethanol, but were insoluble in dichloromethane and chloroform. Epoxide conjugates were readily soluble in solvents commonly used for lithography such as γ-butyrolactone, ethyl lactate, propylene glycol methyl ether acetate (PGMEA), cyclopentanone etc, but were insoluble in methanol and ethanol.

5.3.3.2. IR spectroscopy

Figures 5.2a-5.2c show the IR spectra of G_1-Tris, G_1-Bis and G_1-Dhn respectively, before and after epoxide conjugation.

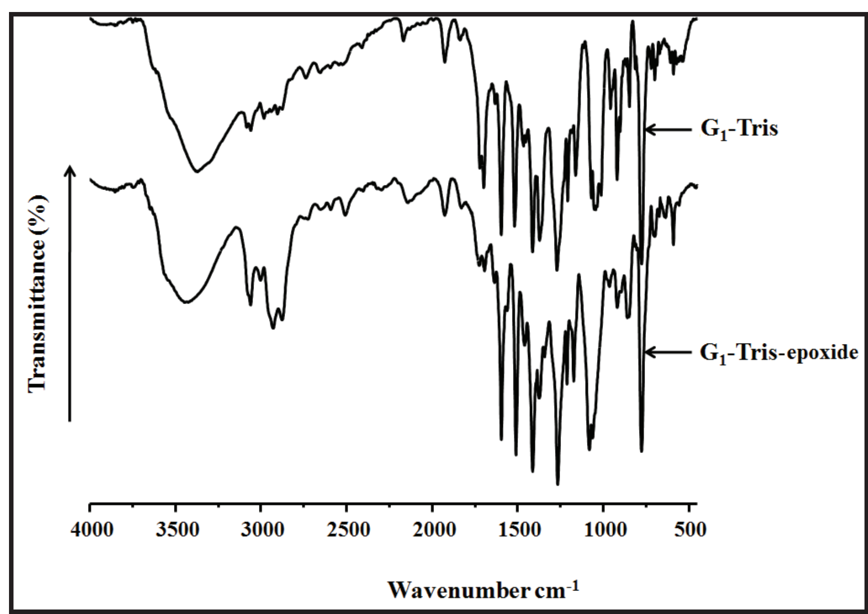

Figure **5.**2a: FTIR spectrum of G_1-Tris and G_1-Tris-epoxide

Absorption bands in the region 3350-3600 cm^{-1} are associated with hydrogen bonding of free hydroxyl groups. Broad absorption bands exhibit a shoulder at 3600 cm^{-1} which corresponds to the free hydroxyls. Presence of epoxide group in the IR spectrum was confirmed by the peaks at 3060 and 3000 cm^{-1} which correspond to

methylene and methyne group. The results obtained demonstrate that, even on conjugation with epoxide group there is no significant change in absorption band in the range 3350-3600 cm^{-1} which corresponds to hydrogen bonding in the conjugates, reflected in band broadening.

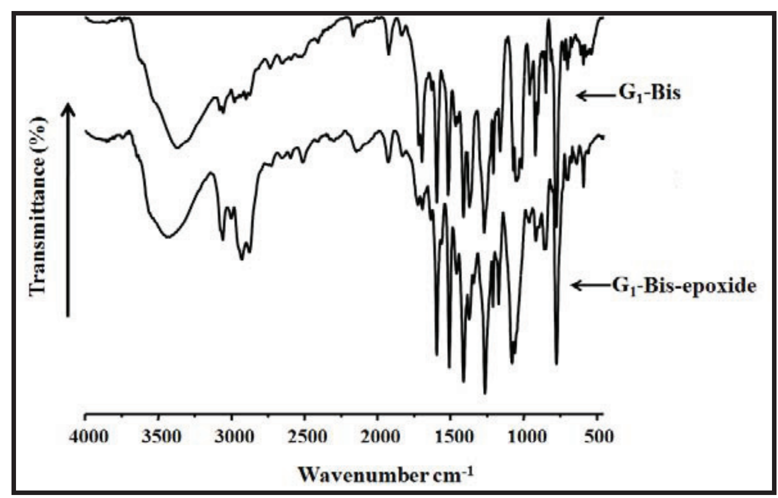

Figure 5.2b: FTIR spectrum of G_1-Bis and G_1-Bis-epoxide

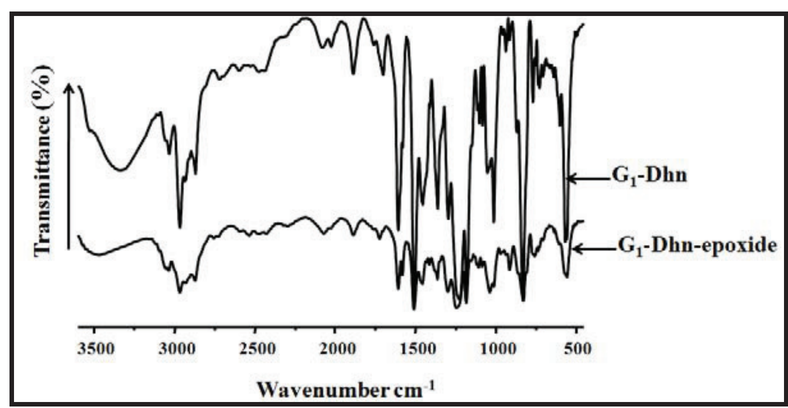

Figure 5.2c: FTIR spectrum of G_1-Dhn and G_1-Dhn-epoxide

5.3.3.3. ^{1}H-NMR spectroscopy

Figure 5.3a shows ^{1}H-NMR spectrum of G_1-Tris in acetone-d_6. Complete disappearance of the peak at 4.50 ppm corresponding to methylene in 1, 3, 5-trisbromomethyl benzene and appearance of the peak at 5.11 ppm confirms formation of G_1-Tris. Peak at 9.28 ppm corresponds to the aromatic hydroxyl functionality of Trisphenol unit and at 7.52 ppm to the aromatic protons of central benzene unit.

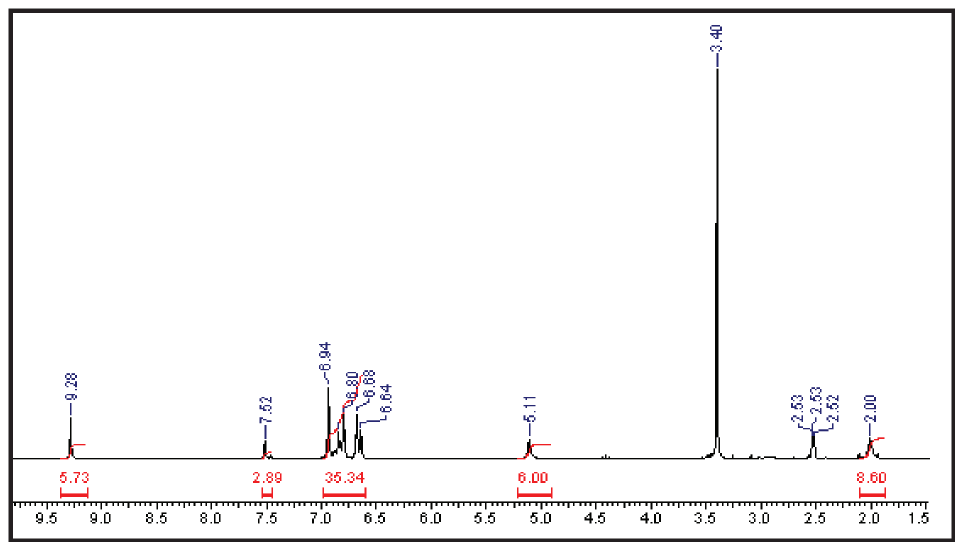

Figure 5.3a: NMR spectrum of G_1-Tris

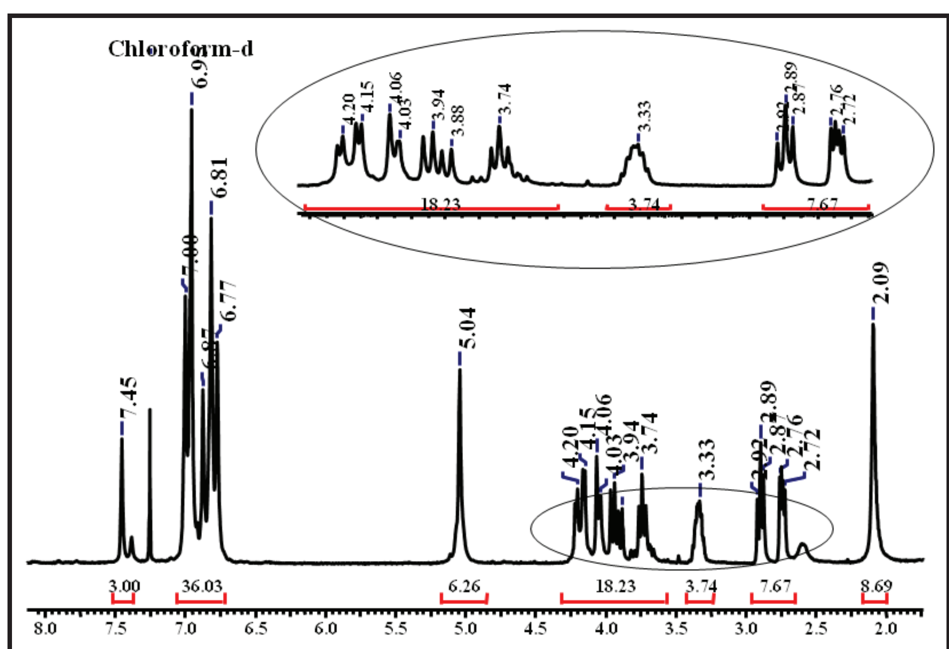

Figure 5.3b: ^{1}H-NMR spectrum of G_1-Tris-epoxide

This confirms conjugation of trisphenol and benzyl groups. Thus, all benzyl bromide groups are converted to corresponding ether groups in G_1-Tris (Figure 5.3a). Figure 5.3b shows ^{1}H-NMR spectrum of G_1-Tris-epoxide in $CDCl_3$, wherein peak at 9.28 ppm corresponding to the aromatic hydroxyl is replaced by peaks corresponding to epoxide ring protons (2.72-4.2 ppm), which confirms conjugation of epoxide groups.

The reaction of bisphenol-A and 1,5-Dhn with 1,3,5-trisbromomethyl benzene and conversion of hydroxyl group to the epoxide was similarly confirmed.

5.3.3.4. Molecular weights

Formation of G_1-Tris was confirmed by comparing peak integrals of 6-methyne protons adjacent to the central benzene ring (5.11 ppm) with 9-methyl protons of the three Trisphenol units as shown in Figure 5.3a. The molecular weight was then calculated from the molecular formula. Similarly formation of G_1-Tris-epoxide was confirmed by considering peak integrals of 6 methyne protons adjacent to the central benzene ring with 30 methyl protons of the 6 epoxide units as shown in Figure 5.3b and the molecular weight was calculated from the molecular formula. Molecular weights of FGDs based on bisphenol-A and 1,5-Dhn and their epoxide conjugates were similarly calculated (Table 5.1).

5.3.3.5. Thermal properties

5.3.3.5.1. Thermal degradation

Thermal stability of the FGDs was evaluated using TGA-7, Perkin Elmer at a heating rate 10 °C/min under nitrogen atmosphere. The temperature T_5 corresponding to 5 wt % loss was considered as the index of thermal stability (Table 5.1). From Figure 5.4a it can be seen that the thermal stability decreases in the order G_1-Tris (273 ^oC) > G_1-Bis (198 ^oC) > G_1-Dhn (139 ^oC). The corresponding values for the epoxide derivatives are G_1-Tris-epoxide (348 ^oC) > G_1-Bis-epoxide (326 ^oC) > G_1-Dhn-epoxide (212 ^oC) (Figure 5.4b). Thus epoxide conjugation enhances thermal stability of the precursors which is desirable. The main skeleton of G_1-Tris-epoxide contains one geminal methyl and two phenyl groups, whereas G_1-Bis-epoxide contains two geminal methyl groups. As compared to the methyl group, the phenyl group is more rigid (De silva et al 2008), which explains higher thermal stability of G_1-Tris-epoxide. In case of G_1-Dhn-epoxide, a fused ring system is present in the structure which enhances the thermal stability.

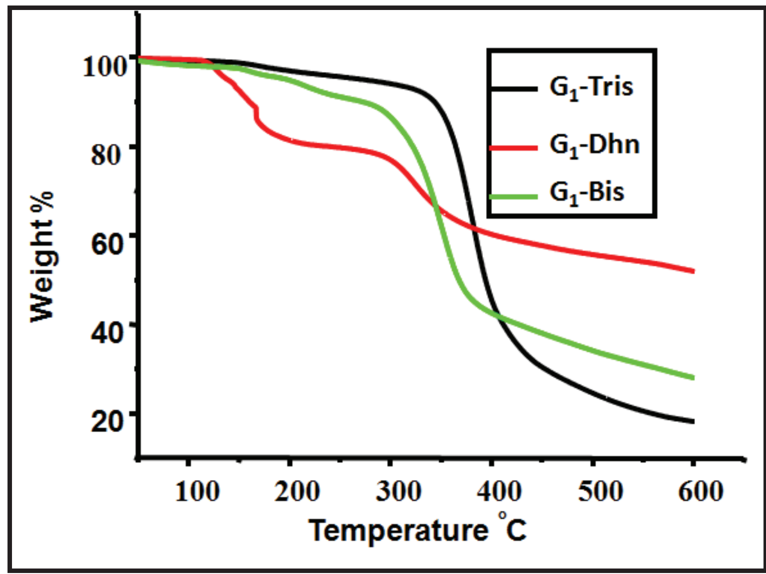

Figure 5.4a: Thermograms of unmodified FGDs

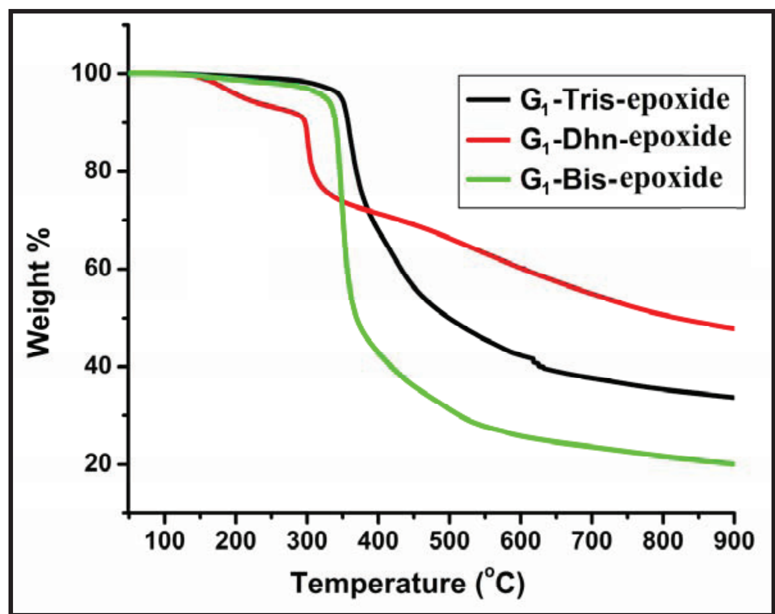

Figure 5.4b: Thermograms of epoxide conjugated FGDs

As a result, the thermal stability is lower (212 °C). Figures 5.4a and 5.4b show a single step degradation which confirms that the epoxides are not deprotected prior to decomposition.

5.3.3.5.2. The glass transition temperature

T_gs of FGDs were determined using TA Instruments DSC Q-10 in nitrogen atmosphere at a heating rate 10°C/min and the data are presented in Table 5.1. DSC

traces recorded during the second heating cycle, shown in Figure 5.5a (unmodified FGDs) and 5.5b (epoxide conjugated FGDs), indicate no melting peak confirming the amorphous nature of the materials.

The rigid core and bulky rigid peripheral segments like bisphenol-A, 1,5-Dhn and trisphenol units effectively decrease free volume in the molecules. T_gs of FGDs increase in the order G_1-Bis (70 ^oC) < G_1-Dhn (87 ^oC) < G_1-Tris (139 ^oC) (Figure 5.5a). Similar trend was observed in the case of T_gs of epoxide conjugated FGDs viz G_1-Bis-epoxide (38 ^oC) < G_1-Dhn-epoxide (66 ^oC) < G_1-Tris-epoxide (80 ^oC) (Figure 5.5b). Although G_1-Tris-epoxide is not a fused ring structure as G_1-Dhn-epoxide, it exhibits higher T_g. This is because three sets of four sterically rigid moieties containing three aromatic rings and one methyl group on the same carbon atom effectively restrict molecular rotation thereby increasing T_g (De Silva et al 2008). In case of G_1-Bis-epoxide, the presence of bulky jeminal methyl groups in bisphenol-A units increases free volume in the molecule (Uthirakumar et al., 2005). Also in the case of G_1-Bis-epoxide there are two aromatic rings and two methyl groups which results in decrease in T_g as compared to that of G_1-Tris-epoxide which has three aromatic rings and one methyl group. G_1-Dhn-epoxide contains three sets of fused ring systems peripheral to the central core, which are bulky and rigid enough to restrict molecular rotation, resulting in increase in T_g as compared to G_1-Bis-epoxide. The intermolecular interaction between the free hydroxyl groups which helps to increase T_g (De silva et al., 2008), is lowered after epoxide conjugation, resulting in decrease in T_g of FGDs. But there is no change in the order. T_g increase in the order phenyl < biphenyl < diphenylphenyl was reported by Kinoshita et al., (2002). The peripheral groups used in this work represent similar substitution. Thus the trends in T_g observed in the case of FGDs are consistent with those reported in the literature.

In case of G_1-Tris, the intermolecular interaction between six peripheral hydroxyl groups enhances T_g compared to other two FGDs, containing three peripheral hydroxyl groups (Figure 5.5c). G_1-Dhn shows relatively higher T_g than G_1-Bis, since 1,5-Dhn unit is more rigid than bisphenol-A unit. After epoxide conjugation significant decrease in T_g was observed in case of G_1-Tris-epoxide followed by that in case of G_1-Bis-epoxide (Figure 5.5c). In contrast, in the case of G_1-Dhn the decrease is much smaller (Figure 5.5c).

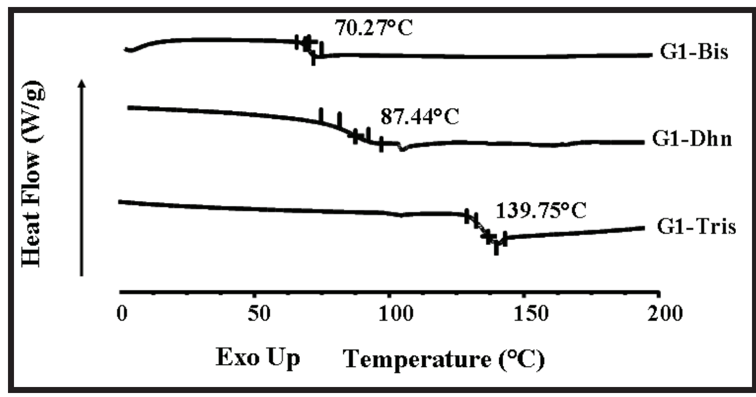

Figure 5.5a: DSC thermograms of FGDs, scan rate 10 °C/min

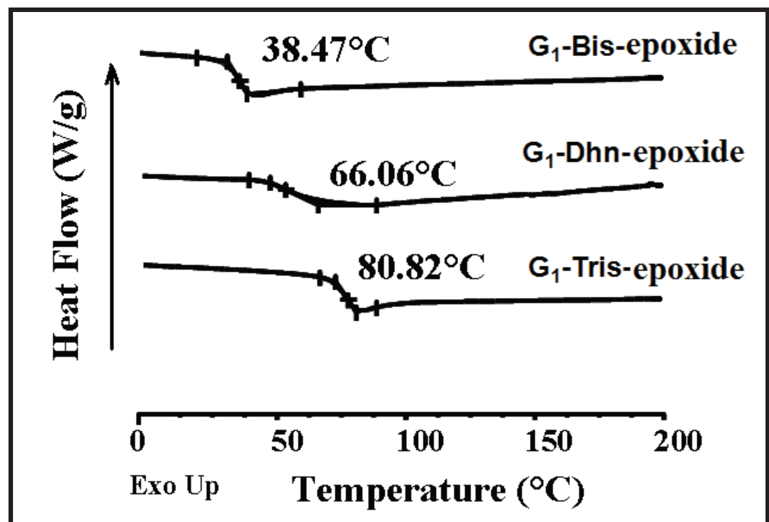

Figure 5.5b: DSC thermograms of FGDs-epoxide scan rate 10 °C/min.

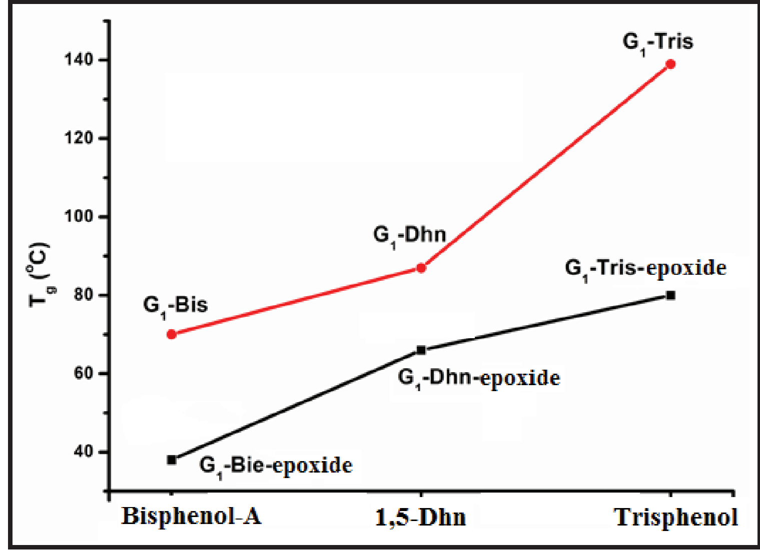

Figure 5.5c: T_gs of FGDs before and after epoxide conjugation

Table 5.1: Characterization of FGDs

Sr.No.	Dendrimer	Molecular weight	T_g °C	T_5 °C
1	G_1-Tris-epoxide	1370	80.00	348
2	G_1-Bis-epoxide	0967	38.47	326
3	G_1-Dhn-epoxide	0763	66.60	212
7	G_1-Tris	1033	139.00	273
8	G_1-Bis	0799	70.00	198
9	G_1-Dhn	0595	87.00	139

5.3.3.6. X-ray diffraction (XRD)

Figure 5.6 shows XRD patterns of G_1-Tris-epoxide; G_1-Bis-epoxide and G_1-Dhn-epoxide. The 2θ values are G_1-Tris-epoxide (19.73°), G_1-Bis-epoxide (18.1°) and G_1-Dhn-epoxide (22.81°) respectively. The nature and 2θ values of the peaks indicate that the compounds are amorphous.

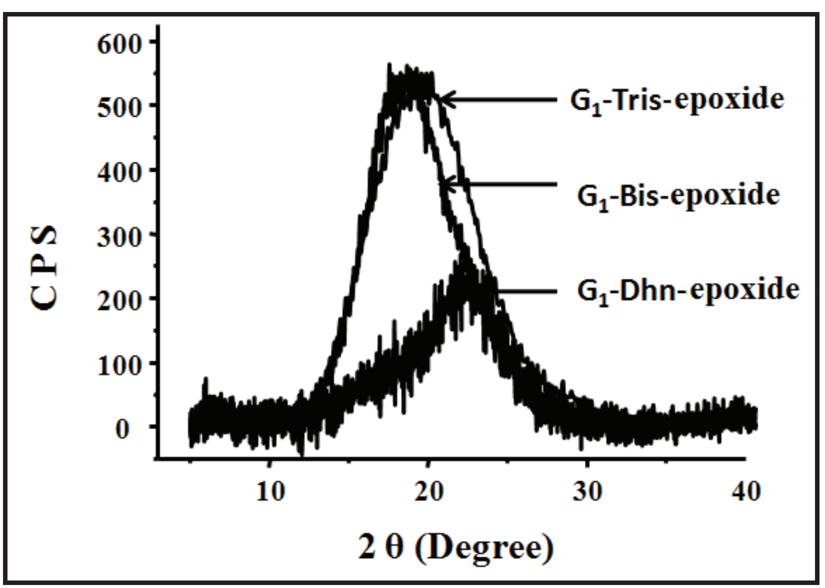

Figure 5.6: XRD of dendrimers

The monomers (bisphenol-A (T_m 158 °C); 1, 5-dihydroxynaphthalene (T_m 180 °C); trisphenol (T_m 246 °C) and 1, 3, 5-trisbromo methyl benzene (T_m 94-99 °C) are highly crystalline in nature. However, the crystallinity is lost during condensation with 1, 3,

5-trisbromo methyl benzene. The ether linkage introduced disrupts the π-π conjugation which assists in crystallization (De Silva and Ober 2008). The ether linkage is also reported to enhance the adhesion to the silicon substrate (Esfandeh et al., 2007, Chattopadhyay et al., 2005; Yonezawa et al., 2002).

5.3.3.7. Lithographic evaluation

5.3.3.7.1. Sensitivity curve for the FGDs

The sensitivity curves for the negative tone resists on exposure to e-beam at 20 kV acceleration voltage, 20 μm aperture, resulting in a beam current of 170 pA are shown in Figures 5.7A and 5.7B. All the resists containing 5 wt % FGDs and 5 wt. % as well as 10 wt. % PAG on the basis of FGDs in PGMEA were spin coated on a silicon substrate and exposed in the dose range 5 $\mu C/cm^2$ to 100 $\mu C/cm^2$. A series of 500 nm lines were patterned at a pitch 1:1 for all the FGDs. Typical patterns for G_1-Tris-epoxide are shown in Figures 5.8A and 5.8B.

The thicknesses of the lines patterned at various dose rates were measured using Raith 150^{Two} SEM. Sensitivity was defined as the lowest dose D_1 at which thickness of the developed pattern was the same as that of the spin coated film (Bilenberg et al., 2006). The resist containing 5 wt % PAG shows a sensitivity of 70 $\mu C/cm^2$ for G_1-Tris-epoxide, 85 $\mu C/cm^2$ for G_1-Bis-epoxide and 95 $\mu C/cm^2$ for G_1-Dhn-epoxide (Figure 5.7 A). G_1-Tris-epoxide resist exhibits slightly higher sensitivity than G_1-Bis-epoxide and G_1-Dhn-epoxide. This could be attributed to higher crosslink density in case of G_1-Tris-epoxide. Although the crosslink density achievable in G_1-Bis-epoxide and G_1-Dhn-epoxide is same, G_1-Dhn-epoxide shows lower sensitivity than G_1-Bis-epoxide, since naphthalene containing resist are less reactive (Pan et al., 2007). However, at 10 wt % PAG all resists showed a sensitivity of 35 $\mu C/cm^2$ (Figure 5.7 B). These resists are more sensitive than the epoxy conjugated calixarene resists containing 30 wt % PAG, which exhibit sensitivity greater than 100 $\mu C/cm^2$ at 30 kV at 90 ^oC and one min PEB (Sailer et al., 2004**).** The increase in sensitivity and contrast with increasing crosslinking density has been reported by Sailer et al., (2002) for calixarene. Similar trend was observed for FGDs, although the molecular architecture is different.

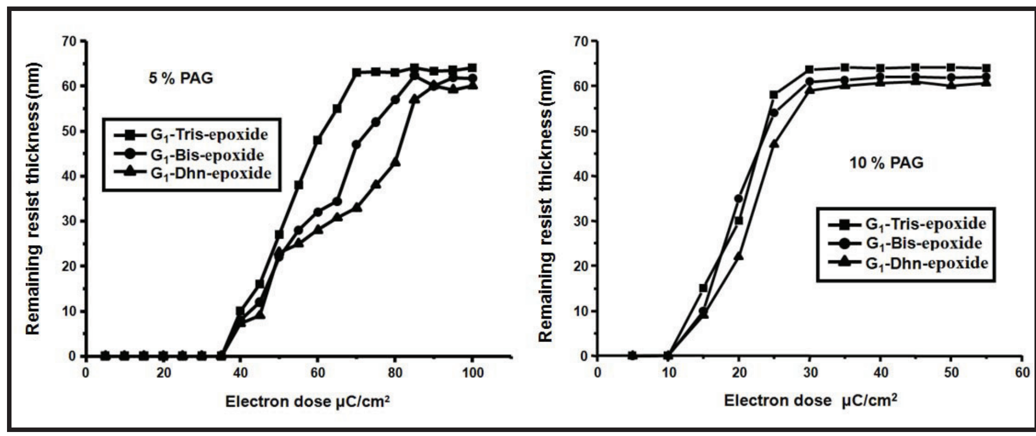

Figure 5.7: Relative resist thickness vs. exposure dose for the FGDs: A) 5 wt % PAG, B) 10 wt % PAG

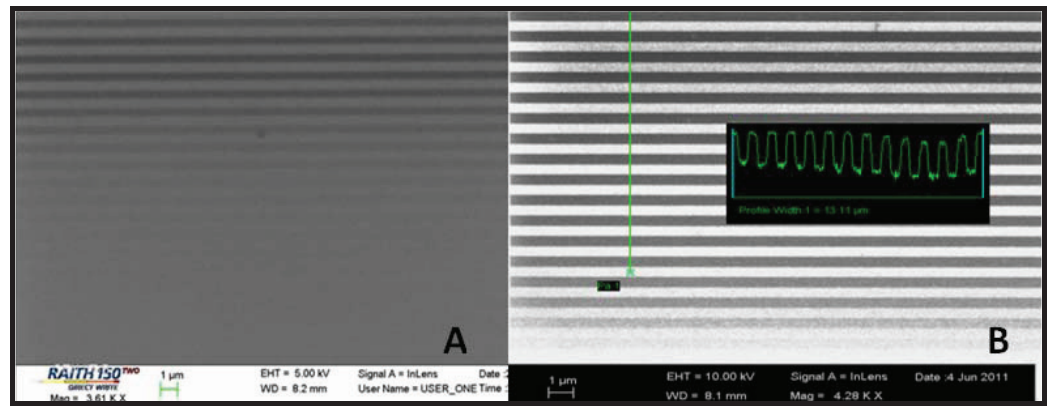

Figure 5.8: SEM images of G_1-Tris-epoxide used for sensitivity and contrast calculation: A) 5 wt %; B) 10 wt. % PAG.

The contrast (γ) was calculated from the formula $\gamma^{-1} = \log D_1 - \log D_0$ (Bilenberg et al., 2006), where D_0 is the highest dose at which the resist is not crosslinked and is washed out completely on development. D_1 is the lowest dose where the resist height after development is the same as the thickness of spin coated film. Figure 5.8A was used to calculate contrast (γ) for the G_1-Tris-epoxide resists containing 5 wt % PAG and Figure 5.8B was used to calculate contrast for the same resist containing 10 wt % PAG. At 5 wt % PAG, the values of contrast are 3.30 for G_1-Tris-epoxide, 2.78 for G_1-Bis-epoxide, 2.43 for G_1-Dhn-epoxide. Corresponding values at 10 wt % PAG were 2.00 for G_1-Tris-epoxide, 1.60 for G_1-Bis-epoxide, 1.53 for G_1-Dhn-epoxide. The values for contrast and sensitivity of FGDs are quite comparable to standard negative tone resists (Table 5.2).

The resists in this work are processed at lower kV and lower line width and pitch compared to the epoxide based calixarene and SU-8. SU-8 resist showed a sensitivity of 19.9 μC/cm^2, at 100 kV, 24 nm lines were resolved at low contrast (0.9) even when pitch was 1:12.5 (Bilenberg et al., 2006), perhaps, because at lower pitch the pattern could not be resolved. Epoxide based calixarene resists showed sensitivity in the range 80-150 μC/cm^2. At 30 kV 25 nm lines were resolved at pitch 1:1 and the contrast was 2.1 (Sailer et al., 2004). The resists synthesized in this work show a sensitivity of 35 μC/cm^2 and lines upto 30 nm and pitch 1:1 could be resolved at high contrast of 2.0 at 20 kV. It would therefore be possible to pattern features lower than 30 nm at higher acceleration.

Table 5.2: Comparison of the FGDs with SU-8 and calixarene based resists

Resist	Acceleration (kV)	Sensitivity (μC/cm^2)	Contrast (γ)	Linewidth (nm)	Pitch (nm)	Reference
SU-8	50	3.6	NA	75	NA	Pepin et al., 2004
SU-8	100	19.9	0.9	24	300	Bilenberg et al., 2006
Epoxy modified Calixarene	30	80	2.1	25	25	Sailer et al., 2004
TOMCA4	25	3000	1.7	40	40	Sailer et al., 2004
G_1-Tris-epoxide	20	35	2.0	30	30	This work
G_1-Bis-epoxide	20	35	1.60	30	30	This work
G_1-Dhn-epoxide	20	35	1.53	50	500	This work

* NA-Not applicable, TOMCA4-tetrakis (oxiran-2-ylmethoxy)-tetra-tert-butylcalix [4]arene.

5.3.3.7.2. Post exposure bake optimization

We examined the effect of PEB in the temperature range 70-110 °C for one min. For 30 nm lines at pitch 1:1, patterns merged due to acid diffusion when baking temperature was 100 °C which is substantially above the T_g of the resist. Pattern distortion was observed at baking temperatures 70 and 80 °C probably because of inadequate crosslinking. The best results were obtained when PEB was carried out at 90 °C, where the patterns were accurately reproduced. Although the PEB temperature is above the T_g of the resists, the patterns are accurately reproduced since crosslinking is rapid. G_1-Tris-epoxide has higher T_g (80 ^oC) and six epoxides, and hence the contrast is greater (3.3) than that for G_1-Bis-epoxide (2.78) which has T_g (38 ^oC) and has three epoxides. While G_1-Dhn-epoxide has three epoxides and higher T_g (66 ^oC) compared to G_1-Bis-epoxide, the lower reactivity of 1,5-Dhn based epoxide results in relatively lower contrast (2.43). Besides the line width is limited to 50 nm and pitch to 1:10.

It is believed that PEB be preferably carried out below T_g of the resist materials in order to ensure that the patterns are not distorted. However, this does not always seem to be the case. The G_1-Bis-epoxide having T_g (38 ^oC) could be satisfactorily processed at 90 ^oC PEB. Mori et al., (2006) also reported that the resist containing 1, 1, 1-tris (4-hydroxyphenyl) ethane and α, α, α-tris(4-hydroxyphenyl)-1-ethyl-4-isopropylbenzene in the core having T_g 55 ^oC could be subjected to PEB 120 ^oC to resolve 200 nm lines at 1:2 pitch. It appears that apart from the initial T_g, the rate of crosslinking at PEB, which results in increase in T_g as the PEB proceeds, is a critical factor. Thus G_1-Dhn-epoxide having a T_g 66 ^oC could be processed only at 50 nm at a pitch 1:10 and yielded a lower contrast as compared to G_1-Bis-epoxide because of lower reactivity.

5.3.3.7.3. Electron beam lithography

Low molecular weight dendrimers have been explored in EBL to reduce the feature size to sub 100 nm ranges (Tully et al., 2000). Our rationale for the choice of phenol and naphthalene based FGDs for EBL has been already explained. The three resists were evaluated for EBL as follows. Oxidised silicon wafers were used to enhance the adhesion of photoresist to the substrate. Resists containing 5 wt. % FGDs and 10 wt. %), triphenylsulfonium perfluoro-1-butanesulfonate (PAG) on the basis of FGDs were spin-coated onto two inch silicon wafers at 6000 rpm which formed 66 nm (G_1-

Tris-epoxide), 63 nm (G_1-Bis-epoxide) and 62 nm (G_1-Dhn-epoxide) thick films respectively. Soft baking of the coated films on the silicon wafer was carried out on hot plate at 70 ^{o}C for 5 min. The resists were patterned using e-beam at 20 kV acceleration voltage, 20 µm aperture and the dose 35µC/cm^2 at beam current 170 pA. Irradiation of triphenylsulfonium perfluoro-1-butanesulfonate generates acid, which subsequently reacts with epoxides leading to initiation of polymerization in the post exposure bake (PEB), carried out at 90 ^{o}C for one min. Post exposure baked films were developed with propylene glycol methyl ether acetate (SU-8 developer MicroChem) for 20 sec, followed by a 10 sec immersion in isopropyl alcohol.

5.3.3.7.4. Scanning electron microscopy

Figures 5.9 (A) and (B) show scanning electron micrographs for 500, 200, 100 and 50 nm patterns of G_1-Tris-epoxide and G_1-Bis-epoxide resists using the same mask. At this magnification 50 nm lines were not seen. At higher magnification 50 nm lines at pitch 1:2 were resolved (Figure 5.10 A). However in the case of G_1-Dhn-epoxide, 50 nm lines could be resolved only at pitch 1:10 (Figure 5.10 B). This could be attributed to the lower reactivity of 1, 5-Dhn based resist during crosslinking. Figures 5.11 and 5.12 show pattern images of FGDs based on trisphenol and bisphenol-A respectively. SEM demonstrates that 30 nm lines could be resolved when the pitch was 1:10 (A), 1:2 (B), and 1:1(C). Thus trisphenol as well as bisphenol based FGDs could be used to pattern features upto 30 nm at pitch 1:1 despite difference in T_g.

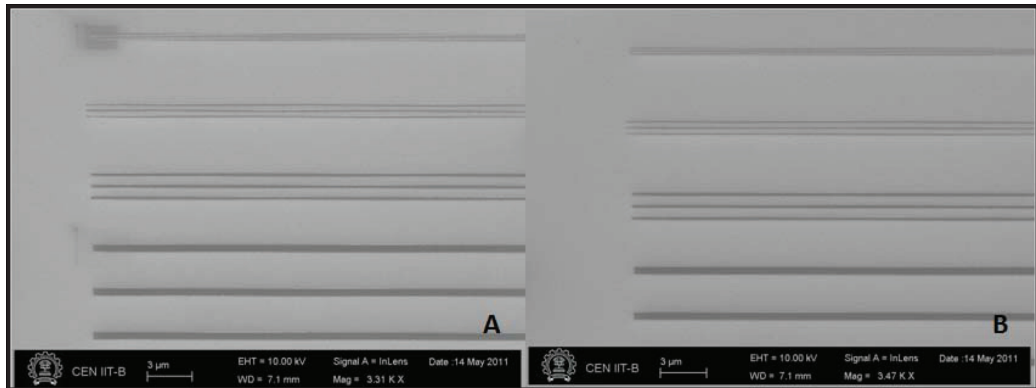

Figure 5.9: SEM images of A) G_1-Tris-epoxide and B) G_1-Bis-epoxide EBL pattern Line thickness 500, 200, 100 and 50 nm bottom upward.

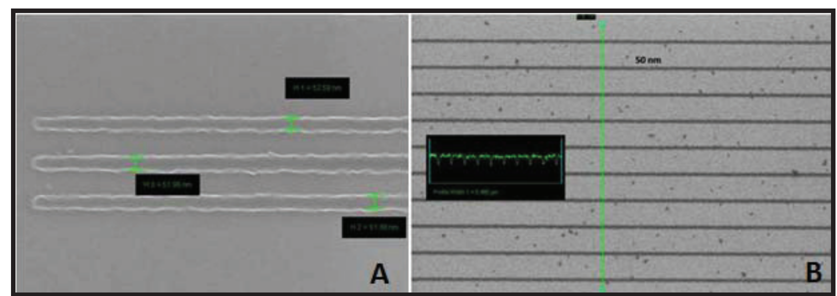

Figure 5.10: A) SEM image of 50 nm lines at 1:2 nm pitch for G_1-tris-epoxide; B) 50 nm lines at 1:10 nm pitch for G_1-Dhn-epoxide.

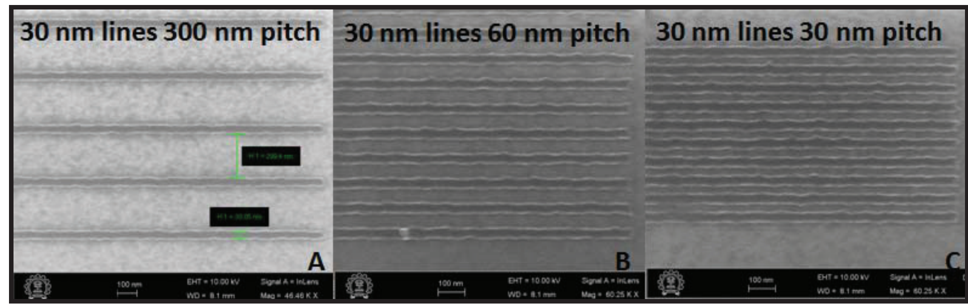

Figure 5.11: 30 nm lines at pitch 1:10 (A), 1:2 (B), 1:1(C) G_1-tris-epoxide

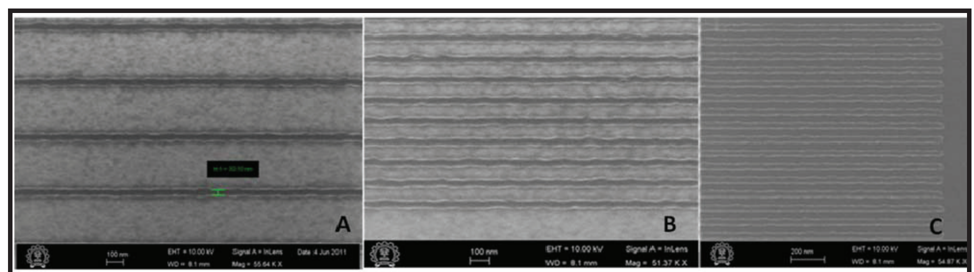

Figure 5.12: 30 nm lines at pitch 1:10 (A), 1:2 (B) and 1:1 (C) G_1-Bis-epoxide

5.3.3.7.5. Line edge roughness (LER)

Low LER is critical to the gate device performance, as gate LER is the primary source of variability for channel lengths below 25 nm (Sun et al., 2010). LER was calculated from the following equation reported by Leunissen et al., (2004) from average of 20 adjacent points on the line for feature size 100, 50 and 30 nm.

$$\sigma = \left(\frac{\sum_{i=1}^{N} (\delta W(z_i) - \delta W)^2}{N-1} \right)^{1/2} \qquad \text{.......1}$$

Figures 13A, 13B and 13C show typical images of 30, 50 and 100 nm lines of G_1-Tris-epoxide, used for LER calculation. The LER values calculated are based on an average of 20 adjacent points along the lines and are summarized in Table 5.3.

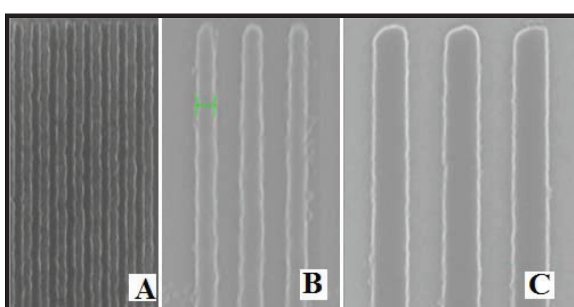

Figure 5.13: Images of patterns of G_1-Tris-epoxide used for LER calculation

The LER increased with decreasing feature size**.** The values obtained for FGDs containing trisphenol and bisphenol-A units are lower than those for FGD based on 1,5-Dhn. The LER is influenced by the molecular size of the resist, as well as lithographic conditions which influence acid diffusion, crosslinking density and swelling during development (Patsis and Gogolides, 2005). Amongst the systems investigated, G_1-Tris-epoxide based FGD containing six epoxide groups for crosslinking shows highest contrast and lowest LER. Although FGDs based on G_1-Bis-epoxide and G_1-Dhn-epoxide contain three epoxides each for crosslinking, G_1-Bis-epoxide shows higher contrast and lower LER compared to that for G_1-Dhn-epoxide. This is because incorporation of naphthalene moieties results in lower degree of crosslinking (Pan et al., 2007). In either case LER values obtained with these FGD resists are comparable to those obtained with molecular glasses (Table 5.3). Yang et al., (2006) reported LER as low as 5 nm for 100 nm lines, when sensitivity was 60 μC/cm^2 at 100 kV for the resist containing blend of 6,69,7,79- tetrahydroxy-4,4,49,49-tetramethyl-2,29-spirobichroman monomer, tetrakis-(methoxylmethyl)-glycoluril (TMMGU) as cross-linker, and 5 wt% triphenylsulfonium nanoflate as a photoacid generator. Similarly Dai et al., (2006) reported a resist system containing 4-[4-[1,1-Bis(4-hydroxyphenyl)ethyl]]-R,R-dimethylbenzylphenol, and the same crosslinker and PAG reported by Yang et al., (2006). The resist could resolve upto 100 nm lines and LER ≈5.1 nm, at a sensitivity of 80 μC/cm^2 at 100 kV. As compared to these resists, FGDs reported in this work resolve features up to 30 nm at 1:1 pitch and exhibit LER 6 nm at 20 kV. It would be possible to achieve lower LER at 30 nm

feature size at 100 kV, as LER decreases with increasing acceleration as reported by Rio et al., (2009) and Wu et al., (2010).

Table 5.3: LER values comparison

Resist	Line width (nm)	LER (3σ)	Sensitivity (μC/cm^2)	Refrence
G_1-Tris-epoxide	100 nm	5.40	35 (20 KV)	This work
	50 nm	5.80		
	30 nm	6.00		
G_1-Bis-epoxide	100 nm	5.63	35 (20 KV)	This work
	50 nm	5.70		
	30 nm	6.30		
G_1-Dhn-epoxid	100 nm	6.80	35 (20 KV)	This work
	50 nm	7.80		
6,6',7,7'-tetrahydroxy-4,4,4',4'-tetramethyl-2, SpirobicHroman	100	5.00	60 (100 KV)	Yang et al., 2006
4-[4-[1,1-Bis(4-hydroxyphenyl)ethyl]] α,α-Dimethyl-benzylphenol	100	5.10	80 (100 KV)	Dai et al., 2006

5.4. Conclusions

FGDs based on 1,3,5-tris bromomethyl benzene as the core and 1, 1, 1-tris-p-4-hydroxyphenyl ethane, bisphenol-A and 1,5-dihydroxynaphthalene peripheral groups were synthesized. The peripheral hydroxyls were converted to epoxide groups and evaluated as negative photoresists for electron beam lithography. The resists based on 1, 1, 1-tris-p-4-hydroxyphenyl ethane and bisphenol-A could resolve 30 nm lines at a pitch 1:1. It should therefore be possible to fabricate features lower in size at the pattern density which would be useful for fabricating devices for future applications.

5.5. References

1. Aktary, M., Jensen, M. O., Westra, K. L., Brett, M. J., Freeman, M. R. J. Vac. Sci. Technol. B 2003, **21**, 4, 5-7.
2. Argitis, P., Boyatzis, S., Raptis, I., Glezos, N., Hatzakis, M. ACS, symposium series 1998, **706**, 345-357.
3. Balakrishnan, M., Faccini, M., Diemeer, M. B. J., Verboom, W., Driessen, A., Reinhoudt, D.N., Leinse, A. Electronics Letters 2006, **42**, 1-2.
4. Bilenberg, B., Jacobsen, S., Schmidt, M. S., Skjolding, L.H.D., Shi, P., Boggild, P., Tegenfeldt, J.O., Kristensen, A., Microelectronic Engineering 2006, **83,** 1609–1612.
5. Bystrova, S., Luttge, R., Berg, Vanden, A. Microelectronic Engineering 2007, **84**, 1113-1116.
6. Carr, B., Evers, A., Weimer, M., Smith, B., Leith, J. Proceedings of SPIE 2010, **7638**, in press.
7. Chattopadhyay, D. K, Panda, S S., Raju, K.V.S.N. Progress in Organic Coatings 2005, **54**, 10–19.
8. Chen, Y., Peng, K., Cui, Z. Microelectronic Engineering 2004, **73-74,** 662–665.
9. Dai, J., Chang, S. W., Hamad, A., Yang, D., Felix, N., Ober, C. K. Chem. Mater. 2006, **18**, 3404-3411.
10. De Silva, A., Felix, N. M., Ober, C. K. Adv. Mater. 2008, **9999**, 1–7.
11. De Silva, A., Ober, C. K., J. Mater. Chem. 2008, **18**, 1903–1910.
12. Duan, H., Winston, D., Yang, J. K. W., Cord, B. M., Manfrinato, V. R., Berggren, K. K. J. Vac. Sci. Technol. B. 2010, **28**, 6, 58-62.
13. Esfandeh, M., Mirabedini, S. M., Pazokifard, S., Tari, M. Colloids and Surfaces A: Physicochem. Eng. Aspects 2007, **302**, 11–16.
14. Feng, R., Farris, R.J. J. Micromech. Microeng. 2003, **13**, 80–88.
15. Jiguet, S., Bertsch, A., Judelewicz, M., Hofmann, H., Renaud, P. Microelectronic Engineering 2006, **83,** 1966–1970.
16. Kamimura, Y., Haba, O., Endo, T., Ueda, M. Journal of Polymer Science: Part A: Polymer Chemistry 2005, **43**, 1210–1215.
17. Kinoshita, M., Kita, H., Shirota, Y. Adv. Fun. Mater. 2002, **12,** 11-12, 780-786.

18. Lee, K. S., Lee, K.T, Kim, Y. S., Jeong, Y.H. Proceedings IEEE Conference on Nanotechnology 2005.
19. Leunissen, L. H. A., Lawrence, W. G., Ercken, M. Microelectronic Engineering 2004, **73–74**, 265–270.
20. Ming, L., Yulin, Q., Baoqin, C., Qiuxia, X., Yinklli, Z. IEEE, 2004, 563-566.
21. Mori, H., Nomura, E., Hosoda, A., Miyake, Y., Taniguchi, H., Macromol. Rapid Commun. 2006, **27**, 1792–1796.
22. Nallani, A.K., Park, S.W., Lee, J.B., Proc. SPIE 2003, **5116**, I, 414-23.
23. Pan, G., Du, Z., Zhang, C., Li, C., Yang, X., Li, H. Polymer 2007, **48,** 3686-3693.
24. Patsis, G. P., Gogolides, E. Journal of Physics: Conference Series 2005, **10**, 389–392.
25. Pepin, A., Studer, V., Decanini, D., Chen, Y., Microelectronic Engineering 2004, **73–74**, 233–237.
26. Pielichowski, J., Czub, P. Die Angewandte Makromolekulare Chemie 1997, **251,** 1-12.
27. Qualtieri, A., Stomeo, T., Martiradonna, L., Cingolani, R., Vittorio, M. D. Lithography Ed. 2010, M INTECH, Croatia, 115-130.
28. Rio, D., Constancias, C., Saied, M., Icard, B., Pain, L. J. Vac. Sci. Technol. B 2009, **27**, 6, 2512-2517.
29. Sailer, H., Ruderisch, A., Henschel, W., Schurig, V., Kern, D.P., J. Vac. Sci. Technol. B 2004, **22**, 6, 3485-3488.
30. Sailer, H., Ruderisch, A., Kern, D. P., Schurigb, V. J. Vac. Sci. Technol. B 2002, **20**, 6, 58-61.
31. Sayah, A., Parashar, V. K., Gijs, M. A. M. Journal of Microelectromechanical Systems, 2007, **16**, 3, 564-570.
32. Shirota, Y., J. Mater. Chem. 2005, **15**, 75–93.
33. Smith, S., Brockie, N. L., Murray, J., Wilson, C. J., Horsfall, A. B., Terry, J. G., Stevenson, J. T. M., Mount, A. R., Walton A. J. IEEE International Conference on Microelectronic Test Structures 2010, **22-25**, 8-13.
34. Sun, X., Liu, T. K. 2010, IEEE Transactions On Semiconductor Manufacturing 2010, **23**, 311-315.

35. Tully, D. C., Trimble, A. R., Frechet, J. M. J. Adv. Mater. 2000, **12**, 15, 1118-1122.
36. Ueda, M., Takahashi, D., Nakayama, T., Haba, O. Chem. Mater. 1998**, 10**, 2230-2234.
37. Uthirakumar, P., Suh, E. K., Hong, C. H., Lee, Y. S., Polymer 2005, **46**, 4640–4646.
38. Wang, C. S., Lee, M. C., Polymer 2000, **41**, 3631–3638.
39. Williamson, F., Shields, E. A., IEEE 2003, 57-60.
40. Wong, W. H., Pun, E. Y. B. J. Vac. Sci. Technol. B 2001, **19,** 3, 732-735.
41. Wu, S. W., Makiuchi, Y., Chen, C., Lithography, 2010, 241-266.
42. Yang, D., Chang, S. W., Ober, C. K. J. Mater. Chem., 2006, **16**, 1693–1696.
43. Yonezawaa, N., Mori S., Miyata, S., Anyashiki, Y. U., Maeyama, K. Reactive & Functional Polymers 2002, **53**, 11–17.

Chapter 6

Chemically amplified positive resists based on first generation dendrimers for electron-beam lithography

6.1. Introduction

The trends in electron beam lithography (EBL) techniques and materials development with reference to negative resist were described in the previous chapter. Positive resists offer advantages such as stripability, ability to re-expose in the case of scumming, and compatibility with a dark field reticle (Flack et al., 2005). The sensitivity of CARs depends on the protecting group structure and photo-acid generator (Reichmanis et al., 1991). Positive (Kadota et al., 2004) and negative (Tully et al., 2000; Felix et al., 2008) chemically amplified resists (CAR) based on t-BOC conjugated dendrimers (FGDs) have been evaluated for EBL.

The irregularity of patterns resulting in case of polymeric resists during the fabrication of nanometer scale patterns arises from high molecular weight molecular weight, distribution and chain entanglement. The positive resists based on molecular glasses for EBL include substituted benzenes as the core and phenols at the periphery to enhance T_g (Kadota et al., 2004; Dai et al., 2006; Hattori et al.,2009) as well as base solubility (De Silva et al., 2008). Phenolic calix[4]resocinarenes were synthesized by the condensation of resorcinols with phenol substituted aldehyde. Conjugation of hydroxyl with t-BOC groups yielded positive resists which were evaluated using optical (Young-Gil et al., 2002) and e-beam (Ito et al., 2008) lithography. However these calix[4]resocinarenes based resists exhibited poor film forming property and adhesion and were used as dissolution rate modifiers (Ito et al., 2008).

The challenge in designing low molecular weight resists for EBL application lies in avoiding crystallization and ensuring high T_g to avoid distortion of patterns during post exposure bake (De Silva et al., 2008, Kadota et al., 2004). There is a need to develop low molecular weight resists which can be processed by EBL to pattern features up to 30 nm at 1:1 pitch.

In the previous chapter we reported synthesis of FGDs starting with 1,3,5-trisbromomethylbenzene as the core and dense, bulky, rigid, bisphenol-A, 1,5-dihydroxy naphthalene (1,5-Dhn) and 1, 1, 1-tris-p-4-hydroxyphenyl ethane (trisphenol) units at the periphery. The peripheral moieties were connected to the core through ether linkage. Number of the peripheral hydroxyl groups and T_g of the FGDs could be manipulated. To evaluate the same skeletons as positive resists, we conjugated peripheral hydroxyls with t-BOC anhydride. The FGD resists so formed exhibited good film forming properties, solubility and adhesion. These were evaluated as positive e-beam resists to fabricate structures upto 30 nm at 1:1 pitch.

6.2. Experimental

6.2.1. Materials

1, 5-Dihydroxy naphthalene (1,5-Dhn), Bisphenol-A, 1, 1, 1-tris-p-4-hydroxyphenyl ethane (Trisphenol), 1, 3, 5-tris (bromomethyl) benzene, propylene glycol methyl ether acetate (PGMEA), triphenylsulfonium perfluoro-1-butanesulfonate (PAG), Tetramethyl ammonium hydroxide (TMAH) 25 wt % solution in water were procured from Aldrich chemicals (USA). Di-t-butyloxy dicarbonate (t-BOC), potassium carbonate (K_2CO_3), 4-Dimethylaminopyridine (DMAP), N-methyl-2-pyrrolidone (NMP) were from spectrochem, N, N-Dimethylformamide (DMF) obtained from Merck was distilled from CaH_2 under reduced pressure before use and all other reagents were used as received.

6.2.2. Synthesis

Synthesis of FGDs containing free hydroxyl at periphery viz G_1-Tris, G_1-Bis and G_1-Dhn was discussed in chapter 5. These were further functionalized to t-BOC conjugates as described below.

6.2.2.1. G_1-Tris-t-BOC100

3 g (2.9×10^{-3} moles) of G_1-Tris and 3.2 g (2.6×10^{-2} moles) DMAP were dissolved in 25 ml NMP and stirred for 20 min. A solution of di-t-BOC 5.7 g (2.6×10^{-2} moles) in 10 ml NMP was then added drop wise to the solution at 0-5 ^{o}C. After complete addition, the mixture was stirred for 24 h at room temperature. The product was precipitated from methanol. White powder was obtained after drying the product in a vacuum oven at 45 ^{o}C. The yield was 3.7 g (78%).

^{1}H NMR (DMSO-d_6); δ [ppm]: 6.83-7.05 (36H, phenolic protons), 7.46 (3H, benzylic protons), 5.04 (6H, Ph-CH_2), 2.16 (9H, -CH_3), 1.54 (54H, -CH_3).

Conjugates containing varying degrees of t-BOC substitution were synthesized by varying the amount of di-t-BOC during synthesis as mentioned below.

6.2.2.2. G_1-Tris-t-BOC80

3 g (2.9×10^{-3} moles) of G_1-Tris and 1.7 g (1.39×10^{-2} moles) DMAP, 25 ml NMP and di-t-BOC 3 g (1.39×10^{-2} moles) in 10 ml NMP were used. Yield 3.2 g (75%).

^{1}H NMR (DMSO-d_6); δ [ppm]: 6.64-7.09 (36H, aromatic protons), 7.49 (3H, benzylic protons), 5.09 (6H, Ph-CH_2), 2.08 (9H, -CH_3), 1.47 (40H, -CH_3), 9.30 (2H, Ph-OH).

6.2.2.3. G_1-Tris-t-BOC60

3 g (2.9 X 10^{-3} moles) of G_1-Tris and 1.3 g (1.04 X 10^{-2} moles) DMAP, 25 ml NMP and di-t-BOC 2.3 g (1.04 X 10^{-2} moles) in 10 ml NMP were used. Yield 2.9 g (73%).
^{1}H NMR (DMSO-d_6); δ [ppm]: 6.65-7.08 (36H, aromatic protons), 7.50 (3H, benzylic protons), 5.10 (6H, Ph-CH_2), 2.09 (9H, -CH_3), 1.48 (29H, -CH_3), 9.25 (2.5H, Ph-OH).

6.2.2.4. G_1-Tris-t-BOC50

3 g (2.9 X 10^{-3} moles) of G_1-Tris and 1.1 g (8.7 X 10^{-3} moles) DMAP, 25 ml NMP and di-t-BOC 1.9 g (8.7 X 10^{-3} moles) in 10 ml NMP were used. Yield 2.9 g (76%).
^{1}H NMR (DMSO-d_6); δ [ppm]: 6.61-7.09 (36H, aromatic protons), 7.49 (3H, benzylic protons), 5.09 (6H, Ph-CH_2), 2.08 (9H, -CH_3), 1.47 (26H, -CH_3), 9.25 (3H, Ph-OH).

6.2.2.5. G_1-Bis-t-BOC100

3 g (3.75 X 10^{-3} moles) of G_1-Bis and 2.1 g (1.68 X 10^{-2} moles) DMAP, 25 ml NMP and di-t-BOC 3.7 g (1.68 X 10^{-2} moles) in 10 ml NMP were used. Yield 3.27 g (79%).
^{1}H NMR (DMSO-d_6); δ [ppm]: 6.90-7.24 (24H, aromatic protons), 7.47 (3H, benzylic protons), 5.08 (6H, Ph-CH_2), 1.60 (18H, -CH_3), 1.47 (27H, -CH_3).

6.2.2.6. G_1-Bis-t-BOC80

3 g (3.75 X 10^{-3} moles) of G_1-Bis and 1.1 g (9 X 10^{-3} moles) DMAP, 25 ml NMP and di-t-BOC 2 g (9 X 10^{-3} moles) in 10 ml NMP were used. Yield 2.6 g (76%).
^{1}H NMR (DMSO-d_6); δ [ppm]: 6.90-7.19 (24H, aromatic protons), 7.47 (3H, benzylic protons), 5.07 (6H, Ph-CH_2), 1.60 (18H, -CH_3), 1.47 (14 H, -CH_3) 9.17 (1.5H, Ph-OH).

6.2.2.7. G_1-Bis-t-BOC60

3 g (3.75 X 10^{-3} moles) of G_1-Bis and 0.8 g (6.75 X 10^{-3} moles) DMAP, 25 ml NMP and di-t-BOC 1.5 g (6.75 X 10^{-3} moles) in 10 ml NMP were used. Yield 2.4 g (72%).
^{1}H NMR (DMSO-d_6); δ [ppm]: 6.62-7.19 (24H, aromatic protons), 7.47 (3H, benzylic protons), 5.07 (6H, Ph-CH_2), 1.55-1.60 (18H, -CH_3), 1.47 (11 H, -CH_3) 9.17 (1.7H, Ph-OH).

6.2.2.8. G_1-Bis-t-BOC50

3 g (3.75 X 10^{-3} moles) of G_1-Bis and 0.7 g (5.62 X 10^{-3} moles) DMAP, 25 ml NMP and di-t-BOC 1.2 g (5.62 X 10^{-3} moles) in 10 ml NMP were used. Yield 2.3 g (70%).
^{1}H NMR (DMSO-d_6); δ [ppm]: 6.62-7.19 (24H, aromatic protons), 7.47 (3H, benzylic protons), 5.07 (6H, Ph-CH_2), 1.55-1.60 (18H, -CH_3), 1.46 (9H, -CH_3) 9.16 (2H, Ph-OH).

6.2.2.9. G_1-Dhn-t-BOC100

3 g (5.04 X 10^{-3} moles) of G_1-Dhn and 2.8 g (2.3 X 10^{-2} moles) DMAP, 25 ml NMP and di-t-BOC 5 g (2.3 X 10^{-2} moles) in 10 ml NMP were used. Yield 3.2 g (72%).
^{1}H NMR (DMSO-d_6); δ [ppm]: 8.16 (3H, protons on 8th carbon of naphthalene ring), 7.75 (3H, protons on 4th carbon of naphthalene ring), 6.59-7.19(6H, protons on 2nd and 6th carbon of naphthalene ring), 7.63 (3H, protons on 3rd carbon of naphthalene ring), 7.34 (3H, protons on 7th carbon of naphthalene ring), 7.46 (3H, benzylic protons), 5.43 (6H, Ph-CH_2), 1.52 (27H, CH_3).

6.2.2.10. G_1-Dhn-t-BOC80

3 g (5.04 X 10^{-3} moles) of G_1-Dhn and 1.5 g (1.2 X 10^{-2} moles) DMAP, 25 ml NMP and di-t-BOC 2.6 g (1.2 X 10^{-2} moles) in 10 ml NMP were used. Yield 2.6 g (66%).
^{1}H NMR (DMSO-d_6); δ [ppm]: 6.59-8.12 (18H, naphthalene ring protons), 7.46 (3H, benzylic protons), 5.42 (6H, Ph-CH_2), 1.52 (17H, CH_3), 10.11 (1H, hydroxyl proton of naphthalene).

6.2.2.11. G_1-Dhn-t-BOC60

3 g (5.04 X 10^{-3} moles) of G_1-Dhn and 1.1 g (9.1 X 10^{-3} moles) DMAP, 25 ml NMP and di-t-BOC 2 g (9.1 X 10^{-3} moles) in 10 ml NMP were used. Yield 2.5 g (67%).
^{1}H NMR (DMSO-d_6); δ [ppm]: 6.59-8.12 (18H, naphthalene ring protons), 7.46 (3H, benzylic protons), 5.42 (6H, Ph-CH_2), 1.52 (14H, CH_3), 10.11 (1.54H, hydroxyl protons of naphthalene).

6.2.2.12. G_1-Dhn-t-BOC50

3 g (5.04 X 10^{-3} moles) of G_1-Dhn and 0.9 g (7.5 X 10^{-3} moles) DMAP, 25 ml NMP and di-t-BOC 1.6 g (7.5 X 10^{-3} moles) in 10 ml NMP were used. Yield 2.4 g (65%).

^1H NMR (DMSO-d_6); δ [ppm]: 6.59-8.12 (18H, naphthalene ring protons), 7.46 (3H, benzylic protons), 5.42 (6H, Ph-CH_2), 1.52 (12H, CH_3), 10.11 (1.84H, hydroxyl protons of naphthalene).

6.2.3. Characterization

The ^{1}H-NMR spectra were recorded in $CDCl_3$ and DMSO-d_6 at 25°C on Bruker 200 MHz spectrometer. Molecular weights of the FGD t-BOC conjugates were calculated by ^{1}H-NMR spectroscopy. The IR spectra were recorded on a Perkin Elmer spectrometer (DRS mode). The differential scanning calorimetery (DSC) was performed using TA Instruments DSC Q-10 at 5 °C/min under a nitrogen atmosphere. Thermo gravimetric analyses (TGA) were conducted using TGA-7, Perkin Elmer at 10 °C/min under nitrogen atmosphere. The resists were spin coated on silicon wafers at 6000 rpm. Raith 150^{TWO} was used a) to measure resist film thickness, b) for pattering, c) imaging the resists structures and d) LER measurements.

6.2.4. Lithographic evaluation of positive tone FGDs

80 % t-BOC conjugated FGDs were dissolved in propylene glycol methyl ether acetate (PGMEA) to obtain 5 wt % solutions. Commercially available triphenylsulfonium perfluoro-1-butanesulfonate (PAG), 10 wt. % on the basis of FGDs was used. The resulting solutions were filtered through a 0.2 µm filter and were spin coated onto 2 inch silicon wafers at 6000 rpm, for 30 sec leading to a film thickness of 70 nm for G_1-Tris-t-BOC, 64 nm for G_1-Bis-t-BOC and 61 nm for G_1-Dhn-t-BOC as measured by Raith-150^{Two} SEM. The coated wafers were prebaked at 70 °C for 5 min, and then exposed to e-beam radiation using Raith-150^{Two}. Post exposure bake was performed at 90 °C for 60 sec. Positive tone images were developed in an aqueous 0.26 N TMAH solution, 70 sec in case of G_1-Tris-t-BOC and for 85 sec in case of G_1-Bis-t-BOC and G_1-Dhn-t-BOC since in the latter case resist were not developed at the end of 70 sec.

6.3. Results and Discussion

6.3.1. Choice of dendrimers

The resist materials to be used for lithography have to be amorphous in nature and have glass transition temperature preferably around 100 °C to ensure image fidelity

(Dai et al., 2006), by minimizing acid diffusion as well as prevent pattern deformation when the film is baked after exposure. Polymers have been used as resist materials because of their amorphous nature, high thermal stability, high T_g and good substrate adhesion (Reichmanis et al., 2001). However, problems are encountered with polymeric resists in the fabrication of nanometer-scale patterns, because of high molecular weight and molecular weight distribution leading to irregular line patterns. Chain entanglement in polymers affects lithographic performance at molecular scale dimensions, where the desired feature size is smaller than the chain length of the polymer (Tully et al., 2000; De Silva et al., 2008).

For sub 50 nm features, low molecular weight dendrimers and molecular glasses which are amorphous in nature are preferred. These materials offer advantages over polymeric materials in terms of high purity, well defined molecular structures and lack of chain entanglement. Dai et al., (2006) reported molecular glass resist based on 4-[4-[1,1-Bis(4-hydroxyphenyl)ethyl]]-R,R-dimethylbenzyl phenol containing three terminal hydroxyl groups which resolved upto 150 nm lines at 1:1 pitch at 40 $\mu C/cm^2$ using 40 kV beam energy. Positive resists based on 1,3,5-tris-p-p-hydroxyphenyl-phenyl-benzene for EBL were reported by Hattori et al., (2009). 70 nm lines at 1:1 pitch were resolved at 6.5 $\mu C/cm^2$ using 5 kV beam energy. Kadota et al., (2004) reported positive resist based on 5,5-bis-(tert-butoxycarbonyloxy) phenyl-5-[4,4-bis(tert-butoxycarbonyloxy)-1,1:3,1-terphenyl-50-yl]-1,1:3,1:3,1:3,1-quinque- phenyl for EBL which exhibited a sensitivity of 66 $\mu C/cm^2$, enabling fabrication of 25 nm line patterns on exposure to 50 kV beam energy. Peripheral hydroxyl group density in the resist plays a key role in resolving lower features when 0.26 N aqueous TMAH solution is used as a developer. Lower the density of peripheral hydroxyl groups, slower the dissolution rate in base developer. Haba et al., (1999) reported a dendrimer based on Calix[4]resorcinarene for optical lithography containing 16 hydroxyl groups at the peripher. The solubility of this dendrimer in aqueous tetramethyl ammonium hydroxide (TMAH) solutions was very high and hence dilute TAH solution had to be used. Kamimura et al., (2005) reported a dendrimer which contained 6 peripheral hydroxyls which could be developed in 0.26 N TMAH. Most of the resists reported in the literature contain 3-6 terminal hydroxyl groups (Dai et al., 2006; Hattori et al., 2009; Kadota et al., 2004). In summary, a positive resist for EBL should have low molecular weight, avoid chain entanglement, have optimum peripheral hydroxyl

groups as to ensure higher T_g, solubility in 0.26 N TMAH and resolve features below 50 nm.

In the preceding chapter we synthesized and evaluated negative resists containing 1,3,5-trisbromomethylbenzene core and bisphenol-A, trisphenol and 1,5-Dhn as peripheral moiety. In order to explore the possibility of developing positive resists from the same skeleton, FGDs in this work were designed (Figure 6.1and 6.2) by conjugating peripheral hydroxyl groups with t-BOC groups and were evaluated as positive resists in EBL. Thus the performance of FGDs containing same skeleton can be evaluated as a negative as well as positive resist

6.3.2. Synthesis of FGDs

The FGDs were synthesized by reacting bisphenol-A, trisphenol and 1, 5-Dhn with 1, 3, 5-trisbromomethyl benzene in the presence of potassium carbonate in DMF.

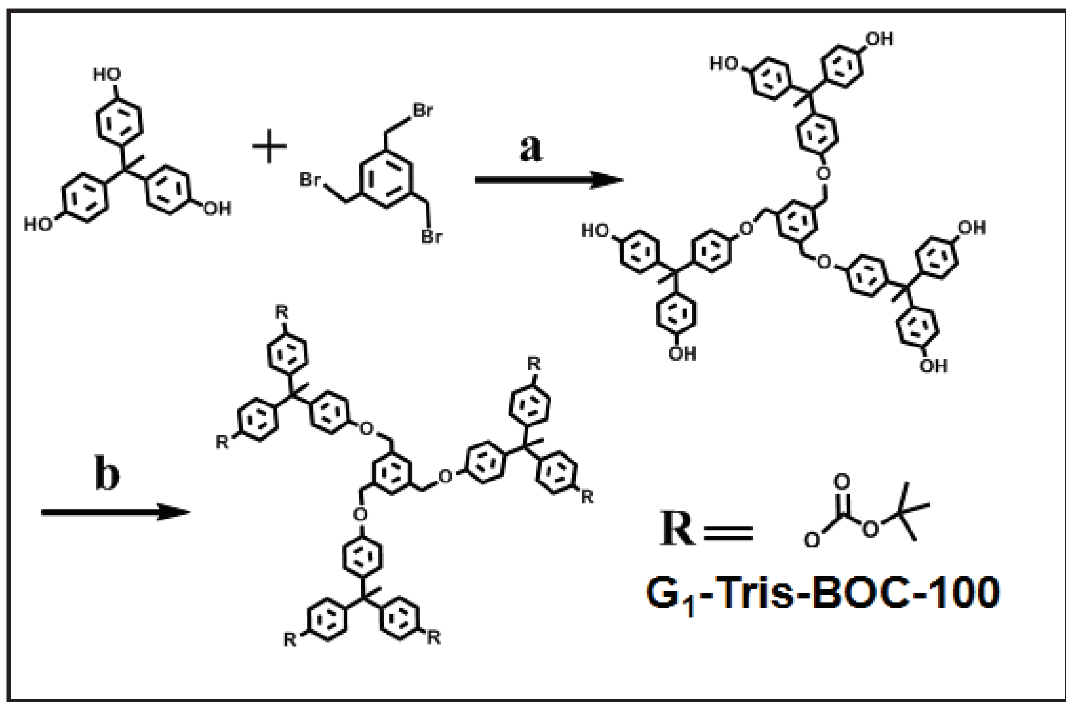

Figure 6.1: Synthesis of t-BOC conjugated FGDs, (a) K_2CO_3, DMF, 60°C; (b) NMP, DMAP, and di-t-butyldicarbonate at room temperature.

Figure 6.2: Structures of G_1-Bis-t-BOC100 and G_1-Dhn-t-BOC100

Peripheral hydroxyl groups were conjugated with t-BOC using procedure reported by Hansen and Riggs, (1998) to yield resists *viz.* G_1-Tris-t-BOC, G_1-Bis-t-BOC and G_1-Dhn-t-BOC. Degree of substitution was controlled by manipulating the ratio di-t-BOC groups to phenolic groups in the FGDs.

6.3.3. FGDs characterization

6.3.3.1. Solubility

FGDs based on Trisphenol (G_1-Tris), Bisphenol-A (G_1-Bis) and 1, 5-Dhn (G_1-Dhn) bearing peripheral hydroxyl groups were readily soluble in TMAH, THF, acetone, DMF, NMP, ethyl acetate, methanol, ethanol, cyclohexanone and 2-methoxyethanol, γ-butyrolactone, ethyl lactate, propylene glycol methyl ether acetate (PGMEA) etc, but were insoluble in chlorinated solvents. The t-BOC conjugated FGD derivatives at 80 % and 100 % degree of substitution were insoluble in methanol, ethanol and 0.26N TMAH, but were readily soluble in chlorinated solvents, toluene, THF, acetone, DMF, ethyl acetate, ethyl lactate and propylene glycol methyl ether acetate (PGMEA). FGDs at t-BOC substitution of 50 and 60 % dissolved slowly in 0.26N TMAH. The solubility differential allows the development of exposed area in 0.26N TMAH.

6.3.3.2. FTIR spectroscopy

The FGDs before and after t-BOC conjugation were analysed by FTIR spectroscopy. Figures 6.3a-6.3c show the FTIR spectra of FGDs at different t-BOC substitution levels.

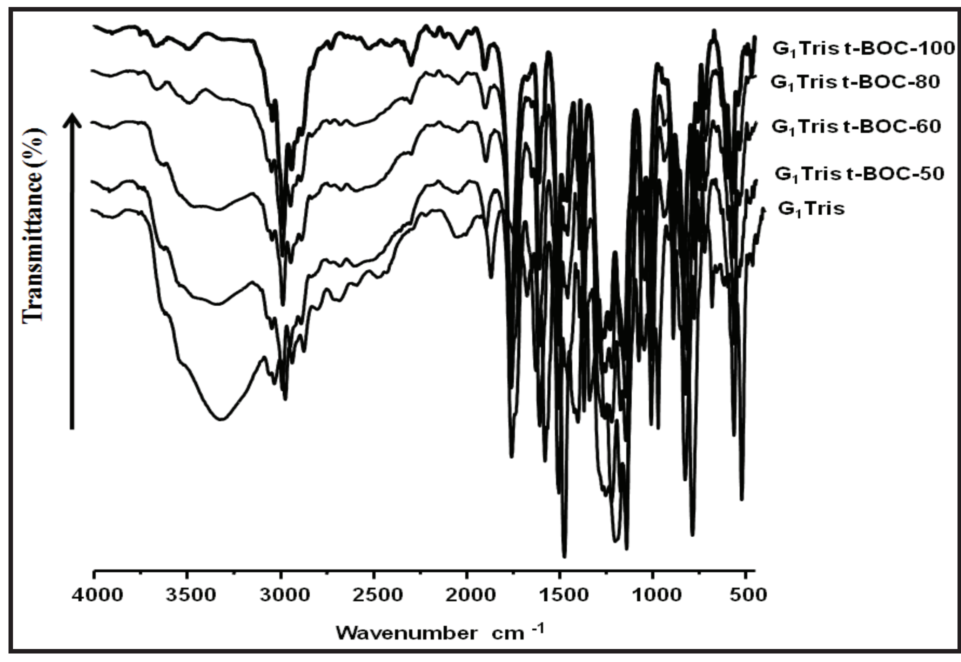

Figure 6.3a: FTIR of G_1-Tris-t-BOC

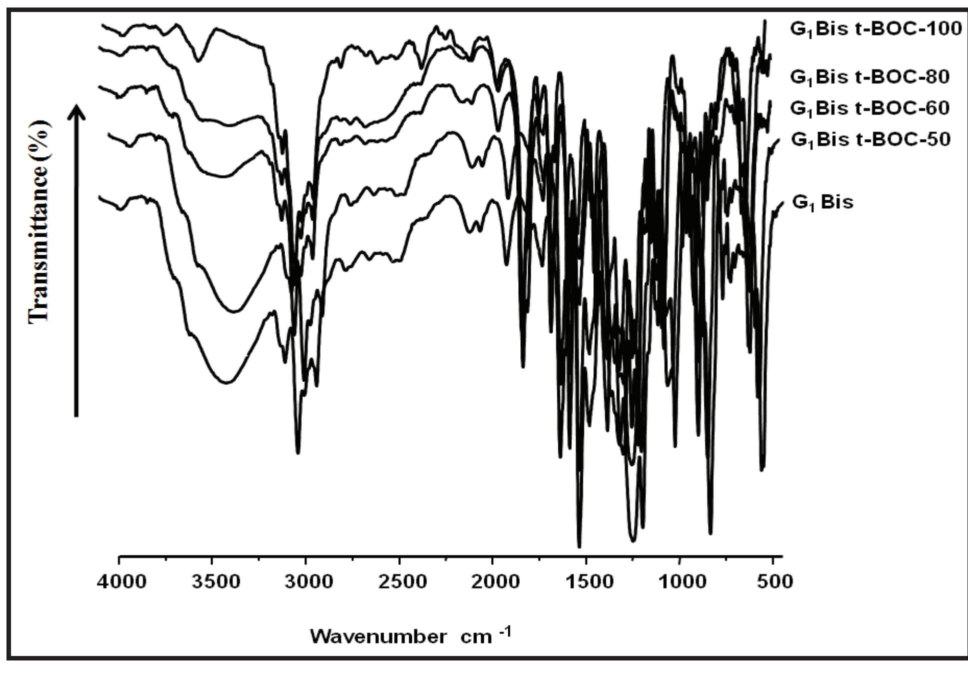

Figure 6.3b: FTIR of G_1-Bis-t-BOC

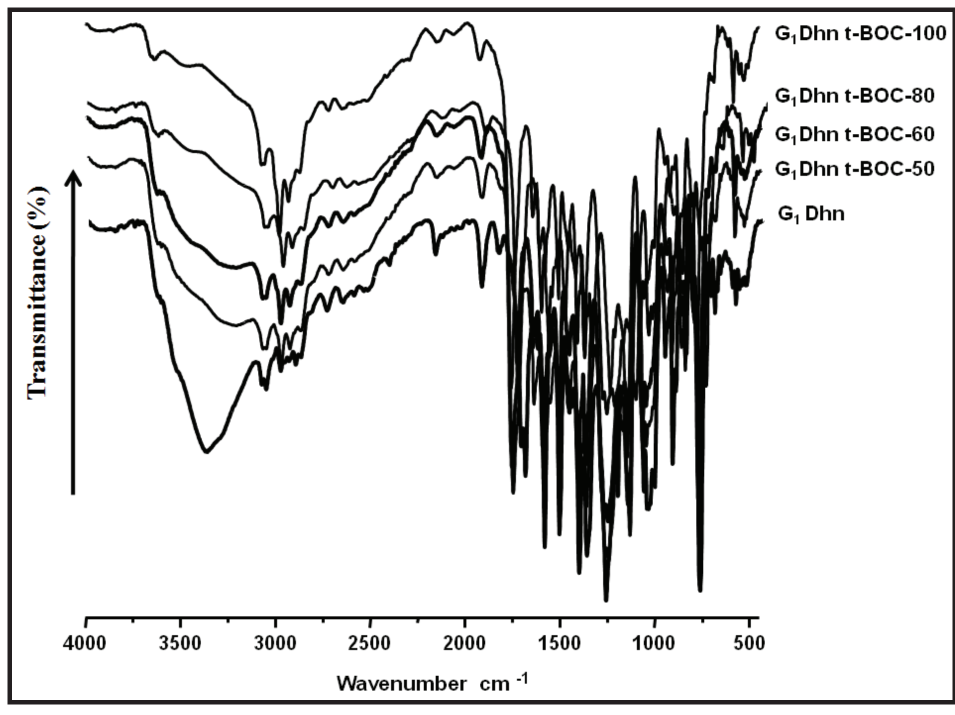

Figure 6.3c: FTIR of G_1-Dhn-t-BOC

From Figures 6.3a-6.3c it is seen that, in all the cases, as the degree of substitution of t-BOC groups increased, the intensity of hydroxyl peaks at 3350 cm^{-1} decreased and that of the peak at 1750 cm^{-1} corresponding to carbonyl group increased.

The free hydroxyl groups at various levels of t-BOC substitution for FGDs based on bisphenol-A and trisphenol show absorption at 3460 cm^{-1}, which is much stronger than the FGD based on 1,5-Dhn. This indicates that hydrogen bonding in the case of 1, 5-Dhn is weak. Similar FTIR characterizations were reported by Dai et al., (2006).

6.3.3.3. ^{1}H-NMR spectroscopy

Figures 6.4a and 6.4b show ^{1}H-NMR spectra of G_1-Tris and G_1-Tris-t-BOC100 in DMSO-d_6 and $CDCl_3$ respectively. Disappearance of the peak at 4.5 ppm corresponding to the methylene of 1,3,5-trisbromomethyl benzene and appearance of new peak at 5.11 ppm confirmed formation of G_1-Tris (Figure 6.4a). After conjugation with t-BOC, peak at 9.28 ppm which corresponds to aromatic hydroxyls is replaced by the peak at 1.54 ppm corresponding to the methyl protons of t-BOC units. This confirms the formation of G_1-Tris-t-BOC100 (Figure 6.4b).

The conversion of G_1-Bis and G_1-Dhn to their corresponding t-BOC conjugates is illustrated by the assignments of the peak positions mentioned in the synthesis section.

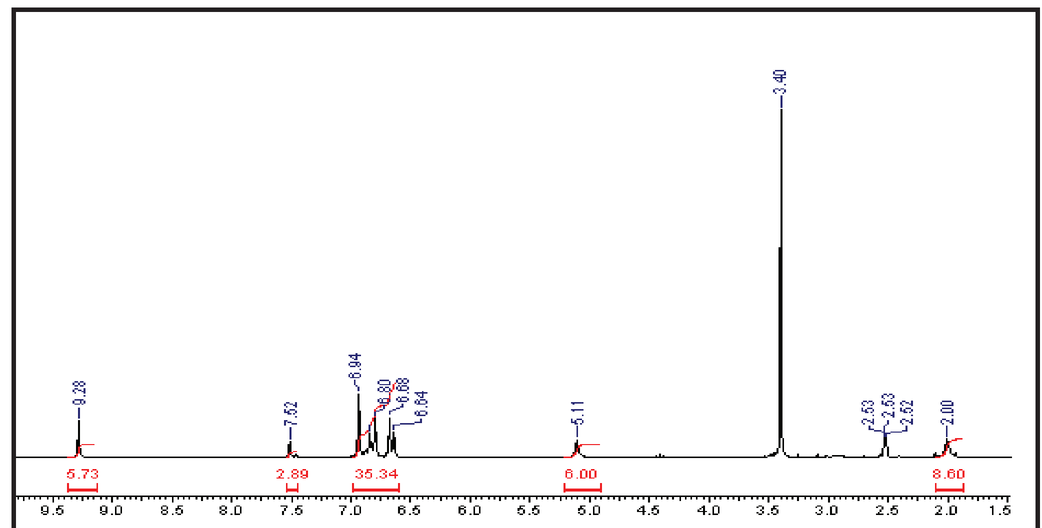

Figure 6.4a: ^{1}H NMR spectrum of G_1-Tris

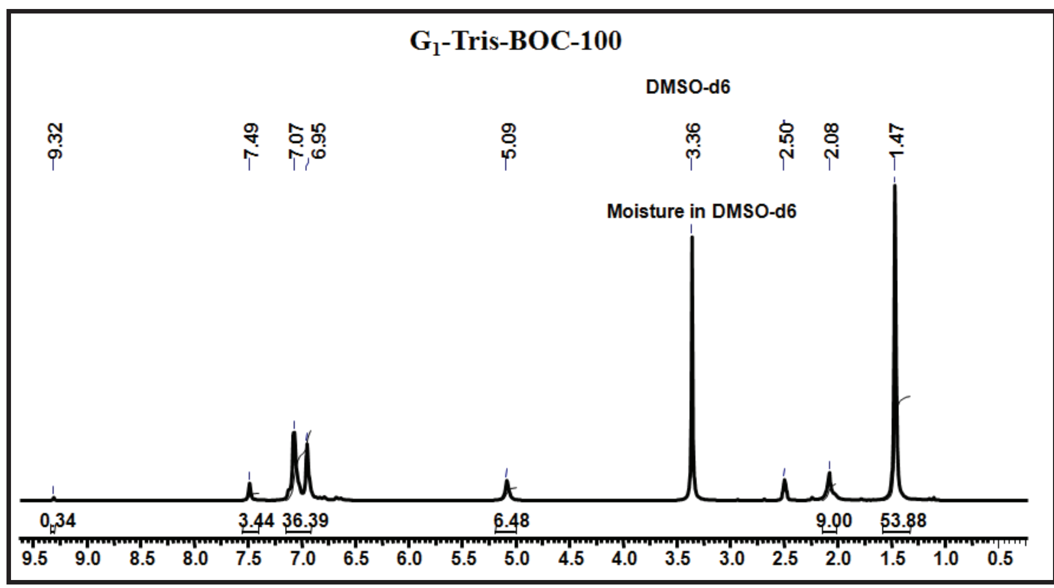

Figure 6.4b: ^{1}H NMR spectrum of G_1-Tris-BOC100

6.3.3.4. Molecular weights

The molecular weights of the FGDs at various level of t-BOC substitution were calculated from ^{1}H NMR measurements. This also helped to estimate exact degree of substitution of t-BOC groups. The results are summarized in Table 6.1.

Molecular weight of G_1-Tris was confirmed by comparing peak integrals of 6-methyne protons adjacent to the core benzene ring (5.11 ppm) with 9 methyl protons of the three trisphenol units (2.08 ppm) as shown in Figure 6.4a. Similarly molecular weight of G_1-Tris-t-BOC100 was calculated by comparing peak integrals of 6 methyne protons adjacent to the core benzene ring with 54 methyl protons of the six t-BOC units (1.47 ppm) as shown in Figure 6.4b. The molecular weights of the FGDs at various level of t-BOC substitution and molecular weights of FGDs based on bisphenol-A and 1,5-Dhn and their t-BOC conjugates were similarly calculated.

Table 6.1: Molecular weights of FGDs

No.	FGDs	MW
1	G_1-Tris-t-BOC100	1633
2	G_1-Tris-t-BOC80	1488
3	G_1-Tris-t-BOC60	1355
4	G_1-Tris-t-BOC50	1318
5	G_1-Tris	1033
6	G_1-Bis-t-BOC100	1102
7	G_1-Bis-t-BOC80	961
8	G_1-Bis-t-BOC60	923
9	G_1-Bis-t-BOC50	902
10	G_1-Bis	799
11	G_1-Dhn-t-BOC100	895
12	G_1-Dhn-t-BOC80	777
13	G_1-Dhn-t-BOC60	753
14	G_1-Dhn-t-BOC50	724
15	G_1-Dhn	595

6.3.3.5. Thermal properties

6.3.3.5.1. Thermal degradation

Thermal stability of t-BOC conjugated FGDs was evaluated using TGA-7, Perkin Elmer at 10 °C/min under nitrogen atmosphere. The TGA plots (Figure 6.5a-6.5c)

show two step degradation profile attributed to the deblocking of t-BOC group in the range 160 to 210 ^{o}C followed by degradation of the skeletal structure beyond 250 ^{o}C. The weight loss in the temperature range 160 ^{o}C to 210 ^{o}C corresponds to the loss of

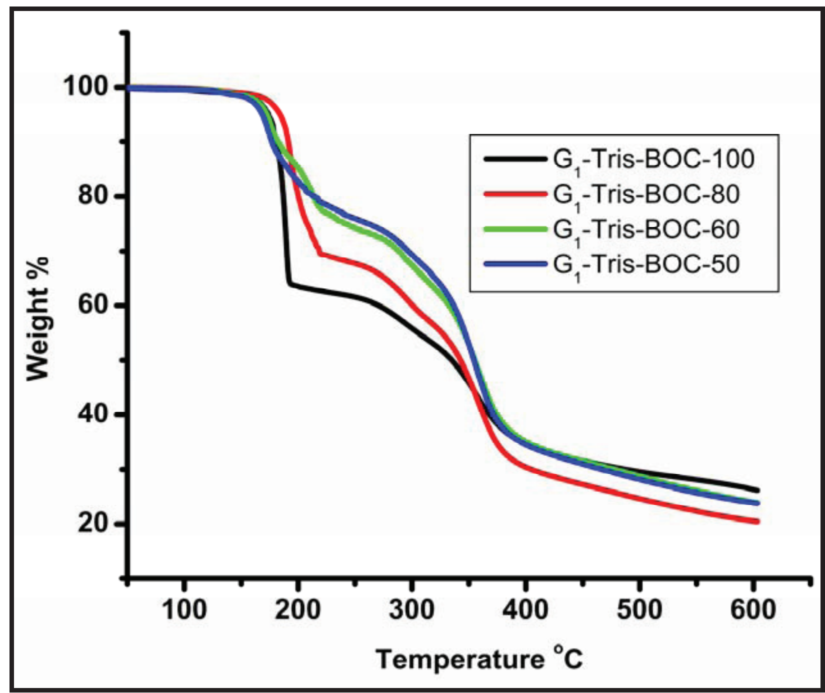

Figure 6.5a: TGA thermograms of G_1-Tris-t-BOC

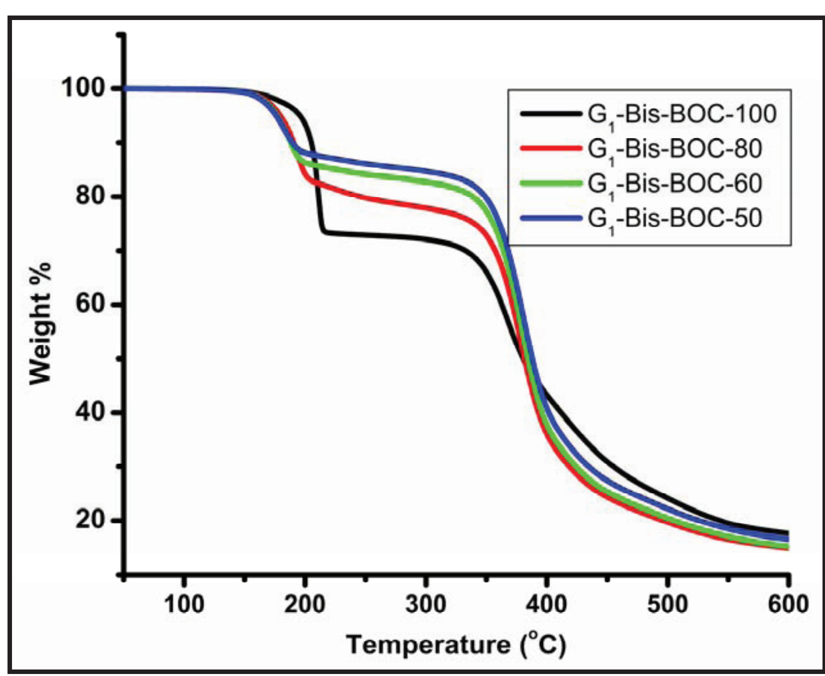

Figure 6.5b: TGA thermograms of G_1-Bis-t-BOC

t-BOC group in the form of carbon dioxide and isobutylene. The values of weight loss calculated from the degree of substitution of t-BOC groups estimated from ^{1}H NMR measurements were compared with experimental values. The results summarized in Table 6.2 show good agreements between the two especially in the case of G_1-Tris-t-BOC and G_1-Bis-t-BOC. Ito et al., (2008) reported a positive e-beam resist based on O-Octa-t-butoxycarbonylmethyl-C-tetramethyl-calix[4]resorcinarene having 8 peripheral hydroxyl groups which were conjugated with t-butyloxycarbonylmethyl groups. The resist exhibited weight loss on heating in the range 175 to 220 °C due to the loss of isobutene and carbon dioxide.

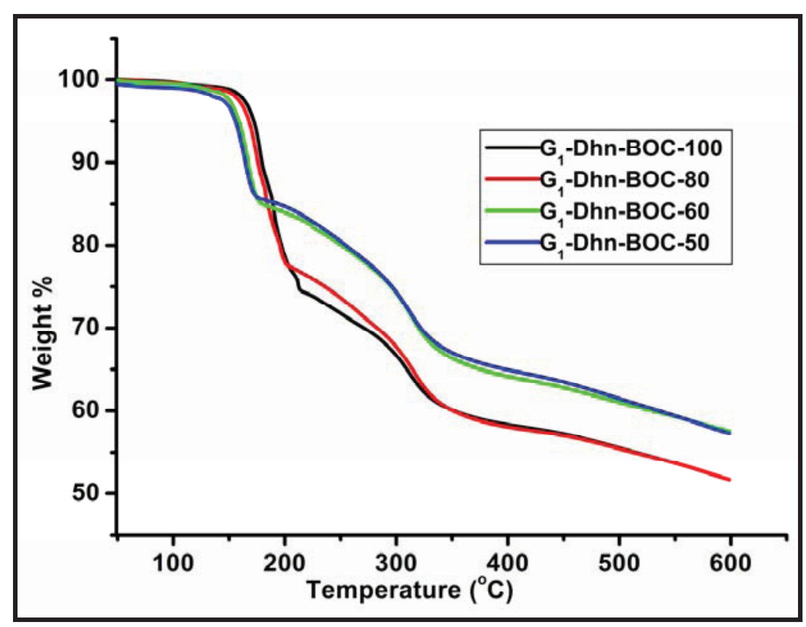

Figure 6.5c: TGA thermograms of G_1-Dhn-t-BOC

Table 6.2: t-BOC content from ^{1}H-NMR and TGA analysis

FGDs	G_1-Tris-BOC				G_1-Bis-BOC				G_1-Dhn-BOC			
t-BOC (mole %) [a]	50	60	80	100	50	60	80	100	50	60	80	100
t-BOC (mole %) [b]	47	53	75	100	34	41	54	100	43	52	60	100
Wt. loss (Calculated)[c]	21	24	30	37	11	13	17	27	18	20	23	33
Wt. loss (Found)[d]	19	23	30	37	11	13	18	27	14	16	23	28

[a]Degree of t-BOC substitution from feed. [b] t-BOC degree of substitution from ^{1}H-NMR). [c] Theoretical % weight loss due to t-BOC deprotection. [d] Actual % weight loss on t-BOC deprotection.

The t-BOC deblocking temperature range reported in this work is comparable to that reported by Ito et al., (2008). Thus it appears that the deblocking temperature for t-BOC conjugated dendrimers is characteristic of the t-BOC group and relatively independent of the substrate. The decomposition temperature on the other hand is governed by the thermal stability of the skeleton involved.

6.3.3.5.2. The glass transition temperature

T_gs of FGDs were measured on TA Instruments DSC Q10 in nitrogen atmosphere at a heating rate 5 ^oC/min and the data are presented in Table 6.3. Figures 6.6a-6.6c show the DSC traces of the FGDs based on trisphenol, bisphenol-A and 1,5-Dhn before and after t-BOC conjugation respectively. T_gs of t-BOC conjugated FGDs were recorded during the first heating cycle whereas those of unconjugated FGDs were recorded during second heating cycle. The traces indicate no melting peak confirming amorphous nature of the materials. The T_gs of unconjugated FGDs decreased in the order G_1-Tris (139 ^oC) > G_1-Dhn (87 ^oC) > G_1-Bis (70 ^oC). The rigid core and branched rigid peripheral segments like trisphenol, bisphenol-A and 1,5-Dhn units effectively restrict molecular mobility.

Although G_1-Tris is not a fused ring structure as G_1-Dhn, it yields higher T_g, since three sets of four sterically rigid moieties (three aromatic rings and one methyl group) on the same carbon effectively restrict molecular rotation. Further, intermolecular interaction between the six free peripheral hydroxyl groups results in enhanced T_g.

In contrast, FGDs based on bisphenol-A and 1,5-Dhn containing three hydroxyl groups each in the periphery result in lower T_g. Presence of jeminal methyl groups in the bisphenol-A units increases free volume in the molecule, which results in decrease in T_g (Uthirakumar et al., 2005) than in the case of the FGD based on 1,5-Dhn.

The T_gs of the conjugated FGDs depended on both core structure and degree of t-BOC substitution. T_gs of the FGDs based on trisphenol and bisphenol-A decreased with t-BOC conjugation from 139 ^oC to 119 ^oC and from 70 ^oC to 45 ^oC respectively. The conjugation of t-BOC group in G_1-Tris and G_1-Bis increases bulkiness of peripheral segments which would enhance T_g. On the other hand t-BOC conjugation disrupts hydrogen bonding which would lower T_g. The overall decrease in T_g with increase in t-BOC substitution indicates that hydrogen bonding contributes significantly to the T_g of G_1-Tris and G_1-Bis. Similar trend was reported by De Silva

et al., (2008) for molecular glass resists containing t-BOC conjugated hydroxyphenylbenzene derivatives wherein T_g decreased from 122 °C to 66 °C. Surprisingly in the case of G_1-Dhn, T_g increased with increasing t-BOC conjugation from 87 to 126 °C.

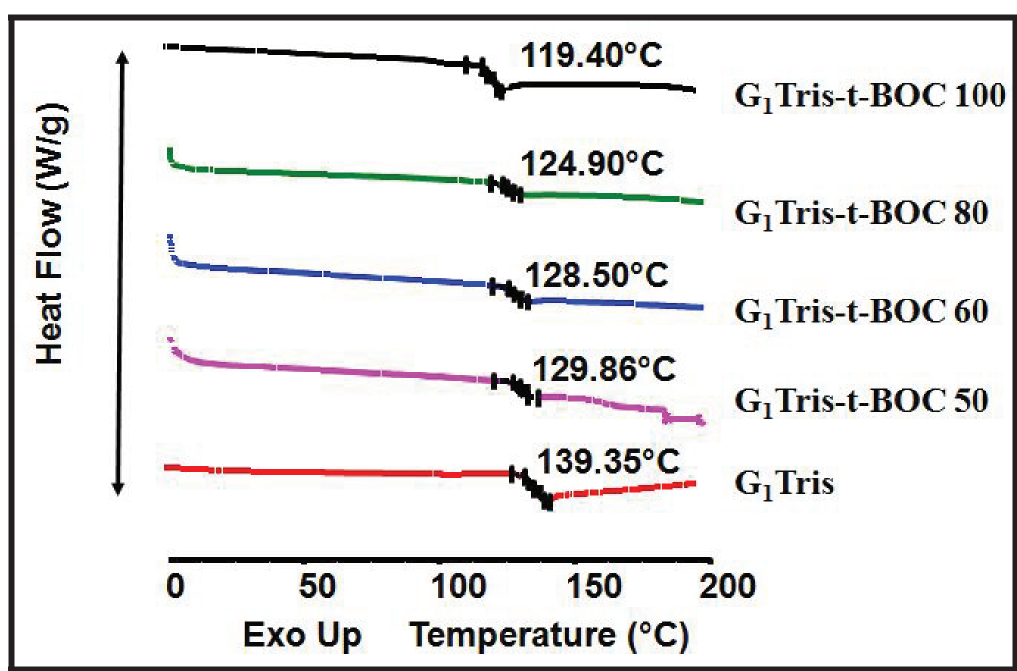

Figure 6.6a: T_g of G_1-Tris and t-BOC derivatives

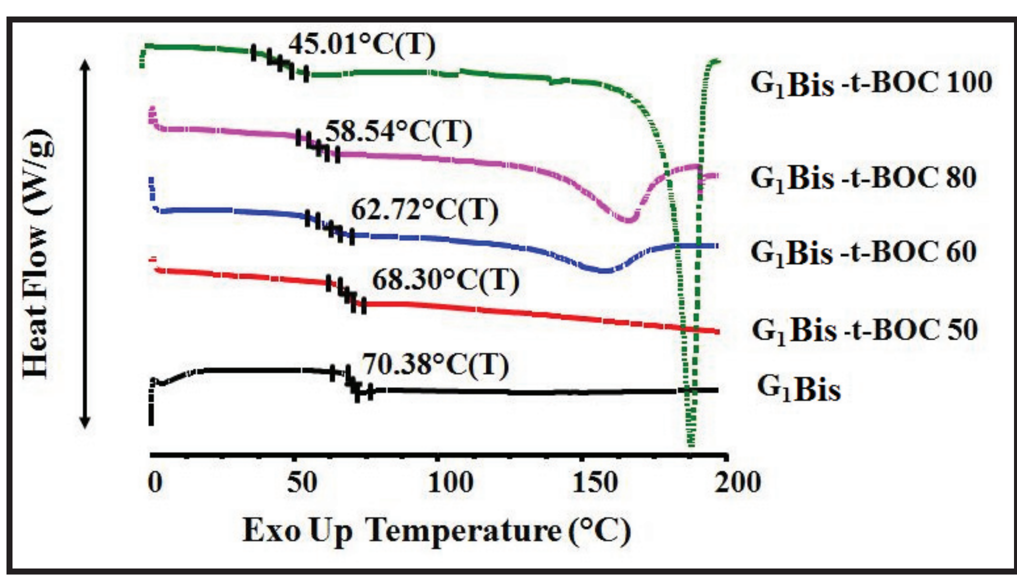

Figure 6.6b: T_g of G_1-Bis and t-BOC derivatives

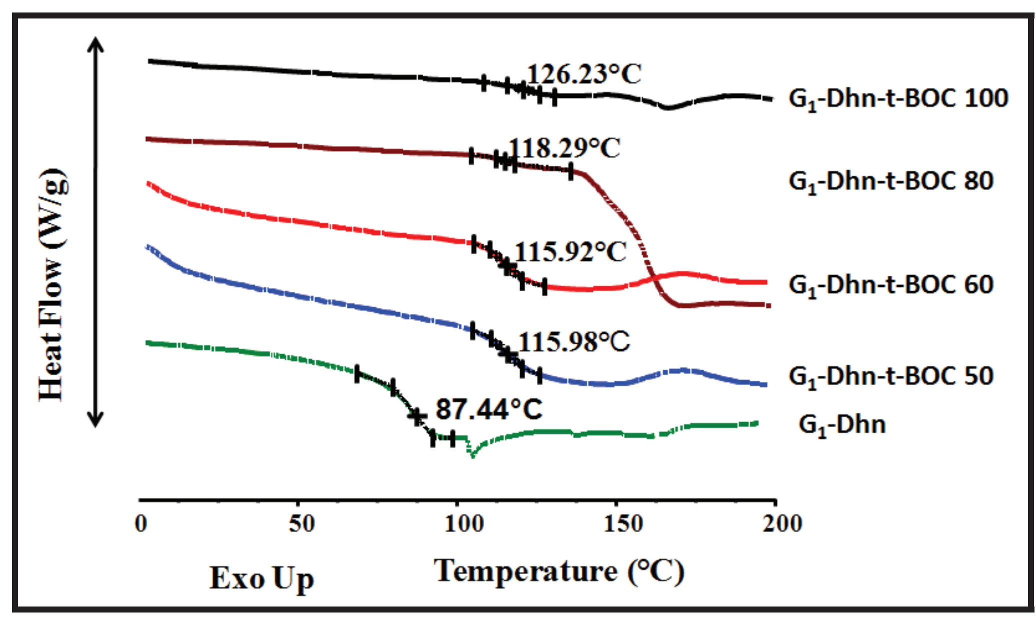

Figure 6.6c: T_g of G_1-Dhn and t-BOC derivatives

Table 6.3: T_g of FGDs

No.	FGDs	T_g °C
1	G_1-Tris-t-BOC100	119
2	G_1-Tris-t-BOC80	125
3	G_1-Tris-t-BOC60	130
4	G_1-Tris-t-BOC50	128
5	G_1-Tris	139
6	G_1-Bis-t-BOC100	45
7	G_1-Bis-t-BOC80	58
8	G_1-Bis-t-BOC60	63
9	G_1-Bis-t-BOC50	68
10	G_1-Bis	70
11	G_1-Dhn-t-BOC100	126
12	G_1-Dhn-t-BOC80	118
13	G_1-Dhn-t-BOC60	116
14	G_1-Dhn-t-BOC50	116
15	G_1-Dhn	87

Incorporation of t-BOC group enhances the rigidity of the fused naphthalene ring structure. Similar trend in T_g was reported by Dai et al., (2006) for positive e-beam resist containing t-BOC conjugated 4-[4-[1,1-Bis(4-hydroxyphenyl) ethyl]]-R,R-dimethyl- benzylphenol, T_g was 47°C when degree of substitution was 33% and increased to 59 °C when fully conjugated. It may be noted that all the conjugates reported by us exhibit higher T_gs than those reported by Dai et al., (2006) for molecular glass which are in the range 7-63 °C.

6.3.3.6. X-ray diffraction (XRD)

During the DSC measurements, no melting peak was observed for FGDs as well as their t-BOC conjugates. Powder samples were examined by X-ray diffraction as well. Figure 6.7 shows XRD patterns of the t-BOC conjugated FGDs. The 2θ values are G_1-Tris-t-BOC100 (17.82°), G_1-Bis-t-BOC100 (16.72°) and G_1-Dhn-t-BOC100 (22.51°) respectively. From the spectrum, it is confirmed that, low molecular weight FGDs are amorphous solids with no peaks indicative of crystallinity.

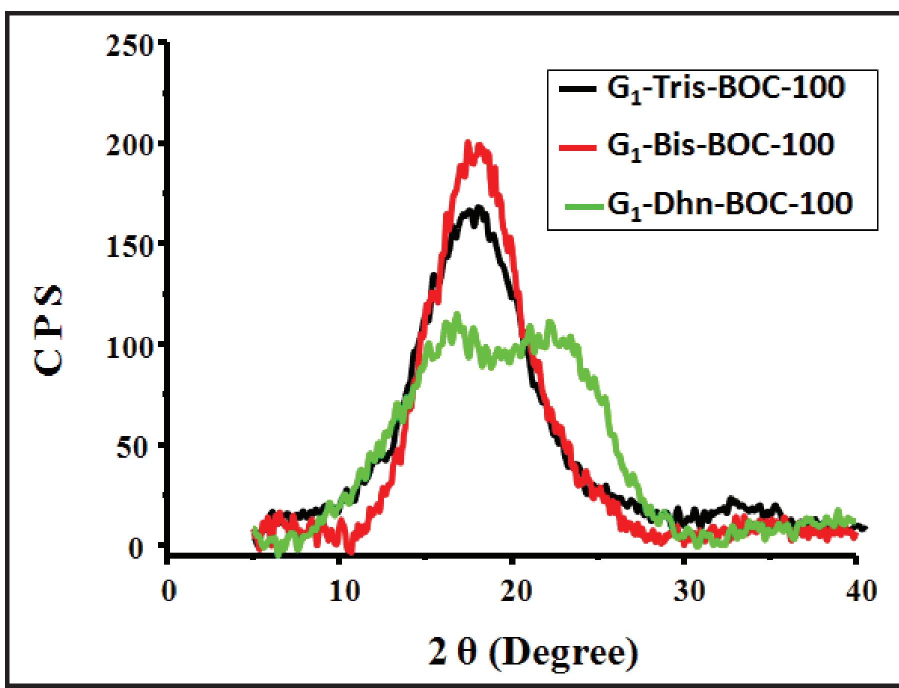

Figure 6.7: XRD of t-BOC conjugated FGDs

The monomers (bisphenol-A (T_m 158 °C); 1, 5-Dhn (T_m 180 °C; trisphenol (T_m 246 °C) and 1, 3, 5-trisbromo methyl benzene (T_m 94-99 °C) are highly crystalline in nature. However, the crystallinity is lost during condensation with 1, 3, 5-trisbromo

methyl benzene. The ether linkage not only disrupts the π-π conjugation between the two benzene rings which assists in crystallization (De Silva and Ober 2008) but also helps to enhance adhesion to the silicon substrate (Chattopadhyay et al., 2005; Yonezawa et al., 2002).

6.3.3.7. Adhesion measurements

Adhesion of FGDs on the silicon substrate was evaluated by calculating work of adhesion (W_{ad}) from the following equation reported by Young Gill et al., (2002).

$$W_{ad} = 2\{(\gamma p^{d}.\gamma s^{d})^{1/2} + (\gamma p^{h}.\gamma s^{h})^{1/2}\} \quad \ldots\ldots(1)$$

(Where γ: surface free energy, P: polymer, S: substrate, d: dispersion force, h: hydrogen bonding). To solve this equation, the contact angles (θ) of water and diiodomethane were measured. The values of contact angle and work of adhesion for various t-BOC conjugated FGD films on silicon wafer are given in Table 6.4.

Table 6.4: Work of adhesion for t-BOC films on silicon substrate

Dendrimers	G_1-Tris-BOC				G_1-Bis-BOC				G_1-Dhn-BOC			
a	50	60	80	100	50	60	80	100	50	60	80	100
θ (H_2O)	88	89.2	78.9	96.9	72.9	73	78.9	90.3	74.8	82.5	81.1	87.8
θ (CH_2I_2)	32	28.7	27	25	29.3	20	15.6	16.3	43	39.9	31.2	27.3
W_{ad}	59.4	55.5	42.3	39.3	82	79	68.8	48.6	83.4	71.8	70.7	57

a= t-BOC (mole %) θ= Contact angle, W_{ad} = work of adhesion (dyne cm^{-1})

Adhesion of resists to silicon substrate depends on the number of free hydroxyl groups in the resist. From Figure 6.8 it can be seen that work of adhesion decreases as t-BOC conjugation level increases. Similar trend was reported by Young Gil et al., (2002) for t-BOC conjugated calix[4]resorcinarene. Values of work of adhesion for 80 % t-BOC conjugated FGDs are 69, 70 and 42 dyne $cm^{-1}$for G_1-Bis-t-BOC, G_1-Dhn-t-BOC and G_1-Tris-t-BOC respectively.

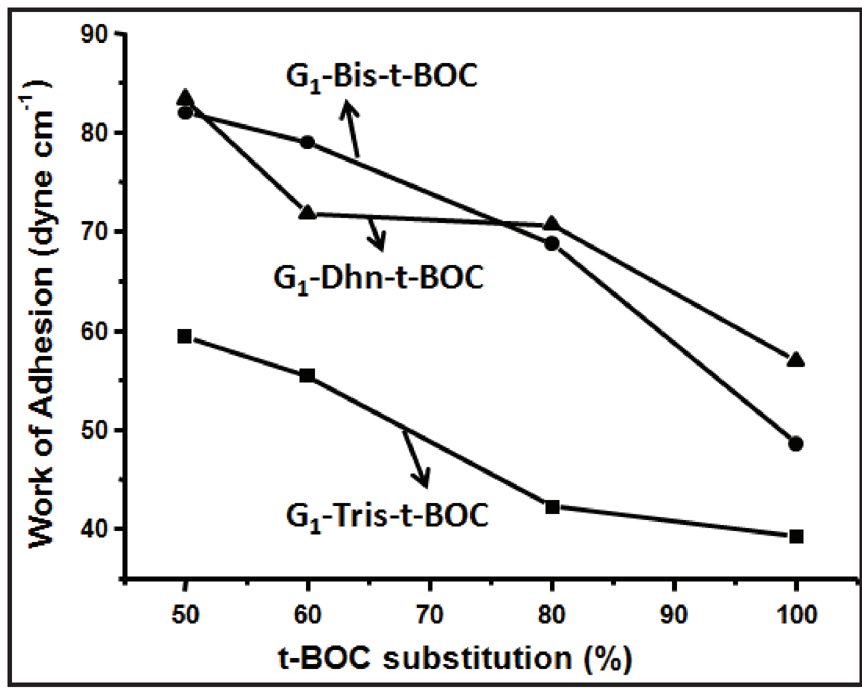

Figure 6.8: Effect of t-BOC protection on adhesion of FGDs

FGDs based on bisphenol-A and 1,5-Dhn even at t-BOC substituted at 80 % show substantially higher adhesion than that exhibited by 60 % t-BOC conjugated calix[4]resorcinarene (60.8 dyne cm^{-1}) (Young Gil et al., 2002). This could be attributed to the presence of polar ether linkages (Esfandeh et al., 2007; Chattopadhyay et al., 2005; Yonezawa et al., 2002).

6.3.4. Lithographic evaluation

6.3.4.1. Sensitivity curves for the FGD resists

To evaluate the sensitivity, 5 wt % solutions of 80 % t-BOC conjugated FGD resists containing 10 wt. % PAG on the basis of FGDs in PGMEA were spin coated on silicon wafers and were exposed in the dose range 20 $\mu C/cm^2$ to 200 $\mu C/cm^2$ in10 $\mu C/cm^2$ intervals with the beam current 157 pA. Exposed films were post baked at 90 ^oC for one min to promote the deprotection reaction and subsequently developed in 0.26 N TMAH for 70 sec in case of (G_1-Tris-t-BOC80) and 85 sec in case of (G_1-Bis-t-BOC80 and G_1-Dhn-t-BOC80). A series of 500 nm lines at 1:1 pitch were patterned. Typical patterns for G_1-Tris-t-BOC80 are shown in Figure 6.9a. Resist sensitivity was calculated by measuring height of the cross-section of the lines drawn at various dose

rates using Raith-150 two. Typical cross-sections of the G_1-Tris-t-BOC80 patterns used for calculating sensitivity and contrast are shown in Figure 6.9b.

The sensitivity curves for the positive tone FGD resists on exposure to e-beam at 20 kV beam energy, 20 µm aperture, resulting in a beam current of 157 pA are shown in Figure 6.10. Sensitivity was defined as the minimum dose D1 at which the exposed resist was completely deprotected and washed out after development.

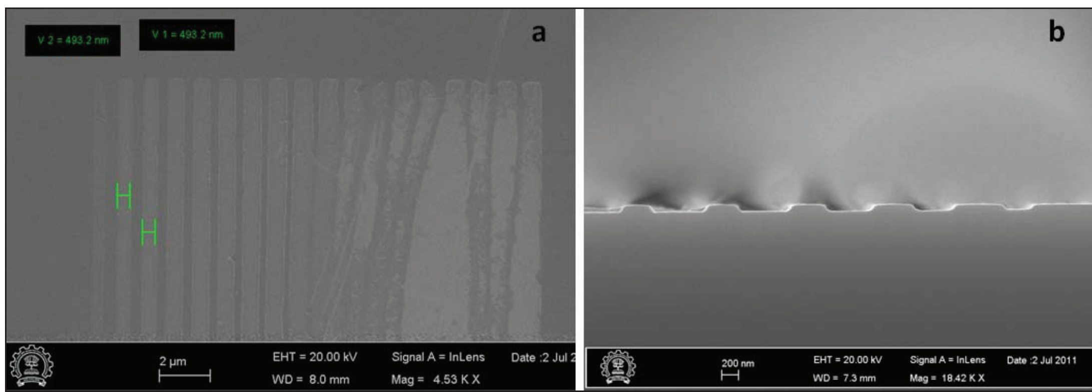

Figure 6.9**:** SEM image of G_1-Tris-t-BOC80 used for sensitivity and contrast calculation a) 500 nm lines with 1:1 pitch, b) Image of cross section of 500 nm lines.

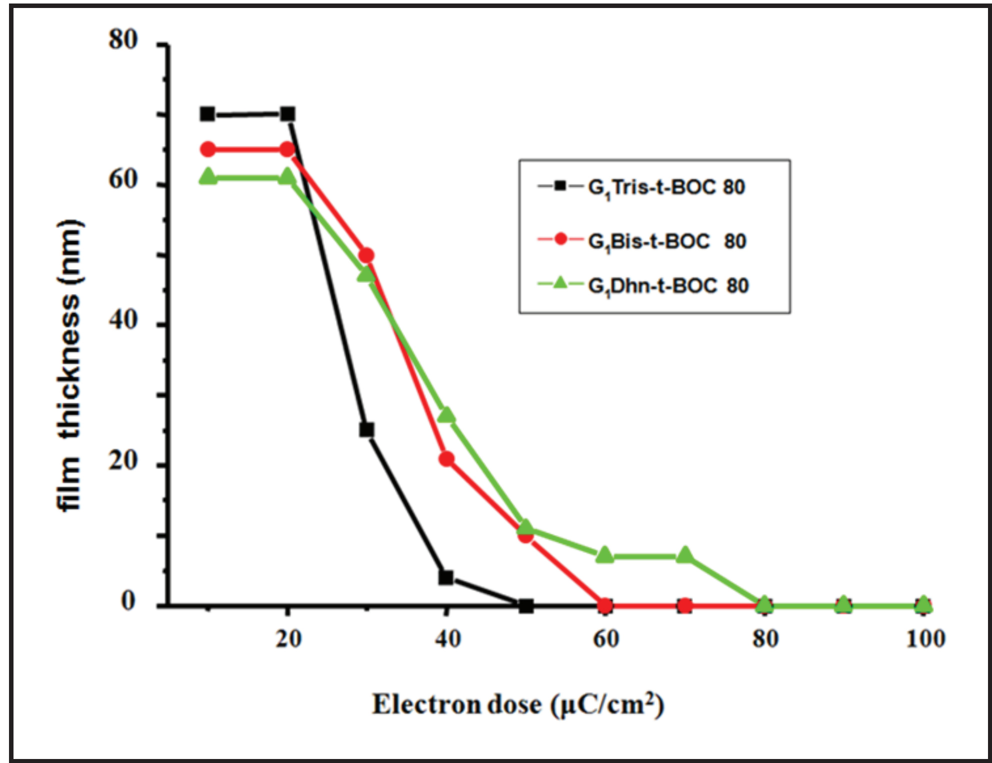

Figure 6.10: Exposure characteristics curves for FGDs containing 80 % t-BOC

Sensitivity values for the resists containing 10 wt % PAG were 50 μC/cm^2 (G_1-Tris-t-BOC80), 60 μC/cm^2 (G_1-Bis-t-BOC80) and 80 μC/cm^2 (G_1-Dhn-t-BOC80). Sensitivity and contrast are governed by the solubility of the resist in developer. Amongst the resists the sensitivity for G_1-Tris-t-BOC80 was highest since it has six hydroxyl groups. Thus at a given degree of substitution it has more hydroxyl groups than G_1-Bis-t-BOC and G_1-Dhn-t-BOC which aid dissolution in 0.26N TMAH. The lowest sensitivity of G_1-Dhn-t-BOC80 could be attributed to the lower reactivity of naphthalene based resist during deblocking (Pan et al., 2007). It thus appears that these positive resists are less sensitive than the corresponding negative resists based on the same skeleton bearing epoxide groups which exhibit a sensitivity of 35 μC/cm^2.

The contrast (γ) was calculated using formula $\gamma^{-1} = \log D_1 - \log D_0$ (Bilenberg et al., 2006), where D_0 is the maximum dose where the resist thickness before development and after development is identical. The values for contrast obtained using 10 wt % PAG, 2.50 for G_1-Tris-t-BOC80, 2.09 for G_1-Bis-t-BOC80 and 1.66 for G_1-Dhn-t-BOC80 follow the same argument as for the variation of sensitivity and are slightly higher than those for the corresponding negative resists reported in the previous chapter. Dai et al., (2006) used molecular glass resist based on 4-[4-[1,1-Bis(4-hydroxyphenyl) ethyl]]-R,R-dimethylbenzyl phenol containing three terminal hydroxyl groups conjugated with t-BOC, which resolved upto 150 nm lines at 1:1 pitch at 40 μC/cm^2 using 40 kV beam energy. Positive resist based on 5,5-bis-(tert-butoxycarbonyloxy) phenyl-5-[4,4-bis(tert-butoxycarbonyloxy)-1,1:3 ,1- terphenyl-50-yl]-1,1:3,1:3,1:3,1-quinquephenyl for EBL reported by Kadota et al., (2004), resolved features upto 25 nm at 66 μC/cm^2 using 50 kV beam energy. Our values for sensitivity at 20 kV beam energy are comparable to those reported for MGs based resist (Dai et al., 2006). It would be possible to pattern features lower than 30 nm at higher beam energy.

6.3.4.2. Post exposure bake (PEB) and development time optimization

We examined the effect of PEB in the temperature range 70-110 °C for 60 sec. All patterns merged during development for PEB at 100 and 110 °C which could be due to acid diffusion effect. Patterns were undeveloped at 70 and 80 °C because of incomplete deprotection.

Figure 6.11 shows typical example of different stages of development of the resist G_1-tris-t-BOC80. The PEB was 90°C for 60 sec. At the end of 40 sec (Figure 6.11 A) and 50 sec (Figure 6.11 B) the patterns were incompletely developed, but were completely developed at the end of 70 sec (Figure 6.11 C).

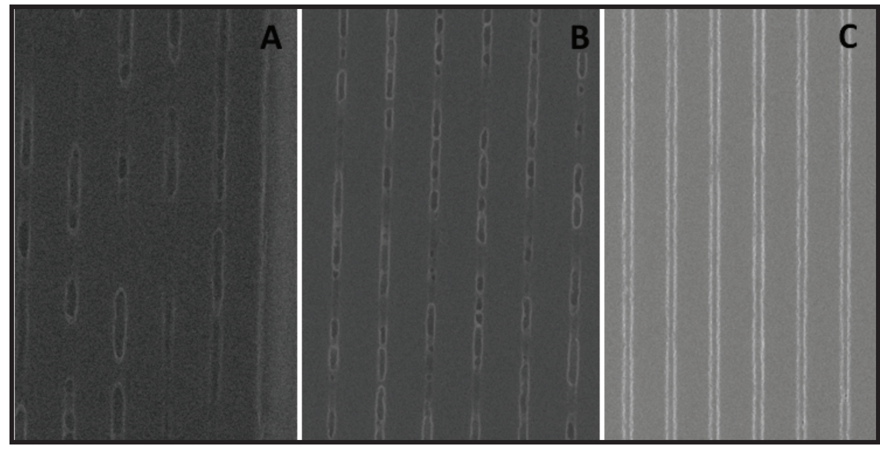

Figure 6.11: Development of G_1-tris-t-BOC in TMAH at varying time A) 40 sec; B) 50 sec and C) 70 sec.

In the case of bisphenol-A as well as 1,5-Dhn based resist, the patterns were fully developed only after 85 sec. Development rate for trisphenol based dendrimer is higher than that for the FGDs based on bisphenol-A and 1,5-Dhn, since trisphenol based FGD containing 6 hydroxyl groups, is more rapidly dissolved compared to FGDs based on bisphenol-A and 1,5-Dhn containing 3 hydroxyl groups each.

6.3.4.3. Electron beam lithography

100% t-BOC conjugated FGDs showed poor adhesion to the silicon wafers during development, whereas FGDs containing 50 and 60 % t-BOC were partially soluble in 0.26N TMAH before exposure, leading to poor image on development. The FGDs containing 80 % t-BOC were therefore evaluated for EBL. Oxidised silicon wafers were used to enhance adhesion of photoresist to the substrate. Resist containing 5 wt. % solution of FGDs and 10 wt. % triphenylsulphonium 2-(phenoxy)tetrafluoroethane-1-sulfonate (based on FGDs) were spin-coated onto a two inch silicon wafer at 6000 rpm which formed 70 nm, 64 nm and 61 nm thick films respectively. Prebaking of the coated films on the silicon wafers was carried out at 70 ^{o}C for 5 min. Positive-tone FGD resists were patterned using 20 kV e-beam and dose 50 $\mu C/cm^2$ for G_1-Tris-t-

BOC80, 60 μC/cm^2 for G_1-Bis-t-BOC80 and 80 μC/cm^2 for G_1-Dhn-t-BOC80 respectively. Irradiation of triphenylsulphonium 2-(phenoxy)tetrafluoroethane-1-sulfonate generates acid, which subsequently reacts with t-BOC conjugate leading to deprotection during the post exposure bake (PEB) carried out at 90 ^{o}C for one min. The films were then developed with 0.26 N TMAH, 70 sec for G_1-Tris-t-BOC, 85 sec for G_1-Bis-t-BOC and G_1-Dhn-t-BOC.

6.3.4.4. Scanning electron microscopy (SEM)

6.3.4.4.1. Positive-tone resists

Positive tone SEM images of 100, 50 and 30 nm patterns of G_1-Tris-BOC 80 resist are shown in Figure 6.12.

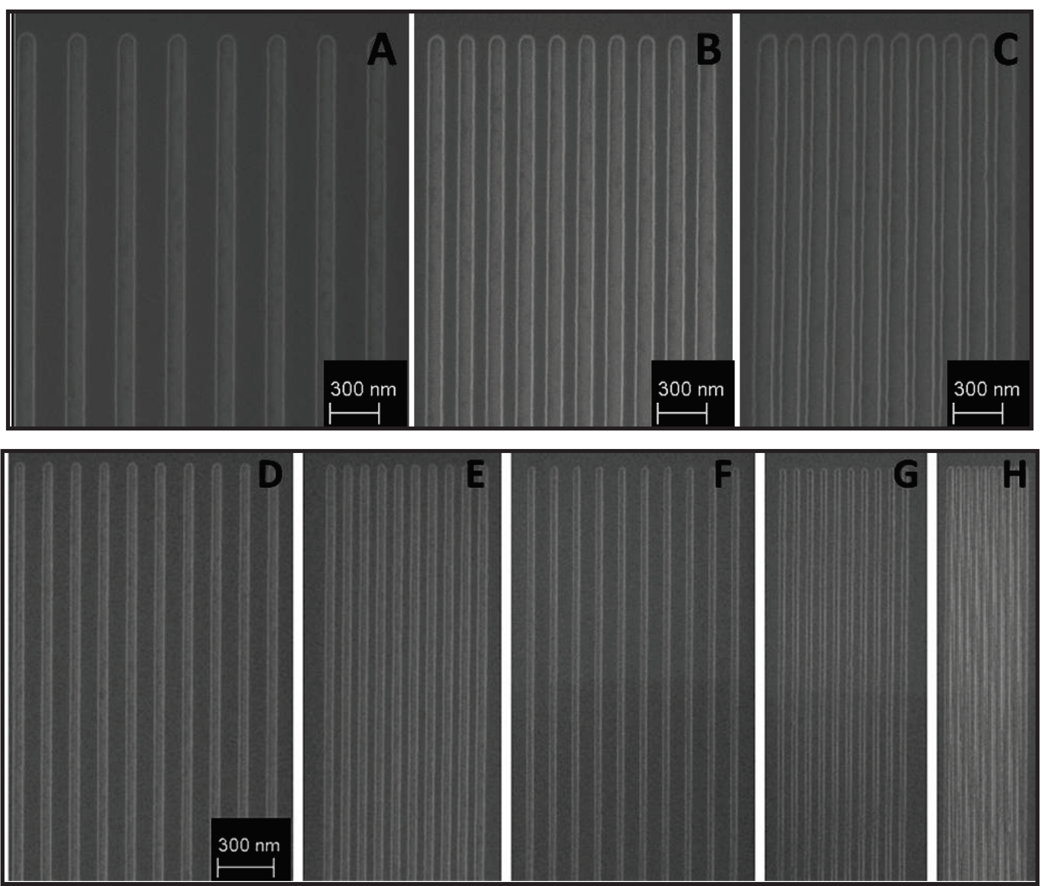

Figure 6.12: SEM images of 100 nm lines at pitch 1:2 (A), 1:1(B), 1:0.7 (C); 50 nm lines at pitch 1:2 (D), 1:1 (E) and 30 nm lines at pitch 1:3 (F), 1:2 (G) and 1:1 (H) for G_1-Tris-BOC 80.

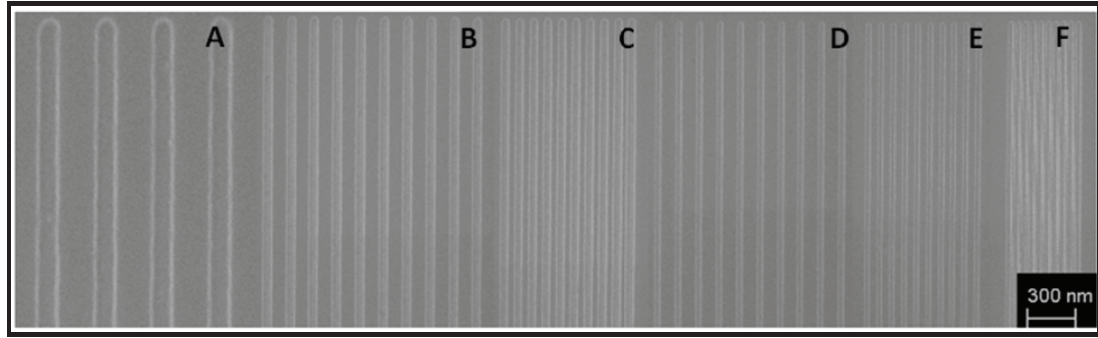

Figure 6.13: SEM images of 100 nm lines at pitch 1:2 (A); 50 nm lines at pitch 1:2 (B), 1:1 (C) and 30 nm lines at pitch 1:3 (D), 1:2 (E) and 1:1 (F) for G_1-Bis-BOC 80.

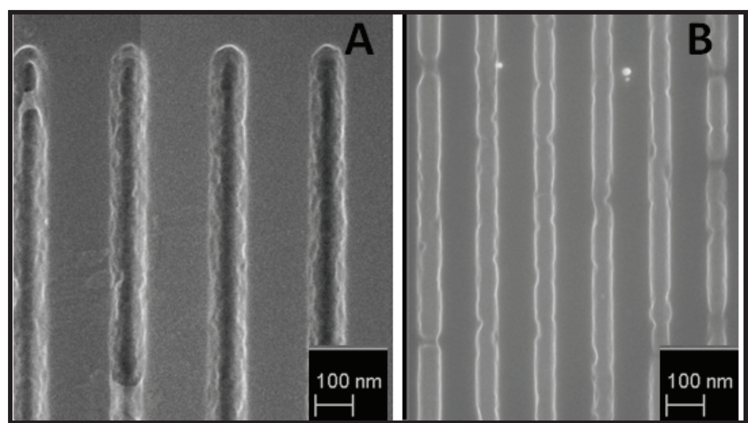

Figure 6.14: SEM images of G_1-Dhn-BOC 80 at pitch 1:2; (A) 100, (B) 50 nm lines.

The results show that 100 nm lines at pitch 1:2 (A), 1:1 (B) and 1:0.7 (C) were resolved. 50 nm lines were resolved at pitch 1:2 and 1:1 (Figures 6.12 D and E) and 30 nm lines were resolved at pitch 1:3, 1:2 and 1:1 (Figures 6.12 F, G and H). These are comparable to 25 nm line patterns reported by Kadota et al., (2004) for BCOQP resist films on exposure to 50 kV beam energy at 66 $\mu C/cm^2$ post baked at 100 ^oC for 90 sec. Similar results were obtained with FGD based on bisphenol-A (Figures 6.13 A-F). FGD based on 1,5-Dhn, resolved features upto 100 nm and 50 nm at pitch 1:2 (Figures 6.14 A and B).

6.3.4.4.2. Line edge roughness (LER)

The LER is inversely proportional to the dissolution rate of the resist (Ma et al., 2003). The dissolution rate increases with to the number of hydroxyl groups in the resist. Compared to polymeric photoresist use of low molecular weight photoresist leads to lower line edge roughness because of higher and more uniform dissolution

rate. LER values were calculated from the equation 2 reported by Leunissen et al., (2004). Averages of 20 adjacent points on the lines were used to calculate LER values summarized in Table 6.5.

$$\sigma = \left(\frac{\sum_{i=1}^{N} (\delta W(z_i) - \delta W)^2}{N-1} \right)^{1/2} \quad \text{.............................} (2)$$

The values obtained for FGDs containing trisphenol and bisphenol-A units are lower than those for FGD based on 1,5-Dhn. Trisphenol based FGD containing 6 hydroxyl groups, results in high solubility compared to FGDs based on bisphenol-A and 1,5-Dhn containing 3 hydroxyl groups each. As compared to G_1-Bis-t-BOC, FGD based on 1,5-Dhn shows higher LER low contrast, since naphthalene containing resist has low reactivity. As compared to epoxide conjugated FGDs based on the same skeleton discussed in previous chapter, t-BOC conjugated FGDs show lower LER and higher contrast. Positive resists show higher resolution at lower feature sizes, since there is no crosslinking which leads to swelling as in case of the negative resist during development.

Table 6.5: LER values for FGD resists.

Resist	Line width (nm)	LER (3σ)	Sensitivity (μC/cm^2) At 20 kV	Contrast (γ)
G_1-Tris-t-BOC80	100 nm	4.9	50	2.5
	50 nm	5.3		
	30 nm	5.8		
G_1-Bis-t-BOC80	100 nm	5.1	60	2.09
	50 nm	5.7		
	30 nm	6.0		
G_1-Dhn-t-BOC 80	100 nm	7.6	80	1.66
	50 nm	7.9		

6.4. Conclusions

Low molecular weight FGDs based on 1, 3, 5-tris bromomethyl benzene as the core and 1,1, 1-tris-p-4-hydroxyphenyl ethane, bisphenol-A and 1,5-dihydroxynaphthalene peripheral groups were synthesized in chapter 5. These FGDs were modified with

varying in t-BOC content. FGD based on trisphenol exhibits lower sensitivity 50 $\mu C/cm^2$ but higher contrast (2.5) compared to FGDs based on bisphenol-A (sensitivity 60 $\mu C/cm^2$ and contrast 2.09) and 1,5-dihydroxynaphthalene (sensitivity 80 $\mu C/cm^2$ and contrast 1.66). 30 nm patterns at 1:1 pitch could be resolved successfully using FGDs based on trisphenol and bisphenol-A whereas 50 nm lines at 1:2 pitch were resolved using 1,5-dihydroxynaphthalene dendrimer. In the case of trisphenol and bisphenol-A dendrimer, the features can be further lowered at higher beam energy. Epoxide conjugated FGDs based on the same skeleton discussed in previous chapter showed high sensitivity (35 $\mu C/cm^2$) compared to t-BOC conjugated FGDs which show lower LER and higher contrast compared to the epoxide based dendrimers. Positive resists show higher resolution at lower feature sizes, since there is no crosslinking which leads to swelling as in case of the negative resist during development.

6.5. References

1. Bilenberg, B., Jacobsen, S., Schmidt, M. S., Skjolding, L.H.D., Shi, P., Boggild, P., Tegenfeldt, J.O., Kristensen, A., Microelectronic Engineering 2006, **83,** 1609–1612.
2. Chattopadhyay, D. K, Panda, S. S., Raju, K. V. S. N. Progress in Organic Coatings 2005, **54**, 10–19.
3. Dai, J., Chang, S. W., Hamad, A., Yang, D., Felix, N., Ober, C. K. Chem. Mater. 2006, **18**, 3404-3411.
4. De Silva, A., Felix, N. M., Ober, C. K. Adv. Mater. 2008, **9999**, 1–7.
5. De Silva, A., Lee J. K., Andre X., Felix N. M., Cao H. B., Deng H., Ober C. K., Chem. Mater., 2008, **20**, 1606–1613.
6. De Silva, A., Ober, C. K., J. Mater. Chem. 2008, **18**, 1903–1910.
7. Esfandeh, M., Mirabedini, S. M., Pazokifard, S., Tari, M. Colloids and Surfaces A: Physicochem. Eng. Aspects 2007, **302,** 11–16.
8. Felix, N. M., De Silva, A., Ober, C. K. Adv. Mater. 2008, **20**, 1303–1309.
9. Haba, O., Haga, K., Morikawa, O., Konishi, H., Ueda, M. Chem. Mater. 1999**, 11**, 427-432.
10. Hansen, M. M., Riggs, J. R., Tetrahedron Letters 1998, **39**, 2705-2706.
11. Hattori, S., Yamada, A., Saito, S., Asakawa, K., Koshiba, T., Nakasugi, T. J. Vac. Sci. Technol. B 2009, **27**, 5, 2138-2144.
12. Ito H., Nakayama T., Sherwood M., Miller D., Ueda M., Chem. Mater., 2008**, 20**, 341–356.
13. Kadota, T., Kageyama, H., Wakaya, F., Kenji, G., Shirota, Y., Chemistry Letters 2004, **33**, 6, 706-707.
14. Kamimura, Y., Haba, O., Endo, T., Ueda, M. Journal of Polymer Science: Part A: Polymer Chemistry 2005, **43**, 1210–1215.
15. Leunissen, L. H. A., Lawrence, W. G., Ercken, M. Microelectronic Engineering 2004, **73–74**, 265–270.
16. Ma, Y., Shin, J., Cerrina, F., J. Vac. Sci. Technol. B 2003, **21**, 1, 112-117.
17. Pan, G., Du, Z., Zhang, C., Li, C., Yang, X., Li, H. Polymer 2007, **48,** 3686-3693.
18. Reichmanis, E., Houlihan, F**.** M., Nalamasu, O., Macromol. Symp. 2001, **175,** 185–196.

19. Reichmanis, E., Houlihan, F. M., Nalamasu, O., Neenan, T. **X.,** Chem. Mater. 1991, **3**, 3, 394-407.
20. Shirota, Y., J. Mater. Chem. 2005, **15**, 75–93.
21. Tully, D. C., Trimble, A. R., Frechet, J. M. J. Adv. Mater. 2000, **12**, 15, 1118-1122.
22. Uthirakumar, P., Suh, E. K., Hong, C. H., Lee, Y. S., Polymer 2005, **46**, 4640–4646.
23. Wang, M, Gonsalves, K. E., Rabinovich, M, Yuehb, W., Roberts, J. M., J. Mater. Chem. 2007, **17**, 1699–1706.
24. Yonezawaa, N., Mori S. I., Miyata, S., Anyashiki, Y. U., Maeyama, K., Reactive & Functional Polymers 2002, **53**, 11–17.
25. Young Gil, K., Kim, J. B., Fujigaya, T., Shibasakib, Y., Ueda, M., J. Mater. Chem., 2002, **12**, 53–57.

Chapter 7

Chemically amplified negative resists based on first generation dendrimers for optical lithography

7.1. Introduction

In semiconductor technology decreasing device size has been necessitated by increasing component density. Advances in optical lithography have enabled reduction in size of semiconductor devices and circuits over the last three decades. A critical step in the manufacture of semiconducting, electronic and optoelectronic devices is pattern transfer for which reactive ion etching (RIE) is most extensively used. The method uses an electrical discharge, reactive fluoride gases and induces ion bombardment on the surface of semiconductor wafers to obtain the designed patterns (Avram et al., 2009; Hong and May. 2003). Compared to wet etching, RIE leads to better uniformity, control and etch selectivity (Rahman et al., 2001).

Negative photoresists based on epoxy resins are used extensively in electronics industry (Chae and Park., 2004) as they offer a unique combination of properties like high strength, thermal stability, moisture resistance, chemical and corrosion resistance, adhesion and requisite mechanical as well as electrical properties (Rwei et al., 2005; Wang and Lee., 2000). SU-8 is a negative tone epoxy photoresist which provides good lithographic performance and low etching rate (Bilenberg et al., 2006) and is extensively used for applications in lithography, for moulding and packaging in semiconductor industry. However, SU-8 suffers from certain limitations. The spin-coating of both thick and thin layers of SU-8 resist often results in non-homogenous films, debonding after post-baking, poor adhesion to substrate (Yang et al., 2007; Sayah et al., 2007), and cracking at the corners of the microstructures caused by excessive residual stress, generated at the corners of the microstructure (Bystrova et al., 2007). Curing of SU-8 resin leads to shrinkage. As the base of the microstructure is bonded to the substrate, it cannot shrink while the surface layer does. This causes the corners to shrink in two different directions, resulting in cracks (Yang et al., 2007).

Negative photoresists based on dendrimers have been extensively investigated for optical lithography. While merits of 1st generation dendrimers have been recognized in the literature, it is believed that low T_g limits their lithographic performance. It was therefore, felt that the first generation dendrimers containing rigid and bulky cores and peripheral epoxy groups would enable overcome the limitations of the dendrimers reported in the past for the lithographic applications (Haba et al., 1999, Kamimura et al., 2005).

In this chapter, we report comparative evaluation of resists based on epoxy functionalized FGDs with SU-8 resist in optical lithography (365 nm) using three different masks and during etching. Epoxy functionalized FGDs based on bisphenol-A and trisphenol formed defect free films at lower thicknesses which could be patterned by UV photolithography. The patterns exhibited lower RIE rates compared to SU-8 and will therefore be useful in the device fabrication using pattern transfer.

7.2. Experimental section

Synthesis of epoxy functionalized FGDs and their characterization was discussed in chapter 5.

7.2.1. Characterization

The resists were spin coated on silicon wafers at 3000 rpm. Optical litho tool, EVG 620 Automated Double Side Mask Aligner, Austria was used for resist patterning. STS RIE 320 PC was used for reactive ion etching. Olympus optical microscope, Japan and Raith 150 ^{TWO}, Germany were used for imaging and resist thickness measurements. Atomic Force Microscope Model MMAFMLN, VEECO Digital Instruments Santa Barbara, CA, USA was used to measure the thickness of the resists and images were taken in tapping mode.

7.2.2. Lithographic evaluation

The resists containing 14 wt % dendrimer (G_1-Tris-epoxide, G_1-Bis-epoxide and G_1-Dhn-epoxide) solutions in PGMEA were used to match the composition of SU-8 2000.5. 10 wt % Triarylsulphonium hexafluoroantimonate (PAG) which is also used in SU-8 2000.5 was added on the basis of FGDs. SU-8 2000.5 resist which has 14 wt. % solid content and is the least viscous amongst the SU-8 series was simultaneously processed for comparative evaluation. For lithographic evaluation we used standard RCA (Radioactive Corporation of America) cleaned 2-inch silicon wafers, which were cleaned by immersion in hydrofluoric acid (HF) and washed with water. Wet oxidation was carried out to grow 490 nm thick silicon oxide layer. This was followed by spin-coating of resists at 3000 rpm. SU-8 2000.5 was first spin-coated onto the substrate to form 460 nm thick resist layer. The FGDs were spin-coated onto the silicon substrate to form resist layers of thickness 200 nm for G_1-Tris-epoxide, 150 nm for G_1-Bis-epoxide and 110 nm for G_1-Dhn-epoxide. Coated samples were

processed using a standard procedure which involved pre-baking on a hotplate at 70 °C for 5 min and 90 °C for 1 min, followed by exposure using a soft-contact mask-aligner of 60 mJ/cm^2 intensity at 365 nm wavelength for 5 sec. Post exposure bake (PEB) was carried out at 60 °C for 1 min and 95 °C for 1 min to accelerate cross linking of the exposed areas of the photoresist. The patterns were developed using PGMEA (SU-8 developer) at room temperature, rinsed with isopropanol and dried with a nitrogen blower.

7.3. Results and Discussion

Retaining dimensions of patterns in silicon oxideafter etching is critical in advanced micromachining processes used for the fabrication of micro devices. To etch these structures, RIE is most commonly used to transfer lithographically defined photoresist patterns onto underlying layers. It is compatible with vacuum processing technologies and offers clean operations.

The findings of this investigation are divided in to three subsections. In the first part, UV lithographic processing of simple line patterns with different width and pitch was explored to validate the concept and evaluate comparative performance of different dendrimers vis a vis SU-8 resist. The second part deals with the performance of resists for patterning of complex structures for gate area used in gate device. Finally, in the third subsection, results of comparative evaluation of the RIE of the dendrimeric resist vis a vis SU-8 resist, are presented.

7.3.1. Lithography

The resists containing 14 wt % dendrimer were used for all the lithographic experiments. The presence of the ether linkages in the base dendrimeric resist structure was expected to provide good adhesion to silicon oxide substrate and hence no additional adhesion promoter such as HMDS was used. During a preliminary study, the resolution capabilities of dendrimeric resist and SU-8 resist were tested. Resists were processed under identical lithographic conditions and same mask containing line patterns ranging from 50 μ to 10 μ at decreasing pitch. Preliminary results showed that PEB at 60 °C for 1 min and 95 °C for 1 min was enough for the completion of the chemical change. The advantage of using low molecular weight resist for lithography is the difference in the T_g of the uncrosslinked and crosslinked dendrimeric photoresists are very high. As a result the development of the

dendrimeric resist is very short which also avoids the swelling of the crosslinked resist were by increasing the performance. Propylene glycol methyl ether acetate was used as a developer, since it has low toxicity, and has been known to offer high resolution, good contrast, develop closely spaced lines of low feature sizes and minimum swelling as compared to 4-methyl-2-pentanone MIBK and 5-methyl-2-hexanone (Argitis et al., 1995).

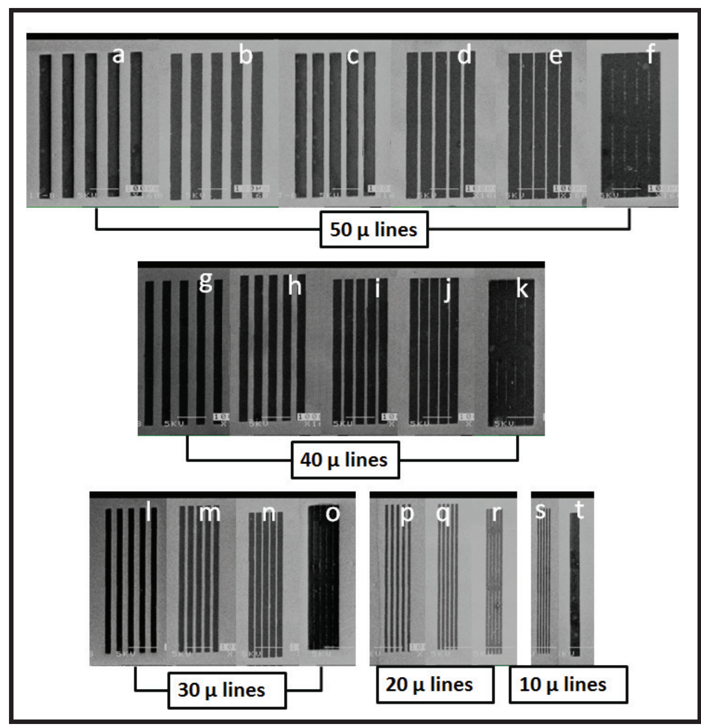

Figure 7.1: Line pattern of the G_1-Tris-epoxide resist

For all the polymer SEM images (Figures 7.1 to 7.4), the lithographic patterns were labelled as discussed in chapter 3. The results of lithography, summarized in Figure 7.1 for G_1-Tris-epoxide, Figure 7.2 for G_1-Bis-epoxide, Figure 7.3 for G_1-Dhn-epoxide and Figure 7.4 for SU-8 resins, show that lines upto 10 μ width and 10 μ spacing could be satisfactorily resolved in all the cases. In this respect the performance of these dendrimers was compared to the SU-8 resin as well as epoxide based linear methacrylate polymers discussed in chapter 4. Features 5 μ width at 5 μ spacing could not be resolved satisfactorily. This was not because of the material limitations but the limitation in the fabrication of the mask.

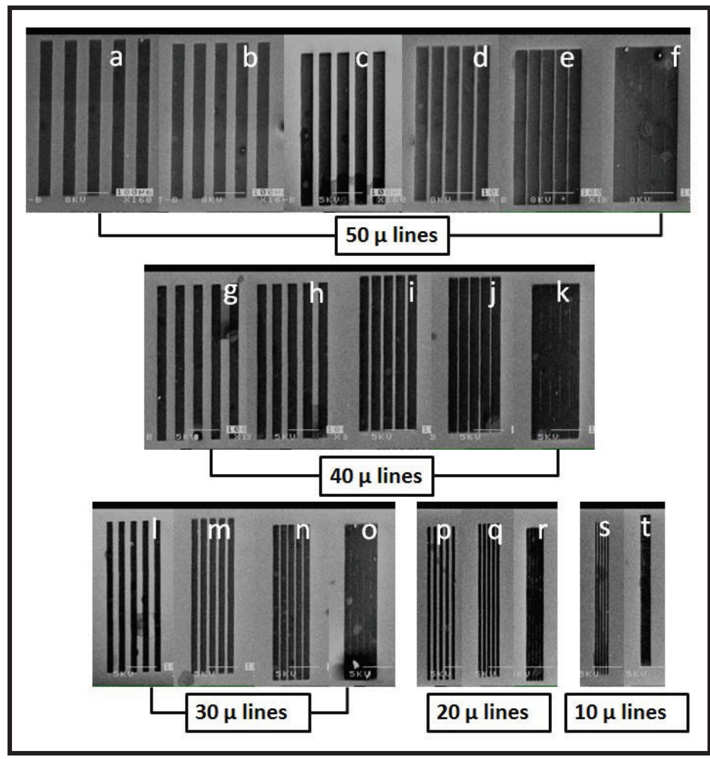

Figure 7.2: Line pattern of the G_1-Bis-epoxide resist

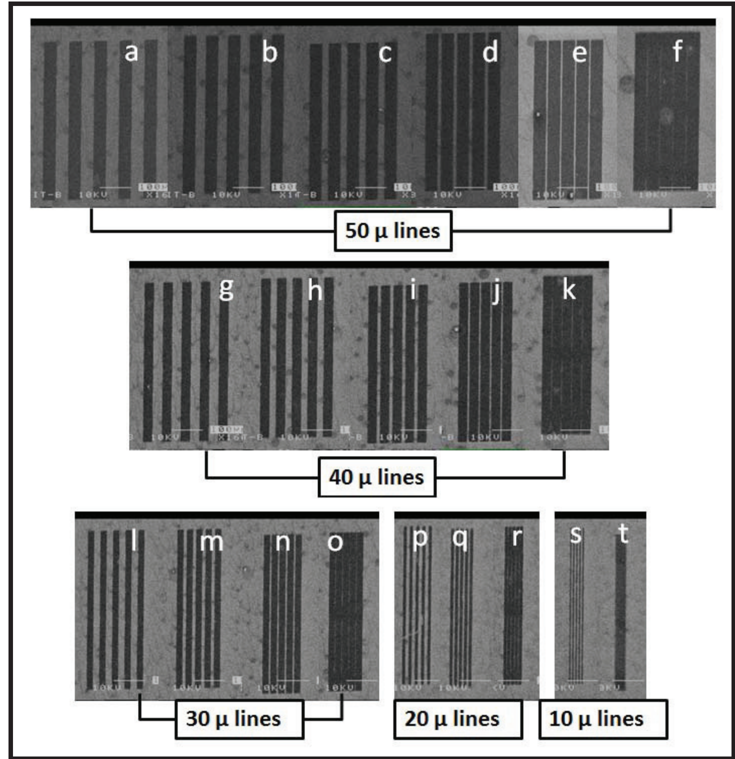

Figure 7.3: Line pattern of the G_1-Dhn-epoxide resist

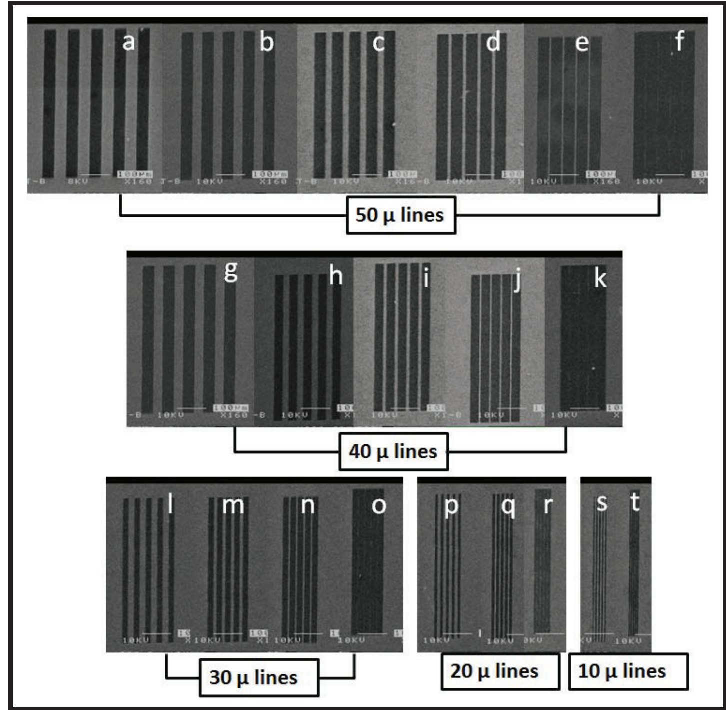

Figure 7.4: Line pattern of the SU-8 resist

7.3.2. Patterns for gate area device

To compare performance of FGD based resists with SU-8 in real life applications, patterns were formed using a mask containing complex structures which would be used in the fabrication of the gate device. Figures 7.5A-D show coloured optical images of gate device area patterned from SU-8, G_1-Tris-epoxide, G_1-Bis-epoxide and G_1-Dhn-epoxide respectively.

The images obtained using SU-8 show roughness at the edges, a blurred shadow effect along pattern edges (gray shade on pale yellowish background) and pinholes (Figure 7.5A). The FGDs based on trisphenol (Figure 7.5B) and bisphenol-A (Figure 7.5C) could resolve defect free features after development under identical conditions. In case of G_1-Dhn-epoxide resist, pin holes were observed after spinning (Figure 7.5D) which indicates poor resist performance as compared to FGDs based on trisphenol and bisphenol-A. This was further confirmed by patterning simple square type structures as discussed in the next section.

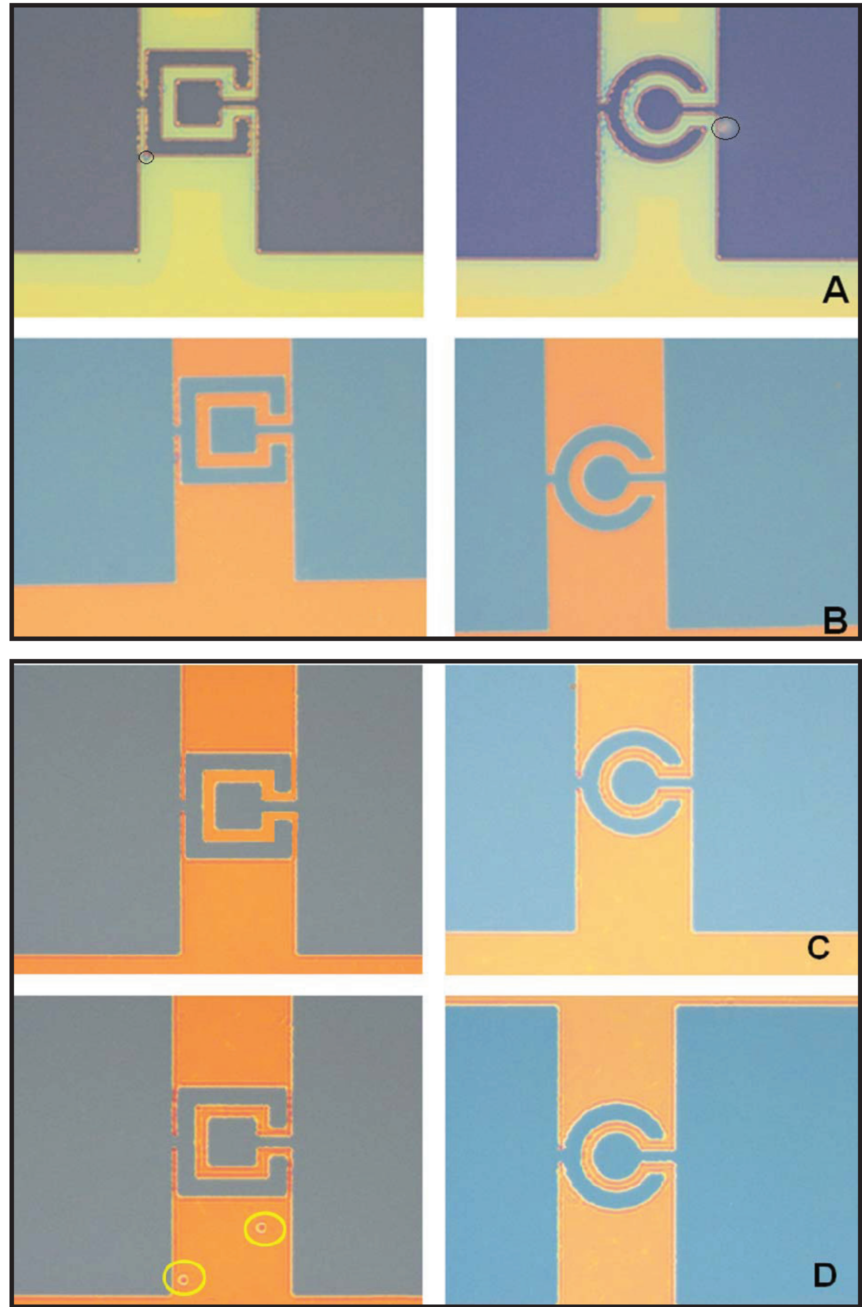

Figure 7.5: Images of the resist SU-8 (A), G_1-Tris-epoxide (B), G_1-Bis-epoxide (C) and G_1-Dhn-epoxide (D)

7.3.3. Reactive ion etching (RIE)

For optimal circuit performance, the dimensions of the features must be most faithfully reproduced and their degree of edge roughness controlled.

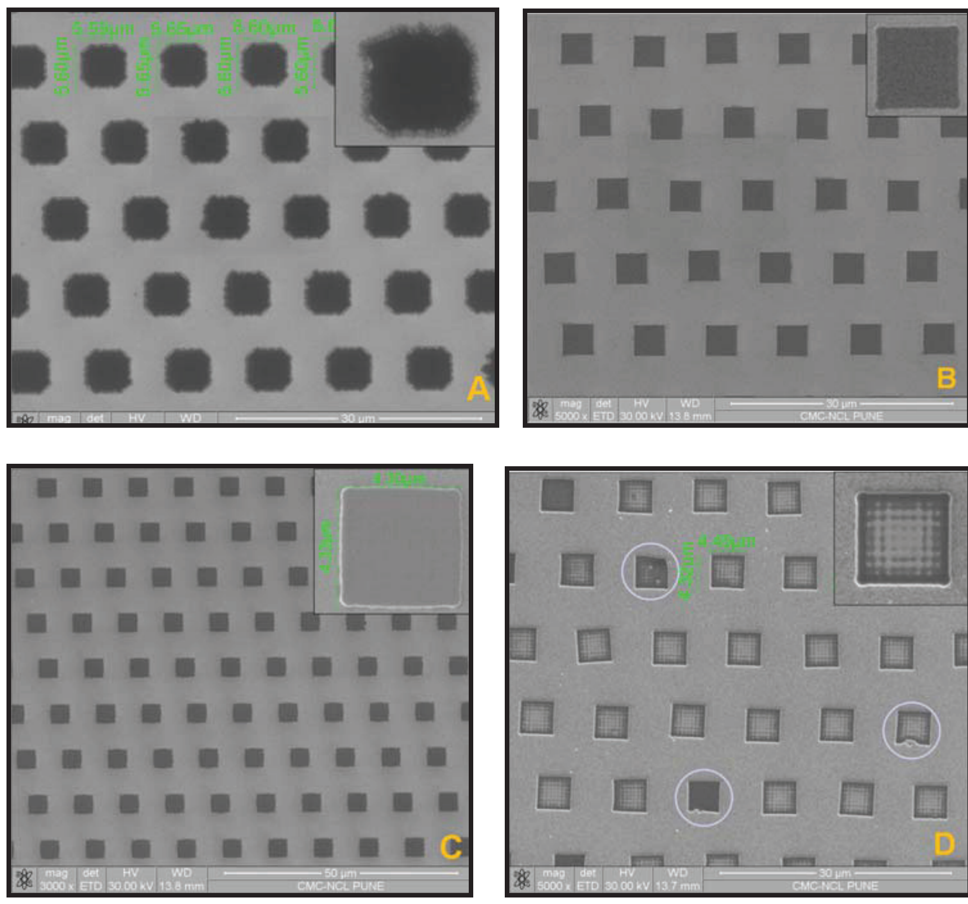

Figure 7.6 SEM images of the resist A) SU-8, B) G_1-Tris-epoxide, C) G_1-Bis-epoxide and D) G_1-Dhn-epoxide

To evaluate the performance of FGDs and SU-8, 4.3 µm squares were patterned under lithographic conditions described in the experimental section. The structures obtained using SU-8 showed roughness at the edges and blunt cuts at the corners (Figure 7.6A). The final pattern size was found to be 5.6 µm as against the mask size of 4.3 µm as a result of acid diffusion and the higher thickness (460 nm). In contrast, the FGDs based on trisphenol (Figure 7.6B) and bisphenol-A (Figure 7.6C) could resolve defect free 4.3 µm square patterns after development. FGD based on G_1-Dhn-epoxide (Figure 7.6D) resulted in 4.3 µm square patterns but resulted in defects indicating poor resist performance. These patterns were further used for RIE to evaluate their stability vis-a-vis SU-8.

Reactive Ion Etching (RIE) is one of the most intensively used techniques in the fabrication of semiconductor devices for transferring patterns from masks to semiconductor substrates. High aspect-ratio reactive ion etching is extensively used for the fabrication of microelectromechanical devices such as high precision motion

sensors (Abdolvand and Ayazi, 2008) and high performance low motional impedance capacitive resonators (Pourkamali and Ayazi, 2005). RIE was carried out to transfer resist patterns onto silicon dioxide, films used as interlayer dielectric material for integrated circuits and multichip modules (Kim and May, 1994).

All experiments were carried out on quarter sections of same 2 inch diameter silicon wafers having a native 490 nm silicon oxide layer so that each sample had the same oxide layer thickness. The samples were first hard baked on a hotplate at 130 ^{o}C for 10 min and slowly cooled to room temperature. The RIE experiment was carried out in STS RIE 320 PC under the standard conditions summarized in Table 7.1. Etching rates were obtained from the differences in the thicknesses of the resist layers by AFM and oxide layers by SEM before and after RIE and the duration of the etching.

Table 7.1: RIE conditions

Process gas	CHF_3 and O_2
Flow	CHF_3 (50): O_2 (2) SCCM
Pressure	100 m TOrr
R F Power	200 watt
Time	300 sec

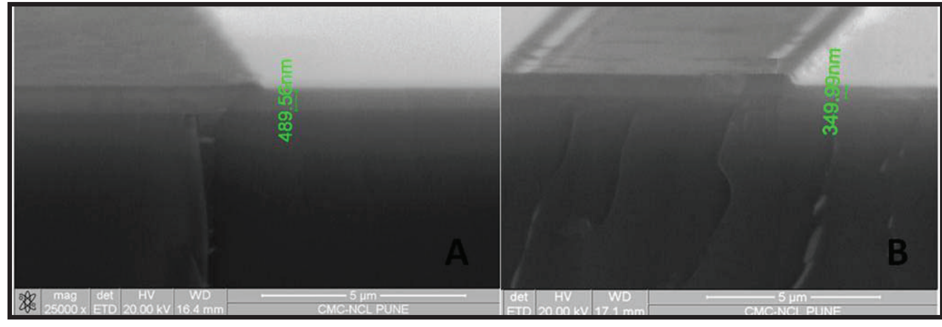

Figure 7.7: Thickness of the squares patterns on silicon oxide before (A) and after (B) RIE

Table 7.2: Reactive ion etching (RIE) of the FGDs and SU-8

Name	A (nm)	B (nm)	C (nm)	D (nm)	E (nm)	F(nm)	G (nm/sec)	H (nm/sec)
G_1-Tris-ep	200	490	690	270	350	620	0.23	0.46
G_1-Bis-ep	150	490	640	200	350	550	0.30	0.46
G_1-Dhn-ep	110	490	600	180	350	530	0.23	0.46
SU-8	460	490	950	500	350	850	0.33	0.46

A= Resist thickness before RIE (AFM measurements); B= Oxidethickness before RIE (SEM measurements); C= Total thickness before RIE (A+B); D= Thickness after RIE (resist + dioxide) (AFM measurements); E= Oxidethickness after RIE (SEM measurements); F= Total thickness after RIE (D+E); G= Resist etching rate (C-F); H= Oxideetching rate (B-E).

Since, it was difficult to measure the thickness of the silicon oxidelayer by AFM technique we measured thickness by taking cross section of the samples using SEM as shown in Figure 7.7. The thickness of the silicon oxidelayer was 490 nm before RIE (Figure 7.7 A) and 350 nm after RIE (Figure 7.7 B).

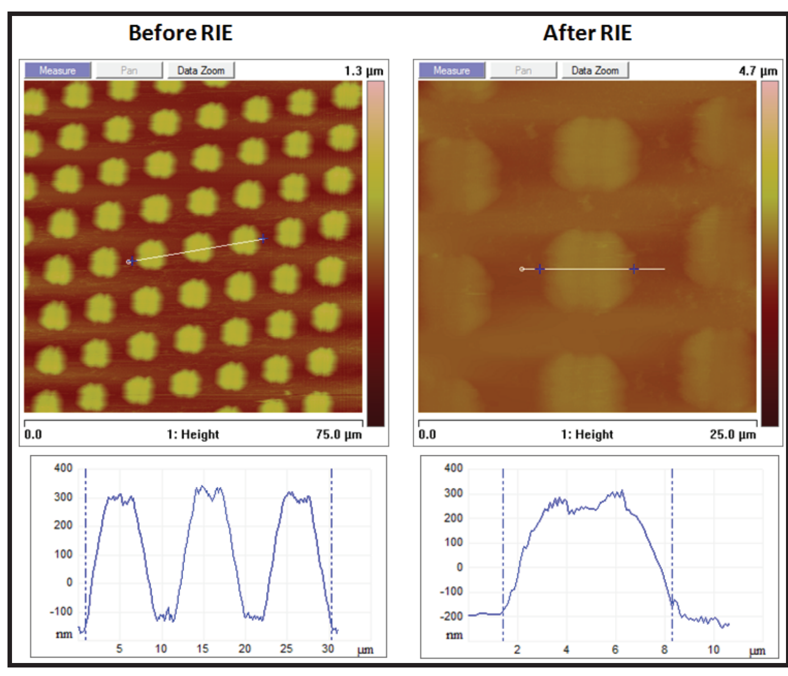

Figure 7.8: AFM images of SU-8 before and after RIE

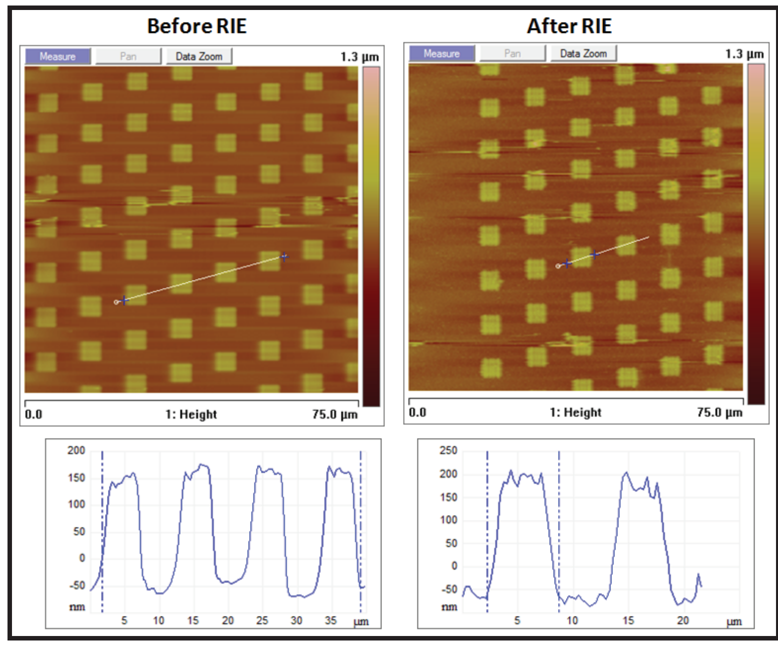

Figure 7.9: AFM images of G_1-Tris-epoxide before and after RIE

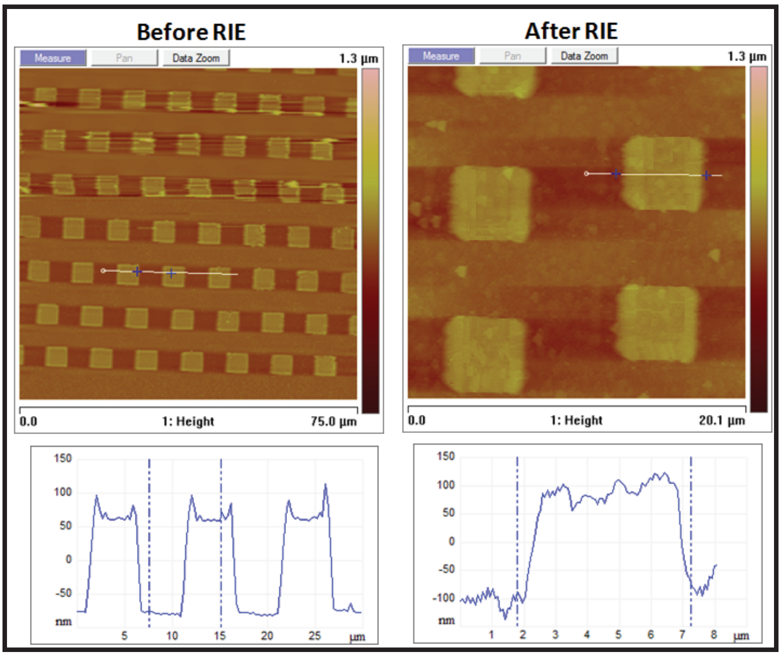

Figure 7.10: AFM images of G_1-Bis-epoxide before and after RIE

Etching rate of the oxide layer was 0.46 nm/sec. Figures 7.8-7.11 show the thickness of SU-8, G_1-Tris-epoxide, G_1-Bis-epoxide and G_1-Dhn-epoxide resist layers before and after RIE. The etching rates of FGD based resist are 30 % lower than that of SU-8 (Table 7.2).

FGD based resist exhibits lower thicknesses because of lower molecular weights which results in lower resist viscosities. As film thickness decreases, exposure time required to harden the resist decreases which minimises acid diffusion. Lower thickness of resists also implies better accuracy of pattern replication. Generally it is difficult to reduce film thickness of SU-8 resists below 100 nm (Bilenberg et al., 2006). Using epoxide conjugated FGDs it is possible to achieve the resist thickness up to 66 nm as discussed in chapter 5. Lower resist thickness as well as lower etching rates is desirable in device fabrication.

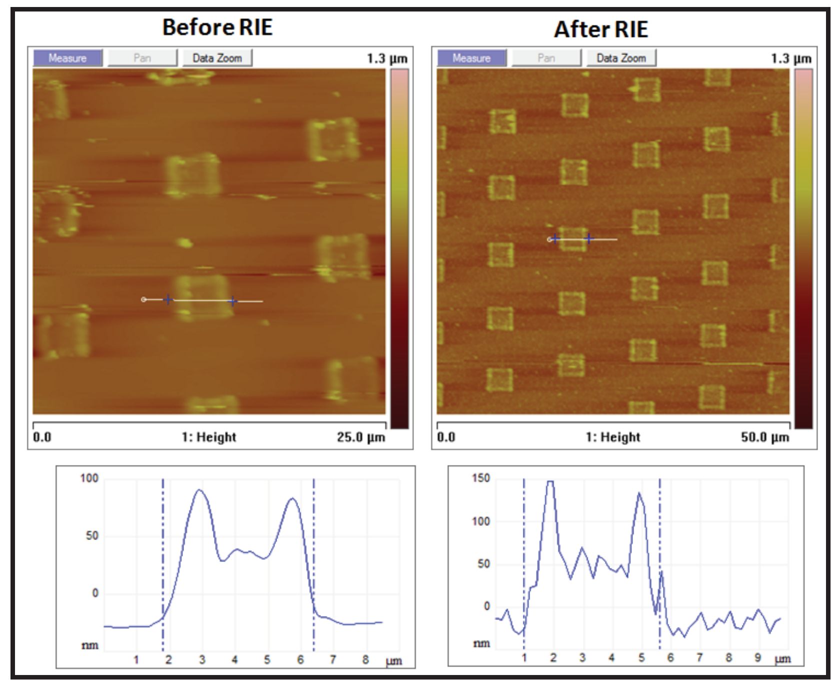

Figure 7.11: AFM images of G_1-Dhn-epoxide before and after RIE

7.4. Conclusions

The resists based on epoxy functionalized FGDs were evaluated for optical lithography as well as RIE. The process conditions were similar to those used with SU-8. Lines upto 10 µ width and 10 µ spacing could be fabricated satisfactorily vis a vis SU-8 resin. Resin could not be evaluated at lower width and spacing because of the mask limitation. Reliable replication of structures of feature size of 4.3 µm feature size was possible using epoxy functionalized FGDs using optical lithography. During RIE the resins exhibited upto 30 % lower RIE rates vis a vis SU-8 resins.

7.**5. References:**

1. Abdolvand, R., Ayazi, F. Sensors and Actuators A 2008, **144**, 109–116.
2. Avram, M., Avram, A., Comanescu, F., Popescu, a. M., Voitincu, C. IEEE 2009, 253-256.
3. Argitis, P., Boyatzis, S., Raptis, I., Glezos, N., Hatzakis, M. ACS, symposium series 1998, **706**, 345-357.
4. Bilenberg, B., Jacobsen, S., Schmidt, M. S., Skjolding, L.H.D., Shi, P., Boggild, P., Tegenfeldt, J.O., Kristensen, A., Microelectronic Engineering 2006, **83,** 1609–1612.
5. Bystrova, S., Luttge, R., Berg, Vanden, A. Microelectronic Engineering 2007, **84**, 1113-1116.
6. Chae, K. H., Park, J. H. Macromolecular Research 2004, **12**, 4, 352-358.
7. De Silva, A., Felix, N. M., Ober, C. K. Adv. Mater. 2008, **9999**, 1–7.
8. Haba, O., Haga,K.,Ueda, M. Chem. Mater. 1999**, 11**, 427-432.
9. Hong, S. J., May, G. S., IEEE TRANSACTIONS ON SEMICONDUCTOR MANUFACTURING, 2003, **16**, 4, 598-608.
10. Kamimura, Y., Haba, O., Endo, T., Ueda, M. Journal of Polymer Science: Part A: Polymer Chemistry 2005, **43**, 1210–1215.
11. Kim, B., May, G. S. IEEE 1994, 273-278.
12. Pourkamali, S., Ho, G. K. Ayazi, F., Proceedings of the IEEE Micro Electro Mechanical Systems Conference'05, 2005, 211–214.
13. Rahman, M., Deng, L., Wilkinson, C., Van Den Berg, J. J. Appl. Phys. 2001, 89, 5, 2792.
14. Rwei, S. P, Cheng, C.Y., Liou, G. S., Cheng, K. C., Polym Eng Sci 2005; 45, 478-486.
15. Sayah, A., Parashar, V. K., Gijs, M. A. M. Journal of Microelectromechanical Systems, 2007, **16**, 3, 564-570.
16. Wang, C. S., Lee, M. C., Polymer 2000, 41, 3631-3638.
17. Yang, R., Steven A. Soper, S. A., Wang, W. Sensors and Actuators A 2007, **135,** 625–636.

Chapter 8

Conclusions and recommendations for further work

Present investigation was undertaken to explore lithographic evaluation of different chemically amplified polymeric and FGD resists for optical lithography and electron beam lithography.

8.1. Major conclusions arrived at from this investigation are summarized below

- Inclusion complex (IC) mediated copolymerization of cyclodextrin complexes of ethylene glycol dimethacrylates and trimethylol propane trimethacrylate with cumylphenol and 1-naphthol methacrylate to yield solvent soluble copolymers containing various levels of pendant vinyl unsaturations was achieved.
- Incorporation of aromatic methacrylate monomers enhanced both thermal stability and T_g of the copolymers compared to the corresponding homopolymers.
- Copolymers containing pendant vinyl unsaturations act as negative photoresists in optical lithography. Cumyl methacrylate based copolymer performed better than 1-naphthol methacrylate based copolymers.
- Synthetic methodology for synthesis of bisphenol-A and 1, 5-dihydroxynaphthalene based linear methacrylate polymers containing varying degree of pendant epoxide was developed.
- The linear methacrylate based polymers containing pendant epoxide could be processed as negative resist for optical lithography.
- Lithographic performance of linear methacrylate polymers of bisphenol-A and 1,5-dihydroxynaphthalene containing pendant epoxide was compared with SU-8 resin. Polymers containing bisphenol-A showed better resolution than SU-8 resin and 1,5-dihydroxynaphthalene polymers.
- FGDs based on 1, 3, 5-tris bromomethyl benzene as the core and 1, 1, 1-tris-p-4-hydroxyphenyl ethane, bisphenol-A and 1,5-dihydroxynaphthalene peripheral groups were synthesized.
- The peripheral hydroxyls when converted to epoxide groups, the FGDs could be processed as negative photoresists for electron beam lithography as well as optical lithography.

- Bisphenol-A and trisphenol based FGDs resolved features upto 30 nm at 1:1 pitch, whereas 1,5-dihydroxynaphthalene based FGD resolve 50 nm lines at 1:10 pitch.
- FGD based on the trisphenol exhibited higher contrast and lower LER as compared to FGDs based on bisphenol-A and 1,5 dihydroxynaphthalene.
- t-BOC conjugated FGDs could be processed as positive resists for electron beam lithography.
- The sensitivity of the t-BOC conjugated FGDs resists was lower than that of the epoxide conjugated negative tone resist containing the same skeleton. The FGDs containing t-BOC peripheral groups exhibited higher contrast and lower LER compared to the epoxide conjugated FGDs.
- As compared to SU-8, FGDs based on trisphenol and 1,5-dihydroxynaphthalene exhibited lower etching rate.

8.2. Recommendations for future work

A research investigation of this kind cannot address all the issues raised, within the limited time period available. The validation of the concept and its application demonstrated in this work opens new areas that could benefit from future work, are summarized below.

- Negative resists based on copolymers containing pendant vinyl unsaturation could be optimized for lower feature sizes and high aspect ratio for optical lithography for evaluating their potential in MEMS.
- The molecular weight of linear polymers containing pendant epoxide groups could be lowered to 2000 and its performance as negative resist could be evaluated in electron beam lithography.
- More detailed evaluation of linear polymers containing pendant epoxide could be undertaken to evaluate the lower pattern size and highest density and aspect ratio that can be achieved in optical lithography as to explore suitability for applications in MEMS.
- Linear polymers containing varying hydroxyl groups could also be conjugated with t-BOC which would act as positive resist having properties similar to PMMA.

- Since FGDs based positive and negative resists resolve features upto 30 nm at 1:1 pitch, their performance for the fabrication of CMOS devices could be evaluated.
- The sensitivity of the positive resist based on FGDs could be increased by conjugating with adamantyl groups.
- The performance of FGD molecular resists in extreme ultraviolet (EUV) lithography could also be evaluated.
- The rheological study of resist synthesized in this work could be undertaken to correlate the resist performance with rheological characteristics. This would also provide insights for manipulating resist structures for enhanced performance.